

A GEOCHEMICAL AND ISOTOPIC STUDY OF PLUTONIC AND HIGH GRADE
METAMORPHIC ROCKS FROM THE CHANDOS TOWNSHIP AREA, GRENVILLE
PROVINCE, ONTARIO

by

LARRY MICHAEL HEAMAN

B.Sc. (University of Western Ontario)

M.Sc. (McMaster University)

A Thesis

Submitted to the School of Graduate Studies
in Partial Fulfilment of the Requirements

for the Degree

Doctor of Philosophy

McMaster University

© December, 1985

A GEOCHEMICAL AND ISOTOPIC STUDY OF PLUTONIC AND HIGH GRADE
METAMORPHIC ROCKS FROM THE CHANDOS TOWNSHIP AREA, GRENVILLE
PROVINCE, ONTARIO.

DOCTOR OF PHILOSOPHY (1985)
(Geology)

McMASTER UNIVERSITY
Hamilton, Ontario

TITLE: A GEOCHEMICAL AND ISOTOPIC STUDY OF PLUTONIC
AND HIGH GRADE METAMORPHIC ROCKS FROM THE
CHANDOS TOWNSHIP AREA, GRENVILLE PROVINCE,
ONTARIO

AUTHOR: LARRY MICHAEL HEAMAN
B.Sc. (University of Western Ontario)
M.Sc. (McMaster University)

SUPERVISORS: Dr. Robert H. McNutt
Dr. Denis M. Shaw

NUMBER OF PAGES: i-xx, 1-307

ABSTRACT

The geological history of the Chandos township region in the Grenville Province of Ontario and the behaviour of the Rb-Sr system in response to an amphibolite grade regional metamorphism have been investigated by comparing Rb-Sr whole rock and U-Pb zircon and sphene ages determined, in most cases, from the same sampling site. A variety of sampling techniques have been employed in order to evaluate the geological significance of Rb-Sr whole rock ages in complex, high grade terrains.

In the case of the layered sodic Apsley gneiss, samples collected from widely spaced sampling sites result in a more precise but anomalously old (1402 Ma) and geologically meaningless age; a consequence of combining genetically unrelated samples. Although Rb-Sr whole rock ages determined using samples collected from homogeneous portions of individual sampling sites are in better agreement with the inferred age of the Grenville Supergroup (ca. 1250 Ma), the best estimate for the age of the sodic Apsley gneiss is 1333 ± 24 Ma, obtained by combining all the samples that have an igneous origin. A minimum estimate for the deposition and extrusion of these supracrustal rocks is the precise U-Pb

zircon age of $1254 \pm 11/-4$ Ma (the Rb-Sr whole rock age for this site is 1244 ± 32 Ma) obtained for the Tallan Lake sill.

Precise U-Pb zircon ages for two other intrusive bodies in the study area, the Methuen quartz monzonite and Loon Lake monzonite, indicate igneous activity at $1242 \pm 22/-6$ and $1090 \pm 7/-4$ Ma, respectively. Most of the granitoid rocks in the Central Metasedimentary Belt have low initial strontium ratios (0.703 to 0.704) and anomalously high oxygen isotopic compositions ($> 8\%$) indicating that these units were derived from a source with a low average Rb/Sr and/or a source with a relatively short crustal residence history, and subsequently interacted with high- ^{18}O rocks (eg. marble) at depth, but did not interact with "old", high Rb/Sr crustal material.

The timing of amphibolite grade metamorphism is unclear, however, a minimum estimate is provided by the 1090 Ma U-Pb zircon age obtained for the post-tectonic Loon Lake monzonite. At present, there is no reliable maximum estimate but the 1150 Ma Rb-Sr study determined using thin slabs from the sodic Apsley gneiss is interpreted to be close to the time of metamorphism. If the occurrence of 1085 Ma U-Pb sphene ages in this region reflects new sphene growth or resetting during metamorphism then these ages, combined with the lack of evidence for new zircon growth, indicate that the region cooled slowly from approximately 600 to 650°C (ie. the

blocking temperature for zircon) at 1150 Ma to approximately 500°C (ie. the blocking temperature for sphene) at 1085 Ma.

The final geological activity in this region was late-stage faulting, injection of pegmatite and associated hydrothermal activity. The effects of this event are recorded in the Rb-Sr whole rock system of the Silent Lake gneiss, the potassic Apsley gneiss and fracture-bearing samples of the Tallan Lake granodiorite. The best estimate for the timing of this activity is the Rb-Sr whole rock age of 1023 ± 17 Ma determined using fracture-bearing samples from the Tallan Lake granodiorite.

The different sampling techniques employed in this study indicate that the scale of Rb and/or Sr migration in the sodic Apsley gneiss, during metamorphism, must be less than one meter (the minimum distance between samples collected from one sampling site) and greater than 1 centimeter (the average width of the slabs). A more profound effect on the mobility of these elements was found in samples that have been affected by the late-stage hydrothermal activity. In certain rock units, the Rb-Sr system has responded to at least two distinct events, a regional amphibolite grade metamorphism at about 1150 Ma and hydrothermal activity at about 1025 Ma; so some caution should be exercised in interpreting the geological significance of Rb-Sr whole rocks ages determined in this region.

ACKNOWLEDGEMENTS

I would like to express my sincere gratitude to my co-supervisors, Dr. R.H. McNutt and Dr. D.M. Shaw, and to the other member of my supervisory committee, Dr. G.R. Purdy, for their valuable guidance, constructive criticism and continued encouragement throughout this study. I am particularly indebted to Dr. McNutt for sharing his wisdom on the "black art" of operating mass spectrometers and occasionally showing me the "black magic" of his driver and to Dr. Shaw for his infinite scientific wisdom and for introducing me to the geological enigmas of Chandos township. The financial support provided by both supervisors to attend field trips, conferences and to carry out part of this research at the Royal Ontario Museum (ROM) is greatly appreciated. I am equally indebted to Dr. T.E. Krogh, who supervised the research at the ROM, for introducing me to U-Pb zircon geochronology, for stimulating discussions, and for sharing the wisdom of his First Law of Isotope Geology "there are a lot of ways to do something wrong"; Dr. Krogh is an inspiration to all geochronologists.

I owe a special note of appreciation to Bob Bowins who

volunteered (with slight persuasion!), on several occasions, to repair and/or fine-tune an ailing mass spectrometer. The interface that Bob built for the mass spectrometer to facilitate computer controlled data acquisition and the numerous squash and hockey outings helped to preserve my sanity. The joys and frustrations of everyday life in Room 406 were shared with G. Beakhouse and K. Connare and the challenges of tracking down Rb contamination or leaks in the vacuum system plus the time spent "theorizing" in the Phoenix will always be remembered.

Many aspects of this study would not be possible without the expertise of numerous individuals. I am especially grateful to Dr. M. Bergeron and Dr. M. Truscott (PGNAA), O. Mudroch (XRF), A. Kabir and B. Bowins (INAA), I. Nicklin (mineral separation), Steve Prevec (sample preparation), and Y.Y. Kwok (U-Pb chemistry) for their assistance. I would also like to extend my appreciation to B. Podstawskyj (ROM) for his uncanny ability to keep two mass spectrometers operating simultaneously with a minimum of problems, to Dr. Y.N. Shieh for willingly analysing several samples for oxygen isotopes, and to J Whorwood and L. Zwiker for the professionalism they showed in preparing photographs and thin sections, respectively.

Stimulating discussions with the following people helped me to clarify, in my own mind, many of the ideas

presented in this dissertation; Drs. G. Beakhouse, F. Corfu, D. Davis, S. Lumbers, N. Machado, C. Rapela, U. Schaerer, and the late C. Rees.

The exceptional patience and understanding shown by my wife Jan over the past year while I tried to finish writing in my "spare time" will always be remembered and to her I express my deepest appreciation.

Finally, I would like to acknowledge the financial support provided by the Natural Sciences and Engineering Research Council (NSERC), the Ontario Graduate Scholarship Program, and McMaster University.

TABLE OF CONTENTS

	Page
ABSTRACT	iii
ACKNOWLEDGEMENTS	vi
CHAPTER 1 INTRODUCTION	1
1.1 OUTLINE OF OBJECTIVES	1
1.2 SELECTION OF A STUDY AREA	3
1.3 THE APPLICATION OF Rb-Sr DATING TO METAMORPHIC ROCKS	6
CHAPTER 2 THE CENTRAL METASEDIMENTARY BELT	10
2.1 INTRODUCTION	10
2.2 GENERAL GEOLOGY	11
2.2.1 Boundaries and Subdivision	11
2.2.2 Metamorphism	12
2.2.3 Supracrustal Rocks	14
2.2.4 Intrusive Rocks	16
2.3 SUMMARY OF PREVIOUS ISOTOPIC STUDIES	18
2.3.1 K-Ar Dating	18
2.3.2 ^{40}Ar - ^{37}Ar Dating by Incremental Heating	20
2.3.3 Strontium Isotopes	23
2.3.4 Lead Isotopes	26
2.3.4.1 U-Pb Ages	26
2.3.4.2 Common-Lead Studies	28
2.3.5 Oxygen Isotopes	29

TABLE OF CONTENTS - CON'D

	Page
4.2 TALLAN LAKE SILL	104
4.2.1 Geological Setting	104
4.2.2 Petrography	106
4.2.3 Geochemistry	111
4.2.3.1 Major Elements	111
4.2.3.2 Trace Elements	123
4.2.4 U-Pb Zircon Geochronology	135
4.2.5 Rb-Sr Geochronology	141
4.2.5.1 Granodiorite	141
4.2.5.2 Amphibolite	146
4.2.6 Oxygen Isotopes	149
4.2.7 Discussion	152
4.2.7.1 Amphibolite Petrogenesis	152
4.2.7.2 Amphibolite-Granodiorite Relationship	161
4.3 METHUEN COMPLEX	166
4.3.1 Geology and Petrography	166
4.3.2 Geochemistry	171
4.3.4 U-Pb Zircon, Sphene Geochronology	176
4.3.5 Rb-Sr Geochronology	181
4.4 LOON LAKE PLUTON	186
4.4.1 Introduction	186
4.4.2 U-Pb Zircon, Sphene Geochronology	191

TABLE OF CONTENTS - CON'D

	Page
CHAPTER 5 DISCUSSION AND CONCLUSIONS	201
5.1 INTRODUCTION	201
5.2 SELECTING SAMPLES FOR Rb-Sr GEOCHRONOLOGY	201
5.3 SUMMARY OF GEOLOGICAL RELATIONSHIPS IN THE CHANDOS TOWNSHIP REGION	203
5.3.1 Supracrustal Rocks	203
5.3.2 Igneous Rocks	205
5.3.3 Effects of Metamorphism	208
5.3.4 Influence of Fractures	212
5.4 TIMING OF IGNEOUS ACTIVITY IN THE CMB	217
5.5 ISOTOPIC CONSTRAINTS ON THE ORIGIN OF CMB GRANITOID ROCKS	220
5.5.1 Initial Strontium Ratios	220
5.5.2 Sr-O Relationships	223
REFERENCES	230
APPENDIX A ANALYTICAL PROCEDURES	247
A1 SAMPLE PREPARATION	247
A2 X-RAY FLUORESCENCE SPECTROSCOPY	248
A2.1 Precision and Accuracy	249
A3 INSTRUMENTAL NEUTRON ACTIVATION ANALYSES	253
A4 PROMPT-GAMMA NEUTRON ACTIVATION ANALYSES	256
A5 ISOTOPIC ANALYSES	257
A5.1 Strontium Isotopes	257
A5.1.1 Chemistry	257

TABLE OF CONTENTS - CON'D

	Page
A5.1.2 Mass Spectrometry	259
A5.1.3 Reproducibility and Accuracy	261
A5.1.4 Age Calculation and Isochron Errors	263
A5.2 Uranium and Lead Isotopes	268
A5.2.1 Mineral Separation	268
A5.2.2 Zircon, Sphene Selection	269
A5.2.3 Air Abrasion	270
A5.2.4 Sample Cleaning	272
A5.2.5 Sample and Spike Weighing	273
A5.2.6 U and Pb Chemistry	274
A5.2.7 Blanks	277
A5.2.8 Mass Spectrometry	278
A5.3 Oxygen Isotopes	280
APPENDIX B MODAL, GEOCHEMICAL AND ISOTOPIC ANALYSES	281

LIST OF FIGURES

Figure		Page
1	Location of the study area within the Central Metasedimentary Belt, Ontario	4
2	Summary of $^{40}\text{Ar}/^{37}\text{Ar}$ data for gabbroic rocks from the Central Metasedimentary Belt	21
3	Summary of U-Pb ages from the Central Metasedimentary Belt	27
4	Summary of oxygen isotopic data from the Central Metasedimentary Belt	30
5	Geologic map of the Chandos township area	38
6	Summary of $\text{K}_2\text{O}/(\text{Na}_2\text{O}+\text{K}_2\text{O})$ ratios for the Apsley Gneiss	45
7	Geochemical profiles across a layered Apsley biotite gneiss sample (AG19)	50
8	Sample location map for the Apsley gneiss	53
9	Rb-Sr isochron diagram for regionally collected samples from the Apsley gneiss	57
10	Rb-Sr isochron diagrams for individual sampling sites of the Apsley gneiss	66
11	Rb-Sr isochron diagram for the Apsley gneiss	71
12	Rb-Sr isochron diagram for the Apsley gneiss slab study (AG19)	75
13	Rb-Sr isochron diagram for the Apsley gneiss slab study (AG50)	81
14	Geologic map of the Silent Lake area	87
15	Rb-Sr isochron diagrams for the Silent Lake gneisses	96
16	Sample location map for the Tallan Lake sill	105
17	Modal quartz-plagioclase-K-feldspar diagram for samples from the Tallan Lake sill	107

LIST OF FIGURES - CON'D

Figure		Page
18	AFM diagram for samples from the Tallan Lake sill	113
19	Enrichment/depletion diagram for fracture-bearing samples from the Tallan Lake sill	121
20	Rb versus Sr diagram for the Tallan Lake sill	126
21	Y, TiO ₂ , P ₂ O ₅ versus Zr for the Tallan Lake sill	128
22	Chondrite normalized REE diagrams for the Tallan Lake sill	132
23	Concordia diagram for the Tallan Lake sill	139
24	Rb-Sr isochron diagrams for the Tallan Lake granodiorite	142
25	Rb-Sr isochron diagram for the Tallan Lake amphibolite	147
26	Oxygen isotopic data from the Tallan Lake sill	150
27	Schematic drawing of the Tallan Lake sill	153
28	Sample location map for the Methuen Complex	168
29	Modal quartz-plagioclase-K-feldspar diagram for the Methuen Complex	169
30	Na ₂ O-K ₂ O-CaO ternary diagram for the Methuen Complex	173
31	Y-Zr diagram for granitoid rocks from the Chandos township region	175
32	Concordia diagram for the Methuen Complex - Site A	177
33	Concordia diagram for the Methuen Complex - Site B	180
34	Rb-Sr isochron diagram for the Methuen Complex	183

LIST OF FIGURES - CON'D

Figure		Page
35	Sample location map for the Loon Lake pluton	192
36	Concordia diagram for the Loon Lake monzonite	194
37	Concordia diagram for the Loon Lake quartz monzonite	196
38	Compilation of U-Pb and Rb-Sr ages from the Chandos township region	204
39	$^{207}\text{Pb}/^{206}\text{Pb}$ versus $^{206}\text{Pb}/^{204}\text{Pb}$ for sphenes from the Chandos township area	210
40	$^{87}\text{Sr}/^{86}\text{Sr}$ versus $1/\text{Sr}$ for the Tallan Lake sill	214
41	Histogram of radiometric ages for granitoids from the Central Metasedimentary Belt	218
42	Histogram of initial strontium isotopic ratios for CMB granitoid rocks	221
43	Sr-O diagram for CMB granitoid rocks	224

LIST OF PLATES

Plate		Page
1.	Exposures of the Apsley biotite gneiss	39
2	Hand specimens of the sodic and potassic Apsley biotite gneiss	40
3	Photograph of the Apsley biotite gneiss sample (AG50) used for the slab study	80
4	Exposures of the Tallan Lake sill amphibolite and granodiorite	108
5	Hand specimens of the Tallan Lake fracture-bearing granodiorite and Methuen Complex	119
6	Zircon fractions from the Tallan Lake sill and Loon Lake pluton	137

LIST OF TABLES

Table		Page
3.1	The average chemical composition of the Apsley gneiss and possible protoliths	47
3.2	Two-error regression results for samples from the Apsley biotite gneiss	63
3.3	The average chemical composition for the Silent Lake leptytes	93
3.4	Two-error regression results for quartz-feldspathic rocks from the Silent Lake area	95
3.5	Comparison of Rb and Sr abundances in the Silent Lake quartz-sillimanite nodules	100
4.1	The average chemical compositions for various sample suites from the Tallan Lake sill	115
4.2	The chemical composition of various slabs sliced from a fracture-bearing granodiorite sample (TL12) from the Tallan Lake sill	122
4.3	The average chemical compositions for two sample suites from the Methuen Complex	172
5.1	Compilation of U-Pb zircon, sphene and Rb-Sr ages from the Chandos township region	206
5.2	Compilation of radiometric ages and initial strontium ratios for granitoid rocks from the Central Metasedimentary Belt	227
A1	Precision and accuracy of major element analyses	251
A2	Precision and accuracy of trace element analyses	251
A3	Precision and accuracy of Rb, Sr and Rb/Sr determinations	252
A4	Accuracy of the REE analyses	255
A5	Comparison of the REE data obtained for samples analysed with both irradiations	255

LIST OF TABLES - CON'D

Table		Page
A6	Interlaboratory comparison of samples analysed for strontium isotopes at McMaster and the Royal Ontario Museum	261
A7	Precision of the strontium isotope measurements	265
A8	Accuracy of the strontium isotope measurements	267
A9	Flow chart illustrating the procedure for separating zircon from a rock sample	271
A10	Summary of bomb blanks used for U and Pb chemistry	278
B1.1	Modal mineral abundances in samples from the Apsley biotite gneiss	282
B1.2	Modal mineral abundances in samples from the Silent Lake Complex	282
B1.3	Modal mineral abundances in samples from the Tallan Lake sill	282
B1.4	Modal mineral abundances in samples from the Methuen Complex	283
B2.1	The chemical composition of samples from the Apsley biotite gneiss	286
B2.2	The chemical composition of samples from the Silent Lake Complex	288
B2.3	The chemical composition of samples from the Tallan Lake sill	290
B2.4	The chemical composition of samples from the Methuen Complex	295
B3.1	Rb-Sr data for samples from the Apsley biotite gneiss	300
B3.2	Rb-Sr data for samples from the Silent Lake Complex	302

LIST OF TABLES - CON'D

Table		Page
B3.3	Rb-Sr and oxygen isotopic data for samples from the Tallan Lake sill	304
B3.4	Rb-Sr data for samples from the Methuen Complex	305
B4	U-Pb results for zircon and sphene fractions from units in the Chandos township area	307

CHAPTER 1

INTRODUCTION

1.1 OUTLINE OF OBJECTIVES

For the past two decades the Rb-Sr whole rock method of age dating has been routinely employed in an attempt to unravel complex geological relationships in metamorphic terrains. The impetus for these Rb-Sr studies was the fact that the whole rock system was shown, in some cases, to be resistant to metamorphic resetting (for a review see section 1.3). However, there are a number of investigations that indicate the Rb-Sr whole rock method can yield spurious age information so there is a definite need to understand the limitations of the technique. This study is an attempt to improve our understanding of the behaviour of the Rb-Sr system in high grade metamorphic rocks and to evaluate the potential of the Rb-Sr method as a viable dating technique for unravelling some complex geological relationships in a part of the Central Metasedimentary Belt (CMB), Grenville

Province, Ontario.

A major consideration before determining the age of any metamorphic rock by the Rb-Sr whole rock method is the scale of Rb and Sr migration during metamorphism. If the migration distances are small (ie. < a few centimeters) then the conventional approach of collecting several hand samples (circa 5 kilograms each) from widely spaced sampling sites, assuming all the samples are cogenetic, should preserve the formation or emplacement age of the rock. To evaluate the scale of Rb and Sr migration during metamorphism in the rocks from the study area, three different sampling techniques have been used; 1) thin slabs from individual samples, 2) multiple samples from individual sampling sites and 3) single samples from widely spaced sampling sites. The Rb-Sr results from these different sampling procedures will be compared to U-Pb zircon and sphene ages obtained for the same units in order to establish whether the method of sample collecting has any bearing on the outcome of a Rb-Sr whole rock age determination.

Another objective of this study is to evaluate the potential of the Rb-Sr whole rock method of age dating for unravelling complex stratigraphic relationships in high grade metamorphic terrains. Stratigraphic relationships in high grade terrains, such as the present study area, are often ambiguous because there is a lack of good marker horizons or clearly recognizable primary structures. In this regard, the

age relationship between two formations that occur in the Bancroft-Apsley area, the Apsley biotite gneiss and the Silent Lake quartzo-feldspathic gneiss, is investigated in detail with the intention that if geologically meaningful ages can be obtained for these units, there is the potential for unravelling some controversial and complex stratigraphic relationships in this region.

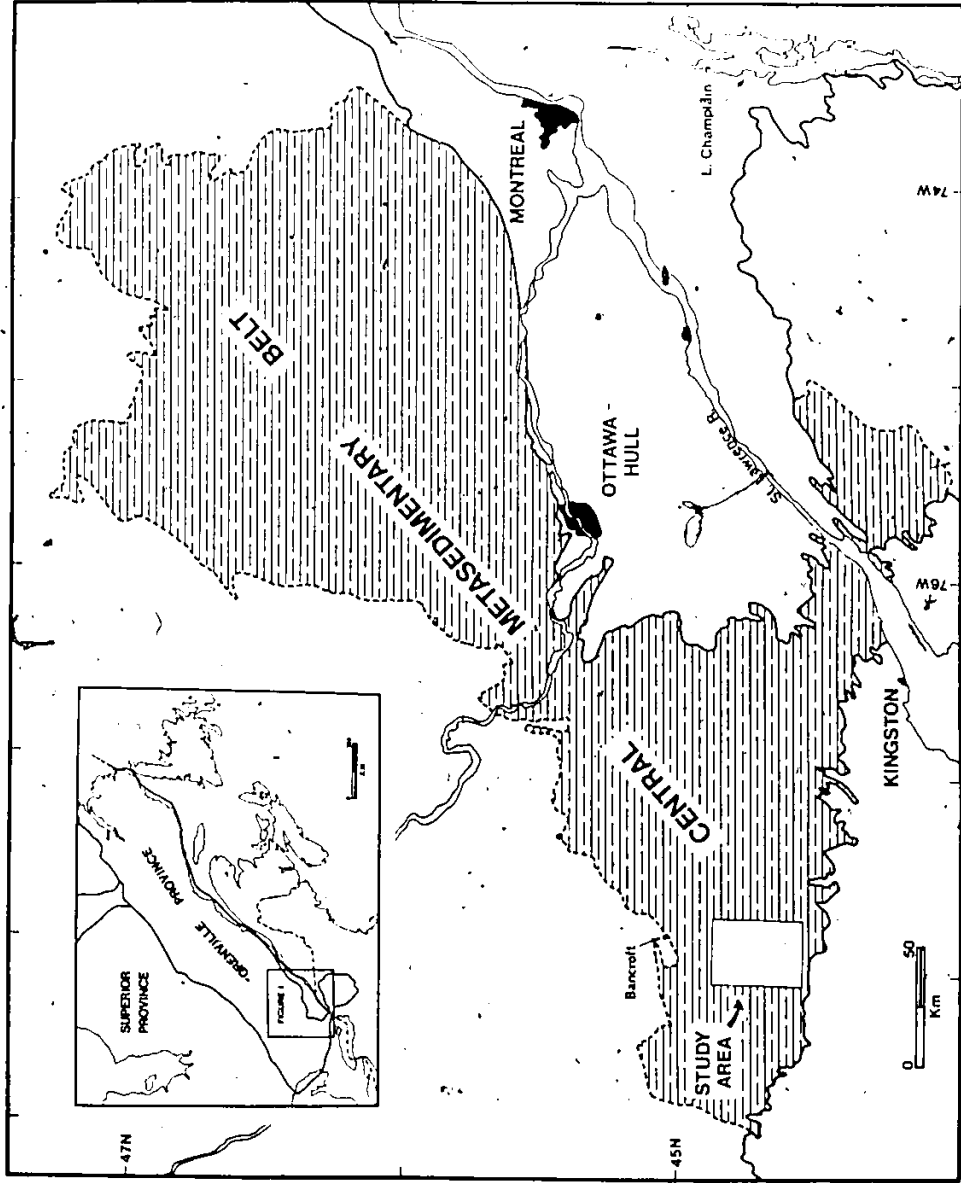
An additional key element in the study area is the ubiquitous presence of plutonic igneous rocks. A variety of intrusive units occur in the CMB but the timing of igneous activity in this belt is not well established. The final objective of this study is to compare the ages obtained by the U-Pb zircon, sphene and Rb-Sr whole rock methods for three igneous bodies; the Tallan Lake sill, Methuen Complex, and Loon Lake pluton. These detailed geochronology studies are expected to provide some insight into the timing of igneous activity in the CMB and, by combining these isotopic data with other petrologic and geochemical information, an attempt will be made to investigate the nature and origin of these units.

1.2 SELECTION OF A STUDY AREA

The area selected for this study is the Chandos township region of Ontario which is located within the Central Metasedimentary Belt, Grenville Province (Fig. 1). Apart from the interesting geological enigmas alluded to in

Figure 1

Location map showing the position of the study area within the Central Metasedimentary Belt (CMB), Grenville Province, Ontario. The dashed line represents the approximate boundary of the CMB. In Ontario and Quebec, this boundary is drawn as the contact between Helikian and Aphebian rocks delineated on the Riviere Gatineau Map Sheet compiled by Baer et al. (1971).



the previous section, this area offers good geological control. For example, all the units investigated in this study have been the subject of detailed (1"=1/2 mile) mapping projects (Shaw, 1962; Hewitt, 1961; Jennings, 1969; Breaks, 1971; Dostal, 1973) and, in most cases, subsequent research involving petrographic and geochemical studies. In other words, the distribution of lithologies and general geology in this area are well documented. It is crucial that there is a good understanding of the geology before attempting a detailed isotopic investigation in such a high grade metamorphic terrain.


Since one of the objectives is to investigate the behaviour of the Rb-Sr system in deformed rocks, it is better to select an area where the disturbance is related to one major period of metamorphism rather than accepting the complications inherent in multiply deformed terrains. In this regard, it is imperative that a considerable amount of time has elapsed between the time the rock formed and the time of metamorphism. Unless there is a significant accumulation of radiogenic strontium in the system, it will be impossible to distinguish geological disturbances from analytical uncertainties. The majority of units investigated from the Chandos twp. area formed at least 100 Ma before Grenvillian metamorphism and, therefore, should be ideal for testing the response of the Rb-Sr system to a metamorphic disturbance.

The final consideration is good access. The study area

has excellent road and lakeshore access with many large and relatively unweathered outcrops; ideal for collecting fresh samples for geochemistry and geochronology.

1.3 THE APPLICATION OF Rb-Sr DATING TO METAMORPHIC ROCKS

The Rb-Sr whole rock method for determining the age of geological samples is rooted in the observations of Schreiner (1958), Compston and Jeffery (1959, 1961), Tilton et al. (1959), Allsopp (1961), Fairbairn et al. (1961), Hart (1961), and Nicolaysen (1961) that the ages calculated for coexisting minerals in a metamorphic rock are commonly lower than the total rock age. This discrepancy in ages was attributed to the susceptibility of the individual minerals, and not the total rock, to isotopic modification during metamorphism. Although the first total rock Rb-Sr analyses were reported by Schreiner (1958), the advantage of the whole rock method for dating metamorphic rocks was originally established by Compston et al. (1960). Three total rock samples from a deformed granite mass located near Mundaring, Western Australia, with different Rb/Sr ratios, were shown to record a significantly older age (ca. 2700 Ma) than microcline (ca. 650 Ma) separated from the same unit. In other words, the Rb-Sr method could be used to determine two discrete geological events; the age of granite emplacement (whole rocks) and the time of metamorphism (minerals).



Despite the enthusiasm generated by the initial investigations, to state that it is possible to determine the formation age of a metamorphic rock implies that the following three assumptions are valid:

- a) all samples used in the age determination are cogenetic and have the same age.
- b) all samples had identical initial strontium ratios at the time of their formation.
- c) there has been no net gain or loss of Rb and/or Sr from the rock unit after it formed.

Unfortunately, it is not always clear that these assumptions are valid when dating metamorphic rocks. For example, Wasserburg et al. (1964) convincingly demonstrated that slightly metamorphosed, mafic samples from dikes and sills located in the Panamint Mountains, California have experienced profound enrichments in radiogenic strontium during a Mesozoic metamorphism, violating assumption (c) above.

Perhaps a more serious problem associated with determining the age of metamorphic rocks is the possibility of obtaining a statistically reasonable Rb-Sr isochron age that has no geological significance. In the example above, the disrupted Rb-Sr system was manifested by anomalous data scatter: however, it is possible to disturb the Rb-Sr system and still retain some colinearity in the data. Isochrons produced this way have been given a variety of names such as

"pseudoisochron" (Birk, 1978), "fictitious isochron" (Faure, 1977), "geologically meaningless isochron" (Field and Raheim, 1980), "artificial isochron" (Butler, 1982) and so on, but the mechanism(s) responsible for their generation is(are) not clearly understood.

In recent years, the detection of fallacious isochrons has been achieved in two ways; by comparison with other radiometric techniques or by deciphering the scale of Sr migration during metamorphism. With regard to the former approach, Page (1978) demonstrated that Rb-Sr whole rock dates obtained for low-grade metamorphic rocks are distinctly younger than corresponding, slightly discordant U-Pb zircon ages from the same rocks. Furthermore, the disturbance in the Rb-Sr system was shown to be related to the high Rb/Sr (ie. $Rb/Sr > 3$) samples because samples from outcrops with low average Rb/Sr ratios approach the U-Pb zircon age.

Recognizing spurious isochrons without the aid of data from other radiometric methods is considerably more difficult. For situations where the scale of Sr migration is small (ie. < a few centimeters), collecting widely spaced samples should yield reliable age data. This is supported by the study of Krogh and Davis (1973) who discovered that Rb-Sr data for small slabs from the central part of granitic layers in a banded gneiss are in excellent agreement with the results obtained for widely spaced samples. On the other hand, if the migration distances for Rb and Sr are large (ie.

> 1 meter) then much more uncertainty is attached to the reliability of a whole rock age. This point was emphasized by Farhat and Wetherill (1975), "there is no reason to believe that widely separated samples represent anything more than individual points on different local metamorphic isochrons, and their colinearity may well be fortuitous, and the age so indicated erroneous".

It is clear from the numerous attempts to determine the age of metamorphic rocks that the limitations of the Rb-Sr whole rock method are poorly understood. The fact that some metamorphic units retain their Rb-Sr integrity while similar rocks in other regions are reset attests to the complex behaviour of the Rb-Sr system to metamorphic processes. Therefore, the Rb-Sr method may be a useful chronometer in unravelling the complex geological history of metamorphic terrains, but a solid understanding of the limitations of the method is required first.

CHAPTER 2

THE CENTRAL METASEDIMENTARY BELT

2.1 INTRODUCTION

The Chandos township area is situated within the Grenville Province of the Canadian Precambrian shield (see Fig. 1). The Grenville Province in Canada alone stretches for some 1500 kilometers between Lake Huron and the Atlantic Ocean and represents the largest continuous exposure of Grenville age rocks in the world. In Canada, the Grenville Province consists predominantly of high grade metamorphic rocks with scattered remnants of younger supracrustal sequences and a host of igneous intrusions. Seven distinctive terrains have been delineated in the Grenville Province based on major changes in lithology and styles of deformation (Wynne-Edwards, 1972). The study area is located within the Central Metasedimentary Belt (CMB); a zone noted for a preponderance of marble and long recognized as containing the thickest, and some of the best preserved, metasedimentary and metavolcanic rocks in the entire Grenville Province.

2.2 GENERAL GEOLOGY

2.2.1 Boundaries and Subdivision

There is a general consensus that the boundary of the CMB is everywhere fault controlled. Perhaps the most dramatic expression of this is the southeastern boundary located in the Adirondack Mountains. Here a prominent lineament, locally called the Carthage-Colton line (Romey et al., 1980) and referred to as the Carthage-Colton mylonite zone by McLelland (1984), marks an abrupt change in metamorphic grade from granulite facies in the Highlands to amphibolite facies in the Lowlands. However, the nature of this boundary in Ontario is quite variable. The presence of tectonic breccias (Davidson, 1982; Easton, 1983) and thrust faults (Brock, 1982) are indicative of intense brittle deformation along this boundary but in other regions the boundary is marked by a wide zone dominated by migmatite (Thivierge, 1982). This boundary has also been considered a possible unconformity between rocks belonging to the Grenville Supergroup and an Aphebian basement (Moore, 1982; Lumbers, pers. comm.).

Within the CMB itself, there are also variations in metamorphic grade, structural style, proportion of metasedimentary versus metavolcanic material, and the size and composition of plutonic rocks. Wynne-Edwards (1972) subdivided the Ontario portion of this belt into three segments. From west to east these are: 1) the Glamorgan-

Cardiff domes (part of the Haliburton Highlands of Hewitt, 1956) - a region of "mantled" gneiss domes with vestiges of amphibolite grade supracrustal rocks; 2) the Hastings Basin (Hastings Lowland of Best, 1966) - a zone containing the thickest preserved section of rocks belonging to the Grenville Supergroup; 3) the Frontenac Axis and Adirondack Lowlands - in some respects a zone similar to the Hastings Basin except that the metamorphic grade is locally very high, reaching granulite facies, and there is a paucity of metavolcanic rocks.

Additional refinements to this subdivision have been made more recently by Moore (1982). Most noteworthy are the recognition of a small scale version of a "granite-greenstone type" terrain referred to as the Elzevir terrain, two regions, dominated by a preponderance of marble (Bancroft and Sharbot Lake terrains) and a fourth zone consisting of a variety of metasedimentary rock (Frontenac terrain). The boundaries between these terrains are generally abrupt and are interpreted by Moore (1982) to possibly represent tectonic boundaries. In this scenario for the CMB, the term "Hastings Basin" has been abandoned so the present study area would be considered part of the Bancroft terrain.

2.2.2 Metamorphism

Within the CMB the metamorphic grade varies from upper greenschist facies near Bishops Corners and Madoc

(Moore and Thompson, 1980) to granulite facies near Westport (Wynne-Edwards, 1972). The diagnostic mineral assemblages in the study area are hornblende-plagioclase (mafic igneous rocks), sillimanite-almandine-biotite (pelitic rocks) and diopside-tremolite (calc-silicate rocks). These assemblages indicate that the prevailing regional metamorphic grade is upper amphibolite facies and corresponds to pressures between 3.5 and 7 kilobars and temperatures in the range 580 to 700°C (Chesworth, 1971).

The timing of prograde mineral development is controversial. In the Bancroft-Madoc area, Silver and Lumbers (1966) suggested there may be two major periods of metamorphism, an older event producing the greenschist paragenesis and a second, more intense, metamorphic culmination generating the amphibolite assemblages in surrounding terrains. Although the possibility of two metamorphic events in the Grenville Province has been postulated again more recently (Baer, 1981), it is difficult to explain how the lower grade terrain would have escaped the effects of a regional, amphibolite grade metamorphism. In the study area, the amphibolite grade assemblages are assumed to have formed during one period of metamorphism, subsequently referred to as Grenvillian metamorphism. Additional information regarding the timing of regional metamorphism in the Grenville Province will be presented in a later section.

In addition to the prograde assemblages outlined

above, there is evidence for a distinct period of retrogression in this area (Lumbers, 1967; Jennings, 1969). For example, Jennings (1969) noted the common breakdown of hornblende to chlorite in mafic rocks along microfractures and small shear zones.

There is also evidence of local metamorphic perturbations related to the emplacement of post-tectonic igneous intrusions. Only a few examples of intrusions that have a well developed contact metamorphic aureole have been reported (eg. Shaw, 1962; Chiang, 1965; Thivierge, 1977) and these tend to be more common in areas of relatively low regional metamorphic grade (Davidson et al., 1979).

2.2.3 Supracrustal Rocks

The abundance of marble in the Grenville Province was noted long ago by Logan (1846) when he reported on the metasedimentary rocks north of the Ottawa River.

Subsequently, the nomenclature for this unique supracrustal succession has evolved to include names like Grenville Series, Hastings Series, and Grenville Group (see the review by Moore and Thompson, 1980). These supracrustal rocks are presently called the Grenville Supergroup and in eastern Ontario can be subdivided into three distinct packages; the Hermon and Mayo Groups (Lumbers, 1967) and the Flinton Group (Moore and Thompson, 1980). According to a regional synthesis of the Bancroft-Madoc area by Lumbers (1967), the oldest f

rocks in the CMB are metavolcanic members belonging to the Hermon Group. The mafic volcanic members have geochemical affinities resembling island arc type (Condie and Moore, 1977) and within plate (Holm et al., 1984) ocean floor basalts. Stratigraphically above, and conformable with, the Hermon Group are members of the Mayo Group (Lumbers, 1967), a succession dominated by metasedimentary material. Detailed descriptions of the individual formations that comprise these two groups have been published elsewhere (Hewitt and James, 1956; Hewitt, 1959; 1961; 1962a; Simony, 1960; Shaw, 1962; Lumbers, 1967; 1969; and Laasko, 1968).

The distinction between Mayo and Hermon Groups was originally proposed for rocks that still retain their primary features. However, regional correlation with more severely deformed rocks such as those in the study area is hindered by the higher grade of regional metamorphism, lack of good marker horizons and paucity of primary structures. The problem of regional correlation is particularly acute in the study area where the terms Mayo and Hermon have been applied to rocks such as tonalite gneiss and amphibolite but bear little resemblance to rocks in the type areas. Therefore, the presence of supracrustal rocks in the CMB "older" than the Grenville Supergroup can not be ruled out and has been suggested for some gneissic rocks in the Howland area (Easton, 1983).

At present, the age of the Grenville Supergroup is not

well known. The 1286 Ma U-Pb zircon age reported for a lower rhyolite horizon within the Tudor volcanics (Silver and Lumbers, 1966; re-calculated using the U decay constants quoted by Steiger and Jager, 1977) provides a minimum estimate for the initiation of volcanism in the belt whereas a 1226 Ma U-Pb zircon age (Lumbers, 1967) for an upper member of the Hermon Group (the Burnt Lake Formation) provides an estimate for the termination of this volcanic activity. Other attempts to date various formations within the Grenville Supergroup in Ontario using the U-Pb zircon technique, including volcanic rocks from Belmont Township (ca. 1250 Ma; D. Davis, pers. comm.) and the Hinchinbrooke gneiss (Wallach, 1974), support the contention that this supracrustal succession formed between 1226 and 1286 Ma. The lower limit of 1226 Ma is also supported by U-Pb zircon ages of about 1226 Ma reported for a number of granitic units that intrude these supracrustal rocks (Silver and Lumbers, 1966).

The Flinton Group is the youngest sequence of supracrustal rocks recognized in the CMB and it unconformably overlies the Hermon and Mayo Groups. The majority of lithologies in this group are clastic metasediments and descriptions of individual units are presented by Moore and Thompson (1980).

2.2.4 Intrusive Rocks

The CMB contains a wide variety of plutonic igneous

rocks ranging from ultramafic lenses (eg. parts of the Umfraville complex; Lumbers, 1969) to large calc-alkaline batholiths (eg. the Elzevir batholith; Pride and Moore, 1983). Based on petrographic and geochronologic criteria, Lumbers (1964; 1967) and Silver and Lumbers (1966) subdivided the plutonic rocks in the Bancroft-Madoc area into two distinct suites, an older biotite diorite and a younger quartz monzonite series. More recently, the subdivision of intrusive rocks in Ontario and western Quebec has been extended to include the following five major plutonic groups (Davidson et al., 1979; Pride and Moore, 1983):

- 1) gabbro - diorite - minor ultramafic bodies
- 2) tonalite - granodiorite - trondhjemite batholiths
- 3) diorite - monzonite - syenite - quartz syenite zoned plutons
- 4) granite
- 5) syenite, nepheline syenite

Not included in this scheme are the minor occurrences of anorthosite in the Frontenac Axis region and the Morin anorthosite (Martignole and Schrijver, 1970), the gneiss domes in the Harvey-Cardiff arch (Hewitt, 1962b) and the post-Grenvillian plutons such as the Chatham-Grenville stock (Doig and Barton, 1968). Moore (1982) pointed out that in eastern Ontario individual plutonic groups listed above are spatially restricted to discrete terrains. For example, the undersaturated rocks (eg. nepheline syenites - group 5) are

conspicuous only in the Bancroft terrain, the large calc-alkaline batholiths (group 2) are restricted to the Elzevir terrain and the majority of zoned plutons (group 3) occur in the Frontenac terrain.

Unfortunately, the relative chronology and tectonic implications of these various plutonic groups with regard to the evolution of the CMB are poorly understood. These topics will be addressed in more detail in a later section.

2.3 SUMMARY OF PREVIOUS ISOTOPIC STUDIES

In the following discussion, pertinent isotopic studies are presented highlighting salient advances in unravelling the geological evolution of the CMB.

2.3.1 K-Ar Dating

The majority of age dates initially reported from the CMB were determined using the K-Ar mineral technique (eg. Aldrich et al., 1958; Lowdon, 1960; MacIntyre et al., 1967). Although many K-Ar mineral ages from this region cluster around 900 Ma (MacIntyre et al., 1967) comparison with other radiometric techniques indicates that the K-Ar mineral ages are generally too low and do not reflect true emplacement ages. For example, the K-Ar riebeckite age determined for the Deloro pluton is 989 Ma (MacIntyre et al., 1967) which is more than 200 Ma younger a corresponding U-Pb zircon age (> 1200 Ma; Lumbers, pers. comm.) and circa 100 Ma younger than

the Rb-Sr whole rock age (1076 Ma; Wanless and Loveridge, 1972). This disparity in ages determined by different techniques partly reflects the greater mobility of ^{40}Ar compared to the less volatile daughter products of other radiometric systems. Therefore, the only conclusion that can be extracted from the K-Ar mineral studies is that the cluster of ages around 900 Ma reflects something about the final cooling history of the CMB. In other words, if the majority of rocks in the CMB are older than 1000 Ma, then the 900 Ma grouping of K-Ar mineral ages represent either a disturbance in the K-Ar system 900 Ma ago or that the region was at an elevated temperature for a prolonged period of time (long cooling history) allowing Ar to migrate freely for over 100 Ma.

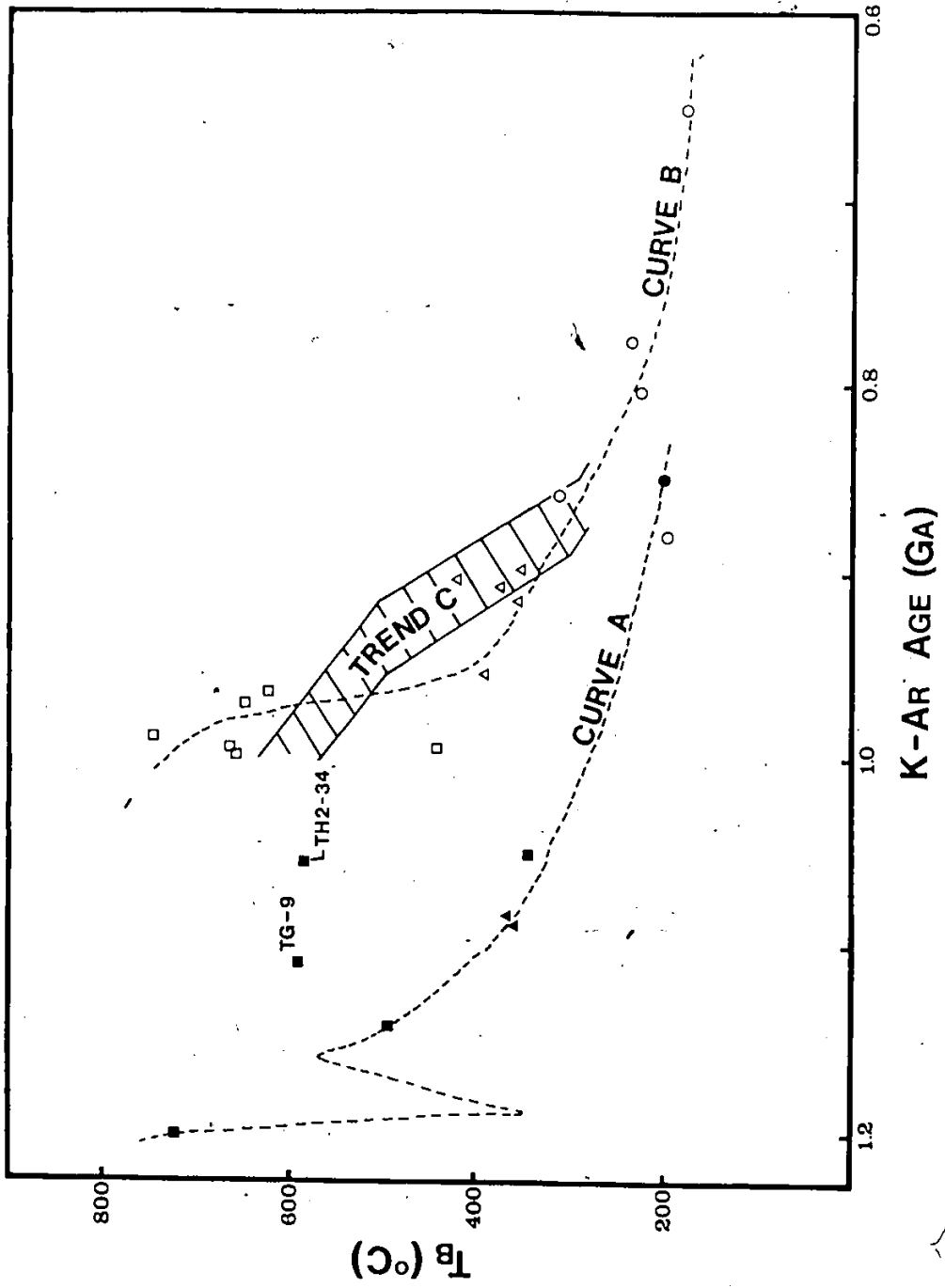
More recently, attempts have been made to use the K-Ar method on whole rock samples (Hayatsu and Palmer, 1975; Palmer et al., 1979). The main advantages of this technique, compared to analysing mineral separates, is that the initial $^{40}\text{Ar}/^{39}\text{Ar}$ ratio is measured, not assumed, and the whole rock may be less likely to lose or gain Ar during metamorphism. However, anomalously young ages were obtained for the Tudor (670 Ma; Hayatsu and Palmer, 1975) and Umfraville (911 Ma; Palmer et al., 1979) gabbros indicating that the K-Ar whole rock method is also not a successful chronometer for dating rocks from the CMB.

2.3.2 $^{40}\text{Ar}/^{37}\text{Ar}$ Dating by Incremental Heating

The $^{40}\text{Ar}/^{37}\text{Ar}$ incremental heating technique has provided important information regarding the cooling history of the CMB. The principal advantage of this technique over the more conventional K-Ar method is that each temperature increment releases Ar from successively more retentive sites in the sample. So, at high temperatures, the isotopic composition of the evolved argon is potentially indicative of the primordial isotopic composition of the mineral (for a review of the method see Faure, 1977). Furthermore, this technique facilitates the calculation of mineral blocking temperatures (Dodson, 1973; York, 1978) and, ultimately, cooling curves for entire regions (Berger and York, 1981a).

A summary of the available $^{40}\text{Ar}/^{37}\text{Ar}$ mineral data and the cooling curves derived from the Glamorgan area (curve A - Berger et al., 1979; Berger and York, 1981a), the Bancroft-Madoc area (curve B - Berger and York, 1981b; Lopez-Martinez and York, 1983) and a portion of the Grenville Province outside the CMB in SW Labrador (trend C - Dallmeyer and Rivers, 1983) are presented in Figure 2. In addition, a single hornblende analysis from the Tudor gabbro (Baksi, 1982) is plotted on Figure 2 for comparison with the other data from the Bancroft-Madoc area. Curves A and B are derived from two regions approximately 50 kilometers apart and demonstrate the profound difference in thermal histories for these regions. In contrast, the cooling curves for the two

Figure 2 Compilation of published $^{40}\text{Ar}/^{39}\text{Ar}$ data obtained for gabbroic rocks from the Central Metasedimentary Belt. These data are plotted on a conventional temperature-time diagram.



high grade regions (curve B and trend C), separated by more than 1200 kilometers, are quite similar.

Curve A (Fig. 2) is based on mineral analyses from two gabbroic units, the Thanet and Cordova gabbros. One hornblende analysis from the former (TH15-86) records the oldest age (1202 Ma) of any $^{40}\text{Ar}/^{37}\text{Ar}$ age determination in the CMB and is interpreted by Berger and York (1981b) to represent the approximate emplacement time of the Thanet body. This appears to be the only sample where the $^{40}\text{Ar}/^{37}\text{Ar}$ system has escaped the effects of Grenvillian metamorphism. A second hornblende analysis from the Thanet gabbro (TH2-34, Berger and York, 1981b) and a single hornblende analysis from the Tudor gabbro (TG-9; Baksi, 1982) fall significantly above curve A and are difficult to interpret in the framework of regional cooling trends. However, the close fit of the Cordova gabbro hornblende data and Thanet gabbro biotite and plagioclase data to curve A lends some credence to the interpretation that curve A is indeed a regional cooling trend. One final consideration is that the biotite ages from the Thanet body (1083 and 1071 Ma; Berger and York, 1981b) provide a minimum estimate for the timing of metamorphism in this region.

In contrast to the cooling history of the Bancroft-Madoc area, the results for a variety of minerals from three mafic intrusions in the Glamorgan region indicate this region was very hot at about 1000 Ma ago and cooled very rapidly

from 700 to 400°C in 50 Ma (see curve B in Fig. 2). Evidently, at 1000 Ma ago the Bark Lake and Glamorgan gabbros were at a temperature around 700 °C while mafic units some 50 kilometers away (ie. the Thanet and Cordova gabbros) were considerably cooler (ca. 275 °C). Although the cooling histories for these two adjacent regions are vastly different, it is remarkable that the Glamorgan cooling curve is quite similar to an equally high grade terrain 1200 kilometers away in the Grenville Province of SW Labrador (trend C in Fig. 2). This similarity may be fortuitous or may indicate that curve B is typical of the cooling histories for many amphibolite grade regions in the entire Grenville Province.

2.3.3 Strontium Isotopes

Until recently, very few Rb-Sr whole rock studies had been made in the CMB. The first published Rb-Sr ages were reported by Krogh and Hurley (1968) and Wanless and Loveridge (1972) and both studies demonstrated that the Rb-Sr system recorded ages older than the presumed age of metamorphism. A good example of the ability of the Rb-Sr system to preserve its isotopic integrity is the relatively old Rb-Sr whole rock age reported by Krogh and Hurley (1968) for the Blue Mountain nepheline syenite (1253 Ma; recalculated using the $1.42 \times 10^{-11} \text{ yr}^{-1}$ ^{87}Rb decay constant). Subsequent to these initial investigations, and partly in response to a renewed interest

towards understanding the geological evolution of the Grenville Province in general, increasingly more Rb-Sr studies have been attempted in the CMB (eg. Davidson et al., 1979; Bell and Blenkinsop, 1980; Heaman et al., 1980a; 1982a; Atkins, 1983; Fowler and Doig, 1983; Miller, 1984).

The strontium isotopic composition of marble samples from the Grenville Supergroup has a range of values from 0.7048 to 0.7084 (Gast, 1960; Krogh and Hurley, 1968; Gittins et al., 1969; Heaman, unpubl. data). If the isotopic composition of the marble has not been modified by post-depositional processes (eg. see Gittins et al., 1969) and the marble precursor was in isotopic equilibrium with Proterozoic seawater then the lower values in this range can be considered representative of the Sr isotopic composition of seawater at about 1250 Ma ago.

There are two Rb-Sr ages reported for rocks that presumably belong to the Grenville Supergroup, 1402 ± 57 Ma for a tonalite gneiss from Chandos township (Heaman, 1980) and 1250 ± 90 Ma for the Tudor metavolcanics (Bell and Blenkinsop, 1980). Although the latter age is considered by Bell and Blenkinsop to be in good agreement with the only published U-Pb zircon age for the Tudor rocks (1286 Ma; Silver and Lumbers, 1966) it is not clear whether the 1402 Ma age is geologically meaningful (this will be discussed further in Chapter 3). However, these data support the

interpretation that the deposition of the Grenville Supergroup occurred at or prior to 1250 Ma ago. The Rb-Sr ages for granitic units in the CMB span a 300 Ma time period (from 1250 to 950 Ma), but details of this distribution will be discussed in Chapter 5).

The only Rb-Sr mineral data available for rocks from the CMB are two biotite ages from pegmatites located in Cardiff township (1000 and 1030 Ma; Aldrich et al., 1958) and feldspar ages from a relatively old tonalite gneiss in Chandos township (Heaman, 1980). These feldspar-whole rock pairs yield a range of ages from 1062 to 666 Ma and were interpreted to reflect the control that bulk rock chemistry has on the blocking temperature of feldspar (Heaman, 1980). The 1062 Ma feldspar-whole rock age also provides a minimum estimate for the time of Grenvillian metamorphism and is somewhat lower but consistent with the $^{40}\text{Ar}/^{39}\text{Ar}$ biotite ages (1083 and 1091 Ma) reported by Berger and York (1981b). However, the unusually young feldspar-whole rock ages indicate that the Rb-Sr system in some feldspar crystals has responded to an extremely long cooling period or, more likely, has been disrupted by a later disturbance such as the circa 450 Ma alteration event recorded by the $^{40}\text{Ar}/^{39}\text{Ar}$ plagioclase data (Lopez-Martinez and York, 1983).

2.3.4 Lead Isotopes

2.3.4.1 U-Pb ages

Historically, rocks from the CMB have been used in the development of the U-Pb dating technique. For example, one of the first U-Pb age determinations was on a uraninite separate from a pegmatite located in the Wilberforce area (Nier, 1939) and some of the first U-Pb zircon and sphene ages were reported from the CMB (Tilton et al., 1955; 1957). However, very few U-Pb ages have been determined in the CMB since the late 1960's.

A summary of U-Pb ages is presented in Figure 3. The majority of these ages were calculated from a single, usually discordant, analysis of minerals such as sphene, thorianite, uraninite and zircon. Except for a few concordia upper intercept ages, the majority of ages compiled in Figure 3 are $^{207}\text{Pb}/^{206}\text{Pb}$ ages. Even with this meager data base there is an indication that at least 400 Ma of geological history is recorded in this belt with possible age maxima at circa 1250 to 1225, 1100 to 1075 and 1025 to 1000 Ma ago. All these maxima are older than the bulk of the K-Ar ages discussed in section 2.3.1. Although the geological significance of these age maxima is unclear, Silver and Lumbers (1966) interpreted the clustering of U-Pb zircon ages at about 1226 and 1104 Ma (re-calculated ages) for several granitoid units to indicate a periodicity of plutonic activity. The oldest age reported

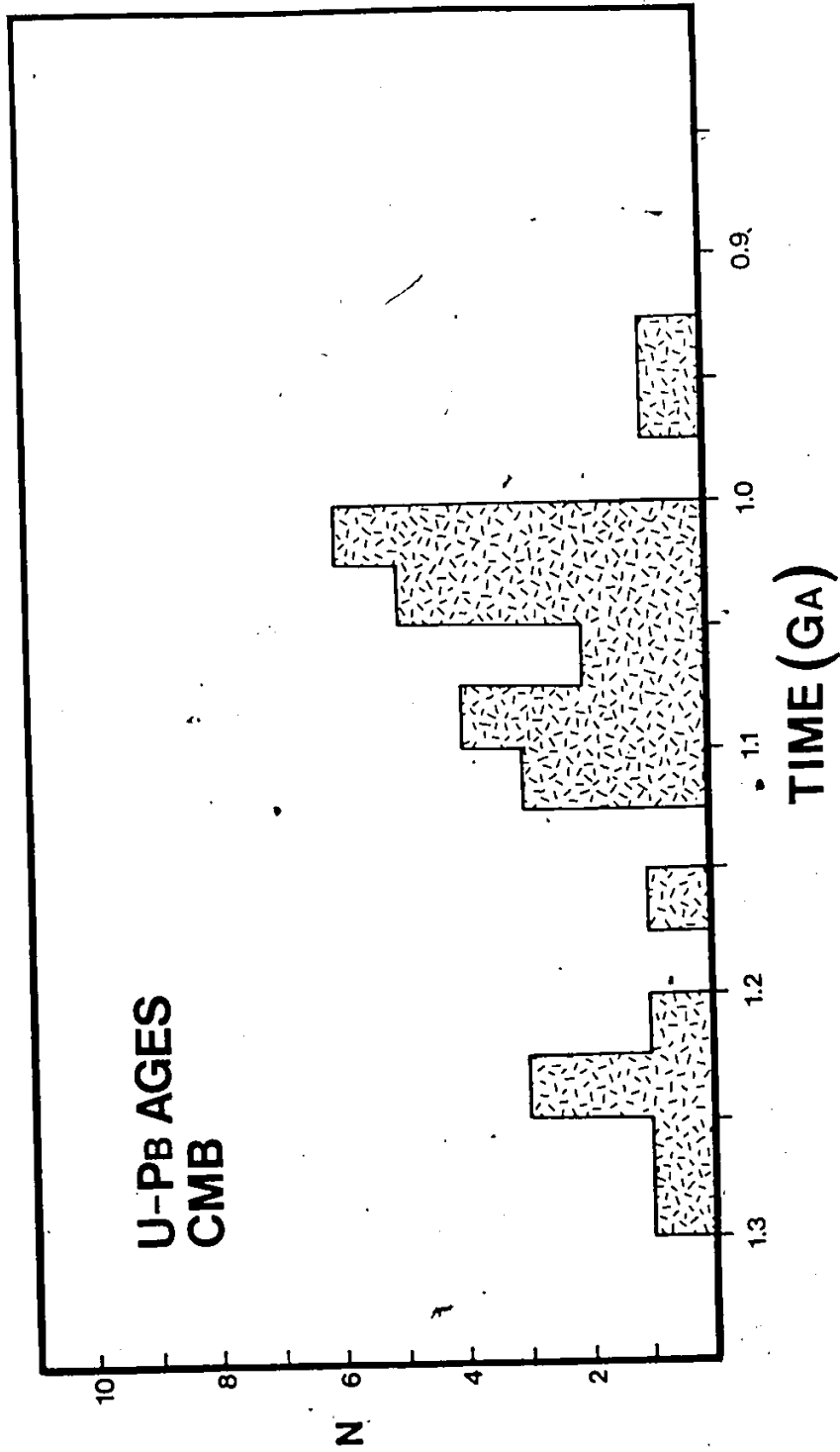


Figure 3 Compilation of published U-Pb ages for rocks from the Central Metasedimentary Belt.

so far is 1286 Ma (re-calculated using the U decay constants recommended by Steiger and Jager, 1977), determined for the lowest felsic volcanic member of the Tudor Formation (Silver and Lumbers, 1966), and provides a minimum age for the beginning of extrusion and deposition of the supracrustal rocks.

Some caution must be used in interpreting a diagram like Figure 3. Recent refinements to the U-Pb technique (Krogh 1973; 1982a; 1982b) have made possible the ability to analyse more than one zircon population from a single sample. This has important implications for samples that contain more than one period of zircon growth because a single analysis of mixed zircon populations will result in an erroneous geological age. In fact, a recent U-Pb zircon study of some alkalic rocks from the CMB (Miller, 1984) has revealed two distinct ages of zircon in one sample so this problem must be considered if the evolution of this area is to be unravelled.

2.3.4.2 Common-Lead Studies

In addition to determining geological ages with the U-Pb chronometer, information regarding the source of the lead can be obtained from Pb bearing minerals such as galena and feldspar. Since there is virtually no U in galena or feldspar, the Pb isotopic composition in these minerals does not change with time unless modified by geological events subsequent to their formation (for a review of the common-

lead method refer to Faure, 1977).

The only investigations specifically concerned with the common-lead component in rocks from the CMB are the studies by Fletcher and Farquhar (1982), and references therein, on ore leads from Pb-Zn sulphide deposits hosted in the Grenville Supergroup, and by Zartman (1969) on the common-lead in feldspars from the Westport pluton. The conclusions from both studies suggest that the Pb in sulphides and feldspars from the CMB is largely derived from a mantle source with little or no contribution from the crust.

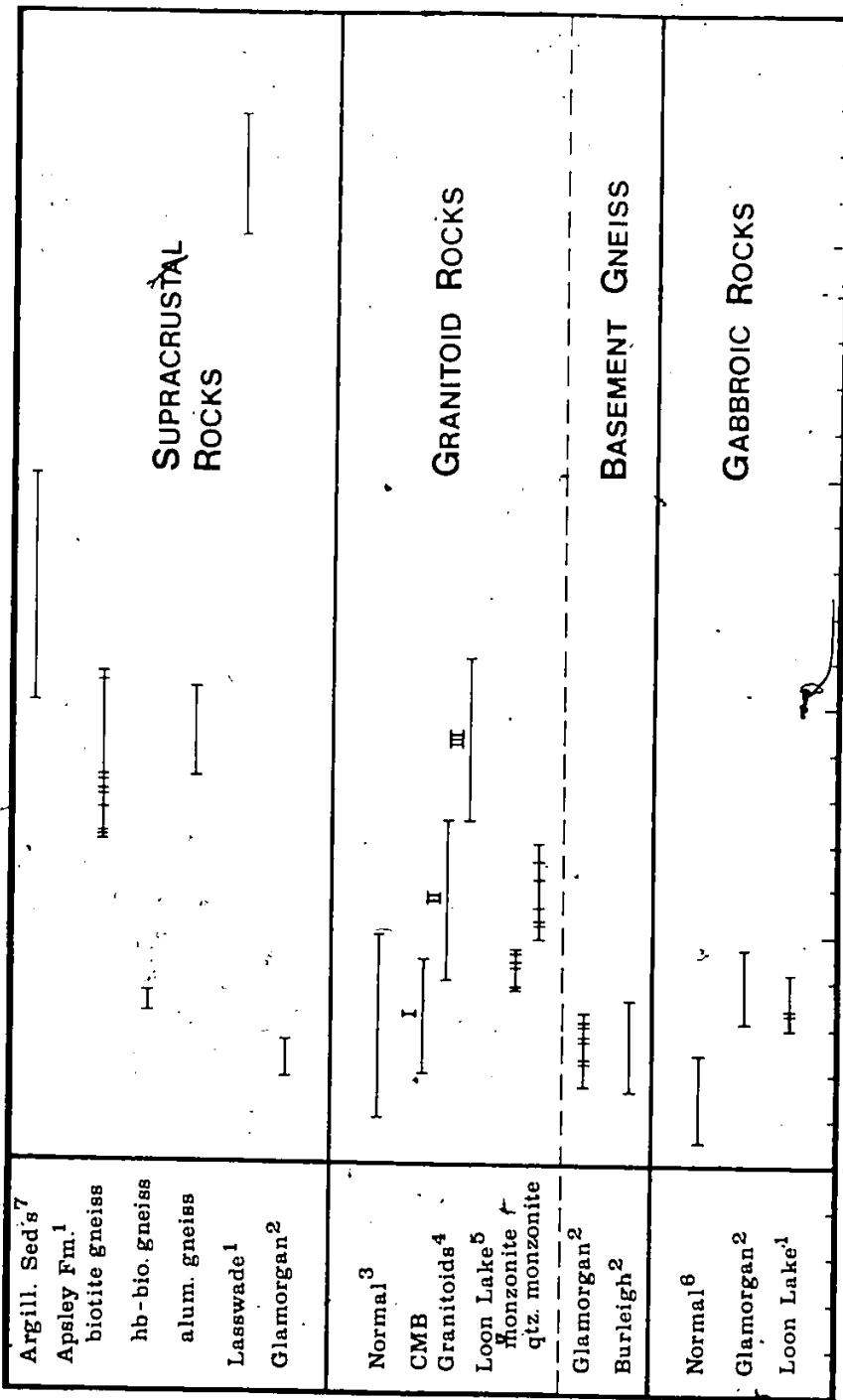
2.3.5 Oxygen Isotopes

A summary of whole rock oxygen isotopic data from the CMB is presented in Figure 4. These data are subdivided into three groups; supracrustal, granitoid and gabbroic rocks. Two granitic units (the Glamorgan and Burleigh gneiss) are separated from other granitic units because they may represent basement(?) to the Grenville Supergroup (Bright, 1977; Morton, 1978).

Although only a few units from the Grenville Supergroup have been analysed, by far the most enriched samples are the marbles (ca. +25 to +28%). Some of the marble samples are lower than this range (ie. +19 to +24%) but these samples were collected near to or are themselves inclusions in post-tectonic intrusions and their lower values

Figure 4 Compilation of published oxygen isotope data available for rocks from the Central Metasedimentary Belt.

References
1 - Shieh et al. (1976) 2 - Shieh and Schwarcz (1974)
3 - Taylor (1978) 4 - Shieh (1980)
5 - Heaman et al. (1982a) 6 - Taylor (1968)



DEL¹⁸ OWR

U

may be a consequence of metamorphic decarbonation reactions (Shieh et al., 1976). Besides the oxygen isotopic composition of marble members, the only other data reported for this supracrustal succession are the results for quartzofeldspathic rocks from Chandos (+8.3 to +16.9%) and Glamorgan (+6.9 to +7.7%) townships. Compared to the range of values reported for unmetamorphosed pelitic and argillaceous sediments (+15 to +20%; Fig.4), the CMB samples have been depleted; possibly during metamorphism. Shieh and Schwarcz (1974) postulated that the low values for rocks such as the Glamorgan paragneiss are a result of large scale oxygen isotopic exchange with a low- ^{18}O reservoir during metamorphism.

In a survey of the oxygen isotopic composition of CMB granitoid rocks, Shieh (1980) proposed that three distinct groups can be recognized: I (+7.0 to +9.5%), II (+9.0 to +12.5%) and III (+12.5 to +16.0%). He also suggested that these individual groups are associated with regions of different metamorphic grade. For example, the group I granitoids are restricted to a region dominated by rocks in the greenschist facies (Elzevir terrain) and the anomalously high- ^{18}O granitoids are associated with rocks in the granulite facies (Frontenac terrain). Furthermore, this progression from low- to high- ^{18}O granitoids with a corresponding increase in metamorphic grade is interpreted to be a reflection of the isotopic composition of the magma

source region. Another factor that may be important in this regard is the presence or absence of marble. The low ^{18}O granitoids occur in regions virtually devoid of carbonates while most of the plutons with high values (ie. > 9%) occur in regions with abundant marble. Using this argument, the oxygen isotopic composition of these granitoid rocks is not a reflection of the isotopic composition of the source material (this will be discussed further in Chapter 5). Compared to the range reported by Taylor (1978) for "normal" granitoid rocks, the majority of CMB granitoid rocks are enriched in ^{18}O , regardless of how they obtained their isotopic signature.

All the mafic rocks that have been analysed from the CMB are also isotopically enriched compared to the range published by Taylor (1968) for "normal" gabbroic rocks (see Fig. 4). Shieh and Schwarcz (1974) attribute this enrichment to isotopic exchange with surrounding country rock during metamorphism.

In addition to the variation in oxygen isotopic composition of whole rock samples throughout the CMB, the isotopic composition of coexisting minerals from metamorphic rocks can provide information regarding temperatures achieved during regional metamorphism. Using the quartz-biotite and quartz-magnetite geothermometers, Shieh and Schwarcz (1974) calculated temperatures in the range 515 to 530°C for paragneiss samples from Glamorgan township. This estimate of

the temperature reached during metamorphism is 50 to 150°C lower than estimates from equilibrium phase assemblages (Chesworth, 1971). Considering the observation of Hoernes and Hoffer (1979) that the $^{18}\text{O}/^{16}\text{O}$ of biotite from a metamorphic rock is fixed at the time (and temperature) of biotite crystallization, it is not surprising that temperatures calculated by this method may be lower than the peak metamorphic conditions. The temperatures calculated from $^{18}\text{O}/^{16}\text{O}$ mineral fractionations do provide a minimum estimate of the temperatures reached in the study area during Grenvillian metamorphism.

2.4 SUMMARY

The CMB is a discrete entity within the Grenville Province of North America that is characterized by a well preserved supracrustal sequence (Grenville Supergroup) but also contains a variety of plutonic igneous rocks. Further subdivision of the belt has been proposed in recent synoptic studies (eg. Moore, 1982) based on the recognition of terrains with abrupt boundaries, distinctive lithologies and contrasting grades of regional metamorphism.

Isotopic studies have contributed substantially to the overall understanding of geological events that have been important in the evolution of this belt. For example, the formation of the Grenville Supergroup is bracketed by the U-Pb zircon age (1286 Ma) obtained for a volcanic unit near

the base of the succession and the emplacement ages for the earliest intrusive rocks, such as the Blue Mountain nepheline syenite (ca. 1250 Ma), that invade the supracrustal sequence. Important information regarding the evolution of the belt has also been obtained from the plutonic igneous rocks. There are indications from U-Pb zircon and Rb-Sr whole rock studies that igneous activity in the belt was episodic with possible culminations circa 1250, 1100 and 1025 Ma ago. In addition, the cooling history for the CMB has been investigated through $^{40}\text{Ar}/^{39}\text{Ar}$ studies of mafic igneous rocks with the important conclusion that adjacent regions in the belt have vastly different cooling histories.

Although progress is being made in unravelling the geological history of the CMB, some very fundamental questions remain to be answered. There is still considerable uncertainty as to the nature of the supracrustal-basement contact, the relationships between various stratigraphic units within regions of high metamorphic grade and the exact timing and nature of igneous and metamorphic activity in the belt. These are some of the enigmas that will be addressed in the following chapters and should be pursued in future studies.

CHAPTER 3

SUPRACRUSTAL ROCKS

3.1 INTRODUCTION

The supracrustal rocks in the study area consist primarily of marble, amphibolite and quartzo-feldspathic gneiss that are interpreted to be part of the Grenville Supergroup (Shaw, 1962; 1972; Lumbers, 1967; Jennings, 1969). However, the paucity of primary structures, lack of marker horizons and high metamorphic grade make correlations with rocks belonging to the Grenville Supergroup in adjacent regions quite tenuous. Furthermore, regional correlation may be complicated by the presence of supracrustal rocks that are older than (eg. the quartzo-feldspathic biotite gneiss in the Howland area; Easton, 1983) and younger than (eg. the Flinton Group; Moore and Thompson, 1980), but similar to, rock units within the CMB previously ascribed to the Grenville Supergroup.

The supracrustal section between Silent Lake and Loon Lake (see Figures 5 and 14) offers a unique opportunity to investigate the relationship between the presumed equivalents

of the Hermon and Mayo Groups in one continuous(?) homoclinal sequence. Samples of quartzo-feldspathic gneiss and biotite-muscovite schist located near Silent Lake, interpreted to be part of the Hermon Group (Lumbers, 1967; Jennings, 1969), and biotite tonalite gneiss from the Apsley area, interpreted to be part of the Mayo Group (Shaw, 1962; 1972), have been collected for petrographic, geochemical and geochronological studies. This chapter reports the results from these studies.

3.2 APSLEY BIOTITE GNEISS

3.2.1 GEOLOGY AND PETROGRAPHY

The most abundant member of the Apsley Formation is a feldspar-quartz-biotite rock referred to in previous studies as Apsley paragneiss (Adams and Barlow, 1910; Hewitt, 1957; Simony, 1960) and Apsley biotite gneiss (Shaw, 1972). The term paragneiss was used to indicate a sedimentary origin for this unit but Simony (1960; p.20) correctly pointed out that "a sedimentary origin, though commonly assumed, needs proof and therefore the term paragneiss is a poor name". In a subsequent study by Shaw (1972) the use of "paragneiss" was abandoned for the term Apsley biotite gneiss, a name that has no genetic connotations but denotes the granular habit of the felsic minerals (feldspar and quartz) and identifies the most abundant mafic mineral as biotite. The distribution of rocks, including the Apsley biotite gneiss, collectively known as

the Apsley Formation is outlined in Figure 5.

The Apsley biotite gneiss is stratified with macroscopic layering that has been previously attributed to variations in the abundance of biotite (Simony, 1960). Simony also noted that individual bands vary in thickness from less than one centimeter to two meters, dip 30 to 70° SE, and are parallel to thin marble horizons within the unit. The latter observation combined with the recognition of a possible conglomerate unit (see Plate 1c) and relict graded bedding (coarse-grained, quartz rich base grading upwards to a finer grained, biotite rich top) were interpreted by Simony as evidence for a sedimentary origin for this unit. An example of this layering is shown in Plates 1a, b, 2a and b. Both layers in sample AG2 (Plate 2a) have similar mineralogies but the lighter band contains less biotite (10% compared to 18% in the dark band). The biotite in the lighter band is also coarser grained (ca. 0.5 to 1.0 mm compared to 0.1 to 0.2 mm).

A second type of layering has been recognized in the Apsley gneiss (Heaman, 1980) and is interpreted to be unrelated to the compositional layering described above. Thin (< 1 cm to 3 cm) and often discontinuous mafic laminae (see Plate 2b) occur sporadically throughout the unit and, in a few instances, these laminae are discordant to the larger scale banding. These laminae consist of an unusual mineral assemblage, with approximately 90% biotite and 10%

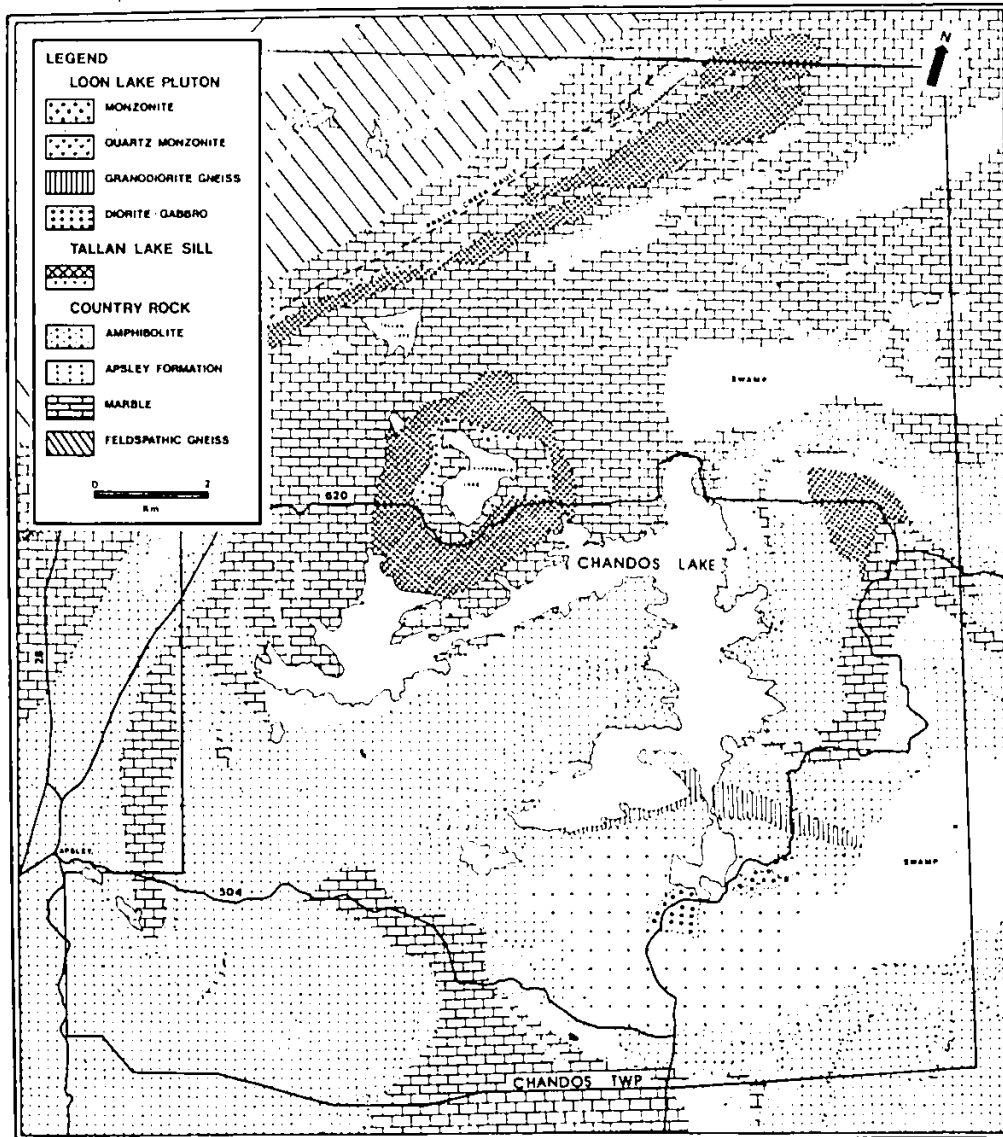


Figure 5 The distribution of lithologies within Chandos township (after Shaw, 1962 and Dostal, 1975) including rocks belonging to the Apsley Formation.

Plate 1 A - An example of the layering that occurs at sample site #1. This outcrop exposure occurs along Hwy 28 approximately 0.2 Km north of the junction between highways 28 and 620

B - The location at site#1 where sample AG19 was collected

C - An exposure of nodular looking Apsley biotite gneiss where samples AG3 and LHB4-1 were collected. This outcrop exposure is located along Hwy. 28 near the town of Apsley

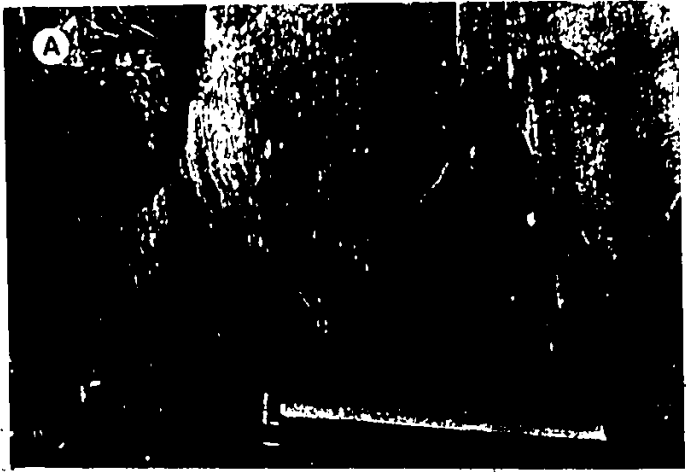


Plate 2 A - Sample AG2 illustrating the layering present in this sample. The total width of the sample is 10 centimeters

B - Sample AG12 illustrating the unique biotite-microcline layer (black). This layer is 3 centimeters wide

C - An example of potassic Apsley gneiss with K-feldspar (white ovoids) poikiloblasts

A



B



C



microcline. The coarse biotite flakes in these laminae (up to 6 mm long) commonly have a random orientation; this shows a definite contrast to the preferred biotite orientation generally observed throughout the unit (see below). One example was observed (AGB) where the large biotite flakes are oriented perpendicular to the contacts between the biotite-microcline layers and the country rock. The origin of these laminae is unclear but may be related to a late stage fracturing event. A sample containing visible fractures sealed with biotite is shown in Plates 3a and b and may represent the incipient stage in the formation of the wider biotite-microcline bands. These fractures are discussed in more detail in section 3.2.3.4.

Two varieties of biotite gneiss were identified by Simony (1960), a sodic and a potassic member. Petrographically, the distinction between the two is based on the proportion of plagioclase: microcline present in the sample. Microcline is abundant (often > 10%) in the potassic variety, sometimes occurring as porphyroblasts or poikiloblasts, but is generally absent in the sodic gneiss. An example of potassic Apsley gneiss with nodular looking microcline poikiloblasts (white patches) is illustrated in Plate 2c. Simony (1960) reported that the sodic and potassic gneisses can be intercalated within an individual outcrop. However, without the presence of microcline porphyroblasts it is difficult to discern these two varieties in the field. The

sodic member was estimated to be five times more abundant than the potassic member (Simony, 1960).

In thin section, the Apsley biotite gneiss is relatively unaltered and consists of a fine- to medium-grained intergrowth of granular quartz and feldspar (120° interfacial angles are common) with a preferred orientation of biotite laths parallel to the banding. Plagioclase (An₁₀-An₁₆) is commonly untwinned (Simony, 1960) and occasionally exhibits a pervasive sericitic alteration, especially near fractures. Microcline is easily recognized by cross-hatched twinning and, as mentioned above, often occurs as porphyroblasts and, more commonly, poikiloblasts (up to 4 mm in diameter). Tiny inclusions of quartz, plagioclase and biotite are common in the poikiloblasts and have been interpreted by Simony (1960) as relicts from a previous mineral assemblage. In this study, microcline was observed to have a variety of habits. In addition to the poikiloblasts, examples of which can be found in samples AG8, 9 and 12, microcline was observed as discrete, fine-grained crystals in an interlocking quartz-plagioclase-microcline-biotite mosaic (eg. AG 3,10) and as isolated nebulous patches (eg. AG 5,7). The samples containing poikiloblasts or isolated patches of microcline clearly demonstrate that this mineral, in some cases, formed subsequent to the crystallization of the other essential minerals. There are two varieties of biotite in the Apsley biotite gneiss, distinguished by differences in

pleochroism; one has a dark to pale brown and the other a dark to pale reddish brown colour scheme (Simony, 1960). A few samples investigated in this study (see Table B1.1) have minor occurrences of Mn-rich garnet, hornblende, muscovite, tourmaline and chlorite (as an alteration product after biotite) and most contain the following accessory minerals; apatite, carbonate, opaques, and zircon. The samples used for the U-Pb study (see section 3.2.4) also contain monazite and/or sphene.

3.2.2 GEOCHEMISTRY

Additional support for the potassic-sodic subdivision for samples from the Apsley biotite gneiss is the bimodal chemical distribution on a K_2O/K_2O+Na_2O histogram (Simony, 1960). Simony noted two maxima (Figure 7 in Simony, 1960) corresponding to K_2O/K_2O+Na_2O values of 0.3 to 0.4 (sodic) and 0.6 to 0.7 (potassic). He also noted the close agreement between the major element composition of the sodic and potassic members to the average chemical composition of graywacke and shale, respectively and to a quartzo-feldspathic biotite gneiss from the Adirondack Mountains region described by Engel and Engel (1958). The major element data base for the Apsley gneiss has been substantially enlarged since Simony's study and the following is a summary of these data.

The K_2O/K_2O+Na_2O values for 140 samples including the

results reported by Simony (1960), Van de Kamp (1968), the unpublished data for samples discussed by Shaw (1972) and data presented in Appendix B (Table B2.1) are summarized in Figure 6 and compared to the results reported by Simony (1960). The majority of the data in Simony's histogram were calculated using one set of chemical analyses for the major K and Na bearing mineral phases (ie. K-feldspar, biotite and plagioclase) in these rocks combined with the corresponding modal mineralogies for each sample. The distribution of K_2O/K_2O+Na_2O values for whole rock samples (non-stipled area) indicates that, although the Apsley gneiss samples may have a bimodal distribution, the majority of samples that have been analysed are "sodic" in that they have K_2O/K_2O+Na_2O values less than 0.5 with a skewness towards more K_2O -rich compositions.

There is some uncertainty as to the meaning of the chemical subdivision shown in Figure 6 for samples of high grade gneiss like the Apsley gneiss. Several samples with greater than 10% modal microcline have K_2O/K_2O+Na_2O values less than 0.5 and on a purely chemical basis would be incorrectly classified as sodic gneiss. Furthermore, some samples with high values (ie. > 0.7) contain the unusual biotite-microcline rich layers described in the previous section and may not be representative of the original sample chemistry.

The major and trace element data obtained for samples

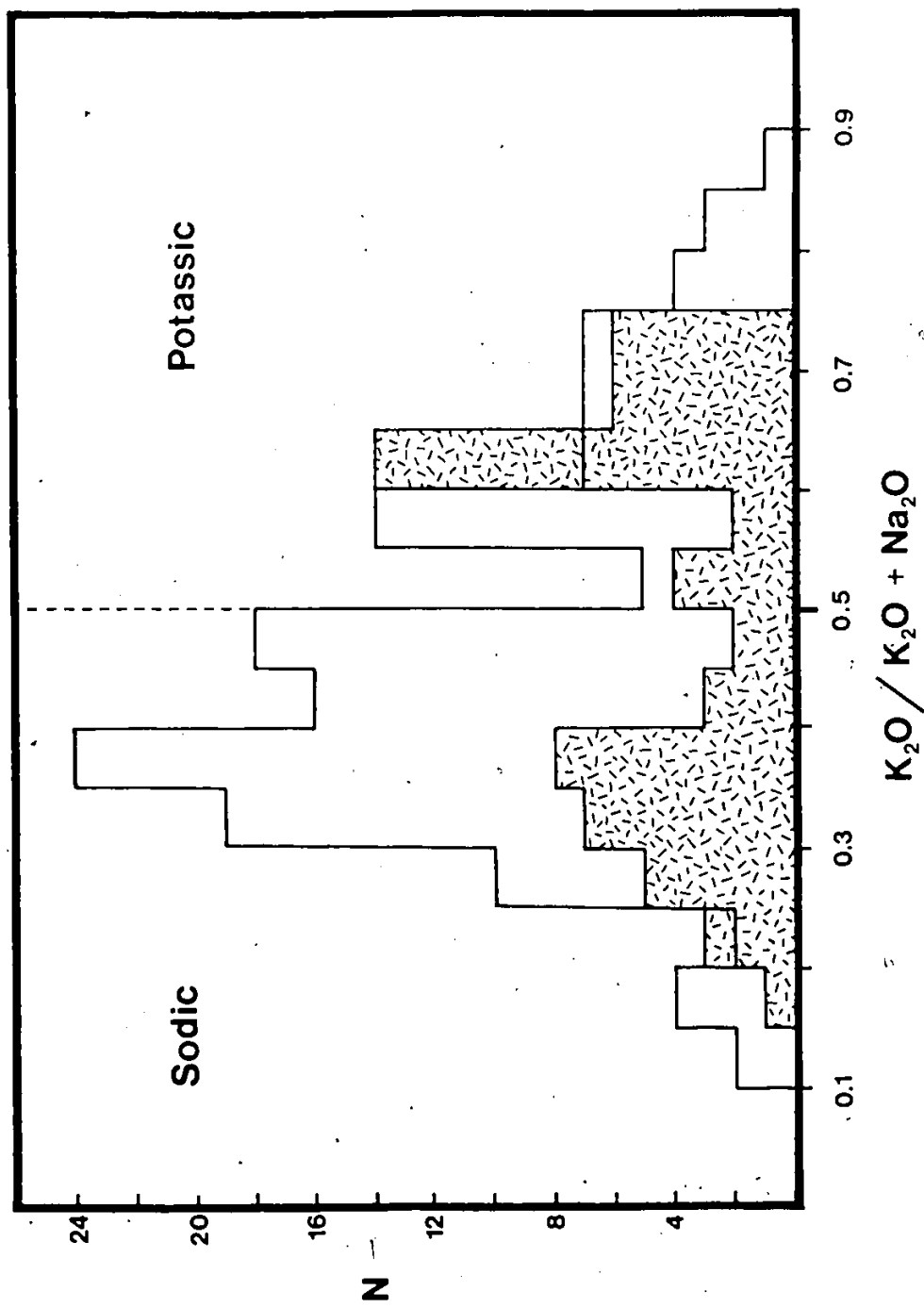


Figure 6 A summary of K_2O/K_2O+Na_2O data for the Apsley biotite gneiss.

of the Apsley biotite gneiss are compiled in Appendix B (Table B2.1). Although the majority of these samples are "grey gneiss" there is a substantial range in sample chemistry (see the range of values reported in Table 3.1). The average chemical composition for all the samples analysed in this study is presented in Table 3.1 and is in reasonable agreement with the average Apsley biotite gneiss composition reported by Shaw (1972).

An examination of the major element data tabulated in Appendix B (Table B2.1) reveals some obvious geochemical anomalies. For example, there are three samples from different sampling sites (AG5, 7 and 19E) that have noticeably higher SiO_2 (78 to 80 weight percent) and lower Al_2O_3 (9 to 11 weight percent) compared to all other samples. The overall chemical composition of these three samples is similar to the average composition of arkose (see Table 3.1) reported by Pettijohn (1963) and it is possible that the different composition of these samples reflects the presence of a primary compositional variation within the unit. Another geochemical anomaly is the high Fe_2O_3 and K_2O values in the samples AG8 and 43. Both samples (plus AG12) contain unusual biotite-microcline layers that might account for these anomalously high Fe and K abundances and, depending on the origin of these unusual mafic layers, may not be representative of the primary composition of the "grey gneiss". Finally, the high CaO, Sr, and P_2O_5 and low SiO_2

TABLE 3.1 - Average chemical composition of Apsley biotite gneiss and possible protoliths

	Apsley Gneiss (n=47)			Site#1 (n=13)		Site#2 (n=6)		Site#3 (n=8)	
	MEAN	s	RANGE	MEAN	s	MEAN	s	MEAN	s
SiO ₂	69.0	6.5	53 - 80	70.2	4.5	59.1	3.8	71.8	3.7
Al ₂ O ₃	13.7	1.8	9 - 17	14.0	1.5	15.5	0.6	13.0	0.8
Fe ₂ O ₃	5.7	1.8	2 - 10	5.4	1.4	7.6	1.2	4.9	0.5
FeO	-	-	-	-	-	-	-	-	-
MgO	1.8	1.2	.4 - 6	1.4	0.7	3.4	1.3	2.9	1.5
CaO	1.9	1.9	.4 - 11	1.3	0.6	5.9	2.6	0.94	0.44
Na ₂ O	4.3	1.1	2 - 7	4.7	1.4	4.0	0.7	4.4	1.2
K ₂ O	2.5	1.2	.8 - 7	2.3	0.8	2.9	0.7	2.0	0.9
TiO ₂	0.54	0.22	.2 - 1	0.48	0.16	0.92	0.06	0.43	0.10
MnO	0.14	0.05	.04 - .3	0.14	0.03	0.17	0.06	0.15	0.02
P ₂ O ₅	0.18	0.20	.03 - 1	0.11	0.04	0.59	0.29	0.11	0.03
Rb	45	22	8 - 103	42	22	70	23	29	13
Sr	153	171	37 - 648	105	22	578	105	90	19

	AB19D (n=4)		AB19E (n=5)		Average AB (a)	Average Arkose (b)	Average Rhyolite (c)
	Mean	s	Mean	s			
SiO ₂	64.0	2.2	77.8	1.9	66.5	77.1	74.2
Al ₂ O ₃	15.9	0.8	10.4	1.1	14.6	8.7	13.6
Fe ₂ O ₃	7.0	0.9	3.6	0.5	3.8	1.5	2.1
FeO	-	-	-	-	1.8	0.7	-
MgO	2.1	0.3	0.89	0.12	2.2	0.5	0.3
CaO	1.6	0.2	2.1	0.7	1.9	2.7	1.1
Na ₂ O	5.8	0.5	3.5	1.1	3.8	1.5	3.0
K ₂ O	2.6	0.3	1.2	0.2	3.1	2.8	5.4
TiO ₂	0.7	0.11	0.35	0.09	0.64	-	0.2
MnO	0.17	0.03	0.12	0.06	0.10	-	-
P ₂ O ₅	0.12	0.01	0.16	0.09	0.17	-	0.1
Rb	58	5	23	5	-	-	-
Sr	148	4	98	7	-	-	-

s - standard deviation-

(a) Shaw (1972)

(b) Pettijohn (1963)

(c) Nockolds (1954)

values of sample AG25 reflects the presence of carbonate-rich zones in this sample.

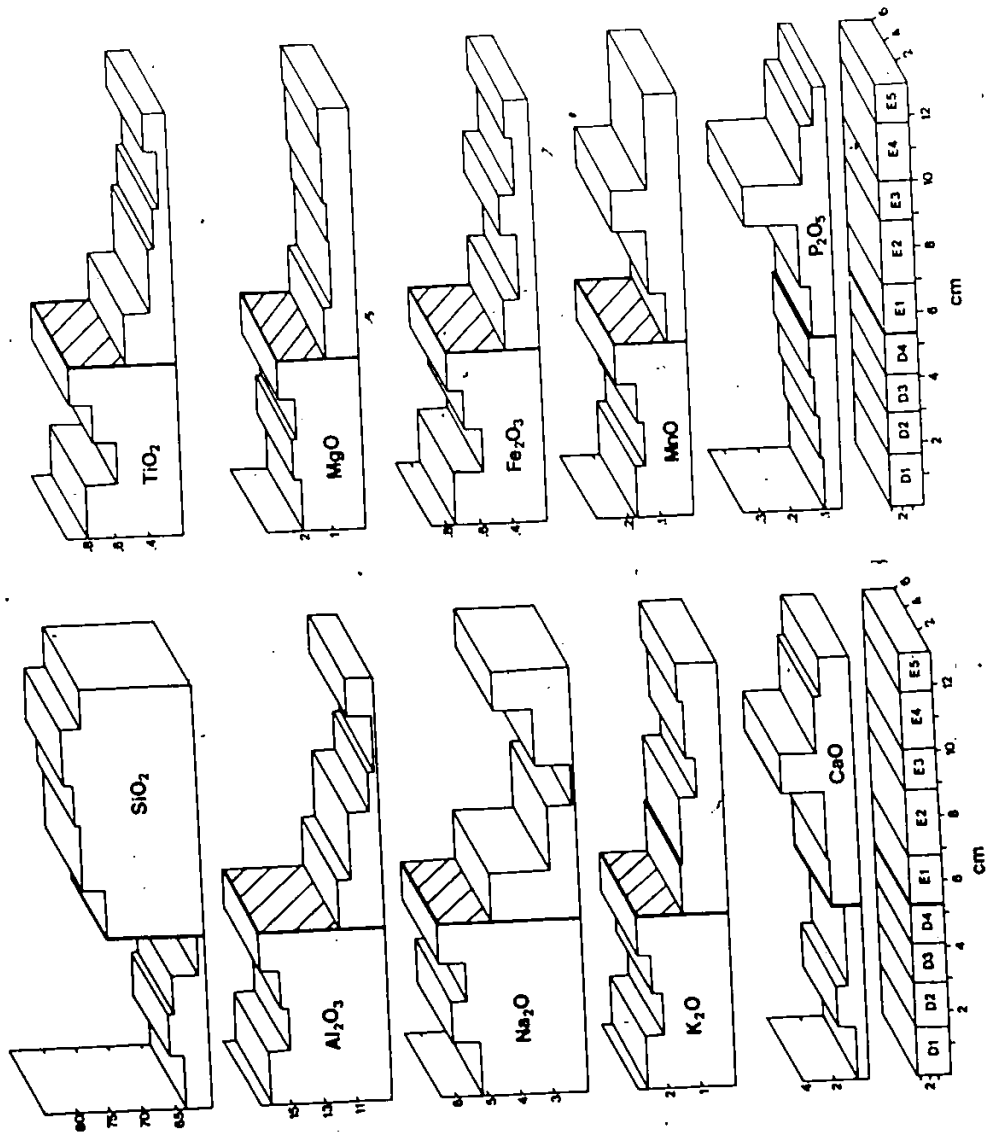
The sampling site where AG25 was collected from, as a whole, has an unusual chemical composition compared to the average Apsley biotite gneiss (Table 3.1). This sampling site is located near the base of the Apsley formation (see Figure 8) and its unusual chemistry, more mafic character, and lack of layering are interpreted to indicate that either the nature of sedimentation and/or volcanism within the unit changed with time or this sampling site does not truly represent an exposure of Apsley biotite gneiss.

The chemical variation observed for the entire unit is also present within individual sampling sites. For the two sites that have visible layering (#1 and #3), the average composition for each sampling site is similar (Table 3.1) but the composition of individual horizons are quite distinct. Perhaps the best example of this is the contrasting compositions of two adjacent layers from one sample (AG19D and E in Table 3.1) where layer D has a composition close to the average composition for the entire unit and layer E, as mentioned above, has a composition more akin to arkose.

Although much of the chemical variation observed for different horizons within the Apsley gneiss is interpreted to be primary, there is always the possibility that some of this

variation has been produced by secondary geological events. To examine the possibility of secondary element mobility in more detail, a series of thin slabs were prepared from one sample (AG19) that contains two lithologic horizons (layers D and E). A portion of sampling site #1 where AG19 was collected is shown in Plate 1b. Layer E is much more heterogeneous in appearance and contains significantly more quartz than layer D. Each layer was sliced parallel to the layering (approximately parallel to the foliation) to give a slab of average dimensions 3 cm x 6 cm x 1.5 cm. The actual slab thickness varies from 1.2 to 2.0 cm. The major element data for the nine slabs prepared from this sample are presented in the form of histograms in Figure 7. The average composition for each layer was described above (see Table 3.1) as being quite different and this difference is visually portrayed in Figure 7 as an abrupt change in composition from layer D4 to E1. In addition to this abrupt change in composition from one layer to the next, there is significant internal chemical variation within individual layers. The most noticeable internal variation is the difference in the composition of slab E3 compared to the other slabs from layer E with anomalously low Na_2O and K_2O and high CaO , Fe_2O_3 , MnO and P_2O_5 abundances. Internal chemical variations such as those in layers E and D might be anticipated for a poorly sorted (immature) sedimentary rock but more likely represent variations induced by secondary processes, possibly

Figure 7 The major element composition (weight percent) for 9 slabs sliced from sample AG19. This sample contains two compositional layers, labelled D and E on this diagram. The approximate slab dimensions are indicated at the bottom of the diagram.



metamorphism.

Several geochemical approaches have been used in the past to decipher the parentage of "grey gneisses" like the Apsley gneiss (see the review by Prabhu and Webber, 1984) with varying degrees of success. Shaw (1972) addressed this same question with regard to the origin of the Apsley biotite gneiss and proposed that the following geochemical discriminant function ($DF = 10.44 - 0.21SiO_2 - 0.32Fe_2O_3 - 0.98MgO + 0.55CaO + 1.46Na_2O + 0.54K_2O$), derived from multivariate analyses, is well suited for discerning igneous ($DF > 0$) from sedimentary ($DF < 0$) protoliths. With reference to the Apsley gneiss, Shaw concluded that this unit represents an intercalated succession of silicic volcanics (ca. 60%) and sandstones. The DF values for samples of Apsley gneiss collected in this study are listed in Table B2.1 and approximately 60% have positive values suggesting an igneous protolith, in agreement with the estimate of Shaw (1972). Of the remaining samples that have negative DF values, the three samples that have compositions similar to an arkose (ie. AG5, 7, and 19E) have large negative DF values, supporting a sedimentary origin. This is in contrast with the observation of Van de Kamp et al. (1976) who reported the inability of this discriminant function to correctly identify some Californian arkoses.

Finally, support for the intercalation of sedimentary and volcanic units within the Apsley gneiss is provided by

the geochemical investigation of an individual sampling site. Samples from visibly layered sampling sites, such as sampling site#1, have a large range in DF values (-1 to +4). In fact, the DF values for the two adjacent layers in sample AG19 (shown in Plate 1b and Figure 7) indicate one layer (E) is sedimentary and the other (D) is igneous.

3.2.3 Strontium Isotopes

3.2.3.1 Introduction - Sample collecting

The most important step in any Rb-Sr age determination is the selection of samples for isotopic analysis. The conventional approach for sample collecting is to obtain fresh hand samples from numerous outcrops so that there is likely to be a range in Rb/Sr; a necessary requirement for a precise age determination. Often, within an individual unit, samples with obvious differences in mineralogy are preferred because they usually have different Rb/Sr ratios. Nothing is more frustrating to a geochronologist than to collect a suite of samples and then subsequently find that there is no variation in the Rb/Sr ratio! The assumptions implicit in all Rb-Sr whole rock studies have already been outlined in section 1.3 along with some serious problems related to determining the age of metamorphic rocks such as the Apsley gneiss. In this regard, a variety of sampling techniques have been employed to test whether the method of sample collecting has any

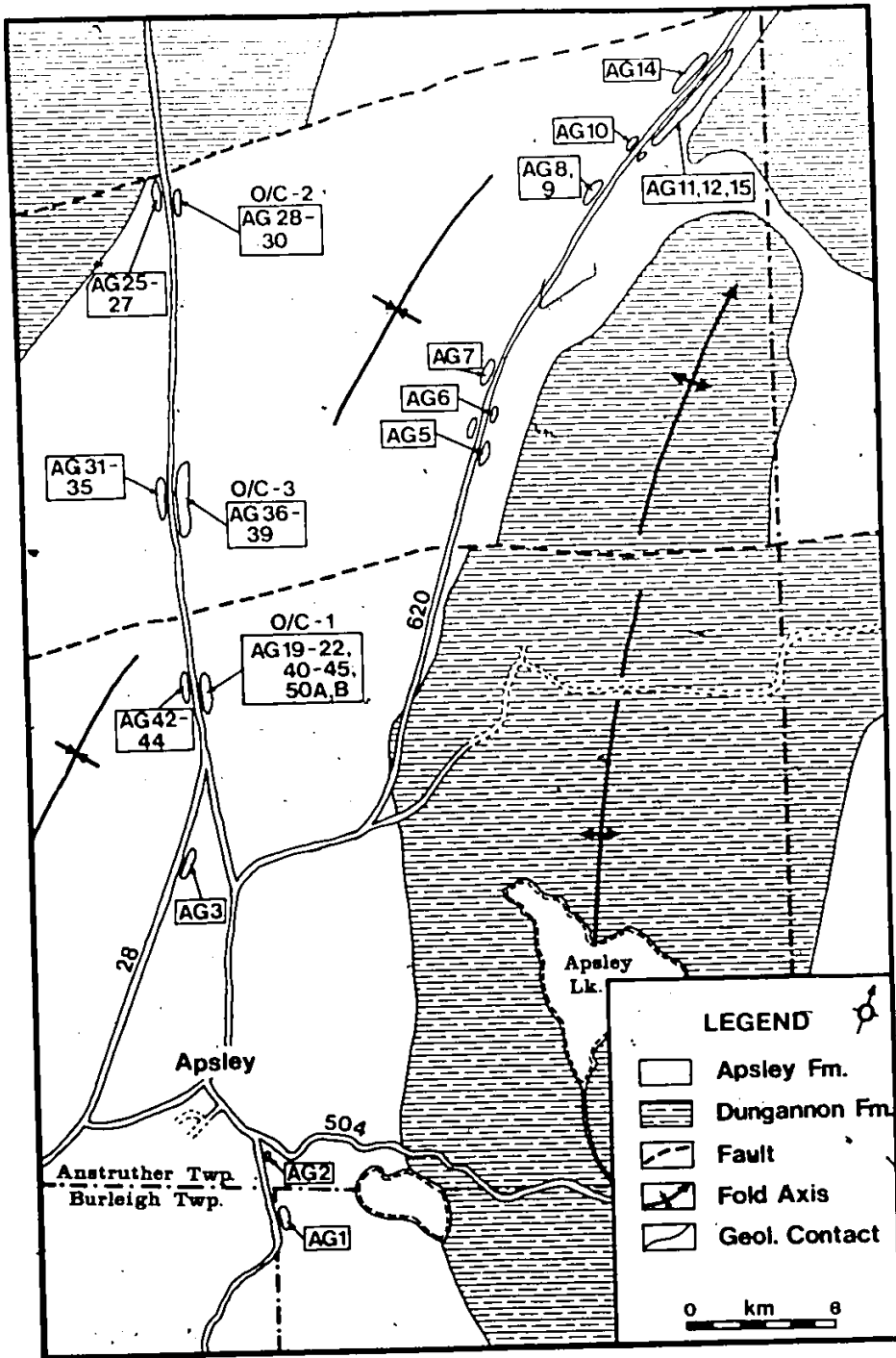


Figure 8 Sample locations for the Apsley biotite gneiss

bearing on the resulting age determination. The locations of Apsley gneiss samples discussed in this study are shown in Figure 8. Many of the samples are from individual, widely spaced sampling sites but multiple samples were collected from three specific sampling sites along highway 28. Two samples, AG19 and 50, were examined in more detail by slicing the hand samples into a series of thin slabs to test for small scale isotopic variations. The analytical procedures for determining the Rb/Sr and strontium isotopic data are outlined in Appendix A2 and A5.

3.2.3.2 Regional Study

Several whole rock samples from the Apsley gneiss were previously analysed (Heaman, 1980; Heaman et al., 1980b; Heaman et al., 1982b) in an attempt to determine the age of the unit. It was noted that certain samples, especially the ones with the unusual mafic layers or abundant microcline, had anomalous isotopic compositions. By isolating the unusual mafic layers it was demonstrated that much of the observed data scatter was related to anomalous isotopic compositions in these mafic layers. Six other samples, without mafic layers, yielded an unusually old age (1444 ± 172 Ma) for rocks in this region but the large error associated with this age, anomalously low R_1 (0.7016) and anomalously high MSWD (10.48) all indicate that this age is suspect. In this case, the data scatter was caused by something other than the presence of

thin mafic bands. One of these samples (AG7) was shown to be very discordant so the age was re-calculated excluding this sample ($t=1402 \pm 57$ Ma; $R_1=0.7022$; $MSWD=3.81$). Although the error associated with this re-calculated age is significantly reduced, the MSWD value still indicates that there is scatter in the data outside analytical error. The main problem with discarding AG7 from the age calculation is that there appeared, at the time, to be no geological reason for doing so. Regardless of whether AG7 is included or not, the previous study indicated that the age of the Apsley gneiss may be as much as 100 Ma older than the age known for any other rocks in the area.

Before discussing the Rb-Sr data obtained in this study it is important to realize the consequences of combining data from sedimentary and igneous rocks for Rb-Sr dating. If a succession of sedimentary and volcanic rocks was deposited in a relatively short period of time, it is likely that different horizons would have different initial strontium ratios, depending on the origin of each horizon. For example, a felsic volcanic rock might have an isotopic signature reflecting the source from which the magma was derived whereas a sedimentary rock, such as an arkose, may inherit a more radiogenic isotopic composition because it was formed by the erosion of older sialic crust. If the various horizons in the supracrustal package retain their isotopic integrity during diagenesis and/or burial metamorphism, then

collecting a variety of samples for age dating from widely spaced outcrops can only lead to data scatter and potentially meaningless geological ages. On the other hand, if the isotopic composition of every horizon is homogenized during diagenesis and/or burial metamorphism and this homogenization took place shortly after deposition or if the sedimentary horizons represent the erosion of nearby felsic volcanic rocks genetically related to the volcanic horizons that occur within the Apsley gneiss, then the Rb-Sr age determined from regionally collected samples should approximate the time when the rocks formed. The fact that excessive data scatter was reported for samples from the Apsley gneiss in a previous Rb-Sr study (Heaman, 1980) combined with the information reported in section 3.2.2, that primary chemical variations exist between adjacent horizons within individual outcrops, implies that some original chemical and isotopic heterogeneity may be preserved in these rocks. The Rb-Sr data reported in this chapter were determined in order to evaluate the nature of the data scatter observed for samples collected from widely spaced outcrops and, ultimately, the geological significance of the "old" age previously reported for the Apsley gneiss.

The Rb-Sr data for the six regionally collected samples discussed by Heaman (1980) are plotted on a Nicolaysen diagram (Figure 9). Additional Rb, Sr and Rb/Sr data were obtained for these samples in this study so the

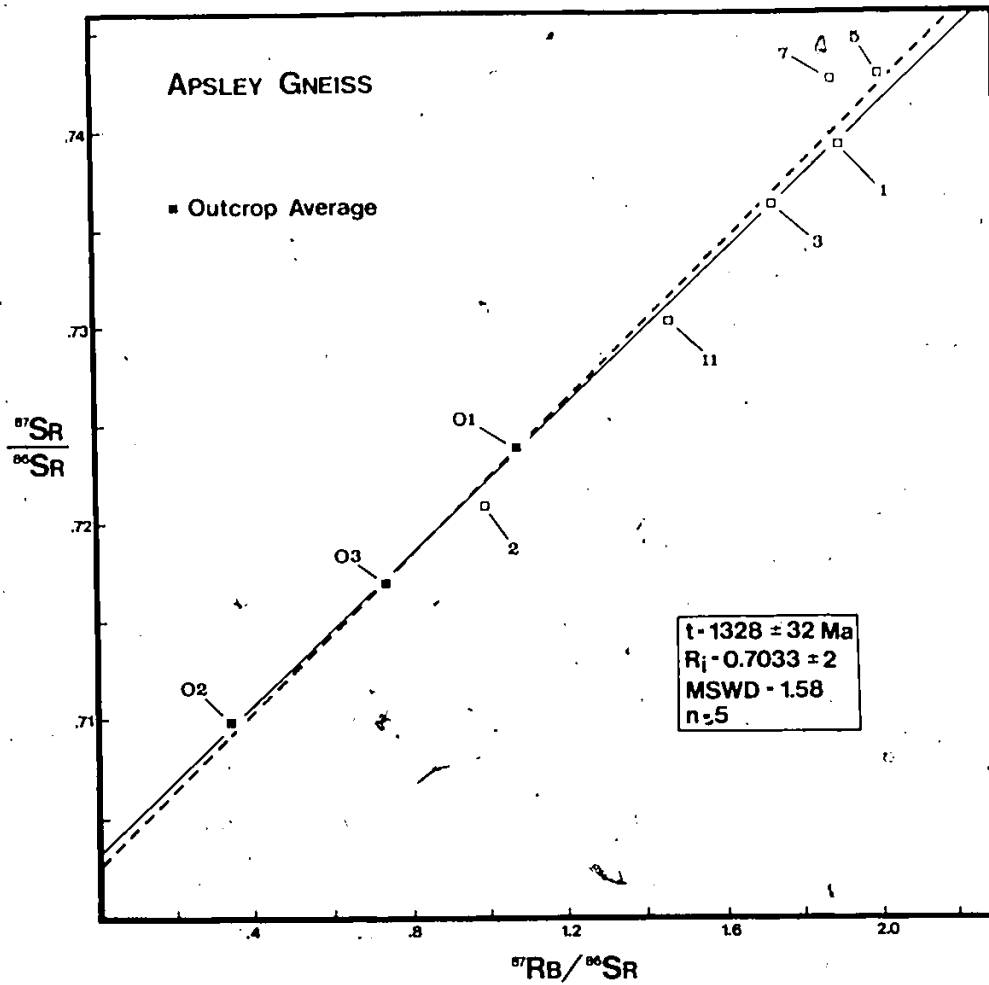


Figure 9 Rb-Sr whole rock data for samples of Sodic Apsley gneiss collected on a regional scale (modified after Heaman, 1980). Also included are the average values (solid squares) calculated for three sampling sites. The dashed line corresponds to 1322 Ma ($R_i = 0.7022$)

data presented in Table B3.1 has been modified slightly compared to the data reported by Heaman (1980). Also plotted on this diagram are the average Rb-Sr data for three isolated sampling sites (these are discussed in more detail in section 3.2.3.3), the 1402 Ma regression line (dashed line) reported by Heaman (1980), and a best fit regression line calculated excluding the four spurious data points AG 2, 5, 7, and 11. The ensuing discussion attempts to explain the geological rationale for omitting these four samples from the age calculation and the advantages of using average outcrop data in regional scale Rb-Sr studies.

In the previous two sections, a petrographic and geochemical investigation of the six regionally collected samples plotted in Figure 9 revealed that three samples (AG 5, 7, and 11) probably have a sedimentary protolith (eg. they all have large negative DF values). It is also apparent that these same three samples have anomalous strontium isotopic compositions and do not plot within analytical uncertainty of the calculated best fit line. Of particular interest is the fact that the two samples AG 5 and 7, samples that also have chemical compositions compatible with an arkosic protolith, plot significantly above the best fit line in Figure 9. These data could be generated either by a net loss of Rb (gain of common Sr) at some time after the unit formed or by the incorporation of excess radiogenic strontium at the time of formation. Since there is no obvious disparity

in Rb and/or Sr abundances in these samples compared to the average composition of the Apsley gneiss, the latter hypothesis is preferred. A scenario can easily be envisaged where excess radiogenic strontium might be preserved in an immature sediment such as an arkose if some allogenic (detrital) minerals are present and retained an inherited isotopic composition through diagenesis to amphibolite grade metamorphism. The net effect of either process (ie. Rb and/or Sr mobility after formation or inherited radiogenic strontium) for Rb-Sr dating is to generate, in most cases, anomalously old and geologically meaningless ages.

One other sample, AG2, is different from the other six regionally collected samples because it contains visible banding (see Plate 2a). It was demonstrated in the previous section that individual layers within a sample can have vastly different chemical compositions possibly reflecting different protoliths, so analysing the strontium isotopic composition of a layered sample such as AG2 may result in the mixing of two unrelated and isotopically distinct layers. This sample is also suspect for a second reason. Although the layering in AG2 is partly a consequence of variations in the abundance of biotite, the biotite laths in the light coloured layer are oriented at an angle to the layering whereas the smaller, more abundant biotite laths in the darker layer show a strong preferred orientation parallel to the layering; indicating that the layering in this sample may not be

primary. This unique layering coupled with the anomalously low K_2O and Rb abundances in AG2 provide support that the chemical, and probably isotopic, composition of this sample has been modified subsequent to the formation of the unit and is not a good choice for Rb-Sr dating. However, further research is required to elucidate the origin of the layering in AG2.

Only two samples, AG1 and 3, out of the six samples analysed by Heaman (1980) have a probable igneous precursor (ie. positive DF values) and have chemical compositions close to the average Apsley biotite gneiss composition reported in Table 3.1. These two samples plot below the 1402 Ma reference line reported by Heaman (1980).

A slightly different approach to determine the age of the Apsley gneiss, using regionally collected samples, is to use the average Rb-Sr data for several samples from an individual sampling site. The main advantage of this approach is that a data point representing the average composition for the sampling site is less susceptible to the effects of local metamorphic resetting that may alter the Rb-Sr systematics of an individual sample. For example, if the strontium isotopic composition of an entire sampling site was homogenized during metamorphism to a value coincident with the average composition for the sampling site then the isotopic composition of any one sample from the sampling site will be modified but the average composition will remain on the

pre-metamorphic isochron. This approach is discussed in more detail by Roddick and Compston (1977).

As mentioned above, three data points representing the average composition for three widely spaced sampling sites (labelled O1, O2, and O3) are also plotted in Figure 9. The majority of samples used to calculate the average outcrop composition probably have an igneous protolith (positive DF values) and in general should not be influenced by problems that can affect sedimentary rocks (eg. excess radiogenic strontium). One possible exception is AG19E because it, like AG5 and 7, has a peculiar chemical composition. However, excluding this sample does not have a significant effect on the age calculation. The interesting result is that these three data points are colinear and define a best-fit regression line with a slope corresponding to an age of 1315 Ma (Table 3.2). It is also interesting that the two meta-igneous samples discussed above, AG1 and 3, plot on this regression line. The regression line shown in Figure 9 was calculated using the three sampling site averages plus AG1 and 3 and corresponds to an age of 1328 ± 32 Ma with no detectable data scatter outside analytical uncertainty (MSWD=1.58) and does not differ significantly from the age calculation using only the three sampling site averages. If the 1328 Ma regression line is geologically meaningful then either the Rb-Sr data obtained for AG1 and 3 must be close to the average composition for their respective sampling sites

or the Rb-Sr system at the sites where AB1 and 3 were collected has not been disrupted on the scale of meters during metamorphism. Support for the latter hypothesis is presented in section 3.2.3.4.

Another piece of evidence that can be used to evaluate the geological significance of a Rb-Sr whole rock age is the initial strontium ratio. A value significantly lower than that predicted for a magma derived from the mantle at the time the rock formed is usually an indication of a rotated isochron and geologically meaningless old age. The low initial strontium ratio (0.7014) obtained when all six regionally collected samples are combined (Heaman, 1980) could reflect the effect of including samples with excess radiogenic strontium or samples that have lost Rb or gained Sr sometime after formation (see the discussion above), producing an anomalously "old" age and low initial strontium ratio. The initial strontium ratio obtained when the regionally collected samples are screened as described above (0.7033 ± 2) is geologically more feasible and is interpreted to reflect the isotopic signature of the source rock from which igneous members of the Apsley gneiss were derived. Based on the strontium isotope initial ratio alone it is impossible to distinguish between a low Rb/Sr source material in the mantle (such as garnet lherzolite; Menzies and Murthy, 1980) or lower crust (such as mafic granulite; Drury, 1973) but it is clear that the Apsley gneiss samples were not

TABLE 3.2 - Two-Error Regression Results for Samples
from the Apsley Biotite Gneiss

SAMPLES	n	t (Ma)	*	R _t	*	MSWD	MODEL
Regional							
a) AB1,3,o/c1,2,3	5	1328	32	0.7033	2	1.58	M1
b) o/c1,2,3	3	1315	113	0.7034	9	3.56	M2
Site#1							
a) AB19,20A,B,22,50A,B	6	1273	66	0.7043	13	1.73	M1
b) AB19D,20A,B,50A,B	5	1303	204	0.7034	31	2.94	M2
c) AB20A,B,50A,B	4	1341	131	0.7035	18	0.68	M1
Site#2							
a) AB25,26,28,29,30	5	1161	195	0.7041	9	5.88	M2
b) AB25,26,28,29	4	1256	119	0.7037	7	1.70	M1
Site#3							
a) AB31,32,33,36,37,38	6	1101	165	0.7051	18	19.88	M2
b) AB31,32,33,38	4	1264	161	0.7037	16	3.28	M2
Composite							
a) AB1,3,20A,B,25,26, 28,29,50A,B	10	1333	24	0.7034	1	1.28	M1
b) AB19,20A,B,22,25, 26,28,29,50A,B	10	1325	27	0.7035	3	2.12	M1
c) AB19,20A,B,25,26, 28,29,50A,B	9	1343	31	0.7033	3	1.23	M1
d) AB20A,B,25,26,28, 29,50A,B	8	1346	32	0.7033	2	1.35	M1
Slab							
a) AB19D1-4,E1,3-5	8	1151	67	0.7056	7	5.02	M2
b) AB19D2,3,E1,4,5	5	1332	269	0.7034	32	4.46	M2
c) AB19D1-4	4	946	154	0.7091	27	0.11	M1
d) AB19E1,3,5	3	1168	65	0.7056	5	0.19	M1

* - error reported at the 95% confidence level

1 M1 = McIntyre Model I; M2 = McIntyre Model II (McIntyre et al., 1966)

derived from or did not interact with relatively old, high Rb/Sr crustal material.

The 1328 Ma age is significantly younger, and more precise, than the 1402 Ma age proposed by Heaman (1980) and, without any other data, is considered a better estimate of the formation age for igneous members of the Apsley biotite gneiss. However, there is still some uncertainty regarding the geological significance of this age because samples from five different sites were used in the age calculation and it is possible that not all the samples analysed are cogenetic; a requisite for Rb-Sr whole rock dating. The following section contains the results from a sampling experiment designed to alleviate the assumption of cogeneticity by analysing numerous samples from the same stratigraphic horizon.

3.2.3.3 Individual Sampling Site Study

To avoid the problems inherent in regional scale sample collecting of a layered metamorphic sequence (see previous section), three large exposures of Apsley biotite gneiss were selected for detailed study. Multiple samples were collected from relatively homogeneous portions of the outcrop at each site where the prerequisites that all the samples are cogenetic and have the same initial strontium ratios are more likely to be satisfied. Sampling sites #1 and #3 have visible layering but some of these layers are thick

(> 1 meter) and relatively homogeneous. The location of each sampling site along highway 28 is shown on Figure 8 and the Rb-Sr data for individual samples are presented in Table B3.1.

The Rb-Sr data for samples from a single sampling site are plotted separately in Figures 10 a-c and the results from a two-error regression treatment of these data are compiled in Table 3.2. Also included in Figure 10 are the average $^{87}\text{Rb}/^{86}\text{Sr}$ compositions for each site (open circles) used in Figure 9. For all three sites a range in Rb/Sr is present even though the samples are very similar in appearance and were collected from relatively homogeneous portions at each site. Although the range for an individual site is not large enough to determine a statistically precise age (note the large errors associated with the quoted ages in Table 3.2), the majority of samples from individual outcrops are colinear.

There are two features about Figure 10 that should be clarified before discussing the results. On all three Nicolaysen diagrams in Figure 10 the solid line represents the preferred regression line calculated by omitting spurious data points. The rationale for omitting certain samples from the age calculation is discussed below. At least one sample from each outcrop is interpreted to have an anomalous isotopic composition and, in all cases, omitting the anomalous samples from the regression treatment increases the

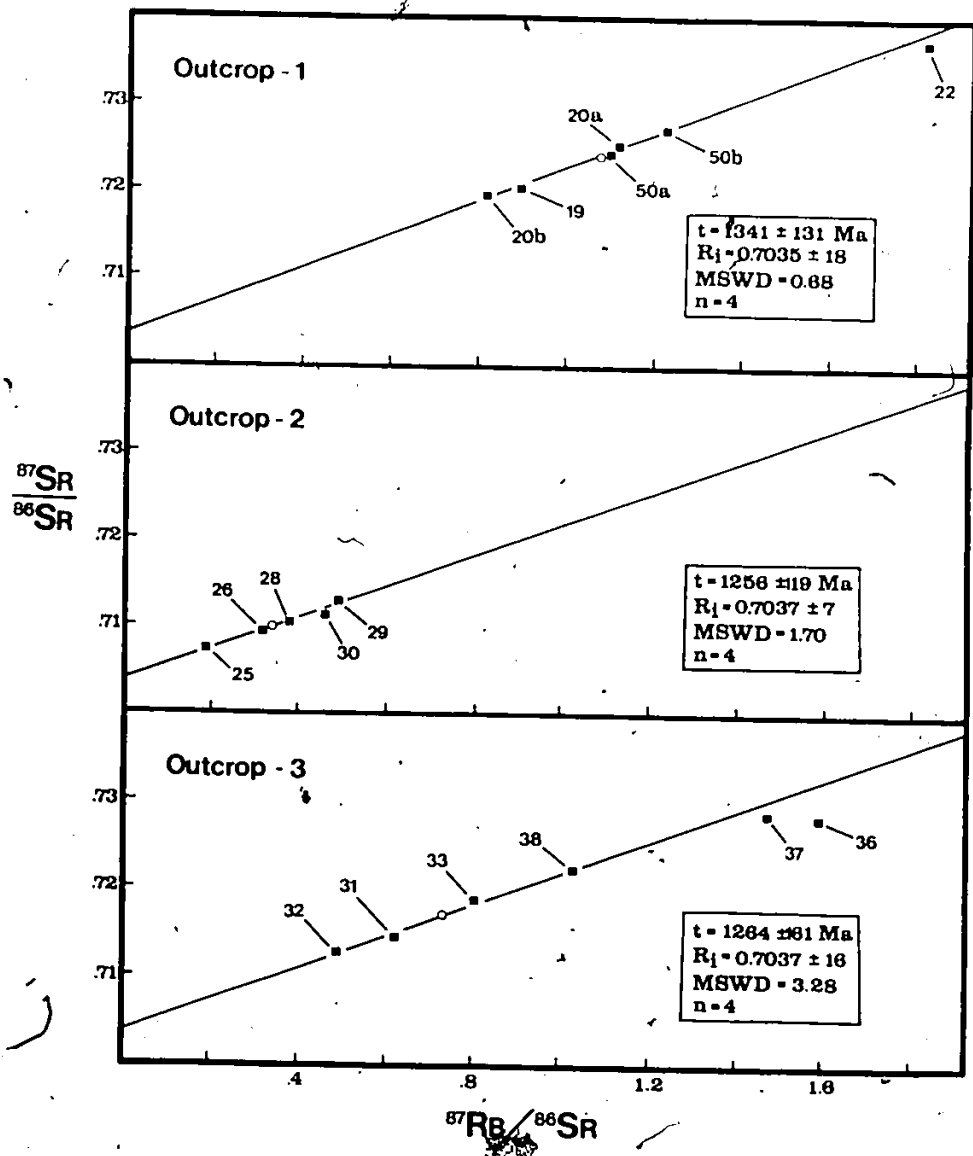


Figure 10 Rb-Sr whole rock data for samples of sodic Apsley gneiss from three selected sampling sites. The open circle on each diagram represents the approximate sampling site mean. a) sample site #1 b) sample site #2 and c) sample site #3

calculated age by about 100 Ma (compare the results in Table 3.2). The second point that should be mentioned is that all the data plotted on Figure 10 represent whole rock analyses except AG19. This sample was sliced into several slabs (see section 3.2.3.4) so the data point plotted on Figure 10a represents the weighted mean of the individual slab analyses. One slab (E2) was omitted in calculating the weighted mean because it has an anomalous isotopic composition (see section 3.2.3.4).

The majority of samples analysed from site#1 were collected from a two meter wide area with four samples (AG20A, 20B, 50A, 50B) collected from one homogeneous layer. The remaining two samples (AG22, 19) were collected from different portions of the outcrop and from different layers. An example of the layering at site#1 is shown in Plates 1a and b. The fact that AG22 was collected from a different stratigraphic horizon may explain the higher Rb and K_2O and hence higher Rb/Sr ratio compared to the other samples from this outcrop. Alternatively, this sample may have gained Rb (and K) subsequent to its formation. In either case, this sample is unique and, because it has a higher Rb/Sr ratio, omitting it from the age calculation has a profound effect; increasing the age from 1273 to 1303 Ma. The unusual chemical composition of layer E in sample AG19 (see section 3.2.2), the similarity to two discordant regionally collected samples (ie. AG5,7), and the fact that it was collected, like AG22,

from a different stratigraphic horizon make this sample likewise less favourable for determining a geologically meaningful age. Although the Rb-Sr age is more precise if AG19 and 22 are included in the age calculation, the preferred age is 1341 ± 131 Ma ($R_1 = 0.7035 \pm 18$; MSWD=0.68); calculated using the four samples collected from the same stratigraphic horizon.

Site#2 is located near the contact between the Apsley gneiss and the underlying marble and amphibolite members of the Dungannon Formation (see Figure 8). This outcrop is relatively homogeneous (ie. no visible layering) except for a cross-cutting amphibolite and pegmatite dike. The samples collected from this site (AG25-30) contain significantly more carbonate (note the high CaO contents in Table B2.17) have the lowest Rb/Sr values, and the smallest range in Rb/Sr compared to samples from the other two sites. A consequence of the latter two features is that a regression treatment of these data (see the results listed in Table 3.2) yield a more precise initial strontium ratio (0.7041 ± 9) but a more imprecise age (1161 ± 195 Ma).

One of the samples collected from this site (AG30), the sample collected closest (ie. 30 meters away) to the amphibolite dike, is enriched in Rb and K_2O (4.1% and 103 ppm) compared to average composition for the other samples (2.8% and 67 ppm). This enrichment in alkalis has been observed in other units within the study area and may be

related to secondary chemical modification either during emplacement of the dikes or during late-stage hydrothermal activity that affected this area (see section 4.2.5.1). If AG30 is omitted from the age calculation for site#2 there is a significant reduction in data scatter about the best-fit regression line (the MSWD value is lowered from 5.88 to 1.70, Table 3.2) and the preferred age for this site is 1256 ± 119 Ma ($R_1 = 0.7037 \pm 7$) using the four samples AG25, 26, 28 and 29.

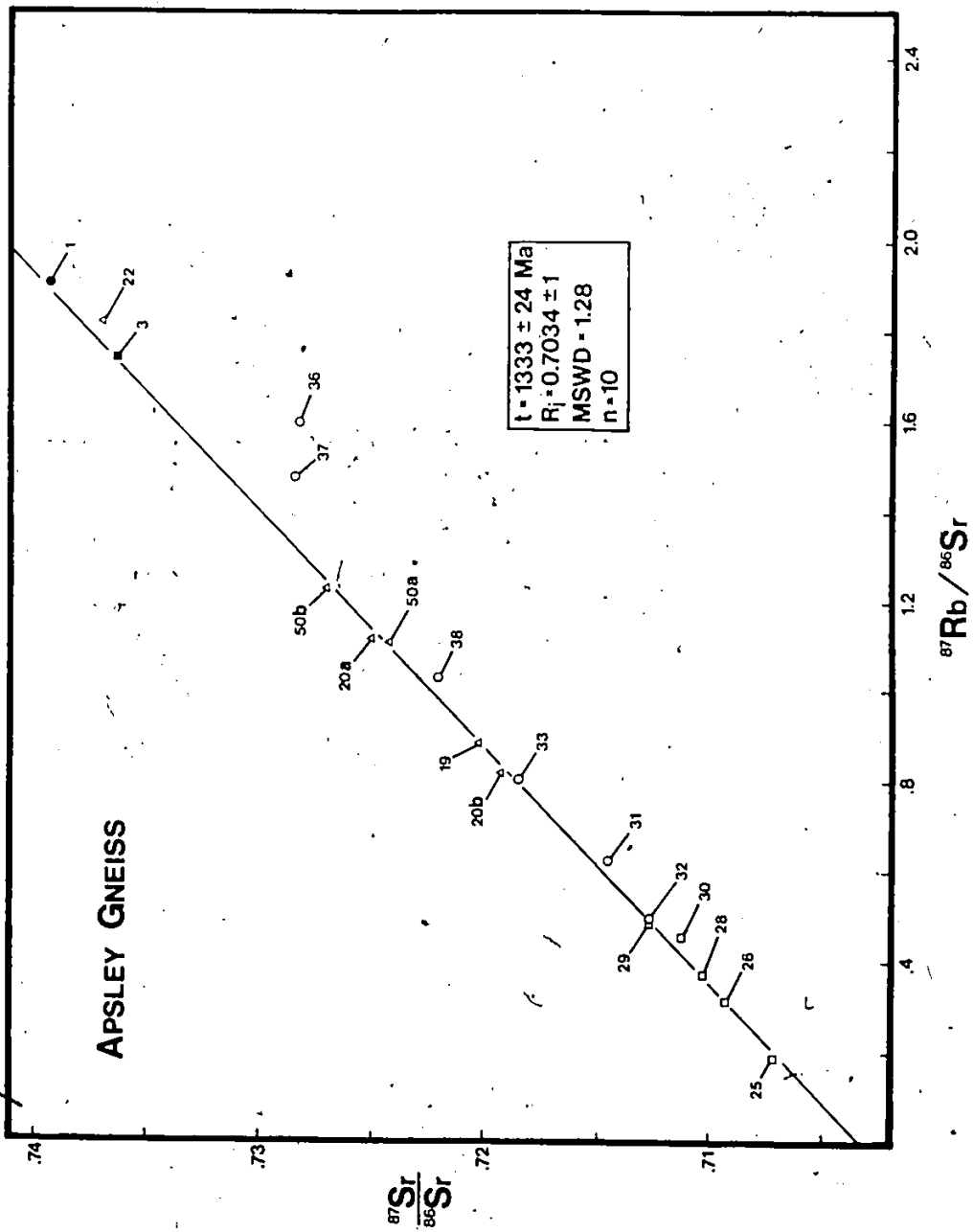
Sampling site#3 also contains visible layering with numerous 1 to 20 centimeter wide biotite-rich horizons, layers with abundant microcline poikiloblasts (see Plate 2c) and a few mafic layers containing garnet coronas. This is the only exposure examined in detail that consists primarily of "potassic" Apsley gneiss. The Rb-Sr results for six samples from this site (AG31-33, 36-38) are presented in Table 3.2 and Figure 10c. The slope of the best-fit regression line through these data corresponds to an imprecise age of 1101 ± 165 Ma ($R_1 = 0.7051$) with considerable data scatter outside analytical uncertainty (MSWD=19.88). The results for site#3 are analagous to the results for site#1 in that samples collected from individual, homogeneous layers, such as AG31, 32, and 33, and have similar chemical compositions, have coherent Rb-Sr systems. Two samples from this site (AG36, 37) have unusual chemical compositions with noticeably higher Na_2O and MgO and lower SiO_2 abundances (Table B2.1). The sample AG36 is also enriched in K_2O and Rb which, in some instances,

reflects secondary chemical modification (see section 4.2.5.1). Omitting these two samples from the age calculation significantly increases the calculated age to 1264 ± 161 Ma, lowers the initial strontium ratio to 0.7037 ± 16 , and reduces the associated data scatter ($MSWD=3.28$). Although there is a significant reduction in data scatter, the calculated errors remain about the same because there is a reduction in the range of Rb/Sr values. The preferred Rb-Sr age for site#3 is 1264 Ma.

The preferred Rb-Sr ages for the three sampling sites range between 1256 and 1341 Ma; clearly older than the presumed age of Grenvillian metamorphism (ca. 1150 Ma) and, except for site#1, in general agreement with the period of time (1286 to 1226 Ma) previously suggested for the deposition of the Grenville Supergroup from U-Pb zircon studies (Silver and Lumbers, 1966). The narrow range in Rb/Sr per site precludes a precise age determination by the Rb-Sr whole rock technique but the results do support the contention expressed in the previous section that the Apsley gneiss is younger than the 1402 Ma age suggested by Heaman (1980).

All the data plotted in Figure 10 are combined into one composite diagram (Figure 11) along with the two regionally collected samples, AG1 and 3. Many of the samples from site#3 (open circles), especially AG36 and 37, are displaced towards higher Rb/Sr values compared to the

Figure 11 Composite diagram combining all the Rb-Sr whole rock data presented in Figure 10 plus the two other "igneous" samples AG1 and AG3. Open triangles - site #1, open squares - site #2 and open circles - site #3



majority of samples analysed and, considering their "potassic" nature, are excluded from the composite age calculation. A similar observation was made by Heaman (1980) for potassic Apsley gneiss samples collected from widely spaced sampling sites. In addition, the three other samples that were omitted from the age calculations above (AG19, 22, 30) are also not included in the composite age calculation. The slope of the resulting isochron in Figure 11, calculated using the remaining ten samples, corresponds to an age of 1333 ± 24 Ma ($R_1 = 0.7034 \pm 1$) with no detectable data scatter outside analytical error (MSWD=1.28). This age is slightly older than the oldest U-Pb zircon age (i.e. 1286 Ma; Silver and Lumbers, 1966) obtained for any unit belonging to the Grenville Supergroup and, if geologically meaningful, challenges the regional stratigraphic correlation proposed by Lumbers (1967), that the Apsley Formation overlies the Tudor meta-volcanics. The fact that these results are in excellent agreement with the results calculated using the average $^{87}\text{Rb}/^{86}\text{Sr}$ and $^{87}\text{Sr}/^{86}\text{Sr}$ values for the three sampling sites plus samples AG1 and 3 (Figure 9; Table 3.2) provides support for the contention that the isotopic systematics of the sodic Apsley gneiss has not been seriously disrupted, on the scale of meters, by Grenvillian metamorphism. If there was large scale homogenization at about 1150 Ma, samples from the same stratigraphic horizon, such as AG20A, 20B, 50A, and 50B, would not lie on the 1333 Ma line in Figure 11.

In the remainder of this chapter, the composite data from Figure 11 are considered the best estimate of the age and initial strontium ratio for igneous members of the Apsley biotite gneiss.

3.2.3.4 Slab Study

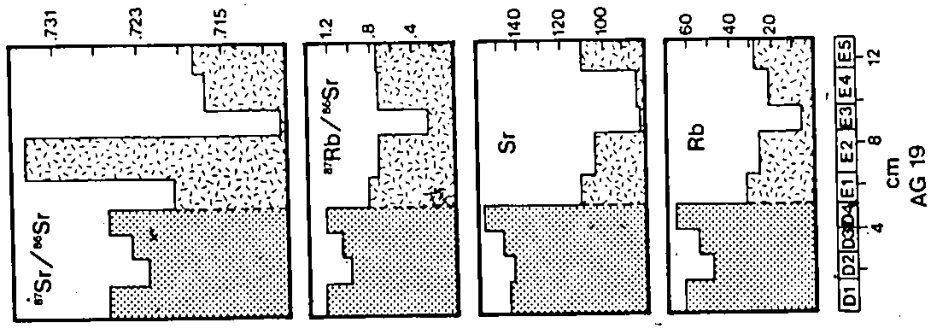
An important observation from the outcrop study is that all the ages determined for a single sampling site are older than the presumed age of metamorphism in the study area (ca. 1150 Ma; Martinez-Lopez and York, 1983). Therefore, the scale of Rb and Sr migration in the sodic Apsley gneiss during Grenvillian metamorphism, as mentioned above, must be less than the minimum distance between adjacent samples (ie. < 1 meter) otherwise the ages determined above would approach the time of metamorphism. It should be possible, however, to sample small subvolumes of rock where the Rb-Sr system has been reset by metamorphism thus recording the age of metamorphism (Hofmann, 1979). With this in mind, two samples from site#1 (AG19 and 50) have been investigated in more detail to:

- a) determine whether the Rb/Sr variation observed within a relatively homogeneous layer also extends to an individual homogeneous sample.
- b) determine how the chemical migration across a lithologic boundary affects the Rb-Sr systematics of a layered sample.
- c) establish the extent of Rb, Sr and Sr isotopic re-distribution associated with a late fracture system.

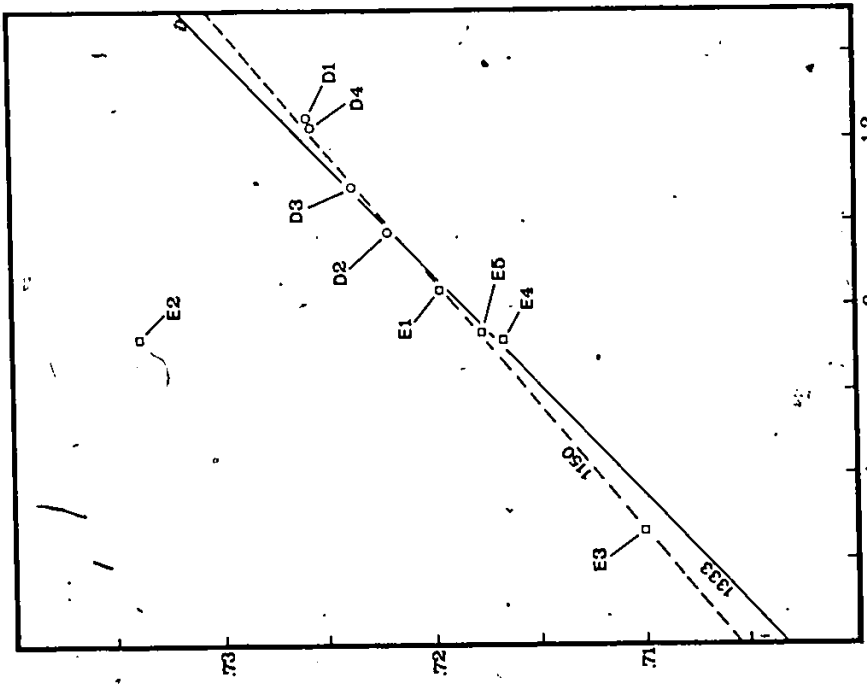
d) better define the scale of Rb and Sr migration in the Apsley gneiss and the age of Grenvillian metamorphism in the study area.

The two samples examined in detail were sliced into a series of thin slabs parallel to the layering in the rock. A description of sample AG19 has been presented in section 3.2.2 and the location of this sample at site#1 is shown in Plate 1b. The Rb-Sr data for the nine slabs prepared from AG19 are presented in Table B3.1 and Figure 12. Accompanying the Nicolaysen diagram in Figure 12 are four bar-diagrams outlining the Rb, Sr, $^{87}\text{Rb}/^{86}\text{Sr}$ and $^{87}\text{Sr}/^{86}\text{Sr}$ composition in each slab. The Rb and Sr profiles in the nine slabs not only indicate a difference in the average composition between the two layers (labelled D and E in Figure 12) but reveal some anomalies within individual slabs. The most noticeable anomaly is the composition of slab E3. Compared to the other slabs from this layer (ie. E1-5), E3 is depleted in both Rb and Sr with a distinctly lower $^{87}\text{Rb}/^{86}\text{Sr}$ and $^{87}\text{Sr}/^{86}\text{Sr}$; consistent with the anomalous major element composition reported earlier (section 3.2.2). Slab E4 is also depleted in Sr although, unlike slab E3, this is not reflected in the $^{87}\text{Rb}/^{86}\text{Sr}$ ratio. Another anomaly is the radiogenic nature of slab E2. The Rb and Sr abundances and $^{87}\text{Rb}/^{86}\text{Sr}$ ratio in this slab are similar to the other slabs from this layer (except E3) which means the excess radiogenic Sr is unsupported (ie. the Rb abundance is too low). This can occur by a net

Figure 12 Rb-Sr whole rock data for the slab study of sample AG19 along with two reference lines for 1333 and 1150 Ma. Also included are bar-diagrams representing the variation in Rb, Sr, Rb/Sr and $^{87}\text{Sr}/^{86}\text{Sr}$ within each slab



AG 19



$^{87}\text{Sr}/^{86}\text{Sr}$
 ^{86}Sr

accumulation of radiogenic strontium, a net loss of Rb, or alternatively, E2 has preserved a very old isotopic component of strontium. For example, model ages for this slab, assuming initial strontium ratios of 0.7035 and 0.7065, would be circa 2890 and 2610 Ma, respectively; suggesting an Archean component of strontium may be present.

Another feature of these profiles is the abrupt change in composition across the boundary between the two layers D (stippled) and E (random slash pattern). There is an indication that slabs E1 and D4 both have elevated Rb and Sr abundances, possibly reflecting an accumulation of Rb and Sr at the boundary. Overall, the chemical and isotopic composition of these two layers are quite heterogeneous.

The results from a two-error regression treatment of the Rb-Sr data for each layer plus the entire sample are tabulated in Table 3.2 and plotted in Figure 12. Also shown is the isochron (solid line) representing the preferred Rb-Sr age for the Apsley gneiss from section 3.2.3.3. Five of the slabs (D2,3,E1,4,5) plot very close to the 1333 Ma reference line and give the impression that they have not been significantly modified during metamorphism. In fact, the regression results for these five slabs ($t=1332$ Ma; $R_s=0.7034$; $MSWD=4.46$) are indistinguishable from the composite data reported in the previous section. However, two slabs (E2,3) plot distinctly above and two others (D1,4) plot below this reference line. It is noteworthy that the two slabs that

plot below this reference line are from the margins of the layer and are also enriched in Rb compared to the slabs sliced from the central portion of the layer. The addition of Rb to these slabs subsequent to the formation of the layer might explain their displacement to the right of the reference line. If the four slabs from layer D are considered separately, they yield a relatively young age ($t=946\pm 154$ Ma; $R_1=0.7091\pm 22$; MSWD=0.11). This young age could represent the time when Rb was added to these slabs or reflect the time when Rb migration on the scale of a few centimeters ceased but is clearly younger than the estimated time of metamorphism (ca. 1150 Ma).

No attempt is made here to calculate an age for layer E because, as mentioned above, at least three of the five slabs (E2, E3, and E4) have anomalous chemical and/or isotopic compositions. It is noteworthy that slab E3, a slab that is interpreted to have lost both Rb and Sr sometime after layer E formed, plots on a 1150 Ma reference line. One interpretation of this datum is that there was some migration of Rb and Sr on the scale of a few centimeters during metamorphism at about 1150 Ma but this element migration was not pervasive throughout the entire layer (otherwise all slabs would plot on a 1150 Ma isochron). The significantly lower Rb/Sr ratio obtained for slab E3, compared to the other slabs, strongly controls the resulting age calculation using all the slabs, excluding E2 ($t=1151\pm 67$ Ma; $R_1=0.7056\pm 7$;

MSWD=5.02).

Additional support for a metamorphic episode at about 1150 Ma ago that disrupted the Rb-Sr systematics of thin slabs is indirectly revealed by calculating the initial strontium isotopic composition of AG19 at 1150 Ma ago assuming the sample has a bulk $^{87}\text{Rb}/^{86}\text{Sr}$ composition equal to the weighted mean of the individual slabs (ie. 0.892) and formed 1333 Ma ago. Therefore, resetting the Rb-Sr system of AG19 at 1150 Ma ago should elevate the initial strontium ratio from 0.7033 to 0.7056; exactly the value determined in this slab study.

Although there is some indication that chemical and isotopic modification has occurred in small subvolumes of the Apsley gneiss during metamorphism, there are anomalies such as the data for slab E2 that are difficult to reconcile with an hypothesis that invokes complete isotopic homogenization during metamorphism. Apparently, anomalous isotopic domains can be preserved or possibly created within relatively small volumes of rock which militates against any model for the resetting of the Rb-Sr system during metamorphism as purely a volume diffusion controlled process.

The second sample examined in detail, AG50, contains numerous fractures and was selected specifically to investigate the effect these fractures might have on the Rb-Sr systematics of an otherwise homogeneous sample of tonalite gneiss. The nature of these fractures is illustrated

in Plates 3a and b. The main fracture that passes through the central portion of the sample (see Plate 3a) is sealed with biotite and bordered by a bleached zone. This bleached zone consists primarily of quartz and plagioclase and, as can be seen in the photomicrograph in Plate 3c, is typically coarser-grained than the rest of the sample. The plagioclase grains in this zone are intensely sericitized. Additional fractures can be recognized in Plate 3b but are not as prominent as the fracture described above. A series of eleven slabs were prepared from this sample with the average slab dimension (1 cm x 1.2 cm x 0.5 cm) considerably smaller than those prepared from AG19. The location of each slab is indicated in Plate 3b.

The Rb-Sr data for each slab from AG50 are compiled in Table B2.1 and presented in a similar manner as the slab study results for AG19 (Figure 13). The Rb and Sr concentrations and Rb/Sr ratios are less precise than the results from AG19 because there was only enough sample powder to prepare one powder pellet per slab for XRF analysis. A thin powder pellet was also prepared from a sample (AG50A) that was analysed repeatedly by the conventional procedure: the results from both methods are identical suggesting that the thin powder pellet results, although not precise, are quite accurate. There are two important features of AG50 revealed through the bar-diagrams in Figure 13. Except for the three slabs S4, S5, and S6, the $^{87}\text{Rb}/^{86}\text{Sr}$ and $^{87}\text{Sr}/^{86}\text{Sr}$

Plate 3 A - Sample AG50 showing an obvious fracture with bleached zone. This sample was used for a slab study

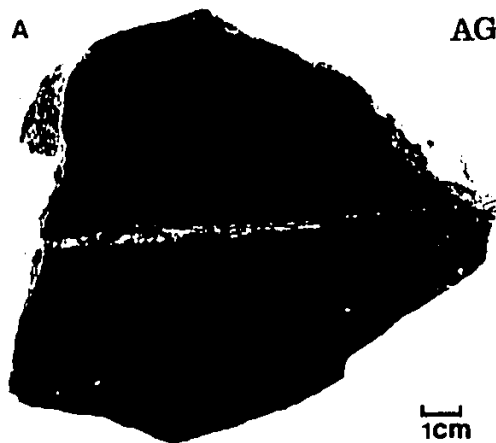
B - Sample AG50 showing the location of individual slabs



C - Photomicrograph of the fracture visible in Plates 3A and 3B. There is a coarsening of grain size near the fracture. The fracture is sealed with biotite and the surrounding bleached zone is depleted in biotite

A

AG50



B

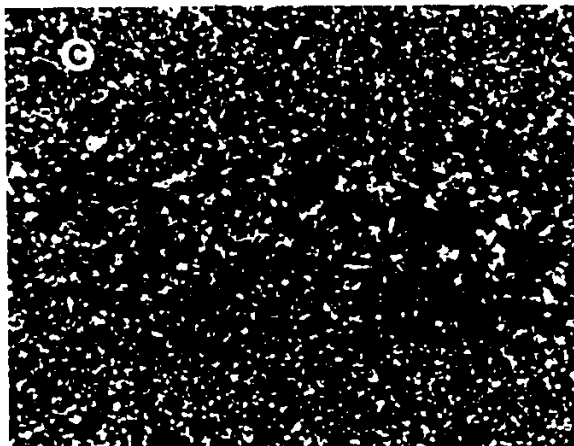
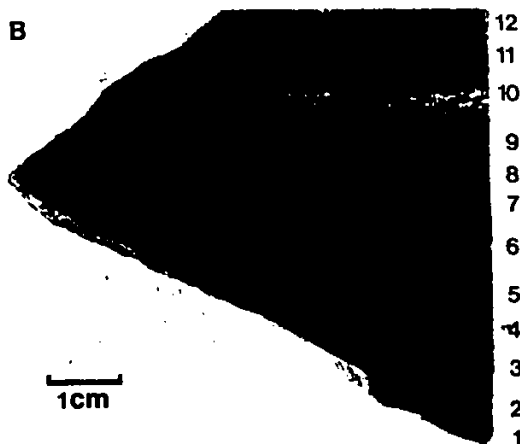
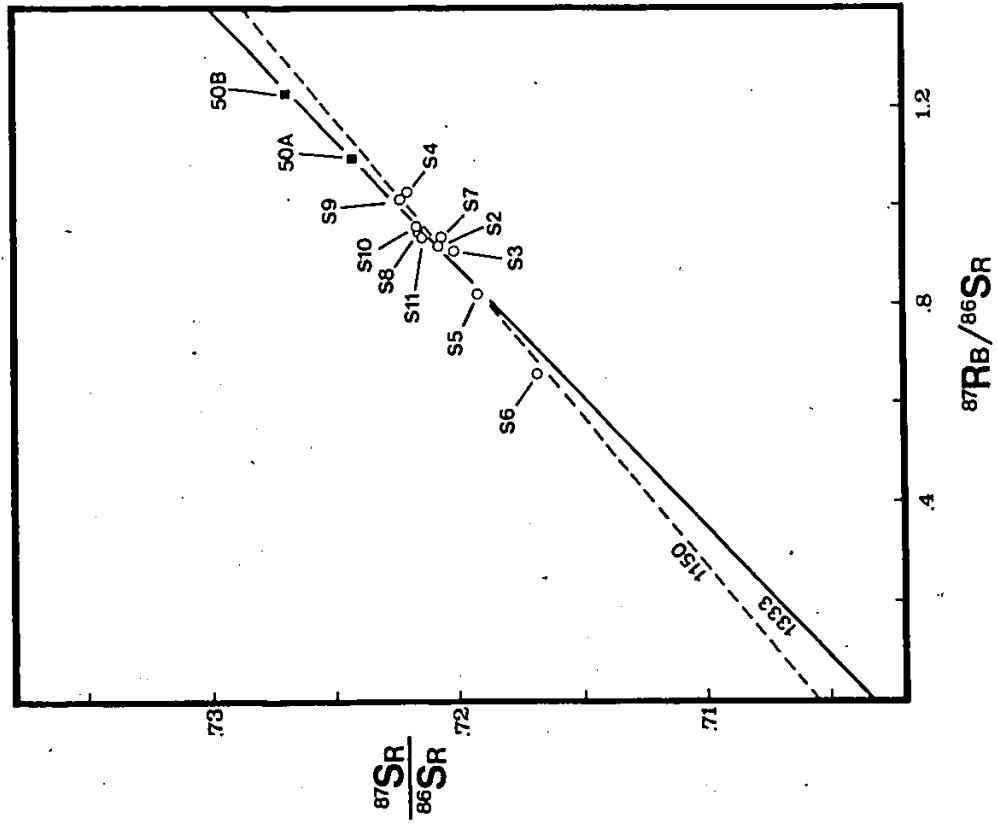
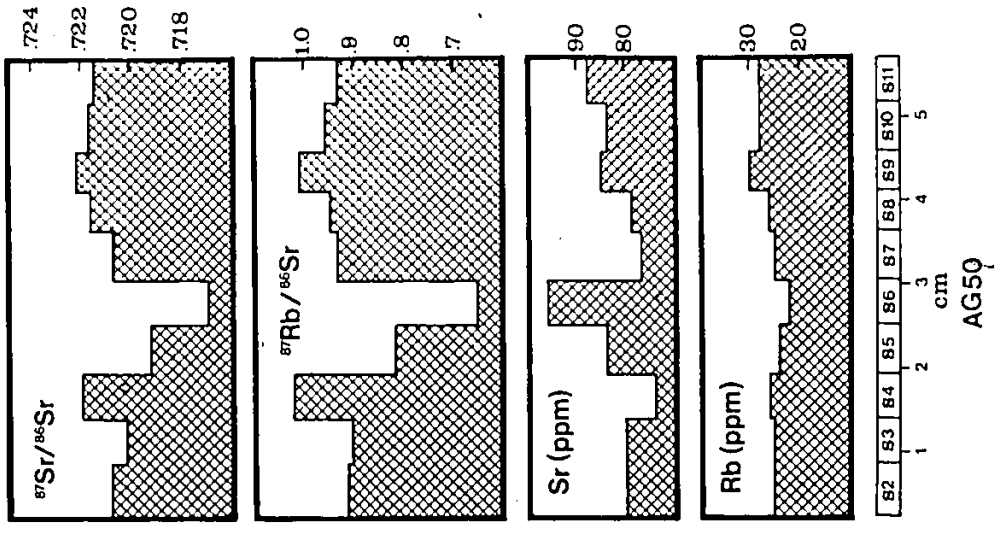




Figure 13 Rb-Sr whole rock data for the slab study of sample AG50. The data is presented in a similar fashion as for sample AG19. Also included are two samples AG50A and AG50B collected at the same sampling site



ratios do not vary significantly compared to the variation observed for the slabs from AG19; especially considering the fact that slab S10 and part of slab S9 contain the prominent fracture discussed above. Compared to the other slabs, S6 and to a lesser extent S5, have noticeably higher Sr contents and lower $^{87}\text{Rb}/^{86}\text{Sr}$ and $^{87}\text{Sr}/^{86}\text{Sr}$ ratios. Both contain a small fracture and, despite the fact that the fracture in S6 is sealed with biotite (a Rb-rich mineral), the major chemical modification is an enrichment in Sr. One might expect the prominent fracture in slab S9 to show a similar chemical alteration because it is also sealed with biotite, but the only noticeable change is a slight enrichment in Rb. Therefore, the two important pieces of information gained from these slab results are that the range in Rb/Sr for slabs without fractures (0.91 to 0.96) does not vary sufficiently to determine a Rb-Sr age and only some of the visible fractures in AG50 have significantly affected the original sample chemistry.

The Rb-Sr data for the individual slabs are plotted on a Nicolaysen diagram in Figure 13 along with the data for two whole rock samples, AG50A and 50B, reported in the previous section. A very large sample (54 kilograms) from site#1 was collected for a U-Pb study (next section) and AG50A and 50B and the sample used here for the slab study represent different hand size pieces from this larger sample. In addition to these data, the 1333 Ma reference isochron (solid

line), representing the best estimate for the age of the Apsley biotite gneiss, and a 1150 Ma reference isochron (dashed line), representing the presumed time of metamorphism, have been included in Figure 13. Many of the slabs (ie. S2,5,8,10,11) plot on or very close to the 1333 Ma reference line possibly indicating that the composition of these slabs has not been modified during metamorphism. However, the Rb/Sr ratios for these slabs (0.82 to 0.96) exactly coincide with the region where the 1333 and 1150 Ma reference lines intersect so it is difficult to interpret.

The remaining five slabs (S3,4,6,7,9) are noticeably discordant from the 1333 Ma line. In fact, three slabs (S3,4,7) also plot below the 1150 Ma reference line. These discordant samples may indicate that the composition of some slabs have been modified by a geological event younger than 1150 Ma ago or has continuously changed in response to slow cooling after the peak of metamorphism. In contrast, slabs S6 and S9 do contain fractures that can account for the observed chemical alteration. The net chemical change in these two slabs is quite different, S6 has gained Sr while S9 has gained Rb. Both slabs plot close to the 1150 Ma line indicating that the fractures, at least some of them, may have formed during or soon after the peak of metamorphism.

3.2.4. U-Pb Study

In addition to the Rb-Sr age dates reported in the

previous three sections, two large samples (ca. 50 kilograms each) were collected for U-Pb zircon, sphene dating. One sample was collected from site#1 (AG50) and the second (LH84-1) was collected from the exposure where sample AG3 was taken (see Fig. 9). Recent refinements to the U-Pb zircon dating technique (Krogh, 1982a; 1982b) combined with a low contamination method for the dissolution of zircon and extraction of U and Pb (Krogh, 1973) have made it possible to determine very precise U-Pb zircon ages using small quantities of zircon. The zircon separation, chemistry and U and Pb isotopic analyses were performed at the Royal Ontario Museum and an outline of the U-Pb zircon dating procedure plus the U-Pb data are presented in Appendix A5.2 and Table B4. Unfortunately, both samples selected from the Apsley biotite gneiss contain relatively few zircons and the majority of these are tiny (< 325 mesh) and rounded (resorbed?). Based on morphology alone these tiny, rounded zircons are similar to zircons formed during metamorphism or found occasionally in felsic volcanic rocks. If these zircons are not metamorphic in origin then the selected samples represent either an intermediate volcanic rock or a sediment derived from the erosion of a volcanic dominated terrain. A second zircon population consisting of large prismatic grains with cloudy cores and clear rims (overgrowths?) was identified in AG50 but this variety is even less abundant.

Two zircon fractions from sample AG50 were prepared for U and Pb extraction and isotopic analyses. Both fractions represent the tiny, rounded and usually clear variety but the clearest grains were hand picked and gently abraded to produce an abraded (0.04 mg) and non-abraded (0.176 mg) fraction. As a consequence of the small sample sizes and small amounts of Pb, the Pb isotopic data for these two samples (Table B4) are very poor and a precise U-Pb zircon age can not be determined for this sample. The $^{207}\text{Pb}/^{206}\text{Pb}$ (7/6) age for the clear, abraded fraction is about 1230 Ma and is approximately 30% discordant whereas the 7/6 age for the unabraded fraction is about 1180 Ma but plots above concordia. Two interpretations can be envisaged for these 7/6 ages. The 1230 Ma age could represent a minimum estimate for the time of deposition of the Apsley gneiss or the tiny zircons are metamorphic in origin with some inheritance. With reference to the latter possibility the two zircon fractions analysed in this study would define a mixing line between the time of metamorphism and the age of the older zircons. However, additional research is required to evaluate the possibility of determining a precise U-Pb zircon age for the Apsley gneiss.

The second Apsley gneiss sample collected for the U-Pb study also contains very little zircon but abundant sphene. The U-Pb data for one sphene fraction is presented in Table B4. Although the sphene contains abundant common lead

(ie. 717 pg) this fraction is slightly discordant with a $7/6$ age of 1078 Ma. Four sphene separates from different units in the study area are colinear on a $^{207}\text{Pb}/^{204}\text{Pb}$ versus $^{206}\text{Pb}/^{204}\text{Pb}$ (Figure 39) and define an age of about 1080 Ma (see section 5.3.3). This 1080 Ma U-Pb sphene age is interpreted to represent a minimum estimate for the time of metamorphism in this area at which time there was new growth of sphene or an older sphene in the Apsley gneiss was totally reset (see the discussion in section 5.3.3).

3.3 SILENT LAKE GNEISS

3.3.1 Introduction

The region surrounding Silent Lake (Figure 14) was mapped on a reconnaissance scale by Adams and Barlow (1910), on a scale of 1"=1/2 mile (Hewitt, 1959), in greater detail (1"=1/4 mile) by Jennings (1969) and Breaks (1971), and more recently by Lumbers and Vertolli (pers. comm.). The main rock types include amphibolite, quartzo-feldspathic gneiss, leptite (a term used by Jennings to denote a pink, fine-grained quartz-feldspar-mica rock of uncertain origin) and marble. These lithologies can be traced along strike for over 60 kilometers from Mayo township, where they are truncated by the McArthur's Mills fault, eastward to the Silent Lake area and through the northern and central portions of Chandos and Anstruther townships, respectively.

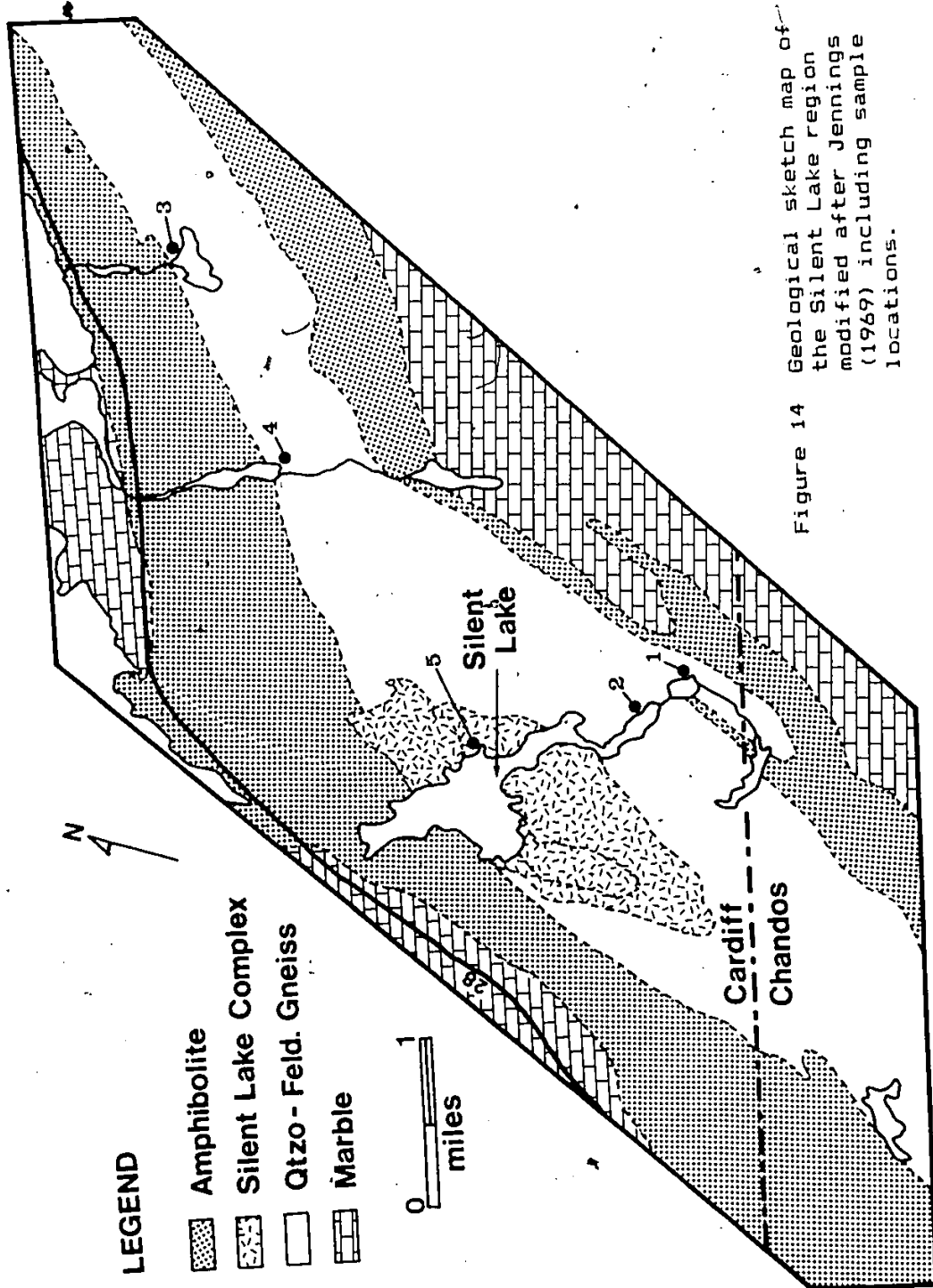


Figure 14 Geological sketch map of the Silent Lake region modified after Jennings (1969) including sample locations.

There is some controversy, however, regarding the stratigraphic position of these rocks. Hewitt and James (1956) referred to these rocks as the Hermon Formation after the exposures of quartz-feldspar-biotite gneiss and schist near the town of Hermon in Mayo township. According to these authors the Hermon Formation belongs to a relatively young metasedimentary package called the Mayo Group. However, an alternative interpretation was proposed by Lumbers (1967). He suggested that the Hermon Formation was predominantly metavolcanic and not part of the Mayo Group but correlative with the metavolcanic members of the Tudor and Oak Lake Formations in Limerick township. If the latter interpretation is correct then the supracrustal rocks in the Silent Lake area are part of the Hermon Group metavolcanic succession and underly the metasedimentary rocks discussed in section 3.2 that occur in central and southern Chandos township.

3.3.2 Geology and Petrography

The distribution of lithologies in the Silent Lake area is shown in Figure 14 and is modified slightly from the detailed map of this area presented by Jennings (1969). The main modification in Figure 14 is that the two map units, quartzo-feldspathic gneiss and leptite, from Jennings map have been combined into one map unit called quartzo-feldspathic gneiss: not an unreasonable simplification since Jennings (p.11) reports that "leptite is seen to grade

laterally into quartzo-feldspathic gneiss parallel to the gneissosity". Therefore, in a simplified way, the supracrustal rocks in the Silent Lake area consist of a NE-SW trending band of quartzo-feldspathic gneiss that is bordered by amphibolite which is, in turn, bounded by marble. According to Jennings (1969; p.28) these rocks are "... right side up underlying marbles of the Dungannon Formation" and "... can be subdivided in a general way into a lower amphibolite, a middle unit of interfingering quartzo-feldspathic gneisses and leptites, an upper amphibolite and an upper leptite".

Of particular interest to this study are the quartzo-feldspathic gneisses and leptites because of their potential, as stratigraphic marker horizons. The leptites are fine-grained, pink, quartz-feldspar-mica rocks with conspicuous muscovite porphyroblasts and tourmaline. Similar rocks are relatively rare in the CMB but have been reported in Methuen, Lake and Wollaston townships (ie. the Oak Lake Formation). Hewitt (1962, p.37) states that fine-grained pink "arkoses" from the Ridge Dome in Wollaston and Lake townships "are very similar to the arkose of the Hermon Formation in Chandos, Cardiff and Faraday townships". Consequently, if the leptites are indeed useful marker horizons then they could be extremely valuable for unravelling the stratigraphy in this geologically complex area. Although Jennings used a non-genetic term to identify the fine-grained, pink rocks in the

Silent Lake area, similar rocks in other areas are interpreted as arkoses. (Hewitt and James, 1956; Hewitt, 1960; 1962; Laasko, 1968), felsites (Adams and Barlow, 1910), recrystallized rhyolitic tuffs (Hewitt, 1962) and felsic metavolcanics (Lumbers, 1967; 1969). An example of the problems facing the field geologist regarding the origin of such rocks is reflected in the statement by Hewitt (1962; p.36) "these pink arkosic rocks much resemble fine grained, pink biotite granite gneiss".

For this study, multiple samples were collected from five separate exposures of quartzo-feldspathic gneiss and leptite in the Silent Lake area (see Figure 14). Four of the sampling sites (#1 - HG1-5; #2 - HG6-10; #3 - HG11-17; #5 - SL1-7) are fine-grained, pink leptite and one site (#4 - HG18-23) is from an area mapped as quartzo-feldspathic gneiss by Jennings (1969). The leptites contain on average 37% quartz, 30% plagioclase, 18% microcline, 9% muscovite with subordinate biotite, garnet, magnetite, carbonate and accessory tourmaline, apatite, zircon, sphene, allanite and pyrite (refer to Table B1.2 for modes). Most of the samples examined show some sign of alteration, from slightly sericitized plagioclase to the more extreme case of quartz-muscovite-microcline-carbonate veining. The concentration of muscovite along grain boundaries in some samples, association with cross-cutting veinlets and fractures and common occurrence as large, anhedral

poikiloblasts all indicate that the presence of muscovite is related to the alteration. This alteration is considered responsible, at least in part, for the variable abundance of muscovite (2 to 22%) and microcline (5 to 35%). Although much of the texture is dominated by alteration products, most samples contain quartz-plagioclase rich domains with good polygonal texture.

The quartzo-feldspathic gneiss samples from site#4 are layered with alternating micaceous and quartz-plagioclase rich bands and have a pronounced schistosity. These rocks contain significantly more mafic minerals than the leptites, especially biotite (up to 35%), generally no K-feldspar and do not show the types of alteration observed in the leptites. There is a weak but pervasive sericitic alteration in the plagioclase grains and biotite in one sample (HG19) is slightly altered to chlorite. A minor component at site#4 is amphibolite (HG21) consisting primarily of hornblende (63%) and plagioclase (31%).

In the immediate vicinity of Silent Lake, an ellipsoidal shaped body, referred to as the Silent Lake Complex in Figure 14, is distinguished from the felsic gneiss and leptite mentioned above because it forms a large discontinuous lense that appears, in places, to be discordant to the regional foliation and contains abundant quartz-sillimanite nodules (Breaks and Shaw, 1973). This unit has been previously referred to as the Pine Lake granite (Adams

and Barlow, 1910), Silent Lake granite (Hewitt, 1957; Jennings, 1969) and the Silent Lake pluton (Breaks and Shaw, 1973) but, except for the nodules, is similar to the fine-grained, pink quartz-feldspar-mica rocks (leptites) reported elsewhere in the belt. In places the nodules are ubiquitous, forming prominent, greyish ovoids (5 mm to 30 cm in length) often surrounded by a biotite-rich zone and, in addition to quartz and sillimanite, contain minor amounts of muscovite, tourmaline, biotite, and plagioclase (Breaks and Shaw, 1973).

3.3.3 Geochemistry

The presence of quartz-muscovite-microcline-carbonate veinlets, concentration of muscovite and other alteration products along grain boundaries and the replacement of plagioclase by muscovite in some samples indicate that at least some of the leptite mineralogy is not primary. There are also indications that the development of this secondary mineralogy has been accompanied by a modification of the original sample chemistry. For example, the leptite sample showing the least amount of alteration (HG16) has a significantly different chemical composition compared to the average leptite composition reported by Jennings (1969) or in this study (see Table 3.1). The most noticeable differences are the lower Al_2O_3 , CaO, K_2O and Rb and the higher Fe_2O_3 , MgO, MnO and Y in sample HG16. The abnormally high modal

TABLE 3.3 - Geochemical comparison of the least altered leptite sample (HG16) with estimates for the average leptite composition

	HG16	a n=9	b n=6
SiO ₂	78.43	78.08	75.66
Al ₂ O ₃	10.99	11.59	11.53
Fe ₂ O ₃	3.87*	2.83*	2.90
FeO	-	-	0.89
MgO	0.93	0.50	0.25
CaO	0.09	0.35	0.61
Na ₂ O	3.58	3.25	2.57
K ₂ O	1.30	2.71	4.57
TiO ₂	0.22	0.16	0.19
MnO	0.24	0.07	0.03
P ₂ O ₅	0.02	0.02	0.06
LOI	0.52	0.44	-
Rb	38	80	93
Sr	33	30	85
Y	158	114	77
Zr	623	514	1119
Nb	39	27	-

a - Average leptite composition from this study

b - Average leptite composition reported by Jennings (1969)

* - Total iron expressed as Fe₂O₃

abundance of biotite in HG16 can account for the high (Fe₂O₃)_T, MgO and MnO contents but the relative enrichment of the other elements mentioned above in the more altered samples is attributed to the development of a secondary paragenesis. One anomaly that was noted by Jennings (1969) and Breaks and Shaw (1973) is the extremely low abundance of CaO, often less than 0.1 weight percent (see Table B2.2), in the leptites. The fact that the samples with higher CaO contents, such as HG8 and HG9, also contain the largest

proportion of carbonate (often associated with veins and fractures) suggests that the effect of alteration has been to increase the CaO and Sr content of the leptite. Therefore, the low CaO is either primary, produced by an earlier period of alteration unrelated to the development of secondary muscovite-microcline-carbonate in veins etc., or reflects an alteration process whereby Ca and Sr are depleted from large quantities of leptite and locally concentrated in veins and fractures. Regardless of the alteration mechanism, the depletion of Sr and enrichment in Rb could seriously affect the Rb-Sr systematics, especially if the alteration occurred a long time after the formation of the rock.

The compositions of two quartzo-feldspathic gneiss samples (HG22 and 23) from site#4 are also presented in Table B2.2. The compositions of these two samples are in close agreement with the average composition for 13 samples reported by Jennings (1969; p.90) except for a noticeably lower Na₂O content (0.19 compared to 2.41 wt.%).

3.3.4 Rb-Sr Whole Rock Study

3.3.4.1 Individual Sampling Sites

The Rb-Sr data for 24 quartzo-feldspathic gneiss and leptite samples, collected from four widely spaced sampling sites (see Figure 14), are tabulated in Table B3.2 and plotted in Figure 15. The Rb-Sr whole rock ages determined

using several samples from each site range between 1021 and 862 Ma (Table 3.4) and are significantly younger than ages, determined in a similar manner, for the sodic Apsley gneiss (see section 3.2.3.3) and the presumed age for the deposition

TABLE 3.4 - Two-error regression results for quartzofeldspathic rocks from the Silent Lake area

SAMPLES*	n	t(Ma)	**	Ri	**	MSWD	MODEL
(2) HG 6-10	5	990	181	0.711	7	18.4	M2
(3) HG 11-17	7	862	137	0.720	10	47.4	M2
(4) HG 18-20,22,23	5	1021	263	0.711	9	53.5	M2
(5) SL 1-7	7	988	53	0.710	1	24.5	M2
(C1) HG6-20,22-23;SL1-7	24	1001	46	0.710	1	45.4	M2
(C2) HG6-17;SL1-7	19	994	44	0.710	1	38.5	M2
(C3) HG6-14,16-17;SL1-7	18	1005	39	0.710	1	27.5	M2

- * - Numbers in parentheses refer to specific sampling sites. The letter C indicates composite data sets.
 ** - errors quoted at the 95% confidence level.

of the Grenville Supergroup (ca. 1250 Ma; see section 2.2.3). Compared to the results obtained for the sodic Apsley gneiss in section 3.2.3.3, the Silent Lake gneisses have a larger range in $^{87}\text{Rb}/^{86}\text{Sr}$, higher initial strontium ratios (0.710 to 0.720) and considerably more data scatter (MSWD=18.4 to 53.5).

It is clear from the anomalous data scatter and unreasonably young ages presented in Figure 15 that the Rb-Sr whole rock ages for the Silent Lake rocks do not represent the primary age of formation but, instead, reflect a disturbance in the Rb-Sr system. In fact, there is very

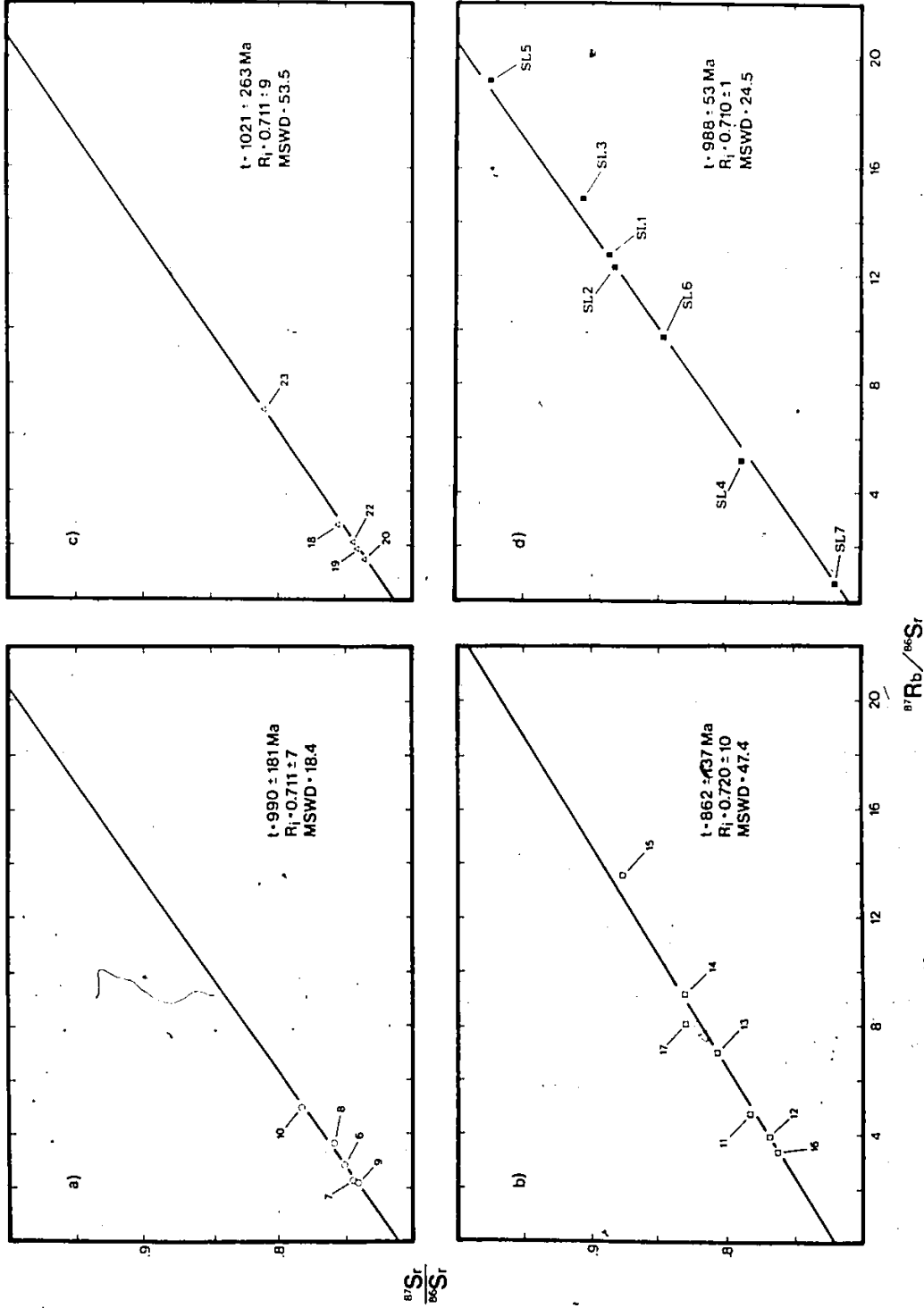


Figure 15 Rb-Sr whole rock data for samples from the Hermon Group quartz-feldspathic gneisses and Silent Lake Complex. a) site #2 b) site #3 c) site #4 and d) site #5.

little difference between the ages calculated using samples from individual sites and those calculated using samples from several widely spaced sites (compare the results obtained for individual sites to the three composite data sets in Table 3.4). The composite data set C1 includes all the samples analysed from the Silent Lake area whereas data set C2 represents only the "leptite" samples and C3 excludes the most discordant leptite sample HG15. Therefore, the common occurrence of 1000 Ma Rb-Sr whole rock ages for the Silent Lake rocks is interpreted to represent a minimum estimate for the time of this disturbance. The high initial strontium ratios are also not primary and, at best (assuming complete isotopic homogenization during the 1000 Ma disturbance), can be interpreted to reflect the average strontium isotopic composition of each sampling site at the time of the 1000 Ma disturbance.

One approach to estimate the time of formation for these rocks is to calculate model ages. To do this, two unknowns have to be approximated; the primary initial strontium and the average Rb/Sr ratios for the rock volume being considered. The initial strontium ratio for most rocks in the CMB varies between 0.7025 and 0.7035 so, to a first approximation, 0.7030 is not an unreasonable estimate of this ratio. To estimate the average Rb/Sr ratio, in the case of the Silent Lake rocks, is more difficult because the primary Rb/Sr ratios have been modified by Rb enrichment (and/or Sr

loss). The best estimate is to select a sample or average of samples that have been least affected by this secondary alteration. To make this calculation, the $^{87}\text{Rb}/^{86}\text{Sr}$ and $^{87}\text{Sr}/^{86}\text{Sr}$ ratios for the least altered sample (HG16) are used (ie. 3.35 and 0.7626, respectively). The model age calculated in this way is 1243 Ma and is within the age range (ie. 1286 to 1226 Ma; Silver and Lumbers, 1966) suggested previously for the deposition of the Grenville Supergroup. This model age is circa 100 Ma younger than the preferred age for the sodic Apsley gneiss (1333 Ma) presented in section 3.2.3.3.

Rb-Sr whole rock ages in the range 900 to 1000 Ma have been reported for other units in this area including pegmatites (970 to 980 Ma; Heaman, 1980; Fowler and Doig, 1983) the potassic Apsley gneiss (979 Ma; Heaman, 1980) and samples from the Tallan Lake sill that are near or contain microfractures (1023 Ma; see section 4.2.5.1). In all cases, these units are enriched in K and Rb and have probably interacted with a K-rich solution. A disturbance around 1000 Ma is also recorded in other parts of the Grenville Province and is considered responsible for generating new, metamorphic zircons in the French River area (Krogh and Davis, 1973) and releasing radiogenic argon trapped in hornblende and biotite from gabbroic rocks located in the Haliburton Highlands (Berger and York, 1981; see section 2.3.2). The nature of the 1000 Ma disturbance in the Chandos township area is discussed further in Chapter 5.

3.3.4.2 Nodules

Rb-Sr data were also obtained for three nodule-matrix pairs from the Silent Lake Complex and are included in Table B3.2. These samples were collected by Breaks (1971; for the sample locations refer to his Figure 3) not far inland from the shoreline exposure where samples SL1-7 (this study) were collected. The abundance of Rb and Sr in these samples reported by Breaks (1971) are included in Table 3.5 for comparison with the data obtained in this study. There is generally good agreement between the two studies for the abundance of Rb, however, the Sr values determined in this study are significantly lower, by as much as 70 ppm. Although it is obvious that the concentration of Sr in these samples is lower than previously reported, it is important to recognize that the nodules have anomalously low Sr concentrations and that both Rb and Sr appear to be depleted in the nodules.

There is considerable uncertainty in the Rb/Sr ratios of the nodules because the Sr concentration is below the level where the abundance of Sr can be determined accurately by XRF. For this reason, these data have not been plotted on a Nicolaysen diagram. However, it is interesting that all the nodules, and their corresponding matrices, are rich in radiogenic strontium with $^{87}\text{Sr}/^{86}\text{Sr}$ ratios greater than 1. This information alone supports the contention of Breaks and

Shaw (1973) that the nodules were involved in a de-alkalini-
zation process unless the anomalously low Sr contents in the
nodules is a primary feature.

TABLE 3.5 - Comparison of Rb and Sr abundances
in the Silent Lake nodules determined
by Breaks (1971) and this study

SAMPLE*	Rb		Sr	
	A	B	A	B
JN24M	198	195	46	18
JN24N	32	40	30	2
JN43M	82	108	87	16
JN43N	27	24	78	2
JN62M	138	154	53	18
JN62N	31	35	45	3

A - Breaks (1971) B - This Study * - N refers to nodule and M
refers to the surrounding matrix

3.4 SUMMARY

The data reported in this chapter for samples from the
Apsley biotite gneiss and the Silent Lake gneiss were
collected with two objectives in mind; to evaluate the
potential for using Rb-Sr whole rock geochronology to unravel
complex stratigraphic relationships in this part of the
Grenville Province and to evaluate the extent of element and
strontium isotope mobility during an amphibolite grade
metamorphic event. To do this, various sampling techniques
were employed to test whether the method of sample collection
affects the resulting age determination and, in the case of

the Apsley gneiss, an attempt was made to compare age information from both the Rb-Sr and U-Pb zircon methods.

The previously reported age (1402 Ma) for the sodic Apsley gneiss (Heaman, 1980; Heaman et al., 1980b; 1982b) is anomalously old and the result of mixing genetically unrelated samples collected from widely spaced sampling sites. A range of ages between 1256 and 1341 Ma was obtained for samples collected from individual sites indicating that extensive migration of Rb and Sr did not occur on the scale of meters in these rocks during metamorphism. The best estimate for the age of the Apsley gneiss is 1333 ± 24 Ma ($R_1 = 0.7034 \pm 1$; MSWD = 1.28) and has been obtained by combining samples that have been examined in detail, have igneous protoliths and have similar, if not identical, initial strontium ratios.

A slab study of one layered sodic Apsley gneiss sample resulted in two relatively young Rb-Sr ages, 1151 and 946 Ma. Since some of these slabs plot close to or on the 1333 Ma reference isochron, there is an indication that the effect of secondary isotopic and chemical modification has not been recorded in every slab. If this is true, then the effect of metamorphism on the Rb-Sr system is not pervasive even on the scale of a few centimeters. The young ages from this slab study are difficult to interpret with any certainty but the 1151 Ma age, using eight of the nine slabs, provides an estimate for the time of metamorphism in this region.

It is difficult to distinguish with any certainty whether the Apsley gneiss is older or younger than the Silent Lake gneiss using the Rb-Sr whole rock data obtained in this study because the latter has been reset at about 1000 Ma ago. However, there is a suggestion that the Apsley gneiss is older than the rocks in the Silent Lake area if the best age estimate for the sodic Apsley gneiss (1333 Ma) is compared to the model age for the least altered Silent Lake sample HG16 (1243 Ma).

The final point worth mentioning is that a range in Rb/Sr values was found for samples collected from homogeneous layers within a single sampling site. Although this range is not large enough to determine a precise Rb-Sr age, these ages are probably more geologically meaningful than ages calculated using samples collected on a regional scale because they avoid the assumption of consanguinity.

CHAPTER 4

INTRUSIVE ROCKS

4.1 INTRODUCTION

The CMB is well known as a unique area in the western portion of the Grenville Province that contains thick accumulations of Neohelikian supracrustal rocks; however, there is another important element present in this belt, the ubiquitous igneous plutonic rocks. Reference has already been made to the variety of igneous rocks present in the CMB in section 2.2.4 and the meager geochronological data available indicates that there is more than one period of igneous activity (Silver and Lumbers, 1966; Bell and Blenkinsop, 1980; Heaman, 1980; Heaman et al., 1980a; Baer, 1981). In this chapter an attempt is made to evaluate the Rb-Sr dating technique as a method for obtaining reliable geological ages for CMB granitoid rocks by comparing the results with the more precise U-Pb zircon technique.

Three units have been selected for detailed study; the

Tallan Lake sill, Methuen Complex and Loon Lake pluton. The isotopic data from these units will be combined with other geochemical and geological information to provide a foundation for discussing the evolution of these granitoid rocks.

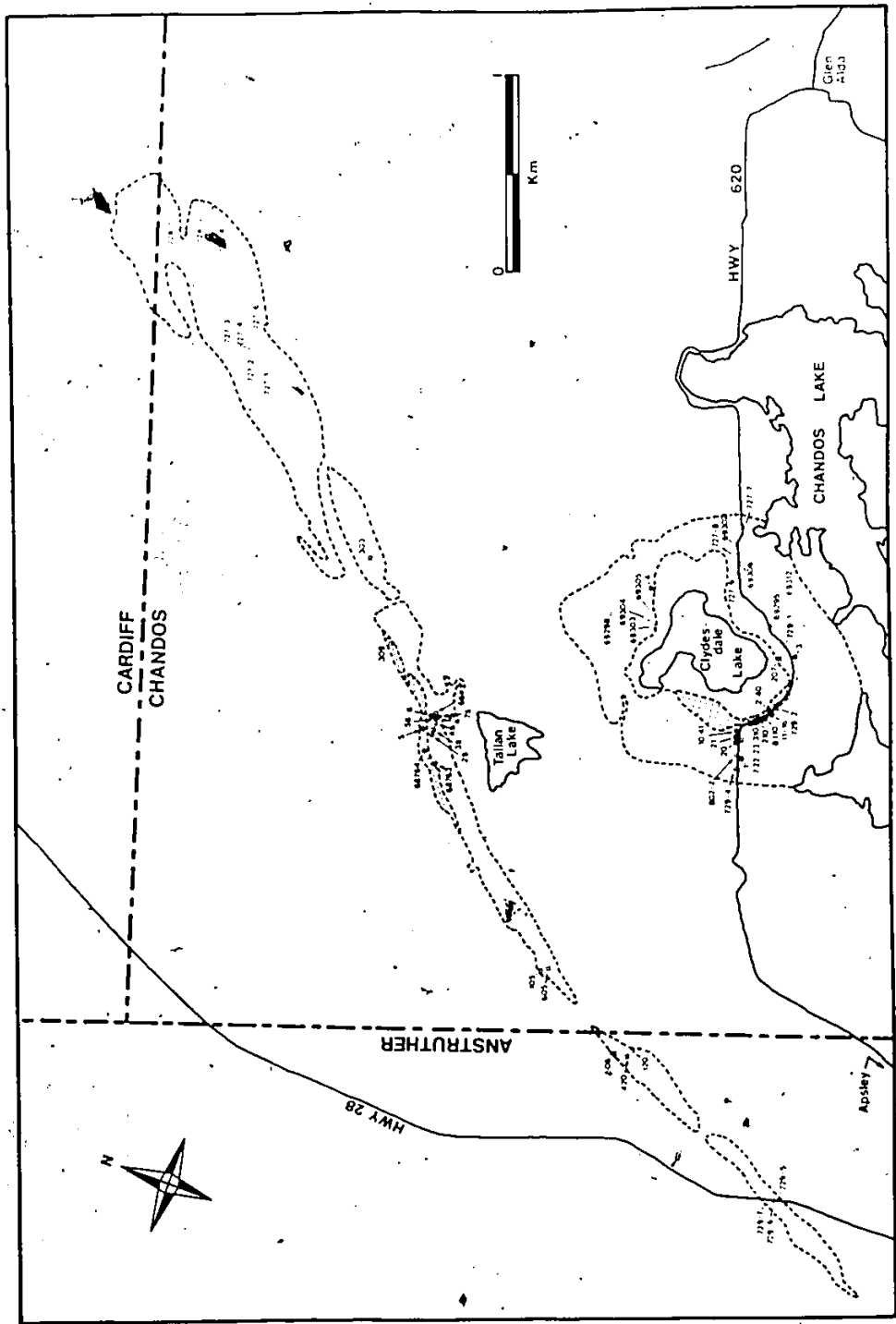
4.2 TALLAN LAKE SILL

4.2.1 Geological Setting

The Tallan Lake sill (TLS) is a NE-SW trending body of amphibolite exposed in the NW portion of Chandos township. There are two outcrop areas of amphibolite presently considered to belong to the sill; the elongated mass north of Tallan Lake (circa 12 km long and 0.3 km wide) that dips 60-70° SE and then re-appears in a domal structure centered around Clydesdale Lake (see Figure 16). The sill is located between marble horizons of the Dungannon Formation and, if truly intrusive, can be used as a unique marker horizon. Field evidence for an intrusive origin is indicated by the presence of a large marble inclusion in an outcrop exposure along Hwy. 620 (Plate 4a) and possible chilled margin (Griep, 1975).

Associated with amphibolite in the two main outcrop areas is a minor amount of felsic rock (Figure 16). Shaw (1962) pointed out the similarity of the felsic rocks in the two outcrop areas and referred to them as syenites. However,

Figure 16 Geological sketch map of Chandos township showing the distribution of rock belonging to the Tallan Lake sill and sample locations. Areas marked with a pattern of crosses represent granodiorite. Solid circles represent samples collected in this study whereas open circles represent samples collected by Kudo (1962) and Shaw (unpublished data) and open squares are from Griep (1975).



most of the samples examined in this study (refer to section 4.2.2 and Table B1.3) contain abundant quartz and are tonalites to granodiorites in the IUGS classification scheme (Figure 17). Although there is some variability in the modal composition of these rocks, in particular K-feldspar abundance, they are referred to as granodiorite throughout this study. Plate 4b illustrates an exposure of foliated granodiorite located immediately south of Clydesdale Lake along Hwy. 620 that is cross-cut by a 25 cm wide felsic dike with coarse-grained margins. Griep (1975) concluded from a petrographic and geochemical study that these rocks are actually part of the sill and the sequence amphibolite grading downward to granodiorite represents an inverted differentiated sill.

To further evaluate the relationship between the amphibolite and granodiorite members of the TLS and the overall evolution of this unit, additional elemental and isotopic data have been obtained to compliment the previous studies by Shaw (1962) and Griep (1975).

4.2.2 Petrography

The following is a summary of the salient petrographic features of the Tallan Lake rocks extracted from the detailed study by Griep (1975) and observations from this study.

The amphibolite samples are medium- to coarse-grained, weakly foliated and consist of amphibole (53%), oligoclase

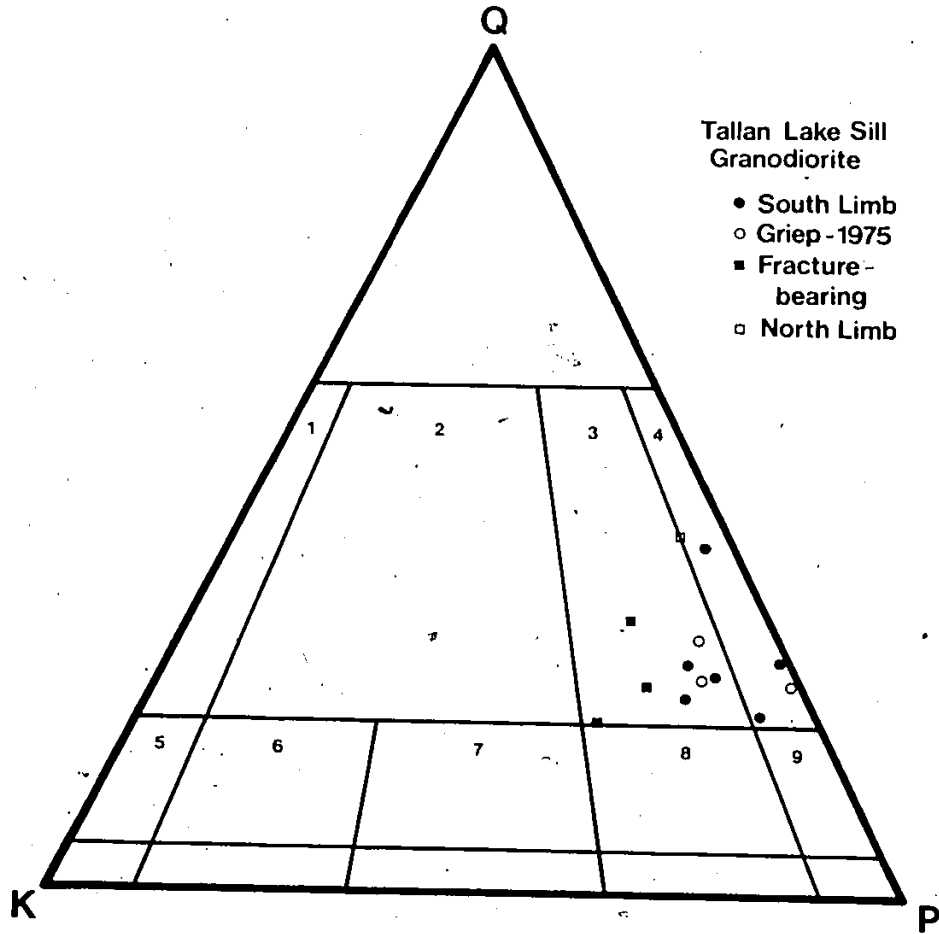
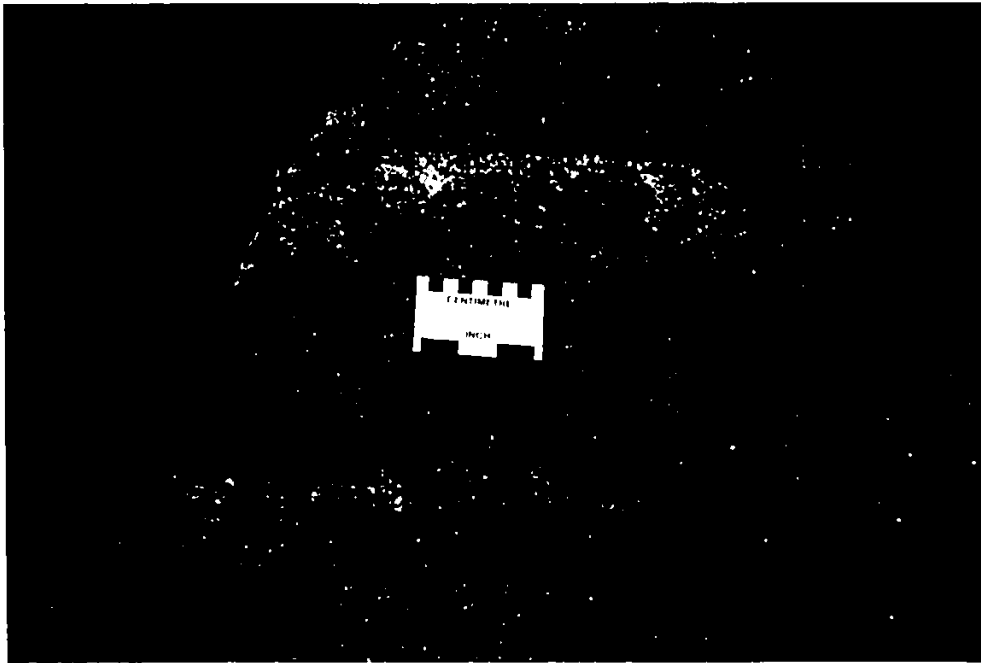
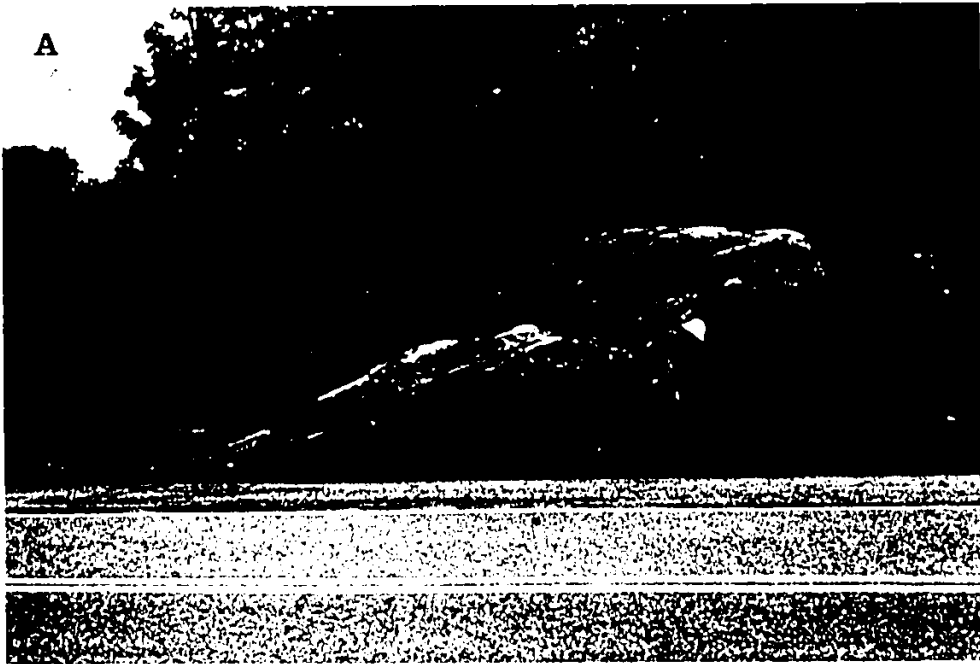


Figure 17 Modal quartz-plagioclase-K-feldspar diagram for samples from the Tallan Lake sill. The various fields are numbered as follows: 1 - Alkali-Feldspar Granite, 2 - Granite, 3 - Granodiorite, 4 - Tonalite, 5 - Alkali-Feldspar Quartz Syenite, 6 - Quartz Syenite, 7 - Quartz Monzonite, 8 - Quartz Monzondiorite, 9 - Quartz Diorite

Plate 4 A - Exposure of the Tallan Lake amphibolite along
Hwy 620 with large marble inclusion (grey)

B - Exposure of the Tallan Lake granodiorite along
Hwy 620 with cross-cutting aplite dike. Note
the large feldspar crystals at the margins



(29%), ilmenite and magnetite (5% combined) with traces of allanite, apatite, biotite, calcite, quartz, sphene, and zircon. Near the amphibolite-granodiorite contact, Griep found that both units contain significant amounts of apatite (up to 7%), cummingtonite (5%) and garnet (2%). One sample examined by Griep (#1317) contains abundant gedrite (19%) and a more detailed microprobe study of this sample (Hawthorne et al., 1980) indicates the presence of a three-amphibole equilibrium assemblage including gedrite-cummingtonite-hornblende. The exposure is not adequate to attempt a comprehensive study of mineralogical variations with depth in the sill but, in a general way, a major mineralogical division was detected by Griep. He noted two varieties of hornblende in the amphibolite samples, a bluish-green and an olive-green variety. The bluish-green variety contains ilmenite inclusions that intersect at right angles and this texture was interpreted by Griep to represent titaniferous clinopyroxene pseudomorphs. In the current position of the sill, the bluish-green variety is absent in samples collected within a 30 meter zone near the amphibolite-granodiorite contact. Note that if the sill is inverted then this variety of amphibole is absent from the upper 30 meters of the amphibolite unit.

A granodiorite outcrop from the south limb of the sill, exposed along Hwy. 620 (Figure 16), has been investigated in detail in this study. In this section, the granodiorite is

medium- to coarse-grained hypidiomorphic granular with an average mode, based on nine samples (Table B1.3), of 47% oligoclase, 21% quartz, 13% biotite, 11% K-feldspar, 7% hornblende, 1% carbonate with subordinate apatite, fluorite, graphite, sphene and zircon. The samples examined from this sampling site have a prominent foliation (Plate 4b and 5b) but generally do not show signs of recrystallization. An exception is sample TL15 which contains a few zones along grain boundaries that are recrystallized to a finer grained polygonal quartz-plagioclase mosaic. These granodiorite samples are also generally free of secondary alteration except for the partial breakdown of hornblende to chlorite along cleavage planes in crystals, grain boundaries and cracks.

However, there are some significant deviations from the average mode reported above. For example, samples TL15 and 16, tonalites in the IUGS classification scheme, contain noticeably more biotite (24 and 26%, respectively) than the other samples (5-17%). In addition, samples identified as containing microfractures, like the one shown in Plate 5b, contain significantly more microcline on average (17%) than the samples without fractures (6%). Other than this greater abundance of microcline, there is no obvious mineralogical difference between the fracture-bearing and fracture-free samples. Griep (1975) also noted the presence of these fractures and claimed they often contain carbonate. The

majority of samples with fractures examined in this study do not contain carbonate mineralization along the fracture. The plagioclase grains near the fractures in some samples show a more severe sericitic alteration but generally the fracture-bearing samples are not associated with any visible alteration. In one fracture-bearing sample, TL12, biotite was observed growing at the expense of plagioclase (Plate 5a). Since these fractures are difficult to recognize at this sampling site, no estimate of fracture density could be made.

The sample collected from the felsic unit in the northern limb of the sill (TL5) has significantly more quartz (Table B1.3) than the majority of granodiorite samples from the south limb and the plagioclase grains exhibit a severe and pervasive alteration to sericite. The altered nature of this sample is also reflected in the presence of a minor amount of secondary muscovite.

4.2.3 Geochemistry

4.2.3.1 Major Elements

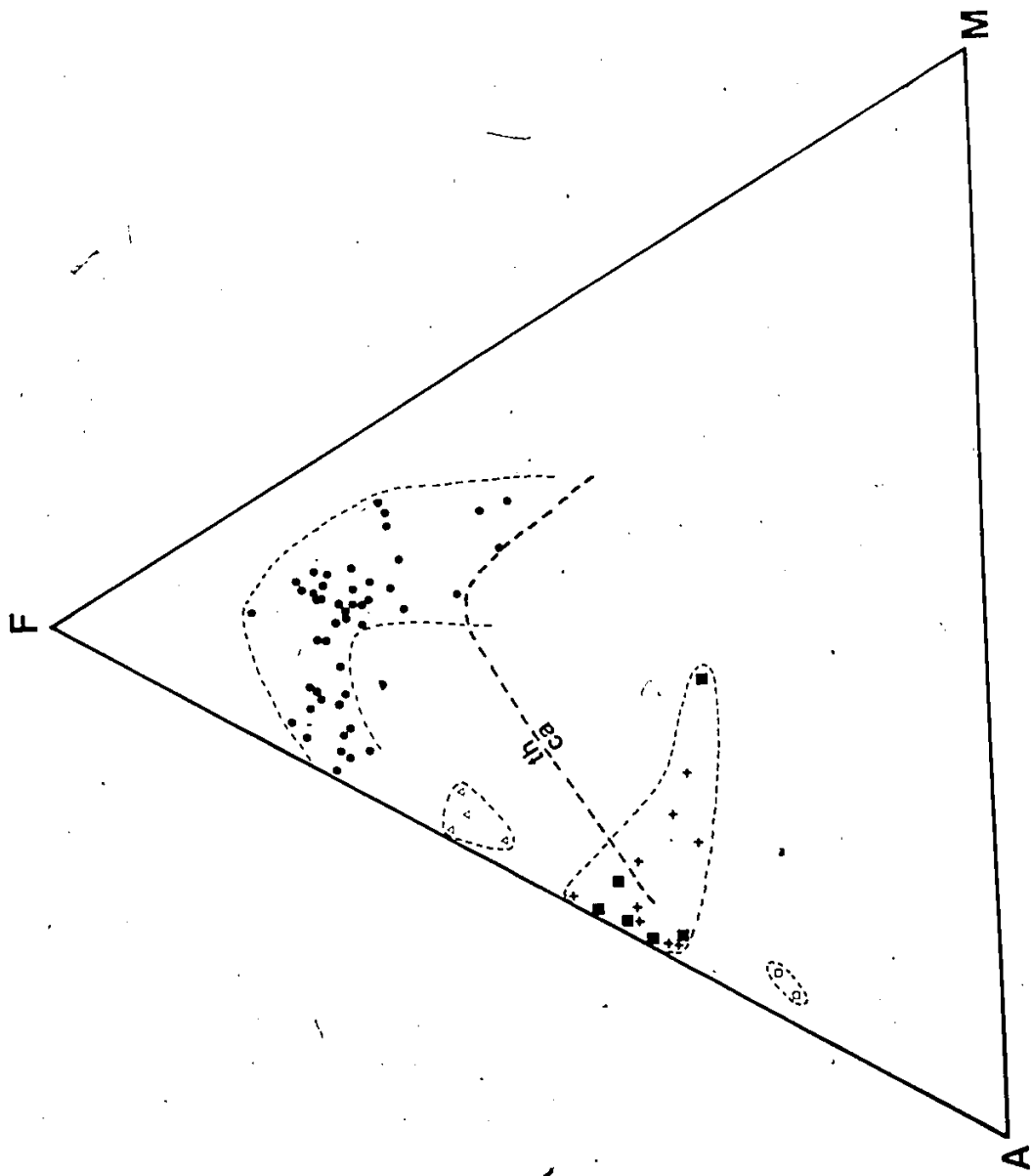
A compilation of major element data available for samples from the TLS is presented in Table B2.3 and include data obtained by two analytical techniques, atomic absorption spectroscopy (AAS) and X-ray fluorescence spectrometry (XRF). The AAS data (denoted by an asterisk in Table B2.3 and 4.1) are from Shaw and Kudo (1965), Griep (1975) and Shaw

(unpublished data) whereas the majority of XRF data were determined in this study, except the results for 11 samples reported by Griep (1975). The analytical procedures used for determining the XRF data are presented in Heaman (1980) and Appendix A2.

In total, 68 samples from the sill have been analysed for major elements. To facilitate comparison, all the data are normalized to 100% excluding loss on ignition. The data for most elements determined by the two techniques agree quite well but the XRF data are presented in Table B2.3 where possible. The two exceptions are Na_2O and MgO where the AAS values are more accurate and precise. Initially, there was a discrepancy between the P_2O_5 values determined by the two techniques, especially the samples with high phosphorus contents (ie. > 1 wt.%). In these cases, the phosphorus content exceeded the levels present in the standards used to define the XRF working curve. Many of the samples were re-analysed for P_2O_5 using a selection of standards with a higher range in P_2O_5 values and these results are in better agreement with the AAS data.

The data presented in Table B2.3 are plotted on a conventional AFM diagram in Figure 18. From this diagram it is clear that the TLS samples can be subdivided into four distinct groups. In order of decreasing total iron content these are amphibolite (high-Fe tholeiite), amphibolite (transitional) and granodiorite from the south and north

Figure 18 An AFM diagram showing the composition of samples from the Tallan Lake sill: solid circles - amphibolite, open triangles - transition, crosses - fracture-free granodiorite from the south limb, solid squares - fracture-bearing granodiorite, open squares - granodiorite from the north limb.



limbs, respectively. Although the data for two groups are meager, the above subdivisions can be distinguished on most major element variation diagrams. Perhaps with more analyses the gaps between adjacent groups might be filled but for the remainder of this chapter this subdivision of the TLS samples will be used. The average major element composition of each group is presented in Table 4.1. By reading across the table from left to right it is apparent that, in addition to a decrease in the average total iron content of each group, there is also a decrease in CaO, TiO₂, MnO and P₂O₅ and an increase in SiO₂ and K₂O.

From a considerably smaller data base, Griep (1975) concluded that the TLS magma has a tholeiitic nature with a strong iron-enrichment trend and is geochemically similar to other differentiated layered mafic bodies such as the Skaergaard and Michikamau intrusions in E. Greenland and Labrador, respectively. The Fe-enriched, tholeiitic nature of the amphibolite samples is clearly illustrated on the AFM diagram in Figure 18. All the amphibolite samples plot above the line separating the tholeiitic from calc-alkaline fields according to the classification scheme of Irvine and Baragar (1972). The field for the amphibolite samples shows a general trend toward extreme iron-enrichment, as previously noted by Griep (1975), followed by a slight increase in alkalis.

One of the most striking features of the data presented in Table B3.2 is the peculiar major element

TABLE 4.1 - The Average Major and Trace Element Composition
for the Four Sample Groups Delineated in Figure 1B

	AMPHIBOLITE			TRANSITION			GRANODIORITE				
	n	X	S	n	X	S	SOUTH LIMB			NORTH LIMB	
	n	X	S	n	X	S	n	X	S	n	X
SiO ₂	48	48.32	4.81	4	63.20	3.95	14	68.98	1.52	2	76.51
Al ₂ O ₃	48	12.78	3.25	4	14.44	1.58	14	14.26	0.92	2	12.80
Fe ₂ O ₃ (t)	40	18.71	3.52	2	9.65	-	11	5.74	0.40	2	2.45
Fe ₂ O ₃	40	3.83*	1.78	3	2.86*	0.34	3	1.76*	0.85	1	0.48*
FeO	40	13.78*	3.48	3	7.71*	0.73	3	4.02*	0.09	1	1.78*
MgO	48	4.07*	2.32	4	0.53	0.35	14	0.71	0.91	2	0.33
CaO	48	8.10	2.03	4	3.33	0.41	14	1.68	0.57	2	0.82
Na ₂ O	48	3.58*	0.90	4	5.71	0.75	14	5.58	0.94	2	4.60
K ₂ O	48	0.71	0.40	4	1.41	0.65	14	2.45	0.67	2	2.41
TiO ₂	48	3.36	0.48	4	0.85	0.30	14	0.40	0.03	2	0.18
MnO	48	0.34	0.09	4	0.24	0.11	14	0.11	0.04	2	0.04
P ₂ O ₅	48	1.01*	0.30	4	0.21	0.09	14	0.08	0.06	2	0.03
As	45	tr	-	2	tr	-	9	tr	-	2	3
B*	7	12.4	4.2	1	7.83	-	4	7.43	1.85	1	13.3
Ba*	34	223	106	1	300	-				1	440
Co*	47	50	11	2	27	-	9	16	4	2	21
Cr*	47	49	54	2	33	-	9	33	25	2	3
Cu	45	74	198	2	tr	-	9	tr	-	2	tr
Hf*	2	13.8	-	1	40	-	1	29	-	1	18
Li*	34	19	9	1	13	-				1	25
Ni*	47	28	15	2	9	-	9	6	5	2	16
Pb	45	11	3	2	15	-	9	7	3	2	tr
Rb	48	21	22	4	29	20	14	57	51	2	25
Sc*	11	40	16								
Sr	48	255	65	2	182	-	14	136	35	2	50
Ta*	2	0.72	-	1	1.9	-	1	1.9	-	1	3.0
Th*	7	1.81	0.75	1	5.8	-	4	9.1	0.8	1	9.6
Tl**	27	588	445	1	150					1	180
V*	47	291	215	2	12	-	9	15	2	2	1
Y	47	96	35	2	203	-	13	290	59	2	234
Zn	45	215	90	2	193	-	9	80	44	2	20
Zr	47	387	390	2	1301	-	13	1089	124	2	491

S - standard deviation

t - Total iron expressed as Fe₂O₃

* - Values determined by Atomic Absorption (Shaw, unpublished data). Scandium was determined by emission spectrograph (Shaw and Kudo, 1965), B by prompt-gamma neutron activation analysis and Hf, Ta and Th by instrumental neutron activation analysis. All others determined by X-ray Fluorescence (Table B2.3). tr - trace

** - All trace element data reported at the ppm level except Tl (ppb).

chemistry of the TLS amphibolites. The high-Fe tholeiitic nature of these samples has already been mentioned but most unusual are the anomalously high TiO_2 (up to 6.44 wt.%) and P_2O_5 (up to 3.69 wt.%) contents of many samples. A review of the major element compositions for other well studied layered mafic intrusions, such as the Skaergaard intrusion in E. Greenland (Wager and Brown, 1967), and differentiated basic sills, such as the Palisades sill in New Jersey (Walker, 1969), indicate that titanium and phosphorus levels above 2 or 3 weight percent are quite rare. Such values are also rare for other amphibolite units studied from the Grenville Province (eg. MacLean et al., 1982). These data, combined with the trace element data reported in the next section, indicate that the TLS magma is either highly evolved, having experienced extreme differentiation, or is a unique magma type. This topic will be discussed in more detail in section 4.2.7.

Another interesting aspect of the amphibolite chemistry is the unusually low CaO and high Na_2O contents of certain samples. The average abundance of these elements reported in Table 4.1 is 8.10 and 3.58 weight percent, respectively, but some amphibolite samples listed in Table B2.3 have CaO contents as low as 5 to 6% (eg. 612S, 68763, 69304, TL4) and Na_2O contents as high as 4 to 5% (eg. 727-8, 728-6, 729-2, 615S, 68763). The anomalous abundances of sodium and calcium in the Tallan Lake amphibolite were also

recognized by Griep (1975) who suggested this probably occurred as a result of spilitization during diagenesis and/or low grade metamorphism. However, it is also conceivable that these anomalous concentrations could be generated by extreme differentiation; a possibility also supported by the high levels of incompatible elements in these samples. Griep (p.53) rejected this hypothesis because of "the difficulty in reconciling alkali contents of the sodic syenites with a simple differentiation mechanism" but there is substantial evidence that the alkali content, especially potassium, has been enriched by late-stage fluid migration (see the ensuing discussion) so differentiation remains a possible explanation. Furthermore, the Na_2O and CaO content of the four transition samples delineated in Figure 18 can be best explained by extreme differentiation of an already highly evolved basaltic magma.

There are two important features of the granodiorite data revealed in Figure 18. The first is that the two granodiorite samples analysed from the northern limb plot in a separate field with what appears to be a higher total alkali content. In fact, the position of the north limb granodiorites in Figure 18 is attributed to a higher SiO_2 and lower total Fe content (compare the data for the two groups in Table 4.1). It is interesting that these data plot within the field for various undeformed pegmatite and aplite dikes from this area (Heaman, unpublished data). The second feature

of the granodiorite chemistry worth noting is the data scatter in the south limb granodiorite field. Some of this scatter appears to be related to the presence of the tiny microfractures alluded to in the previous section. The results from a slab study of one fracture-bearing sample (see below) indicate that there is a profound depletion of MgO in these samples and this might explain why most of the fracture-bearing samples (denoted by solid squares in Figure 18) plot near the AF side of the diagram. Four fracture-free samples (TL8,15,16,40) clearly plot within the calc-alkaline field in Figure 18 and, if these samples are representative of the original granodiorite composition, then it is unlikely that the amphibolite and granodiorite formed by differentiation of a single magma reservoir. One fracture-bearing sample (69303) plotted on Figure 18 appears to be enriched in MgO (refer to Table B2.3).

The chemical composition of the fracture-bearing granodiorite samples has been significantly altered as mentioned above and this alteration has also had a profound effect on the Rb-Sr system (section 4.2.5.1). In order to better understand the nature of this alteration, a detailed investigation of one fracture-bearing sample (TL12) was performed. This sample was sliced into approximately 1 cm slabs parallel to the orientation of the fracture to determine the extent of element and isotopic mobility caused by fluid interaction along the fracture. The location of the

- Plate 5 · A - Photomicrograph of Tallan Lake fracture-bearing granodiorite showing the secondary growth of biotite at the expense of feldspar
- B - Sample of Tallan Lake granodiorite (TL12) that was used for the slab study. The slab containing the fracture is labelled 12FR
- C - Three samples from the Methuen Complex illustrating the variety of rock types present



two slabs that are discussed in detail below are shown in Plate 5b. A slab containing a fracture (TL12FR) and a second slab sliced approximately 4 cm away from the fracture (TL12F) have been analysed for major and trace elements and strontium isotopes. There is no petrographic evidence that slab TL12F was affected by fluid interaction but immediately adjacent to the fracture the plagioclase is more severely sericitized and there is a slight increase in the amount of K-feldspar. The major element data for these two slabs is presented in Table 4.2 combined with the average composition for three samples (TL8, 15 and 16), collected from the same outcrop, that do not contain fractures. It is difficult to establish whether any of the nine granodiorite samples collected from this sampling site have been entirely unaffected by fracturing, however, these three samples are the least affected. The enrichment/depletion factors reported in Table 4.2, and presented graphically in Figure 19, were calculated by dividing the slab composition by the presumed unaltered whole rock composition (ie. column 1 in Table 4.2). Values less than 1 indicate element depletion whereas values greater than 1 indicate element enrichment. The elements plotted in Figure 19 are arranged in order of increasing atomic number.

There are two important results from this slab study. From Figure 19 it is clear that the presence of these microfractures has a profound effect on the sample composition, causing substantial enrichments in P, K, Ca and

Figure 19 Enrichment/depletion patterns determined for a fracture-bearing granodiorite sample (TL12). Solid bars represent the composition of a slab containing a fracture while open bars represent the composition of a slab collected 4 cm away from the fracture. The elements are arranged according to increasing atomic number.

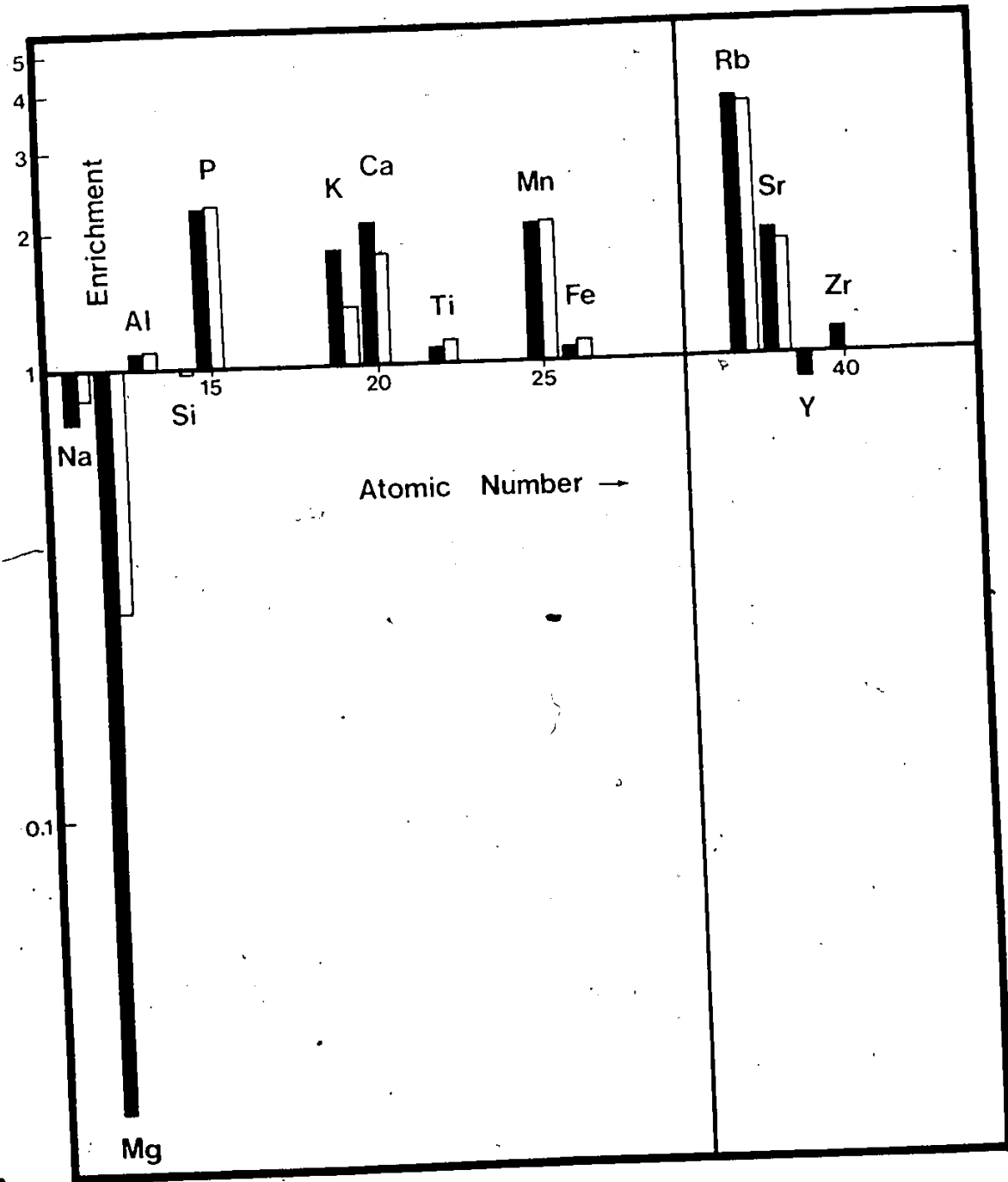


TABLE 4.2 - The Major and Trace Element Results from the TL12 Slab Study

	1	TL12FR	2	TL12F	3
SiO ₂	69.85	69.48	1.00	69.25	0.99
Al ₂ O ₃	13.95	14.42	1.03	14.52	1.04
Fe ₂ O ₃	5.31	5.43	1.02	5.80	1.09
MgO	1.86	0.05	0.02	0.54	0.29
CaO	0.86	1.76	2.05	1.52	1.77
Na ₂ O	5.64	4.37	0.78	4.81	0.85
K ₂ O	2.19	3.86	1.76	2.90	1.32
TiO ₂	0.37	0.39	1.05	0.41	1.11
MnO	0.07	0.14	2.00	0.14	2.00
P ₂ O ₅	0.05	0.11	2.20	0.11	2.20
Rb	41	150	3.66	148	3.61
Sr	81	148	1.83	146	1.80
Y	298	265	0.89		
Zr	1020	1157	1.13		

- 1 - The average chemical composition of TL8, 15 and 16
 2,3 - Enrichment/Depletion factor calculated by dividing the individual slab composition by the unaltered sample chemistry (column 1).

Mn and depletions in Mg and to a lesser extent Na with relatively little effect on the Al, Si, Ti and Fe abundances. The effect of Mg depletion has already been mentioned above with regard to position of the granodiorite samples on an AFM diagram and mobility of Mg may also explain some of the data scatter observed for the amphibolite samples. The second conclusion is that although the enrichment and depletion of certain elements is greater near the fracture there is still evidence of element mobility up to 4 cm or more away from the fracture (compare the data for the two slabs in Figure 19). This is particularly interesting because there is no convincing petrographic evidence for extensive fluid

interaction in this sample.

4.2.3.2 Trace Elements

Over the past 20 years samples from the Tallan Lake sill have been analysed for a number of trace elements utilizing a variety of analytical techniques. A list of 30 trace elements are presented in Table B2.3 and, although some of these elements have been analysed by more than one technique, only the best estimates are listed. The majority of data listed for Li, V, Cr, Co, Ni, Ba, Tl, determined by Atomic Absorption Spectroscopy (Shaw, unpublished data), and Sc, determined by Emission Spectrograph (Shaw and Kudo, 1965), were already available at the time of this study. In this study, most of the Tallan Lake sill samples were analysed for Cu, Zn, As, Rb, Sr, Y, Zr, Nb, and Pb (X-ray Fluorescence Spectrometry - XRF) and a few for REE, Hf, Ta, Th (Instrumental Neutron Activation Analysis - INAA), B and Gd (Prompt-Gamma Neutron Activation Analysis - PGNAA) to compliment the existing data base. The analytical procedures for determining trace element abundances by XRF, INAA and PGNAA are presented in Appendix A. A summary of the average trace element composition for the four groups delineated in the previous section are presented in Table 4.1.

Lithium and Boron

The average abundance of Li and B in the amphibolite

samples is 19 and 12 ppm, respectively (Table 4.1). The abundance of B in these samples is between the B content of relatively unaltered basalts (0 to 3 ppm; Bergeron et al., 1983) and continental spilites from the French Alps (60 to 90 ppm; *ibid*). If B is enriched during hydrothermal alteration and spilitization, as indicated by the enriched nature of the spilites from the French Alps and the experimental data from Seyfried et al. (1984), then the relatively high Na contents of the Tallan Lake samples might be expected to correlate with high B contents if they have experienced spilitization as suggested by Griep (1975). The fact that there is no such correlation indicates that either spilitization is not the reason for the high Na content of some Tallan Lake amphibolite samples or the B content, enriched by spilitization, was subsequently depleted by amphibolite grade regional metamorphism.

The Li content of some amphibolite samples (the total range of Li concentrations is 7 to 123 ppm) overlaps with the Li content reported for unaltered, highly evolved island arc basalts from St. Vincent (6 to 12 ppm; Dostal et al., 1983) so the samples with less than 15 ppm Li could represent primary abundances. However, a number of samples are enriched in Li and these high Li values, assuming Li follows the behaviour of B, could be a result of alteration and/or regional metamorphism.

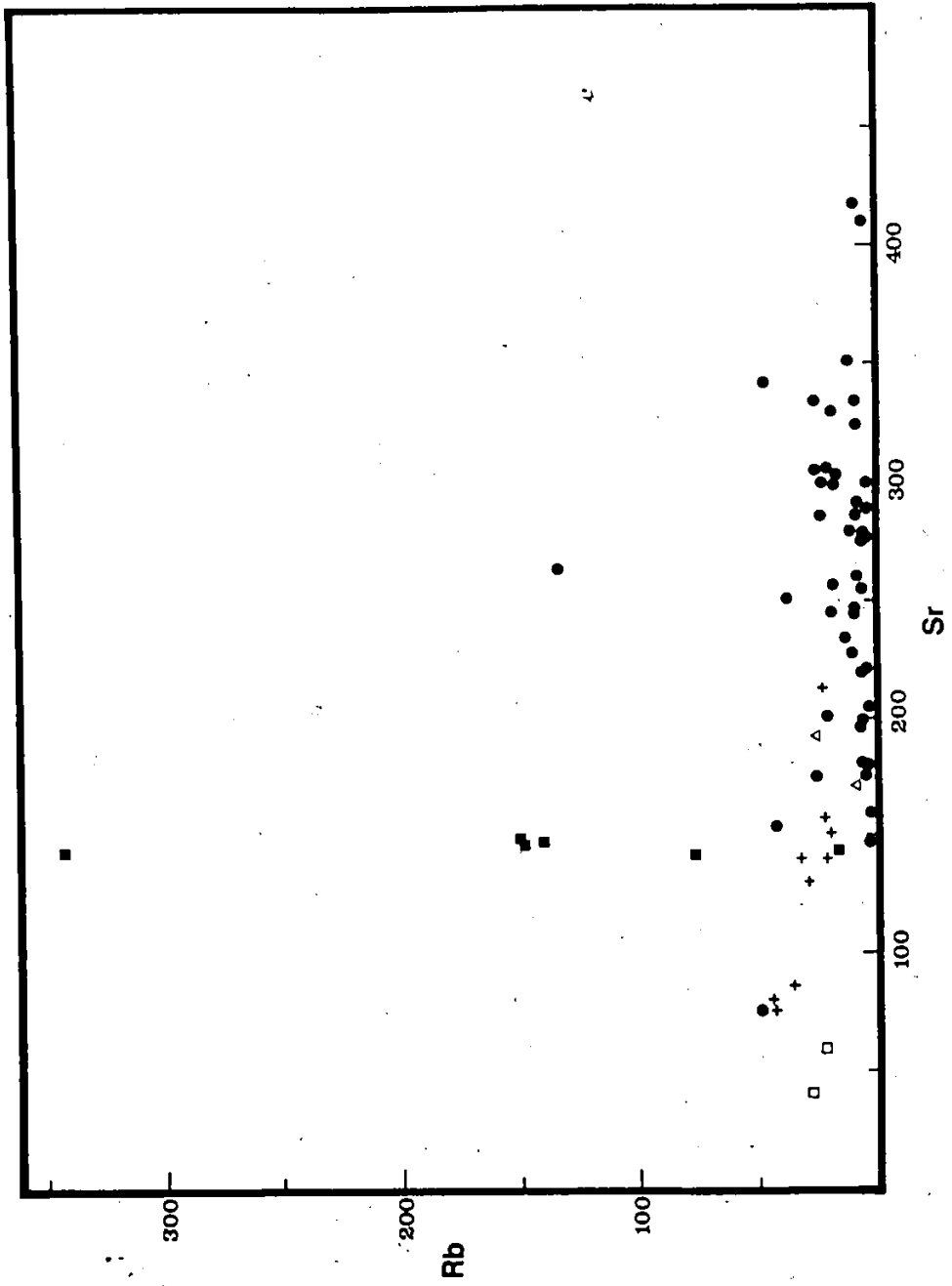
Chromium and Nickel

The Tallan Lake amphibolite samples contain unusually low concentrations of Cr and Ni compared to other differentiated mafic sills (eg. the Palisades Sill; Walker, 1969), layered mafic intrusions (eg. the Skaergaard Intrusion; Wager and Brown, 1967) and other mafic volcanic rocks in the CMB (eg. Condie and Moore, 1977; MacLean et al., 1982; Holm et al., 1984). For example, compared to the average Ni and Cr content in samples from the Palisades Sill (84 and 189 ppm, respectively; Walker, 1969), the Tallan Lake samples are somewhat depleted in these elements (the average Ni and Cr content is 28 and 49 ppm, respectively, Table 4.1). One possible explanation for these low Ni and Cr concentrations is that prior to the emplacement of the sill a significant quantity of olivine and/or clinopyroxene crystallized and settled out of the magma. A model to explain the highly evolved geochemical nature of the Tallan Lake samples will be developed in section 4.2.7.

Rubidium and Strontium

The Rb and Sr data for samples from the Tallan Lake sill are shown in Figure 20 and most samples have Rb and Sr contents close to the average values reported in Table 4.1. A prominent feature on this diagram is the anomalously high Rb contents of several granodiorite samples (eg. 69303, TL12, TL23) and two amphibolite samples (69311, TL20). In the case

Figure 20 Rb-Sr variation diagram for samples from the Tallan Lake sill. Symbols are the same as for Figure 18.



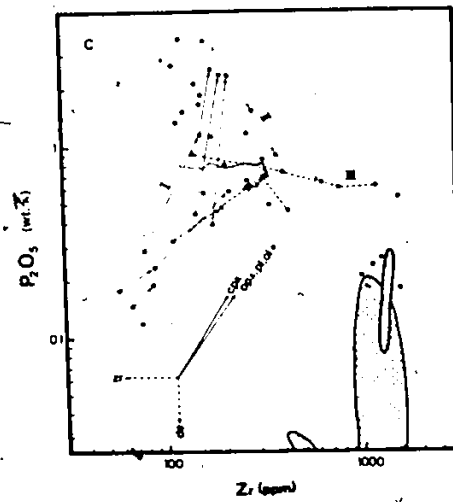
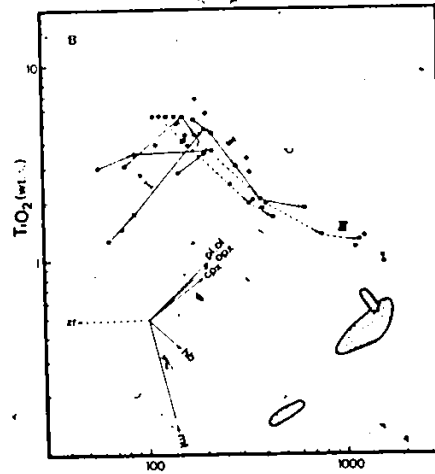
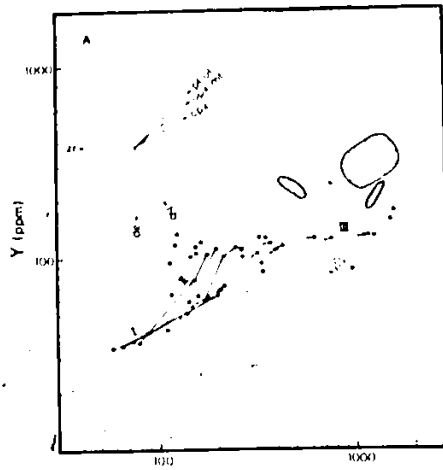
of the granodiorite samples, the Rb enrichment in certain samples can be correlated with the presence of microfractures (refer to the slab study results in Figure 19) and it is probable, although not observed, that the overall chemistry of the amphibolite samples that show this Rb enrichment has been modified by fluid:rock interaction. The association of alkali enrichment with the presence of microfractures will be discussed further in the section 4.2.5.1.

Yttrium and Zirconium

Incompatible trace elements like Y and Zr are particularly useful for characterizing mafic igneous rocks in shield regions because they are relatively immobile elements during metamorphism (eg. Pearce and Cann, 1973; Smith and Smith, 1976; Morrison, 1978). Taking this into consideration, three incompatible element variation diagrams for the Tallan Lake samples are plotted in Figure 21; a) Y-Zr, b) TiO_2 -Zr and c) P_2O_5 -Zr. In all three variation diagrams the results for the amphibolite samples are indicated by closed circles while the other three sample groups are represented as variously shaded fields. In the previous section, reference was made to the anomalously high levels of Ti and P in the amphibolite samples compared to other differentiated mafic suites and this enrichment in incompatible elements is further substantiated by the anomalously high Y and Zr contents in these same samples.

8

Figure 21 Incompatible element variation diagrams for samples from the Tallan Lake sill. a) Y versus Zr, b) TiO_2 versus Zr and c) P_2O_5 versus Zr. The amphibolite samples are represented by solid circles. The fields for transition (dotted pattern), granodiorite from the south limb (cross pattern) and granodiorite from the north limb (random slash pattern) are also shown. The roman numerals refer to specific trends discussed in the text and the mineral vectors represent the composition of a magma crystallizing 50% of the indicated minerals.



The granodiorite samples from the south and north limbs plot in distinctly different fields in Figure 21 with the latter group having distinctly lower Zr and TiO_2 abundances. The significant compositional difference between these two groups on most major and trace element variation diagrams and the similarity between the north limb granodiorite samples and undeformed pegmatite samples from this region indicate that these two granodiorite occurrences are probably not genetically related.

One of the main questions concerning the Tallan Lake sill is the relationship between the granodiorite and amphibolite members. Griep (1975) concluded that both members are part of the same differentiated body. The data presented in Figure 21 could be interpreted in terms of a continuous fractional crystallization model where the amphibolite, transition and granodiorite samples represent progressively more differentiated magma compositions. However, there are two problems with this model. The first is that many of the granodiorite samples have lower Zr contents than some of the amphibolite samples, a feature not easily explained by continuous fractional crystallization. The second problem is that for a mafic magma crystallizing minerals such as clinopyroxene, orthopyroxene, plagioclase, magnetite and possibly even zircon and apatite it is impossible to explain the magnitude of the enrichment in incompatible elements if the starting magma composition is similar to the sample with

the lowest incompatible element content (ie. 72B-3; Table B2.3). This problem will be discussed in more detail later (section 4.2.7).

To evaluate the chemical evolution of the sill further, a series of tie-lines connecting samples that have been collected approximately perpendicular to the strike of the sill have been drawn in Figure 21. The solid and dashed lines represent traverses across the northern and southern limbs of the sill, respectively. For all traverses, the direction of the arrows indicates the relative position of the samples from the present stratigraphic top to bottom (refer to Figure 27). For example, the tie-lines in Figure 21a all point towards the right side of the diagram. Therefore, a sample at the extreme left of any given trend is closer to the stratigraphic top, whereas a sample at the extreme right is closer to the stratigraphic bottom. These trend lines indicate that Y and Zr (Figure 21a) increase systematically from top to bottom but Ti and P (Figures 21b and c) show an initial enrichment followed by a depletion of these elements towards the bottom.

By constructing these crude traverse lines it is possible to delineate three general patterns in the data, denoted by the roman numerals I, II, and III in Figure 21. The change from pattern I to II in Figures 21b and c is marked by the abrupt change in slope at about 150 ppm Zr. Pattern III in all the diagrams is only seen in samples with

high Zr contents and is characterized by a trend with nearly zero slope (ie. there is very little change in Y, TiO_2 and P_2O_5 contents with increasing Zr levels. These trends are interpreted to be primary magmatic variations reflecting changes in the dominant crystallizing phases that control the trace element composition of the Tallan Lake sill magma and will be discussed further in section 4.2.7.

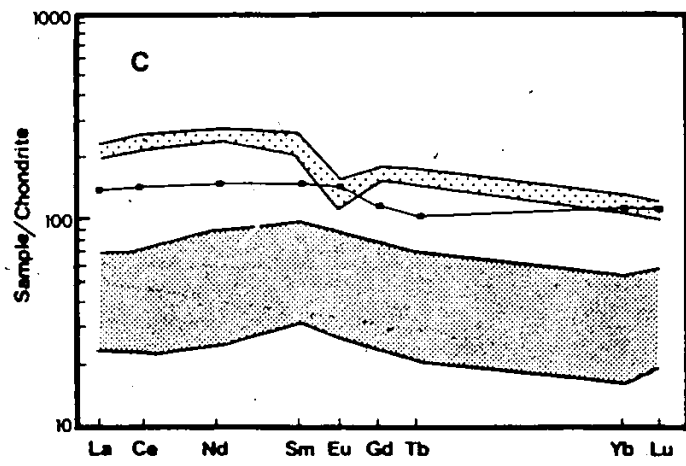
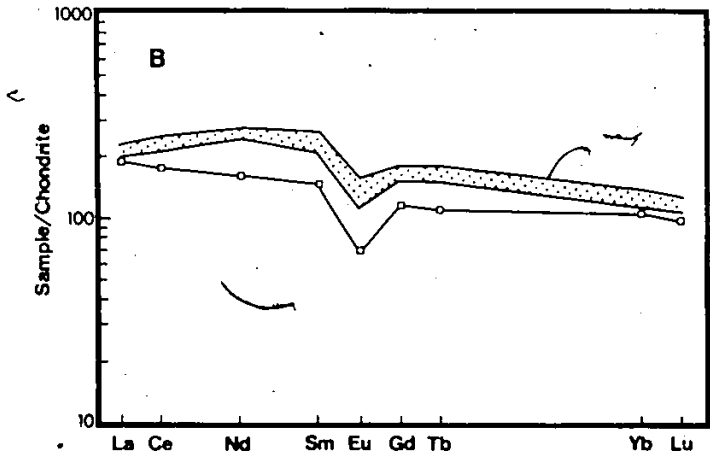
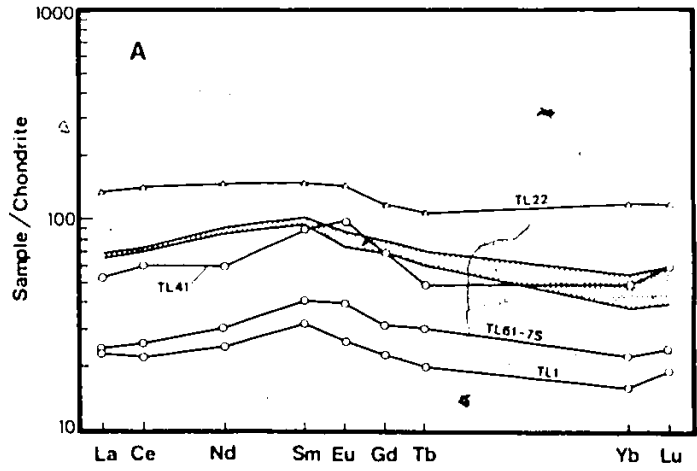
Rare Earth Elements

The chondrite normalized rare earth element patterns for 13 samples from the Tallan Lake sill are shown in Figure 22. Included in this diagram are separate diagrams for samples from the amphibolite and granodiorite members (Figure 22a and b, respectively) and a composite diagram (Figure 22c).

The REE data for four granodiorite samples from the south limb of the sill (Figure 22b) all show identical patterns with nearly flat LREE and slightly fractionated HREE trends with prominent negative Eu anomalies. It was demonstrated in previous sections that the major and trace element composition, especially the alkalis, for one of these samples (TL12) has been altered by fluid:rock interaction but there is no indication that this chemical modification has affected the total REE content or pattern. The REE data for one sample from the north limb granodiorite (TL5) is also included on this diagram (open squares) and,

Figure 22 - Chondrite normalized rare earth element patterns for sample from the Tallan Lake sill; a) amphibolite samples, b) granodiorite samples (open triangle - transition sample) and c) composite.

2



compared to the south limb granodiorite, has a lower total REE content with a more fractionated LREE trend.

The REE patterns for seven mafic samples from the sill, presented in Figure 22a, display a variety of trends with large variations in the total REE content. However, it is clear that the high total REE content in these samples compared to other mafic volcanic rocks in the CMB (eg. Condie and Moore, 1977; MacLean et al., 1982) is consistent with the conclusion reached above that the Tallan Lake amphibolite samples are anomalously enriched in incompatible elements. The C_{Eu}/Y_N value for all samples is greater than 1 (the total range is between 1.2 and 1.9) indicating that there is a slight fractionation from LREE to HREE. A characteristic feature of these patterns is the general enrichment in the middle REE with a slightly positive to negligible Eu anomaly. To investigate the REE variation with depth in the sill a series of five samples (the TL61 series) collected along a traverse perpendicular to the north limb of the sill have been analysed. The following sample sequence indicates the relative position of these samples within the sill starting from the stratigraphic top; T161-7S, 5S, 4S, 3S and 2S (see Figure 27). The stippled pattern in Figure 22a encompasses the REE patterns for the five samples T1612S-5S. It is interesting that most of these samples have identical LREE trends and content and only show variations in the HREE. This could be explained by fractional crystallization of a

mineral phase that concentrates the HREE such as clinopyroxene, orthopyroxene, amphibole or zircon. These data alone suggest that there is no significant variation in the abundance of the REE with depth. However, the sample collected closest to the stratigraphic top (TL61-7S) clearly has a much lower total REE content. The two samples collected from the south limb (TL1 and TL41) also show this difference in total REE content between samples collected near the stratigraphic top and the other samples (ie. the position of sample TL1 within the sill is closer to the stratigraphic top than TL41). The unique REE content of the samples from near the top of the sill can be interpreted in three ways: 1) these samples may represent a primitive magma composition that subsequently evolved by differentiation to produce the high total REE contents observed in the other samples, 2) they may represent a cumulate part of the sill where minerals that do not concentrate the REE have accumulated or 3) they may represent a separate and geochemically distinct magma batch.

In a previous section, a geochemically distinct group of samples from the sill was recognized and called transition because their composition field often falls between the fields for amphibolite and granodiorite on major and trace element variation diagrams. The REE pattern of one transition sample (TL22) is presented in Figure 22a. This sample has the highest total REE content of the mafic samples analysed and

has Eu, Yb and Lu contents similar to those obtained for the granodiorites (see Figure 22b). The overall pattern of this sample is similar to the patterns observed for the other amphibolite samples except for a slight enrichment in the HREE.

A summary of the REE data presented in Figures 22a and b is presented in Figure 22c and some general statements can be made concerning the possible relationship between the amphibolite and granodiorite members. The total REE content of the granodiorite suite is distinctly higher than the amphibolite unit but the general flatness in the trends for both units suggests that they are possibly cogenetic and related by magmatic processes. It is unlikely that a granodioritic magma could be generated from a basaltic source with a REE pattern and content similar to those observed in the Tallan Lake granodiorite (refer to Barker et al., 1976). As an aside, the range in Sm/Nd ratios obtained for the amphibolite samples (0.310 to 0.456) is large enough that a Sm-Nd age could be determined for this unit which would provide an interesting comparison with the U-Pb zircon and Rb-Sr whole rock ages reported in the next two sections.

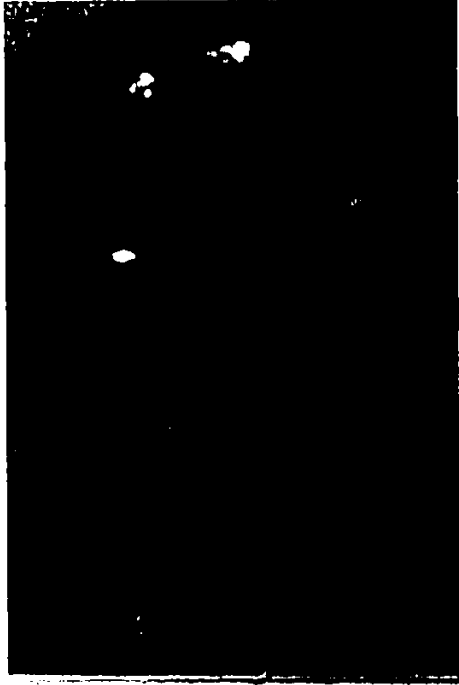
4.2.4 U-Pb Zircon Geochronology

The Tallan Lake sill is an important marker horizon within the supracrustal sequence that occurs in the study area so a precise age for the emplacement of this sill would

also provide a good estimate for the end of volcanism and associated sedimentation in this area. Two samples from the sill were collected for a U-Pb zircon study, one granodiorite (TL40) and one amphibolite (TL41) weighing 20 and 25 kilograms, respectively.

The U-Pb data for six zircon fractions from the sill are presented in Table B4 and Figure 23. Four of the six fractions were separated from the granodiorite sample (open ellipses) and the remaining two are from the amphibolite sample (ellipses with solid circles). All the zircon fractions analysed were hand picked from a single population consisting of euhedral, colourless, prismatic grains. An example of a bulk zircon population from sample TL40 is shown in Plate 6a. The selected grains are devoid of inclusions or visible alteration and have been abraded to remove the outer surfaces. An example of the zircon grains from sample TL41 after abrasion is shown in Plate 6b. It was much more difficult to obtain a large amount of good quality zircon from the amphibolite sample because many of the grains have large magnetite inclusions so many of the grains ended up in magnetic splits during mineral separation using a Frantz isodynamic separator. Most of the zircon fractions analysed were selected from the least magnetic (zero degree tilt, non-magnetic) split from a Frantz isodynamic separator and differ only in the degree of abrasion, the number of grains analysed and the presence or absence of a few cracks. One

- Plate 6
- A - Bulk zircon fraction (+100 mesh) from the Tallan Lake granodiorite (TL40). A single zircon grain in each Plate is approximately 0.1 micron in diameter
 - B - Abraded zircon fraction from the Tallan Lake amphibolite (TL41)
 - C - Bulk zircon fraction (+200 mesh) from the Loon Lake quartz monzonite (LLZ2)
 - D - Abraded zircon fraction from the Loon Lake quartz monzonite (LLZ2). These are a few grains from fraction #21 in Table B4

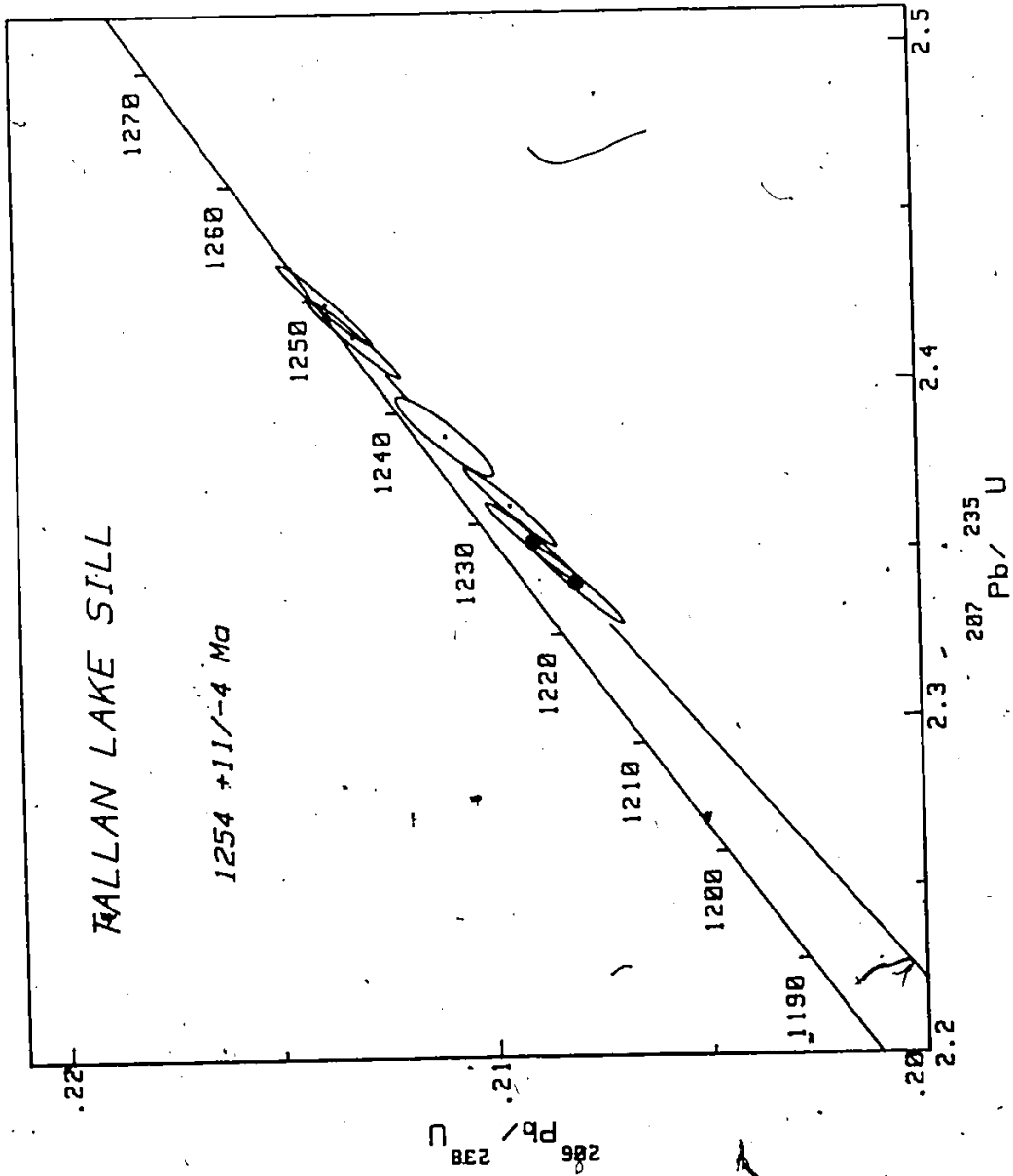


exception is fraction #7 (Table B4). This fraction also consisted of good quality zircon but the grains were smaller (-200 mesh) and more magnetic.

Three features of the U-Pb data are readily discerned from Figure 23; 1) all the zircon fractions analysed are less than 10% discordant, 2) all four fractions from the granodiorite sample are less discordant than the two fractions from the amphibolite sample and 3) zircon fractions from both samples plot on, or very close to, the same discordia line. This latter point is somewhat of a surprise because the amphibolite sample was originally collected to determine the time of metamorphism. Rocks of basaltic composition rarely contain primary zircon but their high grade metamorphic counterparts commonly contain metamorphic zircons formed, in part, with zirconium released during the breakdown of clinopyroxene to amphibole. The Tallan Lake amphibolite apparently contains primary igneous zircon.

The two least discordant fractions in Figure 23 (0.9 and 1.5% discordant, respectively) are so close to concordia that their $^{207}\text{Pb}/^{206}\text{Pb}$ ages (1251 and 1249 Ma) are a reasonable estimate for the time of emplacement of the granodiorite and perhaps the sill as a whole. A slight correction has been made to the data from fraction #4 (Table B4) to compensate for a 3 Ma shift in the $^{207}\text{Pb}/^{206}\text{Pb}$ age that occurs for overspiked analyses. The fact that these two

Figure 23 Concordia diagram for zircon fractions from the Tallan Lake sill. Open ellipses represent U-Pb data for zircon fractions from a granodiorite sample, solid ellipses are data obtained for zircon fractions from an amphibolite sample.



fractions were given the most severe abrasion treatment and have a total common Pb content (13 and 10 pg.) close to the total Pb blank indicates that all the common Pb in these zircons must reside near the surface of the grains. These exceptionally low total common Pb values provide a maximum estimate for the total Pb blank. The greater discordance observed for the remaining samples corresponds with higher common Pb contents (up to 91 pg.) and reflects the effect of analysing zircon grains that contain a few cracks or grains where the outside surfaces have not been completely removed by abrasion.

The four zircon fractions from the granodiorite sample define a discordia line (97% probability of fit) that has an upper intercept age of $1254 \pm 23/-4$ Ma (at the 95% confidence level) and a lower intercept age of 678 Ma. This precise upper intercept age of 1254 Ma is interpreted as the time of zircon crystallization during emplacement of the granodiorite. If all six zircon fractions are combined, there is no change in the upper intercept age but there is a reduction in the associated error (ie. $1254 \pm 11/-4$ Ma). However, including the two fractions from the amphibolite sample reduces the probability of fit to 86% so it is possible that this sample is slightly younger than the granodiorite sample. Additional zircon analyses will be required to test whether there is a significant age difference between these two units. At present, a difference

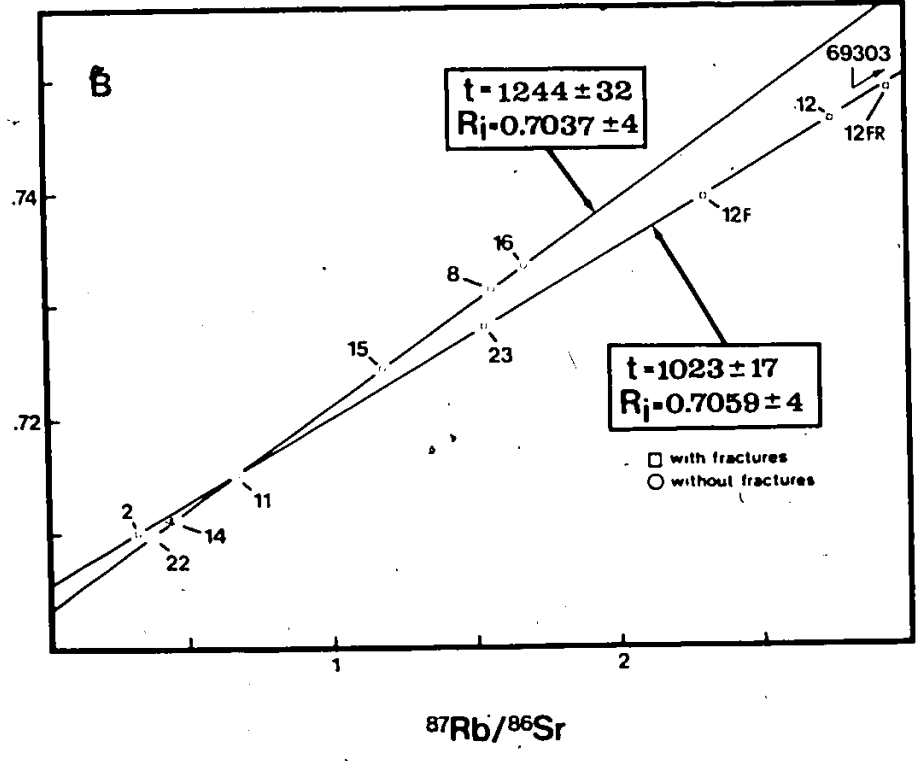
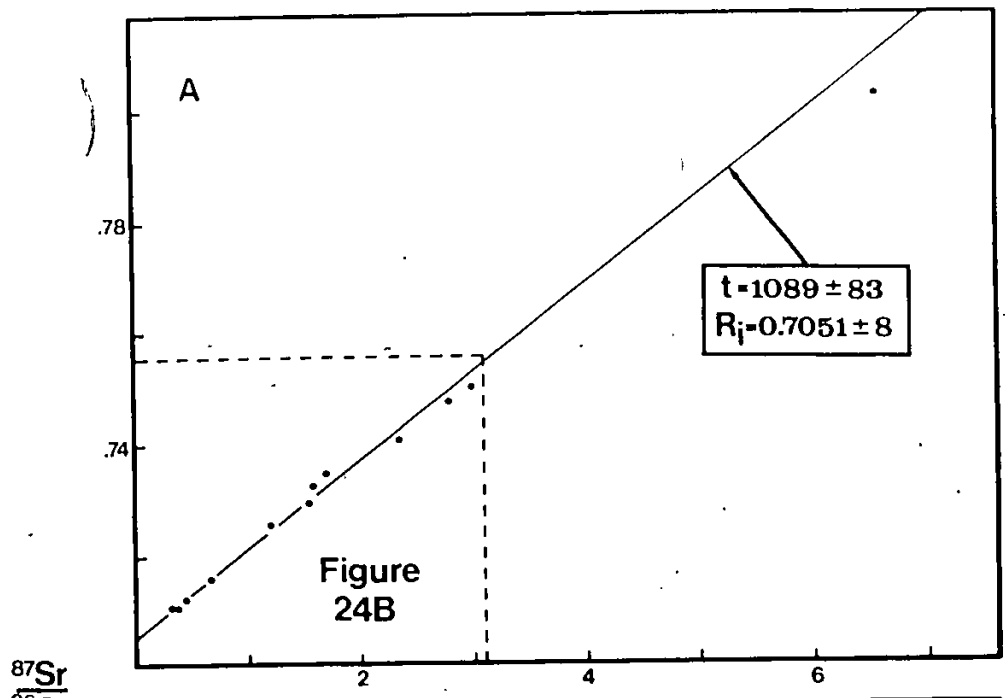
in ages is suggested if the amphibolite zircon data are treated separately (ie. 1239 Ma).

4.2.4 Rb-Sr Geochronology

4.2.5.1 Granodiorite

The Rb-Sr data for ten whole rock samples and two slab sections from one granodiorite sampling site (south limb) are presented in Table B3.3 and Figure 24a. If all the data are combined, the scatter about a best-fit regression line is in excess of analytical error (MSWD=25.7). The slope of this errorchron corresponds to an age of 1089 ± 83 Ma with an elevated initial strontium isotope ratio (R_i) of 0.7051 ± 8 . One sample (69303) has a significantly higher Rb/Sr ratio than the other samples and, at first glance, may be suspected of controlling the Rb-Sr regression results but excluding this sample has only a minor effect on the age calculation ($t=1103$ Ma; $R_i=0.7050$; MSWD=25.5). The source of this "geological error" becomes apparent when the samples are subdivided into fracture-bearing and fracture-free. It has been mentioned already that the fracture-bearing samples are distinguished by a higher modal proportion of K-feldspar and this appears to correlate with Rb concentration. The average Rb content for the 6 samples without fractures is 33 ppm, a value considerably lower than the average (178 ppm) for three of the four fractured samples (TL12, TL23, 69393). One

Figure 24 Rb-Sr whole rock data for samples from the Tallan Lake granodiorite (south limb); a) composite diagram and b) data subdivided based on fracture-bearing (open squares) and fracture-free (open circles). Sample 12FR represents a thin slab from sample 12 that contains a fracture and sample 12F represents a slab sliced 4 cm away from the fracture.



fracture-bearing sample (TL2) is depleted in Rb (16 ppm), compared to the fracture-free samples, even though it also contains abundant K-feldspar.

The results for the six fracture-free samples are treated separately in Figure 24b. The fracture-free sample with the lowest Rb/Sr ratio (TL22) was classified as a transition sample in a previous section, but considering the incompatible element content of this sample it is considered to be genetically related to the granodiorite member. Excluding this sample from the regression treatment has a negligible effect on the calculated age. The best-fit regression line through these data defines a much more precise age of 1244 ± 32 Ma, compared to the composite age reported above, with no detectable scatter outside analytical error (MSWD=0.92). This age is also in excellent agreement with the U-Pb zircon age of 1254 Ma determined using a sample collected from the same outcrop. Therefore, by considering only the samples that are fracture-free, a geologically meaningful Rb-Sr whole rock age is obtained for the granodiorite that does not appear to be affected by subsequent geological disturbances. The initial strontium ratio for the six fracture-free samples is 0.7037 ± 4 and is within the "normal" range for CMB granitoid rocks (refer to Chapter 5.5).

A second Rb-Sr whole rock isochron is obtained for the same outcrop when the fracture-bearing samples are evaluated

separately. The results for four fracture-bearing samples plus the two slab sections from one of these fracture-bearing samples (TL12, see Plate 5b) are treated separately in Figure 24b. The slope of the best-fit regression line corresponds to an age of 1023 ± 17 Ma ($R_i = 0.7059 \pm 4$) with no detectable scatter outside analytical error ($MSWD = 0.38$). The relatively small error associated with this age reflects both the colinearity of the data and the large variation in the Rb/Sr ratio. This age is considerably younger than the age defined by the samples without fractures (1244 Ma) and the age of zircon crystallization (1254 Ma) and represents the time when Rb and Sr ceased to migrate along these fractures. Therefore, the formation of fractures and ensuing fluid migration occurred some 200 Ma or more after the sill was emplaced.

Perhaps the most convincing evidence that these fractures have been instrumental in resetting the Rb-Sr whole rock system, at least on the scale of a few centimeters, is the result obtained from the slab study. Compared to the total rock Rb content of 140 ppm for sample TL12 the slab containing the fracture (TL12FR) is enriched in Rb (149 ppm) while the slab a few centimeters away from the fracture contains significantly less Rb (121 ppm) with only a slight decrease in Sr abundance. Therefore, the total rock Rb content is dominated by the Rb introduced by fluid-rock interaction along the fractures. This effect is evident on Figure 24b. The slab that contains the fracture plots to the

right and of the total rock value but still lies on the 1023 Ma isochron whereas the slab that was sliced 4 cm away from the fracture, which also lies on the 1023 Ma isochron, plots to the left of the total rock value. Although the Rb content of the slab containing the fracture has more influence on the total rock Rb-Sr system, it is interesting that the introduction of Rb via fluids migrating along these fractures also has a profound effect on the behaviour of the Rb-Sr system in the slab sliced 4 cm away from the fracture even though there are no visible signs of alteration. If a linear relationship between Rb gain and distance away from the fracture is assumed then the extent of Rb migration can be estimated to be on the order of 15 to 20 centimeters.

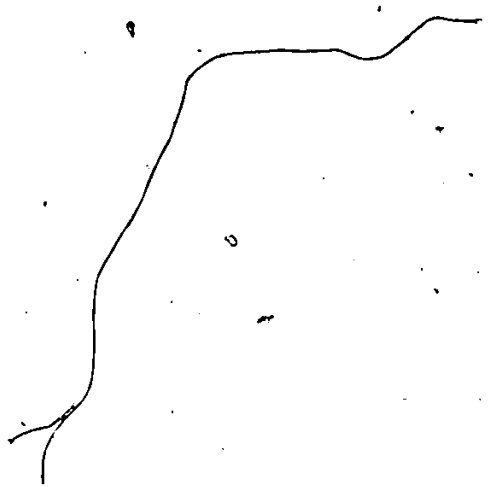
The Rb-Sr data for two samples from the north limb granodiorite are presented in Table B3.3. The slope of a regression line through these two samples indicates an age of about 1150 Ma ($R_i=0.7061$). However, one sample (68764) plots on a 1254 Ma reference line. This may be fortuitous and the north limb granodiorite is really younger than the south limb granodiorite, however, it is also possible that both units were emplaced at about 1250 Ma but the Rb-Sr system of sample TL5 has been modified by a subsequent disturbance. This disturbance might be related to an alteration event that is responsible for the growth of secondary muscovite in this sample.

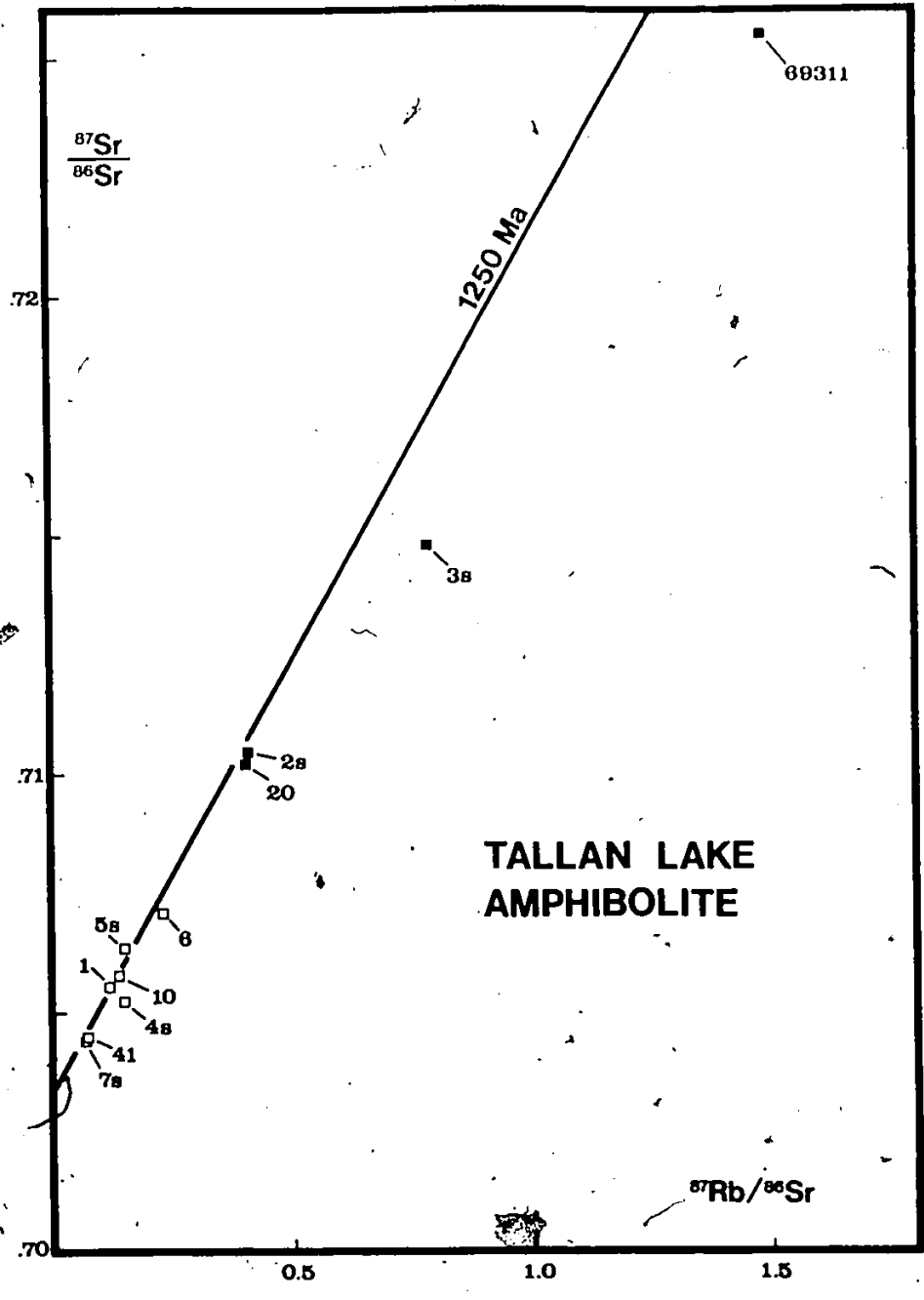
4.2.5.2 Amphibolite

The Rb-Sr data for 11 amphibolite samples are presented in Figure 25 along with a reference line with a slope that corresponds to an age of 1250 Ma., the approximate age of the amphibolite unit determined from the U-Pb zircon study. Unlike the granodiorite Rb-Sr study, many of the amphibolite samples were collected from widely spaced sampling sites. The samples denoted by solid squares on this diagram are anomalously enriched in Rb (eg. sample 69311 contains 135 ppm) and their compositions have probably been altered by alkali metasomatism similar to the effect discussed above for the fracture-bearing granodiorite samples. Two of these "enriched" samples (TL61-3S and 69311) plot significantly to the right of the 1250 Ma reference line. A number of the samples with low Rb/Sr ratios do plot on or very close to the reference line and indicate that the Rb-Sr integrity of these samples has not been significantly modified by subsequent geological disturbances. At present, it is not possible to explain the position of samples like TL61-4S and TL6 that have low Rb/Sr ratios (and Rb contents) but plot significantly below the reference line.

If all the data plotted in Figure 25 are used to calculate an age for the amphibolite unit, an errorchron age of 1099 ± 170 Ma is obtained ($R_i = 0.7035 \pm 5$; $MSWD = 7.93$). This age is probably geologically meaningless and at best approximates the time of metamorphism. Omitting the four

Figure 25 Rb-Sr whole rock data for samples from the Tallan Lake amphibolite. The solid squares represent samples that show anomalous geochemical features and are suspected of containing microfractures.





samples with high Rb contents and sample TL61-4S from the calculation increases the age to 1261 Ma, which is in closer agreement with the U-Pb zircon age, but there is still considerable data scatter outside analytical uncertainty (MSWD=3.23; $R_i=0.7034$). The age calculated for the four samples that are enriched in Rb is 975 Ma ($R_i=0.7045$) indicating that the Rb-Sr system in some of the amphibolite samples may have been disturbed during the late-stage fracture forming and fluid migration event that had a profound effect on the Rb-Sr system of many granodiorite samples. Therefore, it is concluded that the unusually large range in Rb/Sr ratios obtained for the amphibolite unit has been generated by secondary geological processes that have, in part, enriched these samples in Rb. It is also possible that some of the samples such as TL61-2S and -3S (see Table B3.3) have been depleted in Sr.

The best estimate of the initial strontium ratio for the amphibolite unit is the average model R_i (0.7034) for the five samples that plot on or very close to the reference line (ie. TL1, 10, 41, 61-5S, 61-7S); assuming that the age for these samples is similar to the 1254 Ma age determined in the U-Pb zircon study. With the present data, the R_i for the granodiorite (0.7037 ± 4) and amphibolite (0.7034 ± 5) overlap within analytical uncertainty.

4.2.6 Oxygen Isotopes

An interesting aspect of the geochemical study presented above is the recognition that the chemical and isotopic composition of numerous samples from the sill have been altered by fluid:rock interaction along irregularly spaced microfractures. The timing of this fluid infiltration seems to have occurred some 200 Ma or more after the sill was emplaced (refer to section 4.2.5.1). An oxygen isotope study of the Tallan Lake samples was performed in conjunction with Yuch Ning Shieh (Purdue University, Indiana) in order to further characterize this fluid, especially to test whether the fluid may have been derived from decarbonation reactions in the high ^{18}O marbles, and to compare the oxygen isotopic composition of the amphibolite, transition and granodiorite members of the sill.

The oxygen isotopic compositions for sixteen samples from the sill are presented in Table B3.3 and Figure 26. In addition to subdividing the samples according to compositional differences as described above, the granodiorite samples that contain microfractures are denoted by solid symbols. The amphibolite samples have a large range in ^{18}O from 8.1 to 10.7% but clearly do not overlap with the range observed for the fracture-free granodiorite samples (11.1 to 12.0%). The variation observed within each unit as well as the hiatus in oxygen isotopic composition between granodiorite and amphibolite can not be explained by normal

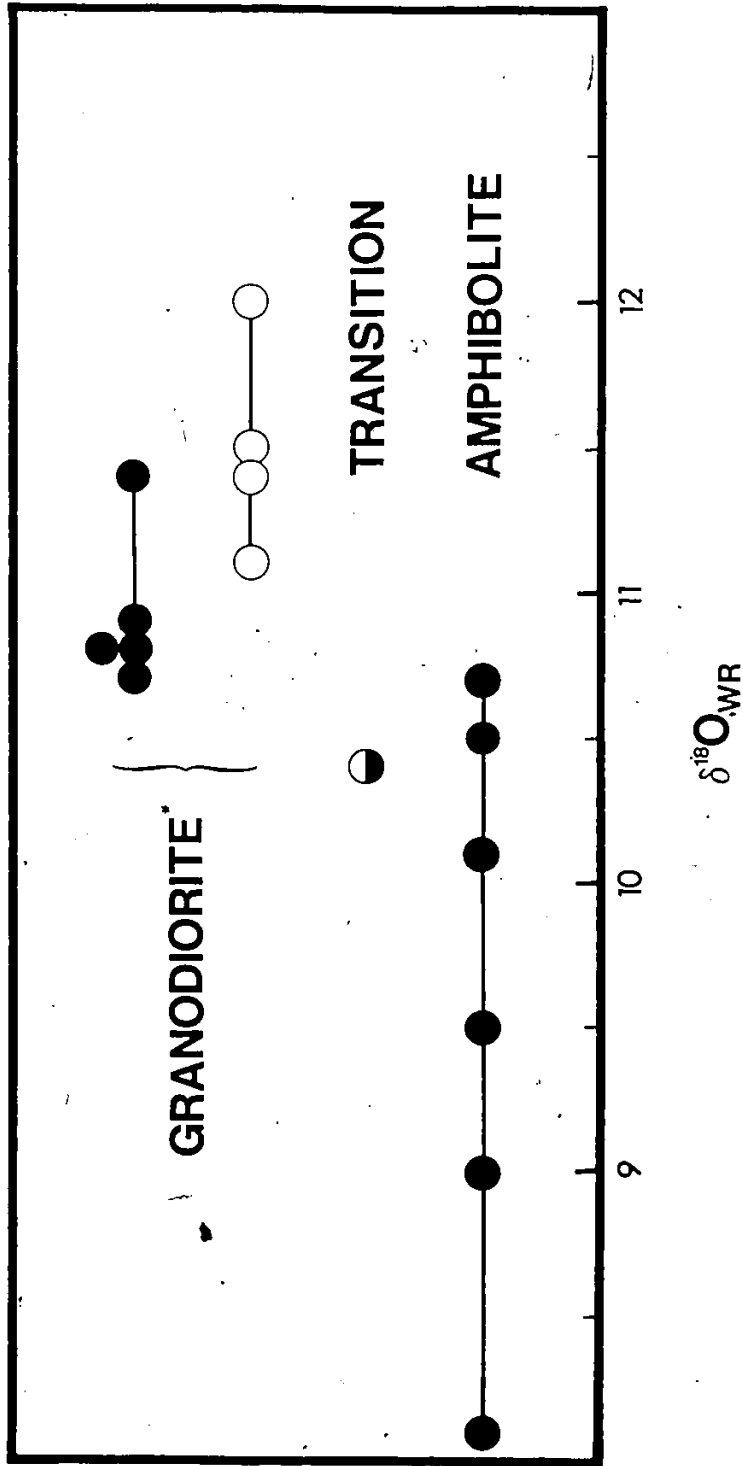


Figure 26 Oxygen isotopic composition of samples from the Tallan Lake sill. The granodiorite samples are subdivided into fracture-bearing (solid circles) and fracture-free (open circles).

igneous processes. The only transition sample analysed (10.4%) falls within the range determined for the amphibolite samples. There are two features of the amphibolite data revealed in this diagram; 1) two samples collected from near the present top of the sill, and possibly representing a cumulate portion of the sill (refer to section 4.2.7.1), have the lowest $\delta^{18}O$ values (8.1 and 9.0%) and 2) a sample that is suspected of chemical modification by fluid:rock interaction (ie. TL61-3S) has one the highest $\delta^{18}O$ values observed for this unit (10.1%).

The majority of fracture-bearing granodiorite samples have a narrow range of $\delta^{18}O$ between 10.7 and 10.9% and are clearly lower than the fracture-free samples. The only exception is sample TL12 (11.4%). The clustering of data for the fracture-bearing samples indicates that fluid interaction has effectively lowered the $\delta^{18}O$ composition of the fracture-free granodiorite samples. This is contrary to what would be expected if the fluid was derived by decarbonation reactions in the adjacent marble horizons (average $\delta^{18}O=26.6\%$; Shieh et al., 1976). Therefore, the fluid must have been derived from some other extraneous source such as emanations from the nearby late-tectonic Loon Lake pluton or metasomatism accompanying the emplacement of post-tectonic felsic dikes.

4.2.7 Discussion

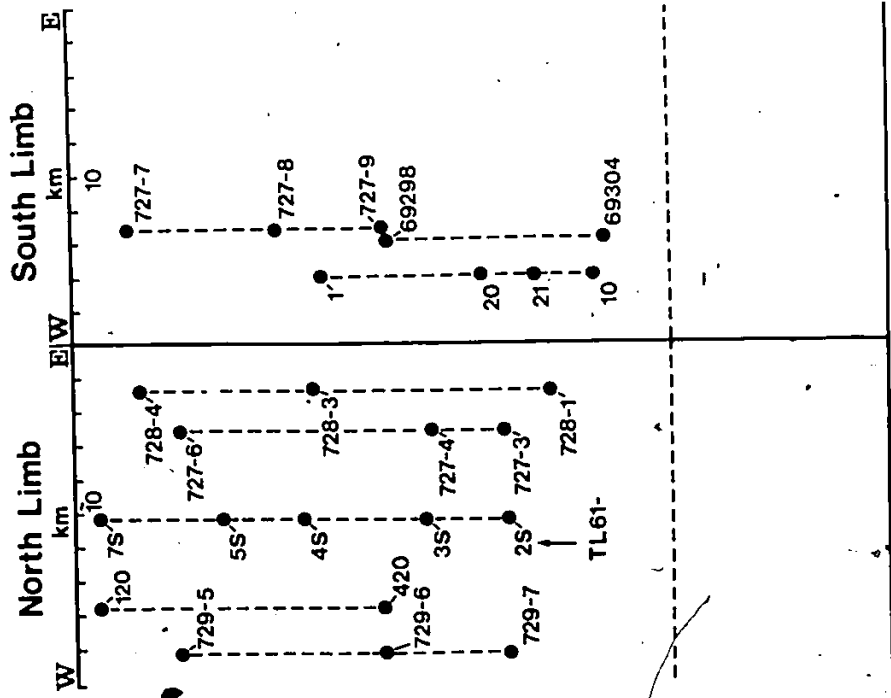
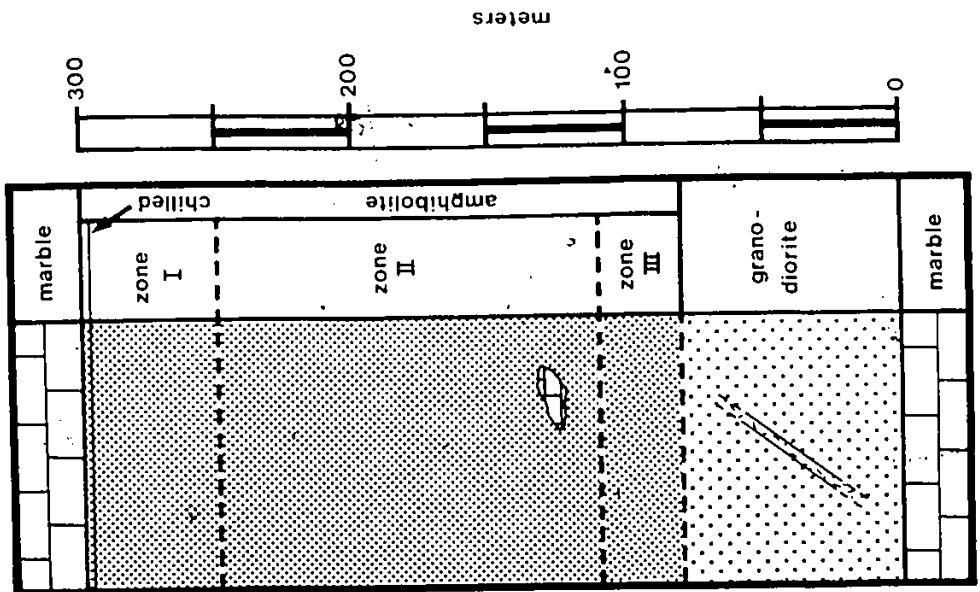
Summarizing the results presented above, it is clear that the Tallan Lake sill was emplaced at about 1250 Ma and, at the time of emplacement, consisted of a unique, highly evolved magma composition. In this section, the critical petrographic, geochemical and isotopic data presently available will be used to discuss the origin and evolution of the amphibolite unit and the relationship between the amphibolite and granodiorite members of the sill.

4.2.7.1 Amphibolite Petrogenesis

A schematic drawing of the sill in its present stratigraphic position is shown in Figure 27 as a visual reference for the following discussion with the approximate location of amphibolite samples collected along traverses perpendicular to the strike of the sill. The following list summarizes the salient features of the amphibolite geology and geochemistry that are considered to pertain to the primary magma characteristics:

- a) one sample, collected at the contact between amphibolite and marble, is ~~fine-grained~~ and interpreted by Griep (1975) as evidence for a chilled margin.
- b) the presence of large marble xenoliths.
- c) clinopyroxene pseudomorphs are absent from a 30 meter wide zone near the amphibolite-granodiorite contact. Samples from this zone show extreme enrichments

Figure 27 Schematic drawing of the Tallan Lake sill in its present stratigraphic position including subdivisions discussed in the text. In addition, the approximate stratigraphic position of samples used to define the geochemical trends shown in Figure 21 are shown. The horizontal scale represents the distance along strike measured in 2 kilometer intervals from the intersection between the N. limb of the sill and Hwy. 28.



Zr (trend III in Figure 21).

- d) the majority of samples are enriched in incompatible elements such as Zr, Y, Ti, P, and the REE and depleted in compatible elements like Ni and Cr.
- e) all samples are high-Fe tholeiites. The samples that contain unusually high Na abundances are also depleted in Ca.
- f) approximately flat REE patterns.
- g) a zone near the top of the sill is characterized by the most primitive incompatible element abundances.
- h) "mantle-like" initial strontium isotope ratio.
- i) presence of primary magmatic zircons with no evidence of inheritance.

The first two features listed above are considered the best geological evidence supporting an intrusive origin for the Tallan Lake amphibolite and the presence of primary magmatic zircons and the low initial strontium ratio also support this contention. Furthermore, this "mantle-like" initial strontium ratio combined with the lack of evidence for inherited zircons indicates that the Tallan Lake magma could not have experienced any appreciable interaction (ie. assimilation or selective contamination) with relatively old upper crustal material. The geochemical evolution of the sill is discussed in more detail below by considering the following aspects in turn; primary magma composition, effects of fractional crystallization and alteration.

Primary Magma Composition

There are two features of the amphibolite chemistry that suggest this unit was derived from a highly evolved mafic magma: 1) the anomalously high incompatible element contents and 2) the anomalously low Ni and Cr abundances. A possible explanation for the anomalously high incompatible element abundances is extreme fractional crystallization. For example, a basaltic magma with normal tholeiitic incompatible element abundances differentiates in situ producing successive liquids that are enriched in these elements. In this case, it would be expected that the least differentiated portion of the sill would approximate the initial magma composition. However, the samples containing the lowest incompatible element contents (eg. TL1 and TL61-7S) are still enriched in these elements above the levels reported for other mafic magmas. In fact, the sample that Griep interpreted as representing a chilled margin (#420), and a reasonable candidate for the approximate primary magma composition, has comparatively high TiO_2 (3.59 wt.%), P_2O_5 (2.32 wt.%), Zr (197 ppm) and Y (108 ppm) plus low Ni (28 ppm) and Cr (13 ppm) abundances.

A more likely explanation for the anomalous composition of the amphibolite is that the starting magma already had a unique composition before it was emplaced as a sill-like body. This could be accomplished by crystallizing large quantities of olivine and clinopyroxene in a deeper

seated primary magma reservoir and, at a late stage in the crystallization history, a part of the remaining magma was emplaced at higher levels to form the Tallan Lake sill. Fractional crystallization of olivine and clinopyroxene would consume much of the Ni and Cr in the primary magma while contributing to the enrichment of incompatible elements in the remaining melt.

Fractional Crystallization

As already stated (section 4.2.3.2), there are three distinct patterns on certain incompatible element variation diagrams (eg. Figure 21) that can best be explained as reflecting primary magmatic processes occurring within the sill. In the remaining discussion, the following three models that might explain these patterns are considered: 1) fractional crystallization of a primitive magma, 2) separate injections of magma and 3) fractional crystallization of a more evolved magma.

To elucidate the possible role of fractional crystallization of a primitive magma (model 1) a series of vectors have been constructed on each diagram in Figure 21 that represent the predicted compositional trends for a magma after crystallizing 50% of the indicated minerals using the well-known Rayleigh Fractionation Law (Rayleigh, 1896). The mineral/melt partition coefficients used are those reported by Pearce and Norry (1979) for Zr, Y, and Ti in a basic magma

and by Anderson and Greenland (1969) for P. These composition vectors were calculated using a starting magma composition with 50 ppm Zr, 30 ppm Y, 1 wt.% TiO_2 and 0.2 wt.% P_2O_5 and, except TiO_2 , represents the approximate abundance of these elements in the sample with the lowest incompatible element content (72B-3; Table B2.3). It is clear from Figure 21 that 50% fractional crystallization of any one phase or combination of phases that are shown, or 99% for that matter, can not produce magma compositions with greater than 600 ppm Zr. Therefore, the starting magma composition must have been more enriched in these elements than the values used in the calculations.

An alternative model is the injection of discrete magma batches (model 2). For example, an initial, more primitive magma batch could have been tapped from a primary reservoir and emplaced to form the clinopyroxene-rich zone (zone 1 in Figure 27) followed by subsequent injections of more differentiated magma. If the first batch of magma was allowed to partially or completely solidified, then this solidified mass might act as a barrier for subsequent magma batches and explain why the more evolved batches of magma appear to underplate the zone 1 amphibolite. A major difference between model 2 and the other models is that the sill does not have to be part of a nappe structure to explain why the least differentiated portion of the amphibolite is at the top of the sill. However, there is no field evidence such

as intrusive contacts or brecciation within the amphibolite horizon so a separate injections model is not favoured here.

Another possible model to explain the observed patterns in Figure 21 is that the starting magma was enriched in these elements and ensuing fractional crystallization formed cumulate portions within the sill that would be depleted in these elements, compared to the starting composition, and a more evolved melt that would be further enriched (model 3). As suggested above, a good candidate for the starting magma composition is sample 420 because it is the only sample analysed from the chilled margin (Griep, 1975). Therefore, trend I in Figure 21a could be explained if these samples represent a cumulate portion of the sill dominated by clinopyroxene accumulation (note the similarity between trend I and the vector for clinopyroxene crystallization); a contention that is supported by the presence of clinopyroxene pseudomorphs (Griep, 1975). A cumulate origin for the samples that plot on trend I is also confirmed by their significantly lower total REE contents (ie. samples TL1 and TL61-2S in Figure 22b).

Continuing with this model, trend II would represent tie-lines joining samples that are predominantly cumulate with samples that contain mixtures of plagioclase and clinopyroxene crystals and intercumulus melt whereas trend III represents an advanced stage in the crystallization history where Zr levels are high enough that zircon becomes a

solidus phase but is unable to settle out of the crystal mush. The TiO_2 -Zr diagram (Figure 21b) adds one more piece of information to the crystallization history of the sill. Trend I on this diagram can be explained as above where the Ti and Zr abundances are controlled predominantly by clinopyroxene accumulation. The abrupt change in slope from trend I to trend II indicates that magnetite and/or amphibole were also crystallizing phases in the magma. Trend II on the P_2O_5 -Zr diagram (Figure 21c) is probably controlled by the crystallization of apatite.

Although the trend lines shown in Figure 21 appear to be continuous from the least differentiated to the most differentiated samples, there are four anomalous samples, from different traverse lines but all from zone II in Figure 27 (729-6, T161-55, 727-4, 728-3), that do not conform to this general pattern. The significance of these "reversals" in the general geochemical trends is not clear but with a more detailed investigation it may be possible to determine if there is a horizon within zone II that represents a separate injection of a more primitive magma composition.

In summary, the best explanation for the trace element patterns observed for the amphibolite samples is that a zone near the present top of the sill is dominated by clinopyroxene accumulation while the remaining magma continued to evolve by crystallizing plagioclase, amphibole, magnetite and possibly apatite followed by a very late stage

of zircon crystallization. If this model is correct, then the occurrence of a clinopyroxene cumulate at the present top indicates that the amphibolite unit must be overturned. It is interesting that the idea of an overturned nappe structure for the sill was originally suggested by Griep (1975) to explain the amphibolite-granodiorite relationship but has been reached here and by Heaman et al. (1982c) based solely on a detailed study of the amphibolite unit.

Alteration

Several features of the amphibolite chemistry, such as the anomalous enrichment in Li, B, Na, Rb and ^{18}O and the disrupted Rb-Sr system observed for some samples, may be a consequence of some form of alteration. From a detailed study of the granodiorite unit (Heaman et al. 1983; section 4.2.5.1) it was concluded that late-stage fluid migration along microfractures had a profound effect on sample chemistry, especially the enrichment in alkalis and depletion in Mg. If similar fluid-rock interaction occurred within the amphibolite unit then some of the unusual features of the amphibolite chemistry listed above might be explained in this way. Magnesium depletion in some samples might explain some of the data scatter observed on the AFM diagram (Figure 18). Unfortunately, no correlation exists between any of the elements that might be considered indices of alteration. For example, the amphibolite sample with the

highest Rb content (134 ppm; 69311) has Na and Mg contents similar to the average value reported in Table 4.1. In fact, of the five amphibolite samples that have Rb contents above 30 ppm only sample TL20 shows a corresponding depletion in MgO (1.44 wt.%) and enrichment in Na₂O (5.04 wt.%).

The unusually high values and the large variation in ¹⁸O (8.1 to 10.7%) can not be explained by normal igneous processes. Compared to the normal range found for mafic igneous rocks (5 to 7%; Taylor, 1974), the Tallan Lake amphibolite has been enriched by as much as 3 to 4%. The fact that the only sample analysed that appears to have been affected by late-stage fluid infiltration (TL61-3S) also has a high ¹⁸O value (10.5%) is suggestive that the migration of fluids along fractures in the amphibolite samples may increase their ¹⁸O values. It is difficult to evaluate whether the enrichment observed in all the amphibolite samples is related to late-stage fluid migration or not without performing a more detailed study on a fracture-bearing sample.

4.2.7.2 Amphibolite - Granodiorite Relationship

The relationship between the amphibolite and granodiorite members of the sill is enigmatic and an attempt is made here to re-evaluate whether the two are genetically related or not. This same question was addressed by Griep (1975) who concluded, from a limited amount of major element

data, that the granodiorite could be derived from the same magma that formed the amphibolite by fractional crystallization. However, some of the results obtained in this study are not consistent with such a model. The most striking is the hiatus observed in the chemical composition for these units on most variation diagrams. Further suspicion is evoked by the hiatus in oxygen isotope composition and the preliminary U-Pb zircon results which indicate that the amphibolite may be slightly younger than the granodiorite. The following four mechanisms are examined in turn as potential processes capable of generating a felsic rock from a mafic magma: 1) liquid immiscibility, 2) partial melting and/or contamination, 3) separate intrusions and 4) fractional crystallization.

Liquid Immiscibility

Liquid immiscibility has been postulated as a viable mechanism for generating two distinct magma compositions from a single magma reservoir (eg. Roedder, 1979). At a certain stage in the crystallization history of some highly evolved, mafic magmas, an immiscibility gap is reached where an Fe-rich mafic magma and a felsic magma are produced. An excellent terrestrial example where this process has occurred is the Cortlandt Complex (Bender et al., 1982) where liquid immiscibility has produced an Fe-rich diorite and a granodiorite. The characteristic feature of co-existing

magmas produced by this mechanism is that the Fe-rich mafic liquid is enriched in high field strength elements like the REE and Zr. Consequently, the mafic liquid has higher total REE contents compared to the felsic liquid; this is in direct contrast with the behaviour of these elements during fractional crystallization. Since the Tallan Lake amphibolite samples have lower total REE abundances than the granodiorite samples, it is unlikely that they formed by liquid immiscibility.

Partial Melting and/or Contamination

Another mechanism capable of producing co-existing mafic and felsic magmas is the fusion of continental crust during emplacement of a mafic magma (eg. Wyllie, 1961; Yoder, 1973; Patchett, 1980). Depending on the time of magma-crust interaction, it is conceivable that a mafic magma with a liquidus temperature around 1200 °C could generate a small volume of granitic melt by fusion of crustal rocks. Although some crustal contamination might be anticipated as suggested by the experiments of Watson (1982), a felsic magma formed in this way should have a distinctive chemical and isotopic composition. It is difficult to envisage the Tallan Lake granodiorite forming by this mechanism because both the granodiorite and amphibolite have similar and generally flat REE patterns. The REE pattern of most tonalite and granodiorite magmas generated by modest degrees of partial

fusion of crustal rocks, even mafic rocks from the lower crust (eg. Barker et al., 1976), are enriched in LREE with low total REE abundances. It also seems unlikely that the granodiorite and amphibolite would have similar "mantle-like" initial strontium ratios if both magmas were derived from different sources.

Separate Intrusions

Included under this heading are the separate intrusions of two compositionally distinct magmas that were derived from different source regions and from a single compositionally stratified magma reservoir. As mentioned above, it is unlikely that two magmas derived from different source regions would have similar REE patterns or initial strontium ratios so only the emplacement of successive magma batches derived from a common source is considered further. Support for the separate intrusion hypothesis is indicated from the U-Pb zircon study where it was suggested that the amphibolite might be slightly younger than the granodiorite. If the primary magma reservoir was compositionally stratified with a more felsic cap (like the model proposed by Hildreth, 1979), then the initial magma batch removed from this reservoir could be derived from the roof zone and have a more felsic composition compared to subsequent magma batches. This would explain a difference in age between the Tallan Lake granodiorite and amphibolite yet maintain the other

features of the sill that suggest these two units are cogenetic. To substantiate this model, it is necessary to demonstrate that there is a significant time difference between the emplacement of the granodiorite and amphibolite units and the existence of an intrusive contact.

Fractional Crystallization

The process favoured by Griep (1975) to generate the mafic and felsic rocks of the sill and the mechanism suggested for the generation of small amounts of felsic magma in layered mafic intrusions (eg. Wager and Brown, 1967) is fractional crystallization. In other words, the composition of a mafic magma evolves towards more felsic differentiates by fractional crystallization of mafic minerals like olivine, clinopyroxene and orthopyroxene. Many of the features of the Tallan Lake rocks, such as the similar initial strontium isotope ratios and REE patterns, are consistent with this model. Therefore, extending the model described above for the amphibolite samples, further differentiation might produce a small amount of liquid with tonalite to granodiorite composition. As stated at the beginning of this section, the hiatus in the chemical composition and oxygen isotope composition are difficult to reconcile with this model. The difference in ^{18}O between the amphibolite and granodiorite samples may not be a primary feature so the main difficulty with the model remains the hiatus in chemical composition and

the indication from the U-Pb zircon study that the amphibolite might be slightly younger than the granodiorite. In particular, it is difficult to envisage how the granodiorite samples that plot in the calc-alkaline field on the AFM diagram (Figure 18) and the amphibolite samples that plot in the tholeiite field could be consanguineous. The REE pattern for the Tallan Lake granodiorite is quite unique compared to other calc-alkaline granitoid rocks in the CMB (eg. the Elzevir batholith, Pride and Moore, 1983) and the similarity between the granodiorite and amphibolite patterns is interpreted as strong support that these two units are indeed cogenetic. It remains to be determined whether fractional crystallization is the only process involved in the evolution of the sill or whether a combination of the processes cited here have been active but it is concluded that the granodiorite and amphibolite members of the sill are cogenetic.

4.3 METHUEN COMPLEX

4.3.1 Geology and Petrography

The Methuen Igneous Complex is one of the larger granitoid bodies in the study area and is located in the central portion of Methuen township (Figure 28). Hewitt (1961) noted that this body consists of at least two distinct phases including a medium- to coarse-grained, well foliated,

pink granite and a fine-grained, grey granodiorite. The relationship between these two phases is uncertain but Hewitt concluded that the grey granodiorite occurs as inclusions within the pink granite. The Methuen Complex intrudes the supracrustal rocks in the area (ie. quartzite, marble, amphibolite, quartzo-feldspathic gneiss) as well as the adjacent Blue Mountain nepheline syenite (Hewitt, 1961).

Samples of the Methuen Complex were collected from several roadcut exposures along County Road 46 (Figure 28). The recent re-construction of this road has created excellent exposures of both the pink granite and the grey granodiorite that are ideal for sample collecting. The majority of samples collected in this study and the samples collected from the same vicinity by Hewitt (1961) fall into the field for granite in the IUGS classification scheme (Figure 29) but four samples are clearly within the granodiorite field. Multiple samples were collected at two sampling sites, referred to as site A and B on Figures 29 and 30 and in the remainder of this chapter. The samples collected at site A define a region in Figure 29 that overlaps the field for granite, granodiorite and quartz monzonite. For simplification, these samples are called quartz monzonite in this study. The rock at site B was originally considered to be part of the grey granodiorite suite as defined by Hewitt (1961) because of the colour and small grain size but all the samples collected at this site are deceptively rich in

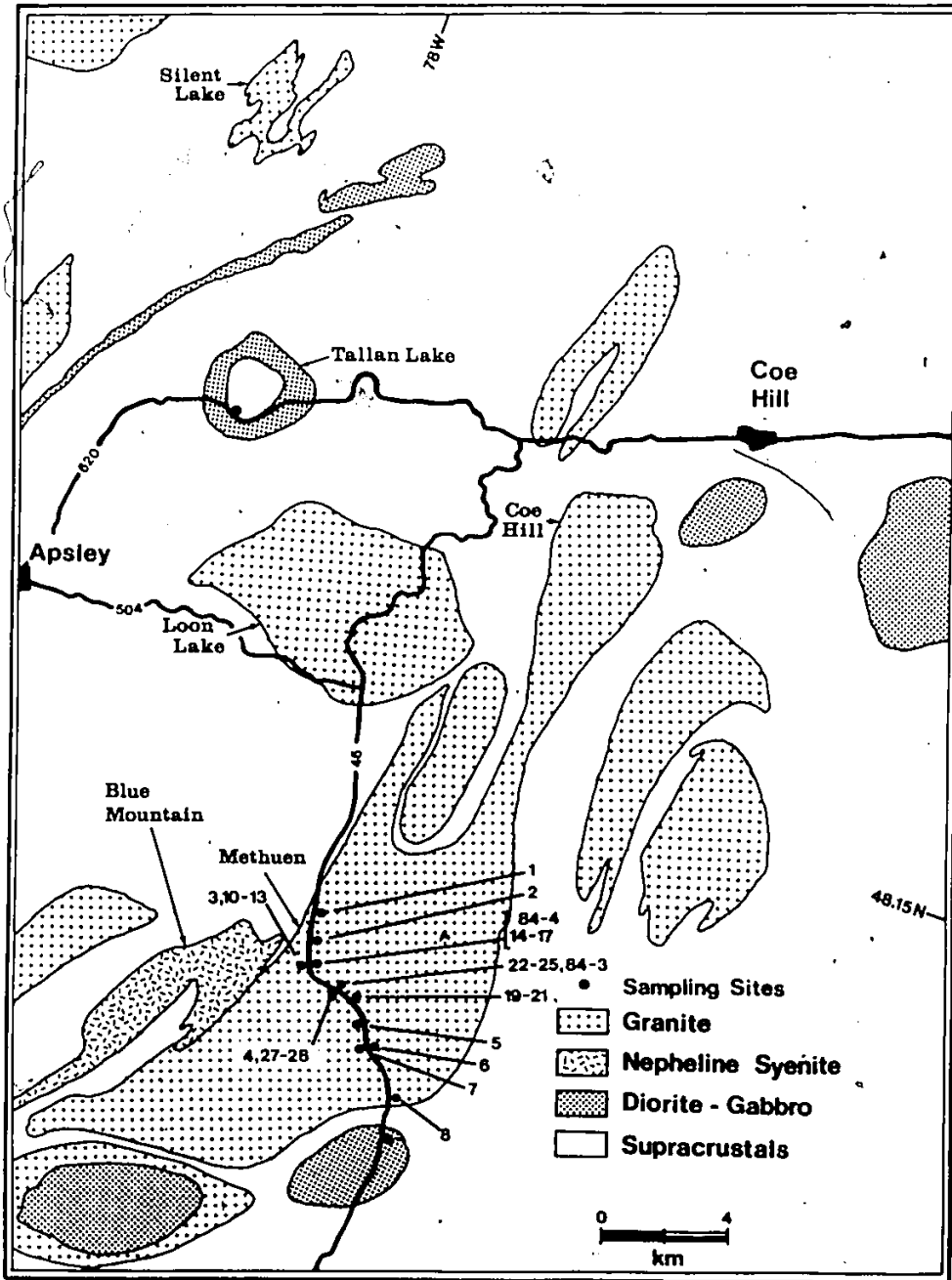


Figure 28 Geological sketch map of the Methuen Township region showing the location of major granitoid bodies. Included are the sample locations referred to in the text.

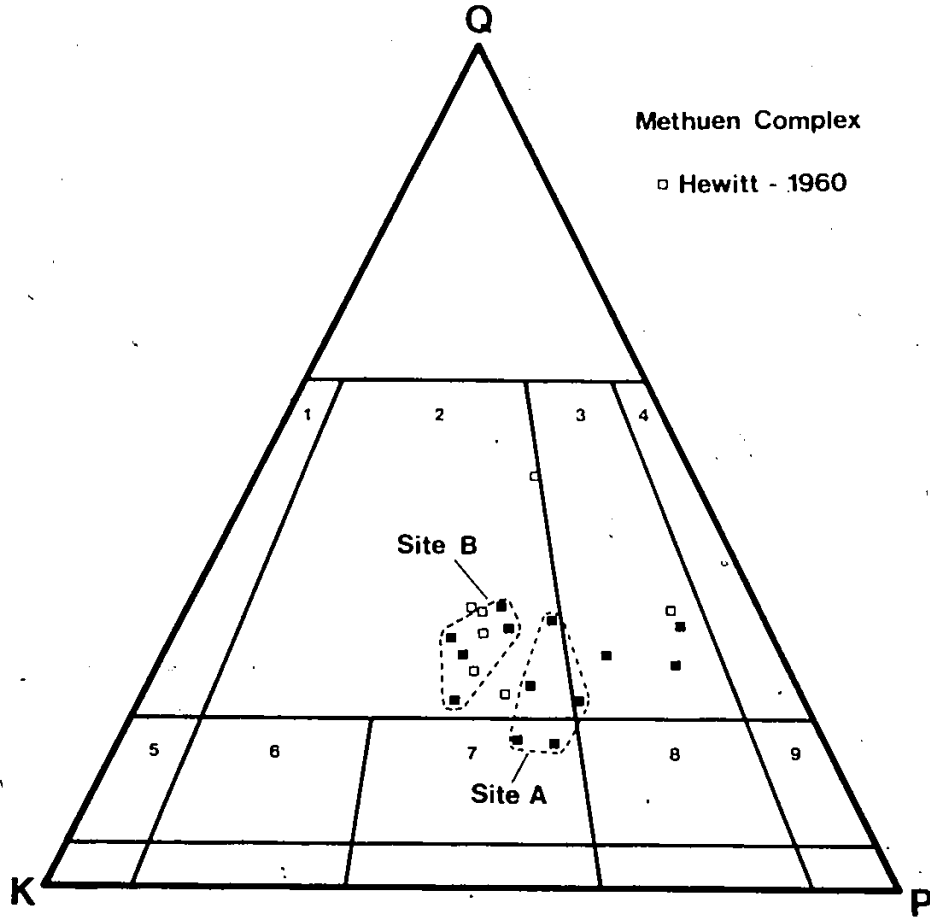


Figure 29 Modal quartz-plagioclase-K-feldspar diagram showing the position of samples collected from the Methuen Complex. The various fields are the same as for Figure 17. Open squares correspond to modal analyses reported by Hewitt (1960).

K-feldspar and plot in the granite field in Figure 29. An example of the diversity in rock types present within the complex is shown in Plate 5c.

At sampling site A, the pink quartz monzonite is medium- to coarse-grained hypidiomorphic granular with an average mode, based on five determinations (Table B1.4), of 43% plagioclase, 27% K-feldspar, 20% quartz, 7% biotite, 3% hornblende with subordinate carbonate, chlorite, muscovite and traces of apatite, fluorite, graphite, opaques, sphene and zircon and is similar to the average mode for three samples (#571, #572, #573) collected from the same vicinity by Hewitt (1961). The samples from this site have a pronounced foliation and are relatively free of alteration. A texture that is commonly observed is the development of distinct zoning at the margins of plagioclase grains where they are in contact with microcline.

The samples of grey granite examined from site B are fine- to medium-grained, hypidiomorphic granular with an average mode, also based on five determinations, of 34% plagioclase, 34% K-feldspar, 27% quartz, 5% biotite and minor amounts of carbonate with subordinate apatite, fluorite, graphite, pyrite and zircon. One sample from site B (M23) contains traces of hornblende and chlorite. The grain size in most samples is bimodal with patches of smaller grains (< 1mm

in width), that show signs of annealing (ie. 120° interfacial angles), dispersed throughout. The feldspar grains are generally free of alteration but the plagioclase grains, like at site A, are zoned wherever they occur in contact with microcline. There are abundant mafic schlieren at site B and a few cross-cutting pegmatite dikes.

One sample (M7), collected from a third sampling site, is unique compared to the other samples because it contains a narrow zone (ca. 1 cm wide) where the plagioclase exhibits a severe sericitic alteration, often most intense at the grain margins, and all the biotite is altered to chlorite.

4.3.2 Geochemistry

The major and trace element contents for 24 samples collected from the Methuen Complex are presented in Table B2.4. The average composition for samples collected from sites A and B are presented in Table 4.3 and the granite samples collected at site B have higher K_2O and SiO_2 and lower CaO , Fe_2O_3 , Al_2O_3 , TiO_2 , Sr and Zr contents than the quartz monzonite samples collected from site A.

The samples analysed from the Methuen Complex are plotted on a Na_2O-K_2O-CaO ternary diagram in Figure 30 along with the range in composition observed for sites A and B and the range in average composition for a number of circa 1250 Ma trondhjemitic batholiths from the nearby Elzevir terrain (Pride and Moore, 1983). Most of the samples from the Methuen

TABLE 4.3 - The average composition for samples collected at sampling site A and B

	Site A	S	Site B	S
SiO ₂	74.05	1.01	76.95	0.27
Al ₂ O ₃	13.56	0.44	12.65	0.09
Fe ₂ O ₃	3.01	0.32	1.86	0.14
MgO	0.44	0.15	0.24	0.17
CaO	1.36	0.32	0.46	0.14
Na ₂ O	3.14	0.45	2.88	0.13
K ₂ O	4.07	0.41	4.77	0.24
TiO ₂	0.26	0.03	0.13	0.02
MnO	0.07	0.01	0.04	0.01
P ₂ O ₅	0.05	0.01	0.01	-
LOI	0.29	0.13	0.32	0.08
Rb	117	9	127	10
Sr	96	11	55	10
Y	58	6	49	2
Zr	291	16	233	24
Nb	14	2	13	1

S - standard deviation

Complex are distinctly more potassic compared to other large batholiths emplaced at approximately the same time in the CMB. The three samples, analysed in this study, that plot within the granodiorite field on Figure 29 also plot close to the field for trondhjemitic rocks delineated on Figure 30. While the samples from the Methuen Complex have a considerable range in chemical composition, it is clear from the petrography, chemistry and U-Pb geochronology (next section) that this unit provides evidence for the existence of a potassic suite of granitoid rocks emplaced in the CMB at around 1250 Ma.

Hewitt (1961; p.149) suggested that "a narrow band of fine-grained, leucocratic pink granite extends north from

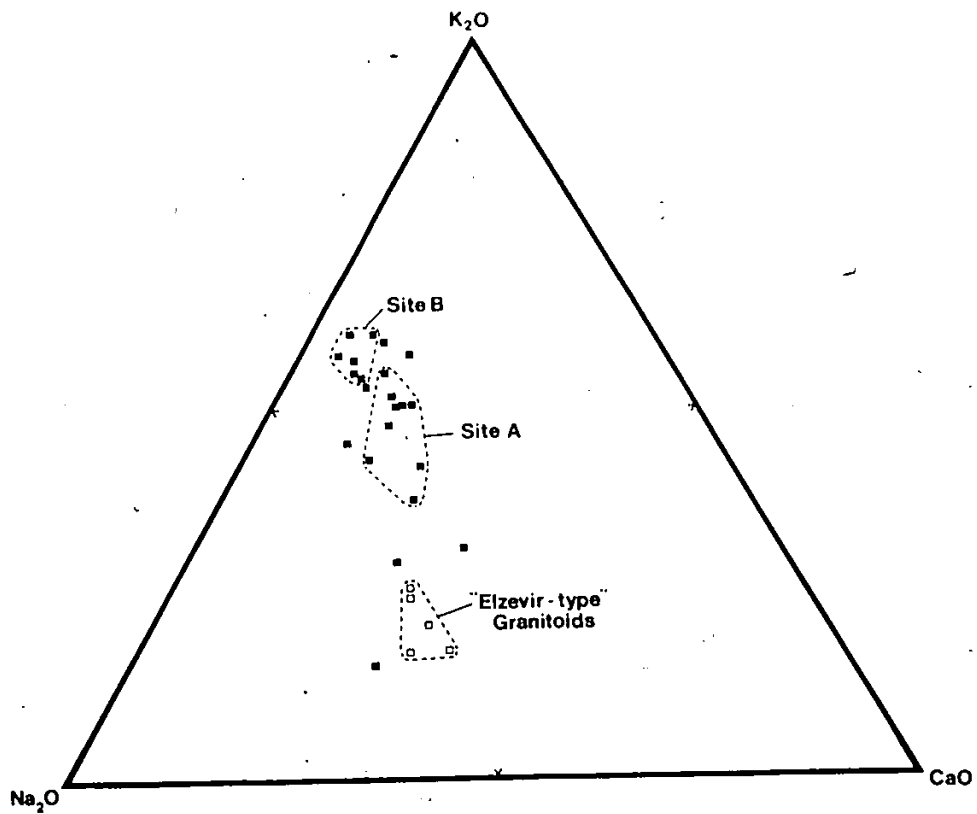


Figure 30 CaO-K₂O-Na₂O ternary diagram showing the composition of granitoid rocks from the Methuen Complex and the range of values reported for trondhjemitic batholiths in the CMB of similar age.

the Methuen granite body into Wollaston township, and may form a connection with the Coe Hill granite". This "connection" between the Methuen and Coe Hill granitoid rocks was further evaluated by Atkins (1983) who claimed that although the mineralogy of the two units is similar, their structural settings are quite distinct. In particular, the Coe Hill pluton does not exhibit the NE-SW trending regional foliation that is characteristic of all phases of the Methuen Complex (Hewitt, 1961).

Additional insight into the relationship between these two spatially related granitoid bodies is provided by the trace element data presented in Tables B2.4 and B2.5 and on the Y-Zr diagram in Figure 31. The samples from each unit plot in different fields except five samples from a marginal phase of the Coe Hill pluton. These five samples plot within, or very close to, the field delineated by the samples from the Methuen Complex indicating that the marginal phase of the Coe Hill pluton might represent a small portion of the older Methuen Complex; a contention supported by the more radiogenic strontium isotopic composition of these same samples (Atkins, 1983; Heaman, unpublished data). Since both units, in general, have similar mineralogies and do not show signs of differentiation, then this difference in the abundance of incompatible elements is not attributed to fractional crystallization of accessory phases like zircon ($ZrSiO_4$) or xenotime (YPO_4) (eg. Tindle and Pearce, 1981) but

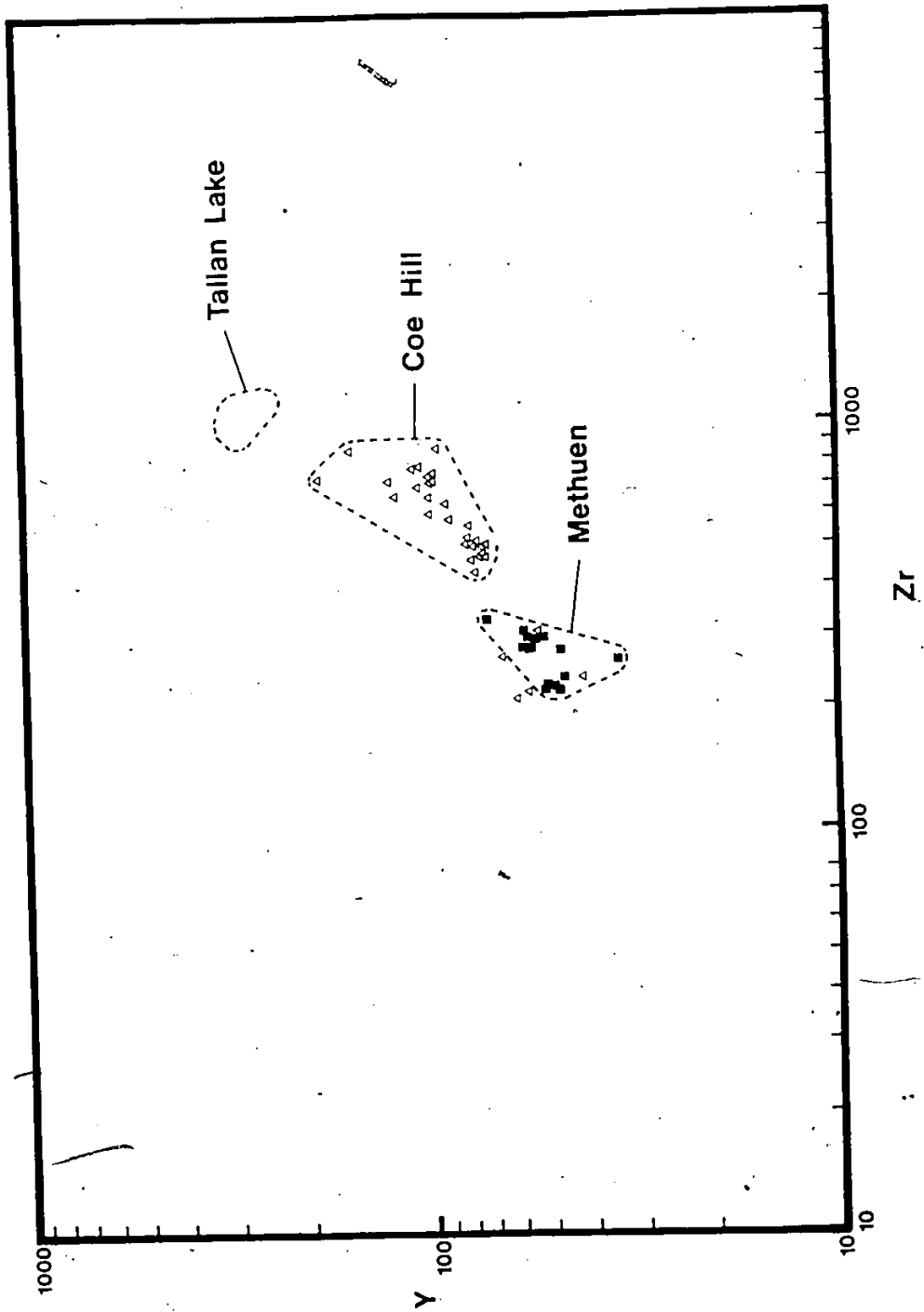


Figure 31 Y versus Zr diagram for samples from the Methuen Complex and Coe Hill pluton.

is interpreted to reflect a primary difference in the source composition. Alternatively, this difference could be generated if the process of contamination has a more important role in the chemical evolution of the younger granitoid plutons.

4.3.3 U-Pb Zircon, Sphene Geochronology

Large samples were collected from site A (LH84-4; 38 kg) and B (LH84-3; 56 kg) for a U-Pb zircon study. The U-Pb data for three zircon fractions and one sphene fraction from the quartz monzonite sample collected at site A and two zircon fractions from the granite sample collected at site B are presented in Table B4. All the zircon fractions have been abraded and selected from a single, colourless, prismatic population.

Site A

The zircon fractions and sphene fraction analysed from the sample (LH84-4) collected at site A are presented on a concordia diagram in Figure 32. The two least discordant fractions (3.1 and 3.2% discordant) are coarser in grain size (-100+200 mesh) and less magnetic than the most discordant fraction (8.3% discordant). All three zircon fractions have relatively low total common Pb contents (19 to 39 pg) and is reflected in the relatively high $^{206}\text{Pb}/^{204}\text{Pb}$ ratios (> 30,000). The calculated discordia line that passes through

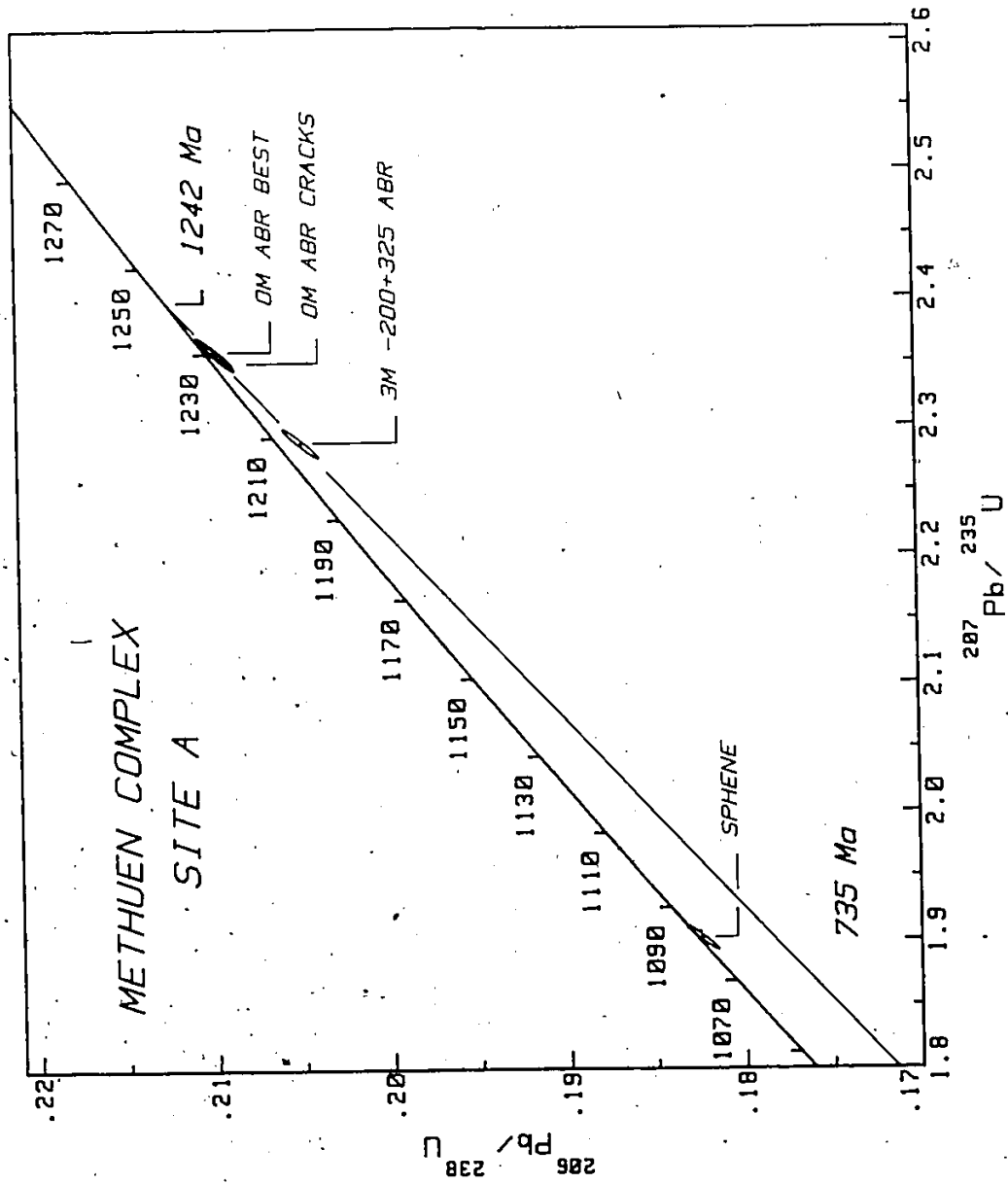


Figure 32 Concordia diagram for zircon and sphene analyses from the Methuen Complex - Site A

these points defines a precise upper intercept age of 1242 $\pm 22/-6$ Ma (62% probability of fit) with a lower intercept age of 735 Ma. The 1242 Ma U-Pb zircon age for this sample is interpreted as the time of emplacement for the quartz monzonite at site A.

The U-Pb data for an abraded sphene fraction from the same sample is also presented on Figure 32 and lies very close to concordia with a $^{207}\text{Pb}/^{206}\text{Pb}$ age of 1085 Ma; an age that is significantly younger than the corresponding U-Pb zircon age of 1242 Ma. Since the $^{206}\text{Pb}/^{204}\text{Pb}$ ratio in the sphene is low (ie. 615) the accuracy of this age depends on how well the common Pb correction can be made. In previous studies (eg. Hanson et al., 1971; Catanzaro and Hanson, 1971) the Pb isotopic composition of a coexisting, U-poor mineral such as feldspar has been used as the best estimate for this correction. If the feldspar lead for comparable Grenvillian granitoid rocks (eg. Tilton et al., 1955; Zartman, 1969) are used for this correction, then a range of $^{207}\text{Pb}/^{206}\text{Pb}$ ages between 1087 and 1094 Ma are obtained. Therefore, the effect of using the feldspar lead only increases the age by 1%. Sphene is generally a relatively resilient mineral to resetting as demonstrated in the study by Hanson et al. (1971) but new growth can occur at high grades of regional metamorphism (Tilton and Grunefelder, 1968). This relatively young sphene age of 1085 Ma implies that a regional geological event occurred at this time that was capable of

either completely resetting the U-Pb system in sphene or, more likely, generating new sphene growth.

Site B

The two zircon fractions analysed from the sample (LHB4-3) collected at site B are presented in Figure 33. It is apparent from this diagram that these two fractions have significantly different $^{207}\text{Pb}/^{206}\text{Pb}$ ages (1232 and 1329 Ma). Both zircon fractions were selected from a larger abraded fraction consisting of about 350 grains. The fraction with the lower $^{207}\text{Pb}/^{206}\text{Pb}$ age (#10 - Table B4) consists of the best 109 abraded zircon grains whereas the remaining 200 to 300 grains had an assortment of imperfections such as cracks or tiny inclusions, but there were no visible signs of cores in either fraction. An interesting feature of the data presented in Table B4 is that the fraction containing the best quality zircon grains has the highest total common Pb and yet plots on concordia. This feature, combined with the lower $^{206}\text{Pb}/^{204}\text{Pb}$ ratio (0.0962), is interpreted as an indication that this population consists primarily of new zircon growth during metamorphism.

The discordia line drawn through these two fractions on Figure 33 is very close to concordia and defines an upper intercept age of 1367 Ma and a lower intercept age of 1180 Ma. The lower intercept age is strongly constrained by the near-concordant nature of fraction #10. This type of

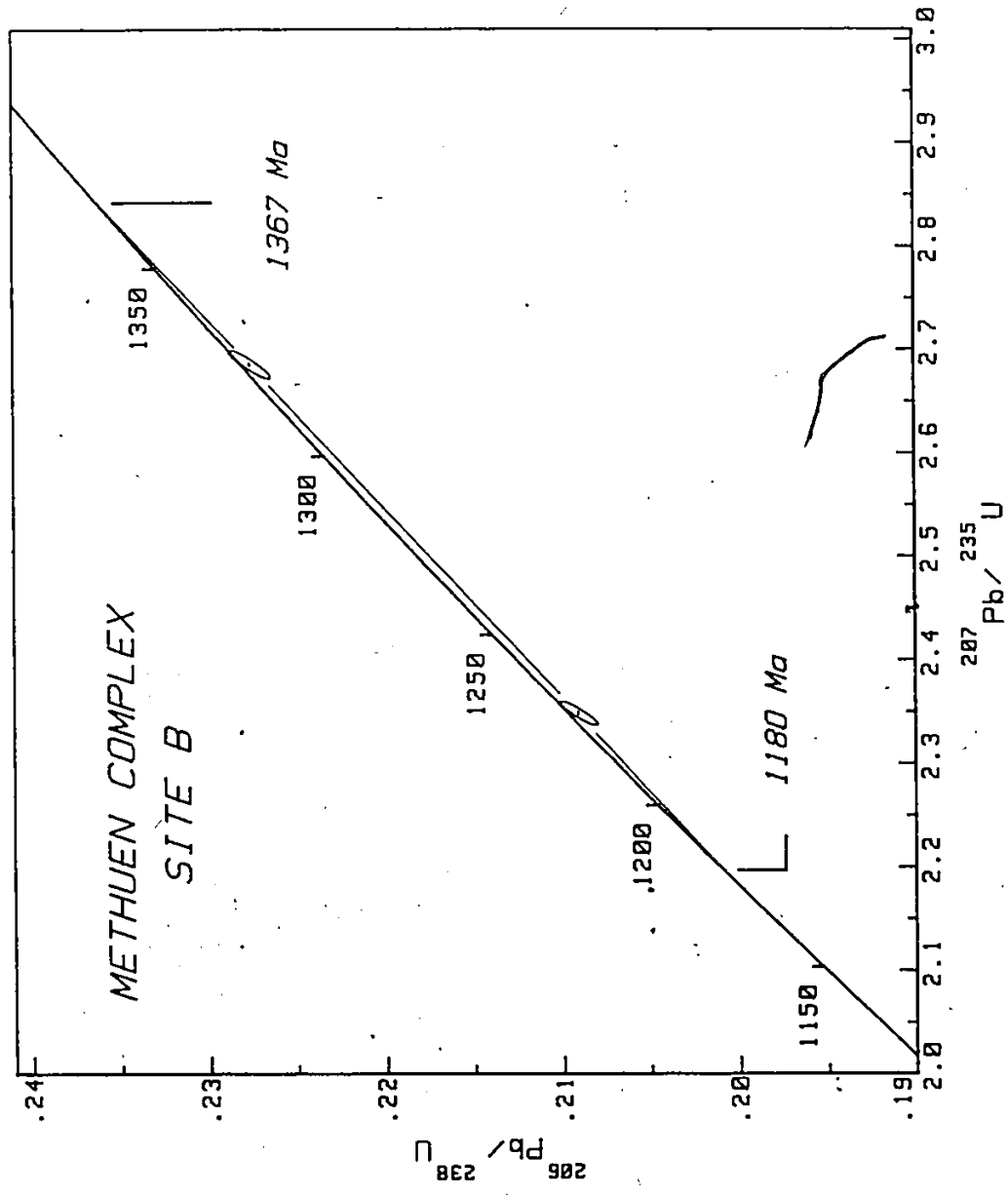


Figure 33 Concordia diagram for zircon analyses from the Methuen Complex - Site B

discordia line can be interpreted in two ways: 1) the rock formed at 1180 Ma but has an inherited component of Pb or 2) the rock formed at approximately 1367 Ma with some new zircon growth occurring at 1180 Ma. More analyses are required to distinguish between these two possibilities but, at present, these data are interpreted to indicate that the rock at site B is one of the oldest granitoid units known to occur within the CMB and was affected by a metamorphic episode that generated some new zircon growth at about 1180 Ma. If the granite at site B truly represents an inclusion in the quartz monzonite phase, then the 1367 Ma upper intercept age is the first indication, from isotopic studies, that older crustal material may exist beneath the CMB. A perplexing feature indicated by this U-Pb study is that new metamorphic zircons grew at site B but there is no indication of a 1180 Ma metamorphic event affecting the zircons at site A, a few hundred meters away?

4.3.4 Rb-Sr Geochronology

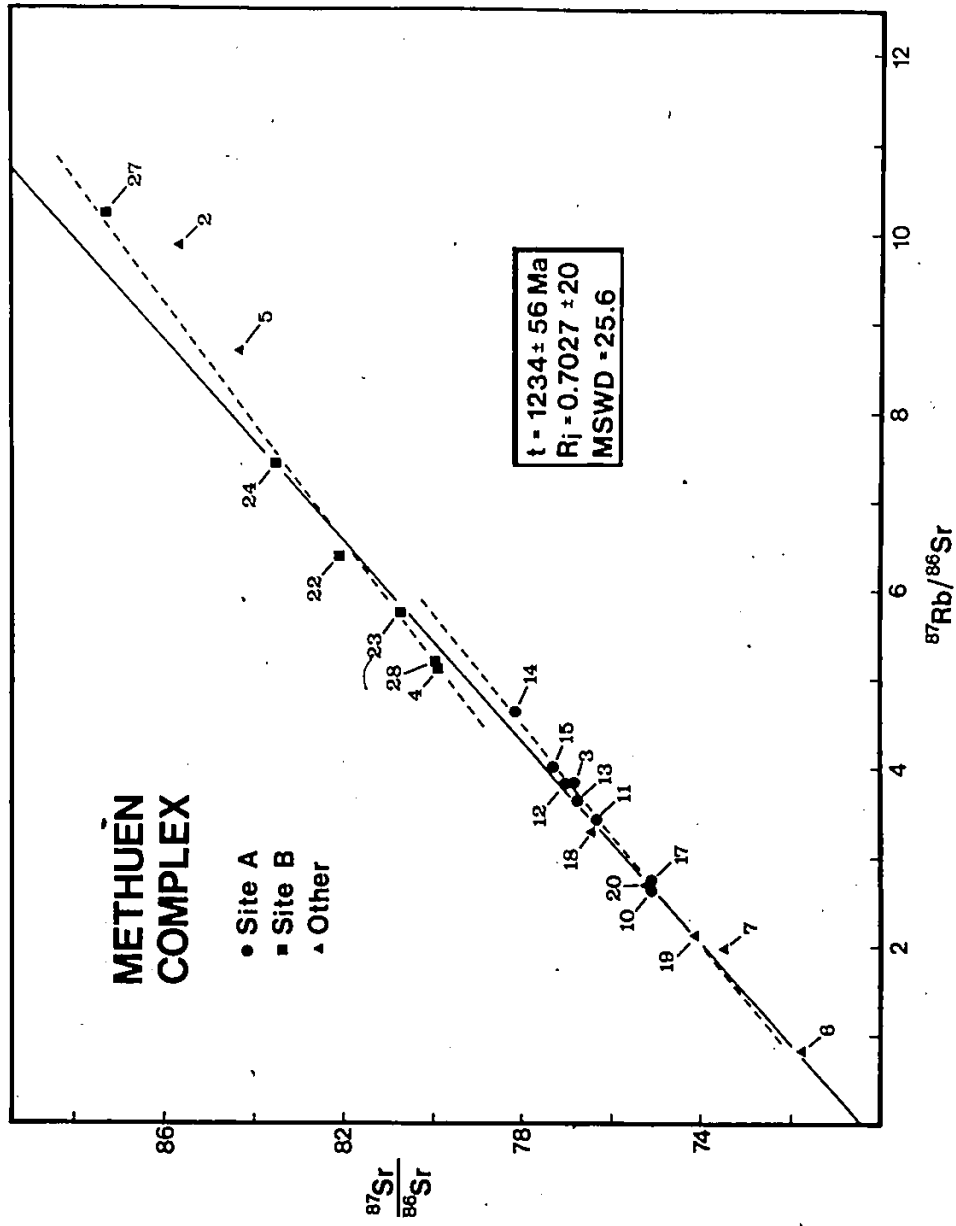
From the U-Pb zircon study presented above it was suggested that as many as three distinctly different periods of zircon growth are present in the two samples collected from the Methuen Complex; at circa 1367, 1242 and 1180 Ma. The two older ages are interpreted as the time of emplacement for two different phases of the complex while the 1180 Ma age is interpreted as the time of new zircon growth during a

metamorphic episode. A possible second regional metamorphic episode, or extremely slow cooling from the 1180 Ma episode, occurred at about 1085 Ma and was responsible for the generation of sphene in these rocks.

To study the behaviour of the Rb-Sr whole rock system in the Methuen Complex, a number of samples, weighing approximately 5 kilograms each, were collected in the conventional way from widely spaced sampling sites (the approximate distance between sites was on the order of a few hundred meters) and multiple samples were collected from the two sites (A and B) described above. The spacing between samples collected from the same sampling site varied between 20 and 50 meters. The Rb-Sr whole rock data for 21 samples from the Methuen Complex are presented in Table B3.4 and on a composite isochron diagram in Figure 34. The samples that were collected from widely spaced sites are represented by solid triangles on Figure 34 while those from sites A and B are represented by circles and squares, respectively.

The slope of the best-fit line through all the data on Figure 34 corresponds to an age of 1235 ± 56 Ma ($R_i = 0.7027 \pm 20$; M2) with data scatter in excess of analytical error (MSWD=25.6). It is not surprising that there is considerable data scatter, especially if there is more than one period of granite emplacement as suggested from the U-Pb zircon study, but it is amazing that the composite age even remotely resembles the U-Pb zircon age for the quartz monzonite at

Figure 34 Rb-Sr whole rock data for samples from the Methuen Complex. Samples represented by solid circles are from Site A, solid squares - Site B and solid triangles - a variety of sampling sites.



site A (ie. 1242 Ma). The remaining discussion will demonstrate that this must be fortuitous. If the three most discordant samples that happen to have the highest Rb/Sr ratios (M2,5,27), plus the sample (M7) that contains a zone of severe chlorite and sericite alteration, are omitted from the age calculation, then the resulting age is significantly older (1274 ± 40 Ma) with a lower initial strontium ratio (0.7020 ± 16) but still with a significant amount of data scatter ($MSWD=9.28; M2$).

In addition to scatter caused by combining genetically unrelated samples, another source of data scatter is evident from the results for an individual sampling site. The best-fit lines calculated for samples collected at a single sampling site are shown as dashed lines in Figure 34 and correspond to ages of 1129 ± 109 Ma ($R_i=0.7080 \pm 53; MSWD=3.98; M2$) and 1053 ± 107 Ma ($R_i=0.7022 \pm 94; MSWD=4.67; M2$), for site A and B, respectively. These ages are significantly younger than the corresponding U-Pb zircon ages determined for the same sites and reflect a disturbance in the Rb-Sr system, on the scale of a few tens of meters, that lowered the age and elevated the initial strontium ratio. It is conceivable that the time of this disturbance corresponds to the metamorphic episode that generated the new growth of zircon at about 1180 Ma.

The Rb-Sr whole rock ages determined for the Methuen Complex are considered geologically meaningless and are

interpreted to be the result of combining genetically unrelated samples and samples that have been disrupted by at least one metamorphic episode. However, some important features about the Rb-Sr system are revealed by this study. It is clear that collecting samples from widely spaced sampling sites increases the risk of unknowingly including genetically unrelated samples in the age calculation. Without the U-Pb zircon and sphene age information, the Rb-Sr whole rock data might have been interpreted as a geologically meaningful age with some data scatter caused by minor effects from metamorphism. Incidentally, the two sigma error associated with the composite age determination is relatively small by Rb-Sr standards but should not be used as a measure of the geological validity of such age determinations. In other words, it is possible to generate a relatively precise but geologically meaningless Rb-Sr whole rock age. It is also evident that the ability to determine geologically meaningful ages from individual sampling sites depends on the extent of Rb and Sr migration as proposed by many authors (eg. Roddick and Compston, 1977). In the case of the potassic members of the Methuen Complex, the migration distances for these elements has been quite large (on the order of a few tens of meters).

One question that is difficult to answer when the Rb-Sr system has been disrupted is what was the original initial strontium isotope ratio for the different phases of

the Methuen Complex? One approach to estimate this value for a unit that has a disturbed Rb-Sr system is to determine a model R_i by using the average $^{87}\text{Rb}/^{86}\text{Sr}$ and $^{87}\text{Sr}/^{86}\text{Sr}$ ratios for a single sampling site, making an age correction corresponding to the age obtained by the U-Pb zircon method. If the bulk Rb/Sr ratio has not changed significantly during the geological disturbance then the model R_i determined in this way should approximate the original initial strontium isotopic composition. The model R_i calculated for site A, using the 1242 Ma U-Pb zircon age, is 0.7021 and, to a first approximation, indicates that the Methuen quartz monzonite originally had a "mantle-like" initial strontium ratio, similar to most granitoid rocks from the CMB (refer to Chapter 5.5). A similar calculation made for site B results in a geologically unrealistic R_i (ie. < 0.700) and possibly indicates that the present bulk rock Rb/Sr ratio for this site is significantly higher than the original bulk rock value. Alternatively, the average bulk rock ratios used in this calculation may not be truly representative of the entire sampling site.

4.4 LOON LAKE PLUTON

4.4.1 Introduction

The Loon Lake pluton is a small body of granitic rock (8 km x 5 km) located in the southeastern corner of Chandos

township (Figure 35) that has been the subject of numerous studies including investigation of the structure (Cloos, 1934; Saha, 1957; 1959), petrography (Saha, 1957; 1959; Shaw, 1962; Dostal, 1973), contact relations (Chiang, 1965), geochemistry (Shaw and Kudo, 1965; McCammon, 1968; Dostal, 1973; 1975), oxygen isotope composition (Shieh et al., 1976; Heaman et al., 1982a), and Rb-Sr systematics (Heaman, 1980; Heaman et al., 1980a; b; Heaman et al., 1982a;). The enormous amount of effort invested to better understand the evolution of this pluton has revealed the following salient features:

- a) the pluton consists primarily of a monzonite (M) core and a quartz monzonite (QM) rim with a band of granodiorite gneiss and isolated occurrences of diorite-gabbro (Saha, 1959; Shaw, 1962; Dostal, 1973).
- b) the contact with the country rock is variable but generally abrupt. The contact is exposed along the western and southern margins and varies from migmatitic in the northwest to brecciated in the southwest. A contact metamorphic aureole is preserved in the southern part of the pluton (Chiang, 1965) where a knife-edge contact between M and country rock is visible.
- c) the QM rim has a prominent foliation that dips steeply toward the center of the pluton and is oriented parallel to the contact (Cloos, 1934).
- d) within the M, there is a general increase in the

biotite/(hornblende + clinopyroxene) ratio, quartz content and decrease in the An content of plagioclase (Saha, 1959; Dostal, 1973).

- e) the composition of samples from the M and QM follow smooth and often continuous trends on many major and trace element variation diagrams (Dostal, 1973; 1975). One notable exception is the unusual enrichment in the abundance of Rb observed for most QM samples (Heaman, 1980).
- f) the REE pattern for some QM samples are less fractionated than the most chemically evolved M sample (Dostal, 1975).
- g) the oxygen isotopic composition of the QM rim (9.9 to 12.0‰) is more heterogeneous and distinctly higher than the range observed for the M core (8.8 to 9.7‰; Shieh et al., 1976; Heaman et al., 1982a).
- h) the M and QM have identical "mantle-like" initial strontium ratios (0.7034) and within analytical uncertainty have similar Rb-Sr whole rock ages. A composite age of 1065 Ma was interpreted by Heaman (1980) and Heaman et al. (1982a) as the time of emplacement.

The relationship between the M core and QM rim has been addressed by numerous authors, however, there is still no clear consensus of opinion. Saha (1959; p.1304) suggested that the monzonite was emplaced prior to the quartz monzonite

because "veins of granite in syenite were observed". This observation is only relevant if the "veins of granite" he refers to are indeed apophyses of the main quartz monzonite mass. Without a detailed evaluation of these "veins" it is difficult to ascertain the importance of this observation because there are numerous cross-cutting dikes throughout the region; many of which have a mineralogy similar to the quartz monzonite. A separate intrusions origin for the M core and QM rim was also proposed by Dostal (1975) for completely different reasons. To explain the smooth and often continuous trends on many major and trace element variation diagrams, Dostal insisted that these two phases must be genetically related but to reconcile the REE data (feature f above) he preferred separate injections from a common magma reservoir. In his model (p.1343) he envisages that the "monzonitic magma was in part intruded into the present position and in part it fractionally melted and reacted with crustal rocks, producing the quartz monzonite and then subsequently intruded". This model was extended by Shieh et al. (1976) to accommodate the unusually high oxygen isotopic composition observed for both the M and QM. They suggested that a monzonite magma was intruded with an oxygen isotopic composition similar to that of normal syenites (5.5 to 7.5 ‰) and was enriched by isotopic exchange with the ^{18}O -rich country rock via a fluid phase. This exchange must have occurred at relatively high temperatures, while the monzonite was still molten, in order

to preserve the normal igneous fractionation values observed for coexisting quartz-biotite and quartz-magnetite pairs and to account for the isotopic homogeneity of the M. The QM, on the other hand, was enriched even further by a mixing process similar to the one described by Dostal (1975).

In an attempt to account for all the features listed above, Heaman et al. (1982a) proposed a model whereby the M core and QM rim represent separate injections of magma from a chemically stratified magma chamber. The involvement of a high temperature fluid was invoked to explain the anomalous Rb abundances and oxygen isotopic composition of the QM but whether this fluid interaction occurred in the magma chamber or after injection of the M and QM magma is uncertain. The identical initial strontium ratios were interpreted as strong evidence that the QM could not be generated by mixing an anatectic melt from the country rock with the same magma that crystallized to form the M core as suggested by other authors. The main problem with this and the other models is the difficulty explaining the less fractionated REE patterns and lower total REE content of some QM samples.

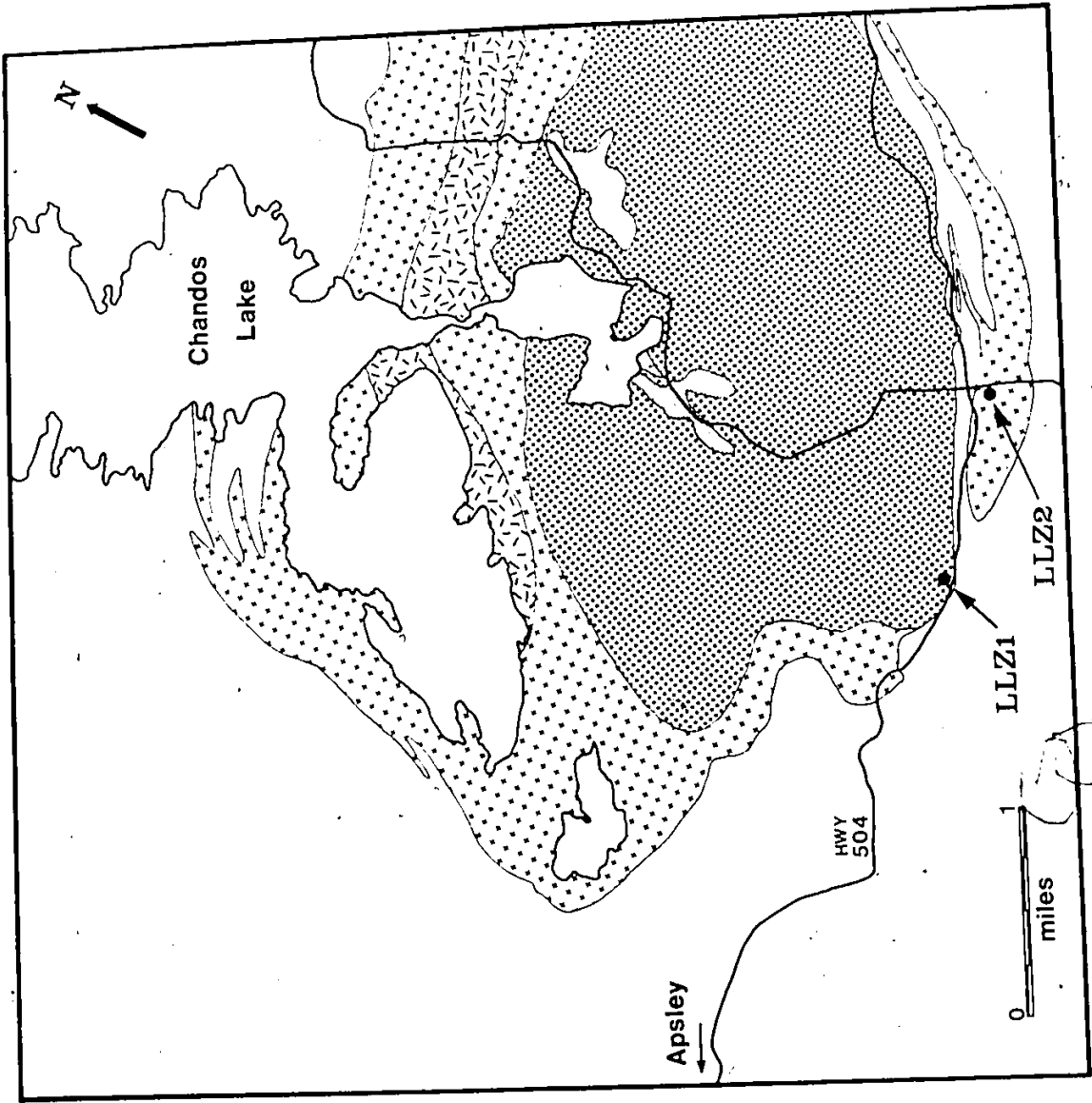
In all the models proposed so far, the M core and QM rim are considered to be the result of separate intrusions. To evaluate whether there has been any significant time hiatus between the emplacement of these two phases, a sample from the M core and QM rim were collected for a U-Pb zircon and sphene study. The location of the two sampling sites is

shown in Figure 35. A U-Pb zircon study should also provide information regarding the relationship between these two phases. For example, if the QM formed by mixing with an anatectic melt as suggested by Dostal (1975) and Shieh et al. (1976) then there might be evidence of an inherited zircon component in the QM magma. A U-Pb study of the Loon Lake monzonite is also of interest because it offers an excellent opportunity to compare the results from two independent dating techniques on an undeformed granitoid rock.

4.4.2 U-Pb Zircon, Sphene Geochronology

The U-Pb data for seven zircon and two sphene fractions from the Loon Lake pluton are presented in Table B4. The zircon grains from both the monzonite and quartz monzonite consist of a single colourless, prismatic population with no visible signs of cores. An example of zircon grains from the quartz monzonite sample (+200 mesh, zero degree non-magnetic), before final selection, is shown in Plate 6c and some abraded grains from fraction #21 are shown in Plate 6d. Of the ten zircon grains shown in Plate 6c only the tiny, euhedral grain in the center of the photo, with no visible cracks or alteration, would be selected for analysis. The sphene grains from both samples vary in colour from light orange to dark orange-brown and tend to form multi-faceted, subrounded crystals with a similar morphology to the crystals grown in experiments at high temperatures

Figure 35 . Geological sketch map of the Loon Lake pluton (after Shaw, 1962 and Dostal, 1975) showing the distribution of lithologies and the location of two sampling sites selected for the U-Pb zircon and sphene study. Quartz monzonite - cross pattern, Monzonite - coarse stipple pattern, Diorite-gabbro - fine stipple pattern, Granodiorite gneiss - random slash pattern.



(Franke and Ghobarkar, 1980).

The U-Pb data for three zircon fractions and one sphene fraction from the monzonite sample (LLZ1) are plotted on a conventional concordia diagram in Figure 36. The least discordant fraction (0.5% discordant) consists of the best quality zircon grains that were abraded to remove the outer surfaces. It is interesting that the more discordant fractions (3.2 and 4.1% discordant) were not abraded and yet have lower total common Pb contents than the abraded fraction. Therefore, most of the common Pb in these grains must reside within the grains; possibly associated with cracks, invisible altered domains or minute inclusions. All three zircon fractions are close to concordia and together define a discordia line that has a precise upper intercept age of $1090 \pm 7/-4$ Ma (76% probability of fit). The lower intercept age of 216 Ma is much less precise because of the long extrapolation. The U-Pb sphene fraction separated from the same sample plots within analytical error of concordia with a $^{207}\text{Pb}/^{206}\text{Pb}$ age of 1086 Ma so the U-Pb sphene and zircon ages are identical within analytical uncertainty. This implies that the monzonite magma must have cooled quite rapidly from about 650 °C (the approximate temperature for a granite minimum melt and U-Pb blocking temperature for zircon) to 500 °C (the U-Pb blocking temperature for sphene; Hanson et al., 1971).

The U-Pb data for four zircon fractions and a sphene

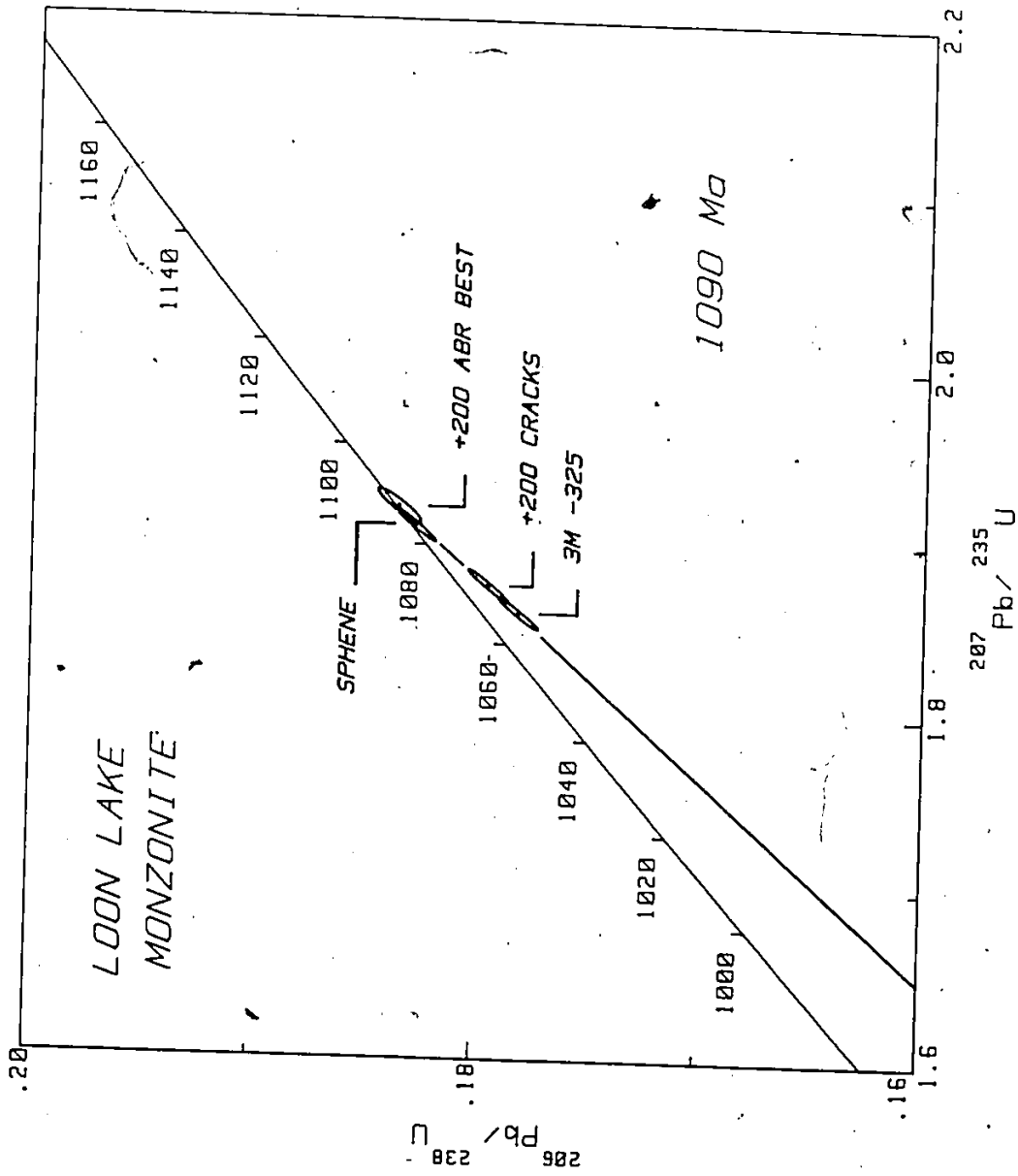


Figure 36 Concordia diagram with U-Pb zircon and sphene data from the Loon Lake monzonite.

fraction from the quartz monzonite sample are presented in Figure 37. Initially, three zircon fractions were prepared from the quartz monzonite sample in a similar way as the monzonite study above. These fractions (#21, 22, and 23 in Table B4), including one abraded fraction (#21), define a discordia line with a precise upper intercept age of 1205 ± 3 Ma even though the percent probability of fit is quite low (ie. 19%). When the U-Pb zircon data from the monzonite and quartz monzonite are compared, it is apparent that the quartz monzonite zircons have suffered a stronger Pb loss history than comparable zircon fractions from the monzonite. For example, zircons from the monzonite sample that are magnetic at 3 degrees tilt on a Frantz isodynamic separator (#18 in Table B4) are 4.1% discordant whereas similar zircons from the quartz monzonite sample (#23) are 16.5% discordant. However, most of the total common Pb in the latter must reside near the surface of the grains as witnessed by the reduction of common Pb in the same fraction from a value of 60 pg before abrasion (#22; Table B4) to a value of 17 pg after abrasion (#21; Table B4). The 1205 Ma age for the quartz monzonite sample is considerably older than the U-Pb zircon and sphene age and the Rb-Sr whole rock age (Heaman et al., 1982a) obtained for the monzonite. This difference in age between these two samples is somewhat surprising since all the models proposed for the origin of the pluton so far require that the monzonite and quartz monzonite are

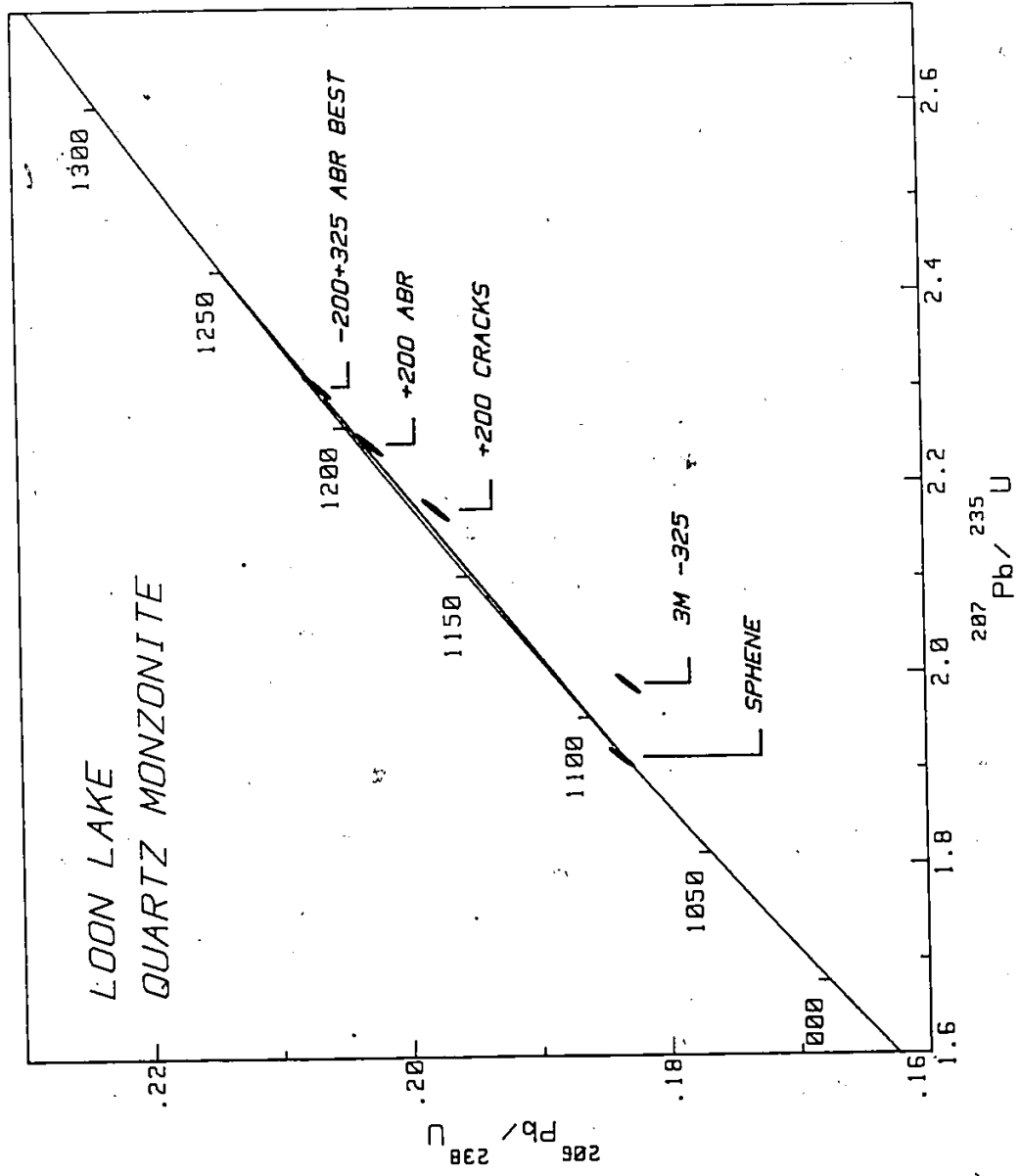


Figure 37 Concordia diagram with U-Pb zircon and sphene data from the Loon Lake quartz monzonite.

consanguineous.

A fourth zircon fraction (#20 in Table B4) was analysed from the quartz monzonite sample to investigate the reason for the low percentage probability of fit for the original three analyses. This fourth fraction was also selected from the least magnetic grains but from a smaller size fraction (-200+100 mesh). In addition, this fraction was given a more severe abrasion treatment and is reflected in the low total common Pb (14 pg) and high $^{206}\text{Pb}/^{204}\text{Pb}$ ratio (< 600,000). This fraction plots within experimental error of concordia with a $^{207}\text{Pb}/^{206}\text{Pb}$ age of 1217 Ma and clearly plots to the right of the 1205 Ma discordia line. Therefore, the $^{207}\text{Pb}/^{206}\text{Pb}$ age of 1217 Ma for this fraction provides a minimum age for the quartz monzonite at this sampling site. An important feature of the U-Pb zircon systematics is illustrated by this data. Although a very precise U-Pb zircon age was defined with the initial three analyses, the 1205 Ma age is geologically too young. If all four zircon fractions are used to define a discordia line, the percent probability of fit is even lower (0.1%) than the 19% quoted above using the original three analyses so the 1217 Ma age is not considered a reliable estimate for the emplacement age of the quartz monzonite. The following discussion evaluates other possible explanations for the data scatter in Figure 37.

An alternative explanation for the U-Pb zircon data presented above is that the zircons analysed from the quartz

monzonite sample contain an inherited component of Pb. A possible mixing line has been constructed in Figure 37 to pass through the least discordant, abraded zircon fraction and the sphene analysis discussed below. This mixing line intersects concordia at approximately 1250 and 1080 Ma and is virtually impossible to resolve because it passes very close to concordia such that every analysis that plots on the mixing line also plots within analytical uncertainty of concordia. If such a mixing line exists, the zircon analyses that plot below the mixing line must have experienced a relatively strong and recent Pb-loss history. In this case, the quartz monzonite could have been emplaced at about the same time as the monzonite (ie. 1090 Ma) but has incorporated older (ca. 1250 Ma) xenocrystic zircon.

The incorporation of xenocrystic zircon combined with recent lead loss to explain the U-Pb zircon data in Figure 37 is not favoured here because there are no visible signs of cores in these zircons, most of the zircon in the quartz monzonite would have to be xenocrystic; this is unlikely since all the granitoid rocks from this area contain abundant primary zircon, and that an inherited Pb component is usually associated with anomalous data scatter, much more than observed in Figure 37, when zircons of different size and magnetic susceptibility are analysed (eg. Corfu and Ayres, 1984). A more likely explanation for these data is that the sample of quartz monzonite used in this study is actually

from a relatively old (ca. 1250 Ma) granitoid unit, like the nearby Methuen quartz monzonite, and not from the Loon Lake pluton proper, that has experienced some thermal disturbance during the emplacement of the adjacent monzonite body at 1090 Ma. Therefore, the zircons from this sample lost some lead at 1090 Ma and again during some recent lead loss event.

The U-Pb data for a sphene fraction separated from the quartz monzonite sample is presented in Table B4. The $^{207}\text{Pb}/^{206}\text{Pb}$ age for this sphene fraction is 1083 Ma and is identical, within analytical uncertainty, to the sphene age obtained for the monzonite. In the case of the quartz monzonite, the sphene age can be interpreted in two ways: a) it may represent the resetting or new growth of sphene during the emplacement of the monzonite. In this regard, it is important to note that the quartz monzonite sample was collected within 2000 meters of the monzonite-quartz monzonite contact. b) it may also represent the resetting or new growth of sphene during metamorphism as suggested for a similar sphene age reported for the Methuen quartz monzonite (refer to section 4.3.3). If the Loon Lake monzonite is late-tectonic instead of post-tectonic then there would be little difference between these two interpretations.

There are a number of striking similarities between the U-Pb zircon and sphene results obtained for the Methuen quartz monzonite reported in section 4.3.3 (the sampling site for this unit is some 10 kilometers south of the Loon Lake

sampling site) and the Loon Lake quartz monzonite data presented here. At both sampling sites, the U-Pb zircon data indicate that the quartz monzonite was emplaced around 1250 Ma and the U-Pb sphene ages are identical indicating that there has been new growth of sphene (or resetting) at around 1085 Ma. It is also interesting that the U and Th content in the zircon fractions analysed from both sites are similar (compare the U concentrations and $^{206}\text{Pb}/^{208}\text{Pb}$ ratios for fractions #12-14 to fractions #20-23 in Table B4). The most likely explanation for these similarities is that the quartz monzonite at both sampling sites is part of the same 1250 Ma granitoid unit. Therefore, it is concluded that the quartz monzonite at the southern margin of the Loon Lake pluton is part of an older granitoid unit. To properly address the question of whether there is any significant time hiatus between the ~~emplac~~ placement of the Loon Lake monzonite and quartz monzonite requires additional U-Pb zircon studies on a sample collected from the main quartz monzonite mass exposed in the northern and western part of the pluton.

CHAPTER 5

DISCUSSION AND CONCLUSIONS

5.1 INTRODUCTION.

One of the primary objectives of this research has been to evaluate the potential of the Rb-Sr whole rock method of age dating for determining geologically meaningful ages in high grade metamorphic terrains. The approach adopted has been to compare Rb-Sr whole rock ages, determined using a variety of sample collecting techniques, to U-Pb zircon and sphene ages obtained from the same unit. The results from this comparative study are discussed in this chapter and provide, in addition to a better understanding of the behaviour of the Rb-Sr system in deformed rocks, valuable information regarding the timing of igneous and metamorphic events in the Chandos township area.

5.2 SELECTING SAMPLES FOR Rb-Sr GEOCHRONOLOGY

The most important question that must be considered before attempting a Rb-Sr whole rock age determination is how

should the samples be collected so that a geologically meaningful age can be obtained? This study indicates that there is no simple answer to this question. For some units, like the Apsley gneiss, different ages are obtained depending on the sampling technique used and for other units, like the Methuen Complex, there is convincing evidence that Rb-Sr whole rock ages can be precise but geologically meaningless. However, there are two general comments that can be made with regard to collecting samples from the Chandos township area.

The first concerns the range in Rb/Sr ratios found at a single sampling site. For all units examined in this study, that have been affected by metamorphism, there is a insufficient range in the Rb/Sr ratio to determine a Rb-Sr whole rock age from a single sampling site. The advantage of determining a Rb-Sr age from a single sampling site is that there is less risk of collecting samples that are not cogenetic. In at least one example, the Tallan Lake granodiorite, the age determined in this manner is in excellent agreement with a U-Pb zircon age determined for the same sampling site. On the other hand this is not the case for late- to post-tectonic intrusions like the Coe Hill pluton (Atkins, 1983). The question then arises whether this range in Rb/Sr for samples collected at a single sampling site in deformed units is a primary feature or a consequence of metamorphism?

The second conclusion from the sampling experiment is

that the magnitude of the response of the Rb-Sr system to a geological disturbance is related to bulk rock composition. This can be demonstrated by comparing the results obtained for the Tallan Lake granodiorite and Methuen quartz monzonite (site A). As mentioned above, the Rb-Sr whole rock and U-Pb zircon ages obtained for the Tallan Lake granodiorite are in excellent agreement but a geologically meaningless Rb-Sr whole rock age (1129 Ma) was obtained for the Methuen quartz monzonite that is between the time of emplacement (1242 Ma) and metamorphism (ca. 1100 Ma). Therefore, a more promising application of Rb-Sr whole rock dating in the CMB is determining the age of emplacement of the more sodic granitoid bodies from a single sampling site.

5.3 SUMMARY OF GEOLOGICAL RELATIONSHIPS IN THE CHANDOS TOWNSHIP REGION

5.3.1 Supracrustal Rocks

A summary of the Rb-Sr and U-Pb zircon, sphene ages determined for supracrustal rocks in the Chandos township region is presented in Figure 38 and Table 5.1. The majority of these ages were determined using the Rb-Sr whole rock technique and most have large associated errors. It is clear from this diagram that it is not possible to resolve detailed stratigraphic relationships with this method. The Rb-Sr whole rock ages that cluster around 1000 Ma were determined on

Figure 38 - Compilation of Rb-Sr whole rock and mineral ages and U-Pb zircon and sphene ages for rock units from the Chandos Township area determined in this study and Heaman (1980).

Rb-Sr Ages

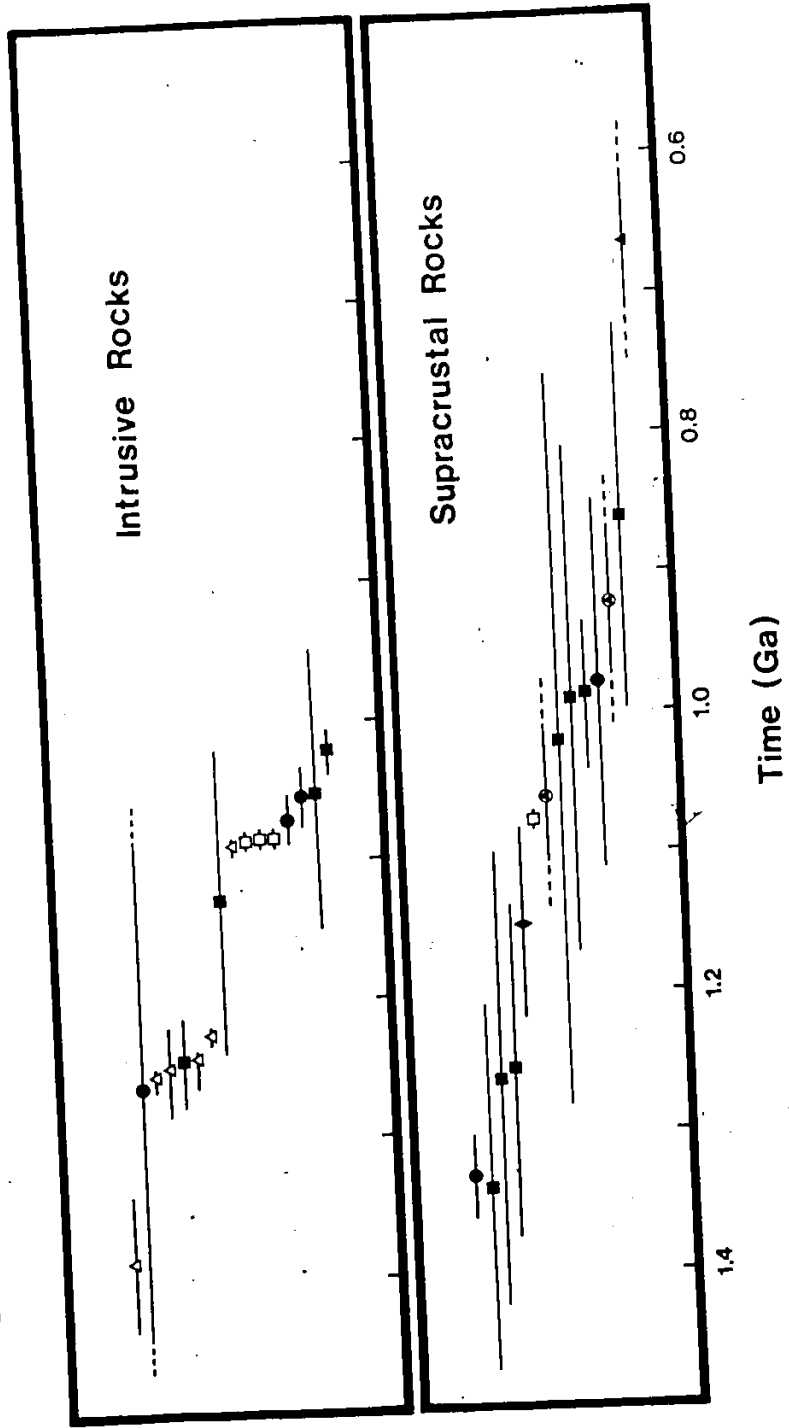
- Whole Rock (regional)
- Whole Rock (single sampling site)
- ◆ Whole Rock (slab study)
- ⊕ Plagioclase - Whole Rock Pair
- ▲ Biotite - Whole Rock Pair

U-Pb Ages

- △ Zircon
- Sphene

Figure 38

U-Pb and Rb-Sr Ages from the Chandos Township Area



potassium-rich members of the Hermon Group (in the vicinity of Silent Lake) and on the potassic Apsley gneiss and are significantly younger than the presumed age (ca. 1250 Ma) for deposition and extrusion of these rocks. The Rb-Sr system in these potassium-rich rocks has either responded to a disturbance at about 1000 Ma or has remained open for a considerable period of time following regional metamorphism (see section 5.3.3). The Rb-Sr whole rock results for the sodic Apsley gneiss (1341 to 1256 Ma) overlap, within error, the range of ages determined for the Tudor felsic volcanics (1286 to 1226 Ma; Silver and Lumbers, 1966) but are also not precise enough to unravel complex stratigraphic relationships in this region. Unfortunately, no reliable U-Pb zircon ages are available for the units examined in this study. The significance of the precise U-Pb sphene age is discussed in section 5.3.3.

5.3.2 Igneous Rocks

The Rb-Sr and U-Pb zircon, sphene ages for igneous rocks from the Chandos township area, determined in this study, are also presented in Figure 38 and Table 5.1. Many of these ages are much more precise than the ages determined for the supracrustal rocks with the suggestion of two distinct periods of igneous activity, 1250 to 1240 Ma and 1090 Ma. Units examined in this study that belong to the 1250 to 1240 Ma period of igneous activity include the Tallan Lake sill

TABLE 5.1 - Compilation of U-Pb zircon, sphene and Rb-Sr ages (Ma) from the Chandos township area determined in this study and Heaman (1980)

<u>UNIT</u>	<u>Rb-Sr</u>	<u>Ri</u>	<u>U-Pb</u>
APSELEY GNEISS			
Sodic Suite			
a) Regional	*1402±57	0.7022±12	
b) Site A	1341±131	0.7035±18	
- Slab	1151±67	0.7056±7	
- Plag-WR	*1062		
c) Site B	1256±119	0.7037±7	
d) Site C	1264±161	0.7037±16	
e) Composite	1333±24	0.7034±1	
f) Plag-WR	*924		
g) Sphene			1078±5
Potassic Suite			
a) Regional	*979±131	0.7143±70	
b) Plag-Bio-WR	*666		
SILENT LAKE COMPLEX			
a) Site A	990±181	0.711±7	
b) Site B	862±137	0.720±10	
c) Site C	1021±263	0.711±9	
d) Site D	988±53	0.710±1	
METHUEN COMPLEX			
a) Site A	1129±109	0.7080±53	1242±22/-6
- Sphene			1085±5
b) Site B	1053±107	0.7222±94	1367±54/-41
			1180±5
c) Composite	1234±56	0.7027±20	
TALLAN LAKE SILL			
a) Granodiorite	1244±32	0.7037±4	1254±11/-4
b) With Fractures	1023±17	0.7059±4	
c) Amphibolite	1261±268	0.7034±2	1239
LOON LAKE PLUTON			
a) Monzonite	*1055± 22	0.7034±4	1090±7/-4
- Sphene			1086±5
b) Quartz Monzonite	*1071± 18	0.7034±4	
- Sphene			1083±5

* - Ages reported by Heaman (1980)

and Methuen quartz monzonite. The Tallan Lake sill occurs between horizons of the Dungannon Formation and the precise U-Pb zircon age of $1254 \pm 11/-4$ Ma for this unit provides the best minimum estimate for the deposition of the Mayo Group.

The only indication that there may be older crustal material beneath the rocks exposed in the study area is the 1367 Ma U-Pb zircon upper intercept age for a granite inclusion within the Methuen Complex. There is considerable uncertainty attached to this age and further research is required to verify this finding.

The U-Pb zircon and sphene ages determined for the post-tectonic Loon Lake monzonite (1090 and 1085, respectively) are older than the Rb-Sr whole rock age (1055 ± 22 Ma) indicating that the Rb-Sr system may have remained open for approximately 30 Ma after emplacement of the body, possibly reflecting slow cooling or may have been affected by subsequent geological disturbances such as late-stage hydrothermal activity (see section 5.3.4). The colinearity of the Rb-Sr data supports the slow cooling hypothesis. Alternatively, if the currently used decay constant for ^{87}Rb is 2% too high then the ages determined by these two techniques would be in agreement.

The last recorded event in the Chandos township region is a period of fracturing and hydrothermal activity at about 1023 Ma (Rb-Sr whole rock age) that affected samples from the Tallan Lake sill (see section 5.3.4). This

hydrothermal activity may also coincide with the emplacement of pegmatites (U-Pb zircon ages) in the Bancroft and surrounding region (Silver and Lumbers, 1966; Rimsaite, 1981).

5.3.3 Effects of Metamorphism

In parts of the Grenville Province in North America there is evidence for at least two major periods of metamorphism at about 1650 and 1000 Ma (Krogh and Wardle, 1984) but the timing of regional metamorphism in the CMB is controversial. As mentioned in section 2.2.2, Silver and Lumbers (1966) suggested that there may be two periods of metamorphism within the CMB, an older (circa 1250 Ma) event, subsequently referred to as the Elzevirian orogeny (Moore, 1982), producing the lower grade metamorphic assemblages and a younger and more intense episode that is responsible for the amphibolite grade assemblages (Ottawan orogeny; Moore, 1982). At present, there is no consensus on the timing of this younger metamorphic episode. Moore and Thompson (1980) proposed that polyphase deformation and regional metamorphism occurred at about 1050 to 1000 Ma, after the deposition of the Flinton Group, whereas Baer (1981) interpreted the distribution of radiometric ages in the Grenville Province to indicate two distinct thermal events at about 1100 and 950 Ma.

The U-Pb zircon, sphene and Rb-Sr whole rock ages

determined in this study (Figure 38 and Table 5.1) provide some constraints for the timing of regional metamorphism in the Chandos township area and possibly for the entire CMB. A good estimate for the minimum age of regional deformation and metamorphism is the U-Pb zircon age (1090 Ma) for the late-tectonic Loon Lake monzonite (refer to section 4.4.2 and Heaman and Krogh, 1985). A minimum age for regional metamorphism at about 1090 Ma is also supported by the Pb isotopic data obtained for sphene fractions separated from samples of the Apsley gneiss, Methuen Complex and Loon Lake pluton. The results for four sphene fractions from different rock units are plotted on a $^{207}\text{Pb}/^{206}\text{Pb}$ versus $^{204}\text{Pb}/^{206}\text{Pb}$ diagram in Figure 39 and the slope of the isochron corresponds to an age of 1080 Ma. The colinearity of these data indicates that new sphene growth was occurring at about 1080 Ma throughout the region. Since the U-Pb blocking temperature for sphene is about 500°C (Hanson et al., 1971) it is possible that the sphenes grew sometime before 1080 Ma and responded to regional cooling. Therefore, the 1080 Ma age records the time when the region cooled below 500°C and is consistent with the contention that regional metamorphism must have occurred prior to 1090 Ma.

Another feature of the rocks examined in this study is that very few samples contain evidence of new zircon growth during a period of regional deformation and metamorphism. Therefore, the temperatures reached during this metamorphic

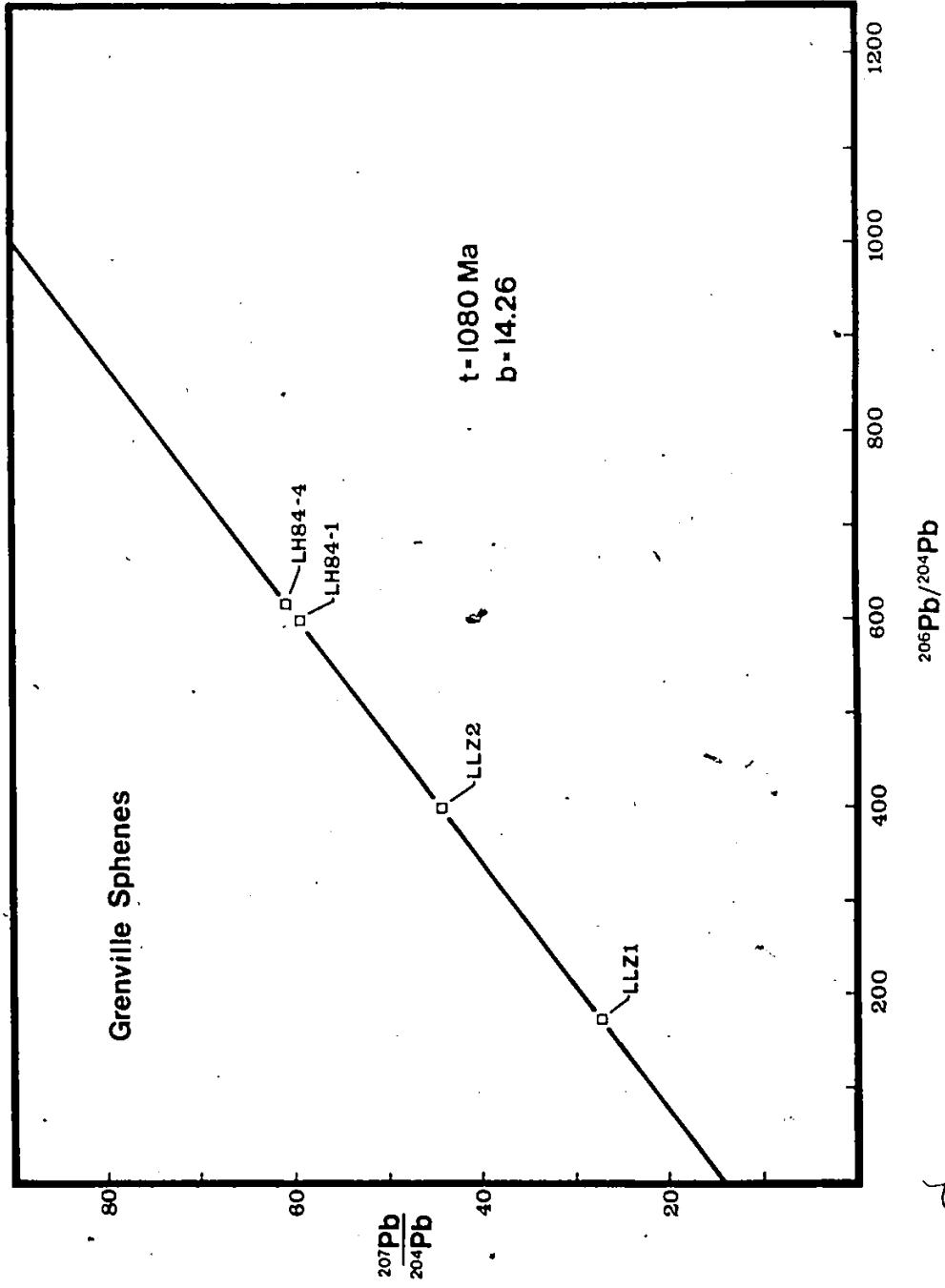


Figure 39 $^{207}\text{Pb}/^{204}\text{Pb}$ versus $^{206}\text{Pb}/^{204}\text{Pb}$ diagram for sphene samples from the Chondos Township area.

episode could not have exceeded approximately 650°C, the temperature at which zircon would show signs of significant Pb loss. Therefore, either this portion of the CMB was maintained at temperatures between 500 and 650°C for a long period of time or the culmination of regional deformation and metamorphism could not have occurred much before 1090 Ma. Slow cooling (ca. 2°C/Ma) between 1150 and 1050 Ma has been proposed for this region by Lopez-Martinez and York (1983) based on $^{40}\text{Ar}/^{37}\text{Ar}$ studies of hornblende, biotite and plagioclase mineral separates from the Thanet and Cordova gabbros and it is interesting that the biotite ages obtained from the Thanet gabbro (1083 and 1091 Ma) are consistent with the interpretation that regional metamorphism culminated prior to 1090 Ma. The only exception to this generalization is the new zircon growth at about 1180 Ma indicated for a granite inclusion within the Methuen Complex (site B). However, there is considerable uncertainty attached to the accuracy of the age and to the interpretation that there is actually new zircon growth.

Although there is good evidence that 1090 Ma is a minimum estimate for the time of regional metamorphism, it is more difficult to establish a maximum estimate. Hofmann (1979) suggested that Rb-Sr dating of thin slabs might provide a means to determine the age of metamorphism. The Rb-Sr results for several 1 to 2 cm wide slabs from the Apsley gneiss indicate an age of 1151 ± 67 Ma and, although not

very precise, do suggest a maximum estimate for the time of metamorphism. Therefore, regional metamorphism in the Chandos township area seems to have culminated some time between 1150 and 1090 Ma. This estimate is higher than the age of polyphase deformation (1050 to 1000 Ma) proposed by Moore and Thompson (1980) and lower than the age (1170 Ma) proposed by Lopez-Martinez and York (1983) from $^{40}\text{Ar}/^{37}\text{Ar}$ studies but correlates with a high grade metamorphic event at about 1100 Ma that has been found for other regions within the Grenville Province of Quebec (eg. Doig, 1977) and the Sveconorwegian Province of SW Sweden (eg. Daly et al., 1983).

The effect of regional metamorphism on the behaviour of the Rb-Sr system appears to be minimal in sodic rocks, like the sodic Apsley gneiss and Tallan Lake granodiorite, where the migration distances for Rb and Sr during metamorphism are on the order of a few centimeters. However, the Rb-Sr system in potassic granitoid rocks, like the Methuen quartz monzonite, has been disrupted by metamorphism. At the present time, it is difficult to distinguish between effects of regional metamorphism and the profound disturbance in the Rb-Sr system generated by late-stage fluid migration (next section).

5.3.4 Influence of Fractures

A particularly interesting result from the Rb-Sr study of the Tallan Lake granodiorite is that, when the samples

from one sampling site are subdivided into fracture-bearing and fracture-free, two distinct and relatively precise Rb-Sr whole rock ages are obtained. As mentioned in section 4.2.5.1, the older age (1244 Ma) defined by the fracture-free samples is in excellent agreement with a U-Pb zircon age (1254 Ma) determined for the same sampling site and represents the time of granodiorite emplacement. The younger age of 1023 Ma, defined by the fracture-bearing samples, demonstrates that fluid migration associated with these fractures has had a profound effect on the Rb-Sr whole rock system even though they do not show any visible signs of alteration, except the slight chloritization of hornblende. However, the higher abundance of K-feldspar could indicate that the resetting of the Rb-Sr system, largely by copious additions of Rb, is related to new growth of this mineral.

The Rb-Sr results for the samples that contain fractures provides some insight into the mechanism by which the Rb-Sr whole rock system is reset. The Rb-Sr data for these samples are colinear, despite large variations in the Rb/Sr ratio, indicating that the process of homogenization has been similar in every fracture-bearing sample. This is contrary to the results obtained by Field and Raheim (1979) where the Rb-Sr system for fracture-bearing samples of charnockitic gneiss was disturbed by a low grade metamorphic event. Their results indicate that variations in the intensity of secondary alteration contributed to

Figure 40 $^{87}\text{Sr}/^{86}\text{Sr}$ versus $1/\text{Sr}$ diagram for samples from the Tallan Lake sill. Solid circles - amphibolite, solid squares - fracture-bearing granodiorite, open squares - fracture-free granodiorite, open triangle - transitional, solid triangle - N. limb granodiorite



anomalous data scatter and not to a totally reset isochron. One possible explanation for the colinearity of the present data is that the net effect of fluid:rock interaction along the fractures is primarily the addition of Rb, with little or no change in Sr content. This can be seen quite clearly on the mixing diagram ($^{87}\text{Sr}/^{86}\text{Sr}$ versus $1/\text{Sr}$) shown in Figure 40. If the Rb-Sr systematics of a particular unit are controlled by mixing of two components that have different strontium isotopic ratios and Sr concentrations (in the present example the two end-members would be the compositions of the fluid and rock) then the results should follow a straight line with, most commonly, a positive slope. However, the fracture-bearing samples define a vertical trend on this diagram with only a small variation in Sr abundance but an enormous variation in the strontium isotopic composition. This can only be explained by addition, or depletion in the case of sample TL2, of Rb. This appears to hold true for the amphibolite samples as well (see Figure 40). The introduction of alkalis by fluid:rock interaction along microfractures is supported by the slab study where Rb enrichment in the total rock is most intense near the fracture. Therefore, fluid-rock interaction along irregularly spaced fractures appears to be an effective mechanism for generating large variations in the Rb/Sr ratio on the scale of a few meters. The corollary is that the Rb/Sr ratio of the granodiorite before the fractures developed must have been quite uniform otherwise a net

addition of Rb would be expected to cause some data scatter.

At least three different hypotheses can be postulated for the origin of the fractures in the Tallan Lake granodiorite. They could have formed; 1) during outgassing that accompanied regional metamorphism (circa 1100 Ma), 2) as a consequence to hydraulic fracturing associated with the emplacement of the nearby Loon Lake pluton or 3) in response to a minor geological event during regional cooling. If these fractures formed by either of the first two mechanisms, then migration of fluids along the fractures must have continued for about 70 Ma in order to preserve a colinear Rb-Sr data array at 1023 Ma. A more plausible explanation is that the 1023 Ma age reflects a minor event during regional cooling that is characterized by brittle deformation and migration of fluids. There are also a number of U-Pb zircon ages for undeformed pegmatite dikes in the Bancroft area that cluster around 1020 to 1030 Ma (eg. Silver and Lumbers, 1965; Rimsaite, 1981) and it is conceivable that the fluid migration in the Chandos township region is also related to this injection of pegmatite near Bancroft.

A second fracture study was performed on a sample from the sodic Apsley gneiss where the fractures are sealed with biotite and much easier to recognize in the field. The Rb-Sr data for this fracture-bearing sample (AG50), including a slab containing a fracture, plot close to a 1150 Ma reference line indicating that these fractures were sealed at about

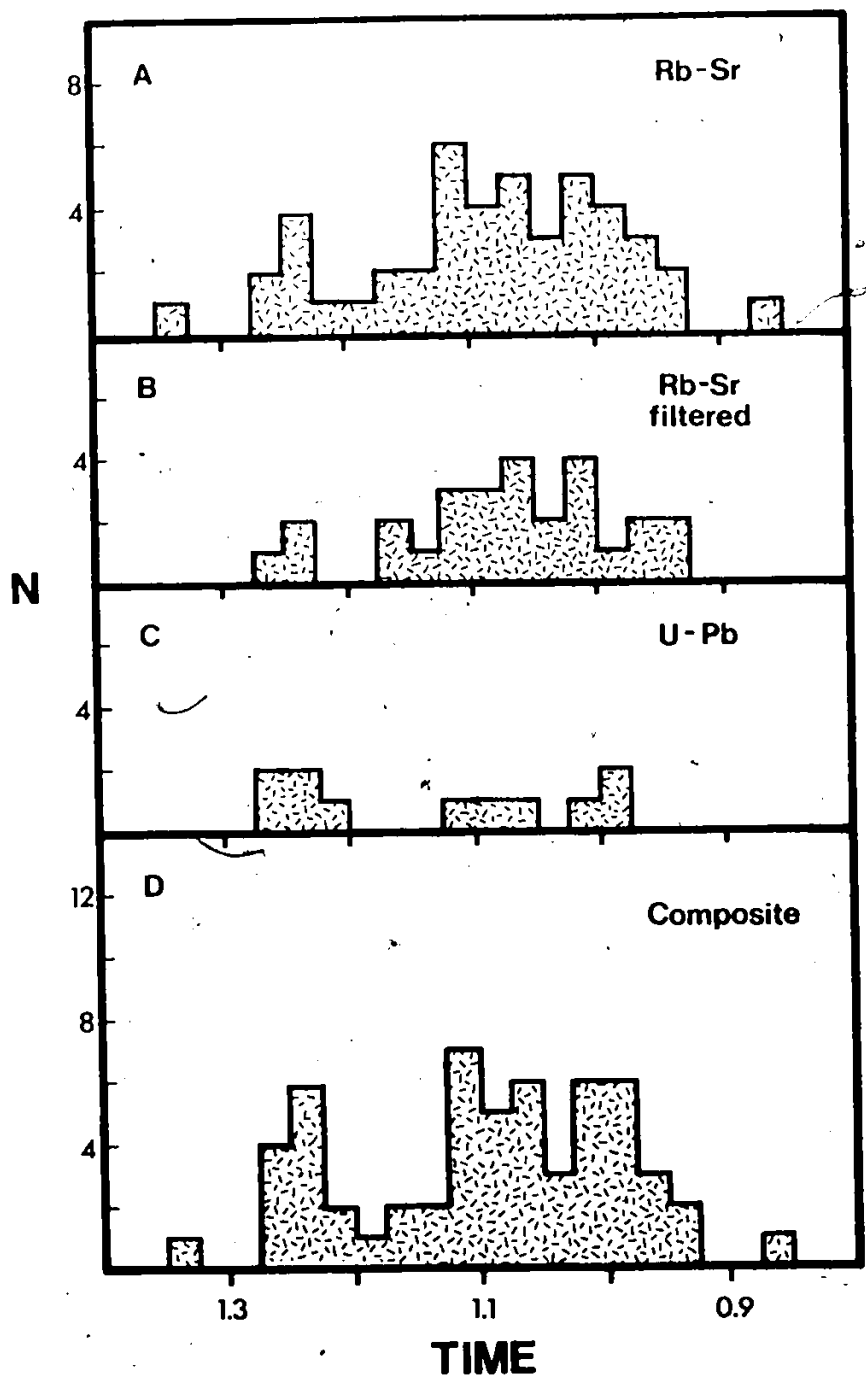
this time and probably, in some way, are related to the circa 1090 to 1150 Ma regional metamorphic event suggested above. These fracture studies indicate that there are at least two distinct periods of fracturing in the study area.

5.4 TIMING OF IGNEOUS ACTIVITY IN THE CMB

One conclusion reached from the present study is that not all Rb-Sr whole rock age determinations for granitoid rocks from the CMB provide geologically meaningful age information. Therefore, any compilation of Rb-Sr whole rock ages, including the ones determined in this study, will be a mixture of geologically meaningful and meaningless ages. It is difficult to assess the geological significance of most published Rb-Sr data from the CMB because there is no independent check for these ages but it is clear from the examples presented in this study that geologically meaningless ages are commonly associated with anomalous data scatter (ie. high MSWD values and large associated errors). A compilation of Rb-Sr whole rock and U-Pb zircon ages, plus initial strontium ratios, for granitoid rocks from the CMB in Ontario and Quebec (Table 5.2) is presented here with the aim of evaluating the existing data base and commenting on the nature and timing of this igneous activity.

The age data compiled in Table 5.2 are depicted in the form of histograms in Figures 41. In addition to a composite age diagram (Figure 41d), three other histograms are

Figure 41 - Compilation of Rb-Sr whole rock and U-Pb zircon ages for granitoid units from the CMB in Ontario and Quebec. a) all Rb-Sr whole rock ages, b) filtered Rb-Sr data set, c) U-Pb zircon ages, and d) composite



presented to illustrate the distribution and proportion of Rb-Sr whole rock ages (Figure 41a), the distribution of Rb-Sr whole rock ages excluding geologically "suspect" ages (Figure 41b) and U-Pb zircon ages (Figure 41c). A Rb-Sr whole rock age in Table 5.2 is considered geologically "suspect" if there are less than four samples used in the age calculation, the MSWD value is greater than 3, and the initial strontium ratio is lower than the lowest acceptable value for mantle strontium for this time period (ie. 0.702). There are two features of the age distribution that are immediately evident from Figure 41. Almost 50% of the Rb-Sr ages would be classified as geologically "suspect" by the filtering technique used (compare Figure 41a and b) and comparatively few U-Pb zircon ages have been published.

There is clearly an indication of igneous activity in the CMB at about 1250 Ma in both the Rb-Sr (Figures 41a and b) and U-Pb zircon (Figure 41c) data and two examples of granitoids that were emplaced at this time have been found in the study area; the Tallan Lake granodiorite and the Methuen quartz monzonite. There are relatively few radiometric ages in the period 1225 to 1125 Ma possibly indicating a period of quiescence in igneous activity during this time. The majority of ages for granitoid rocks occur in the range 1150 to 925 Ma and represent a combination of geologically meaningful (eg. the 1090 \pm 7/-4 Ma U-Pb zircon age determined for the post-tectonic Loon Lake pluton) and geologically meaningless

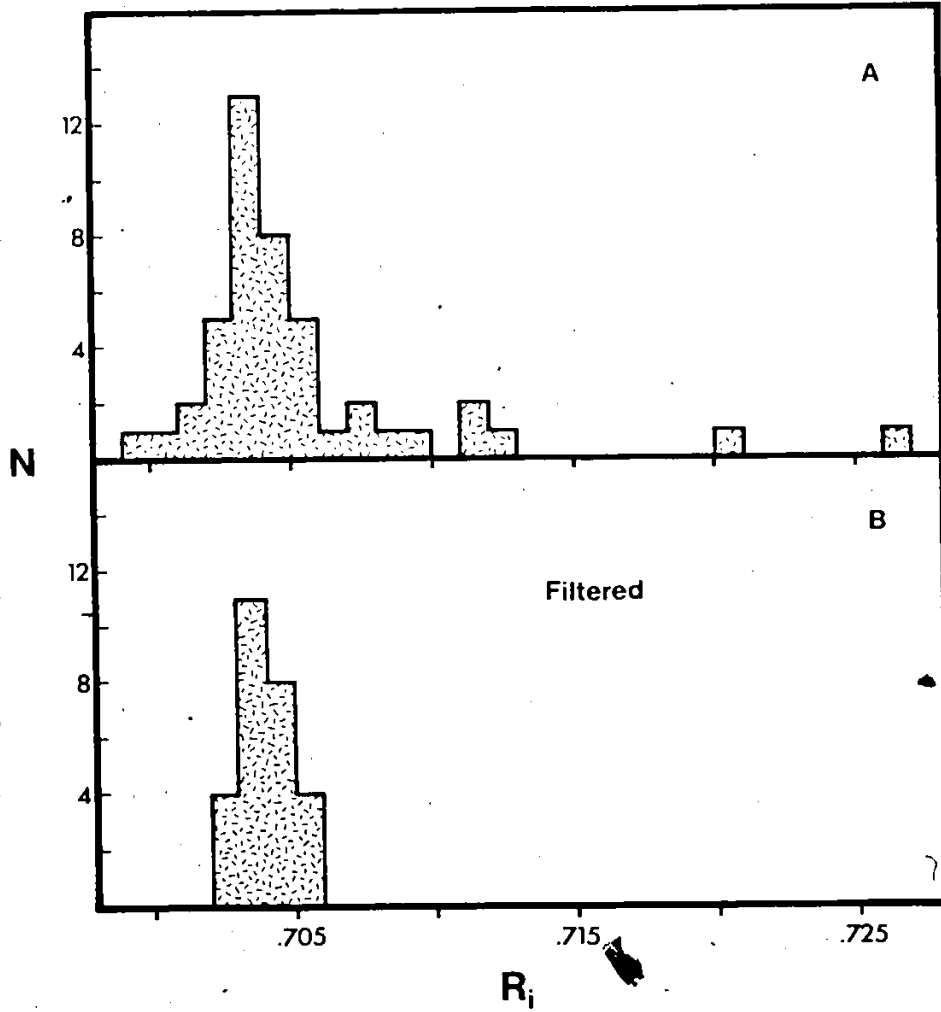
(eg. the 1129 ± 109 Ma errorchron age determined for the Methuen quartz monzonite). It is not surprising, therefore, that there are no prominent peaks of igneous activity discernable during this time period. At best, the concentration of radiometric ages in the period 1150 to 925 Ma reflects a prolonged period of igneous activity after regional metamorphism (ca. 1150 Ma) or, more likely, reflects the difficulty in determining precise and geologically meaningful Rb-Sr whole rock ages in the CMB. It is clear that in order to better understand the timing of igneous activity in the CMB it will be necessary to obtain many more precise and geologically meaningful age dates.

5.5 ISOTOPIC CONSTRAINTS ON THE ORIGIN OF CMB GRANITOID ROCKS

5.5.1 Initial Strontium Ratios

A compilation of initial strontium ratios for granitoid rocks from the CMB is presented in Table 5.2 and portrayed in the form of histograms in Figures 42a and b. In both diagrams it is obvious that the majority of initial strontium ratios fall within the range 0.702 to 0.706 with a maximum between 0.703 to 0.704. The abundance of low initial strontium ratios indicates that the majority of granitoid rocks have been derived by partial melting of material with a low average Rb/Sr ratio (< 0.2) or, alternatively, material

Figure 42 Compilation of initial strontium ratios for
granitoid rocks from the CMB. a) composite
(n=45) - the R_i for unit 23 in Table 5.2 has
been omitted. b) filtered.



with a higher average Rb/Sr ratio that has experienced a short (< 200 Ma) crustal residence history, but there is clearly no evidence that these rocks interacted (ie. partial melting or contamination) with relatively old sialic crust. The low initial strontium ratios combined with the general absence of inherited zircons is considered strong evidence that old (ie. Archean to Proterozoic) sialic crust does not form the basement upon which the Grenville Supergroup was deposited.

These data do not, however, exclude the possibility that the basement could be similar in composition to the low Rb/Sr tonalites etc. found in the "Algonquin Batholith" (circa 1400 to 1500 Ma old; Lumbers, 1982), to the north of the study area. The presence of such a basement beneath the CMB also provides a more likely candidate (compared to a mantle rock such as a garnet lherzolite) for the source material from which the large volume of granitic magma in the CMB was derived. It appears that the 1367 Ma U-Pb zircon upper intercept age for the granite inclusion in the Methuen Complex, although questionable, is the only evidence, so far, that supports the suggestion above. Additional geochemical and isotopic investigations are required to elucidate the origin of these granitoid bodies.

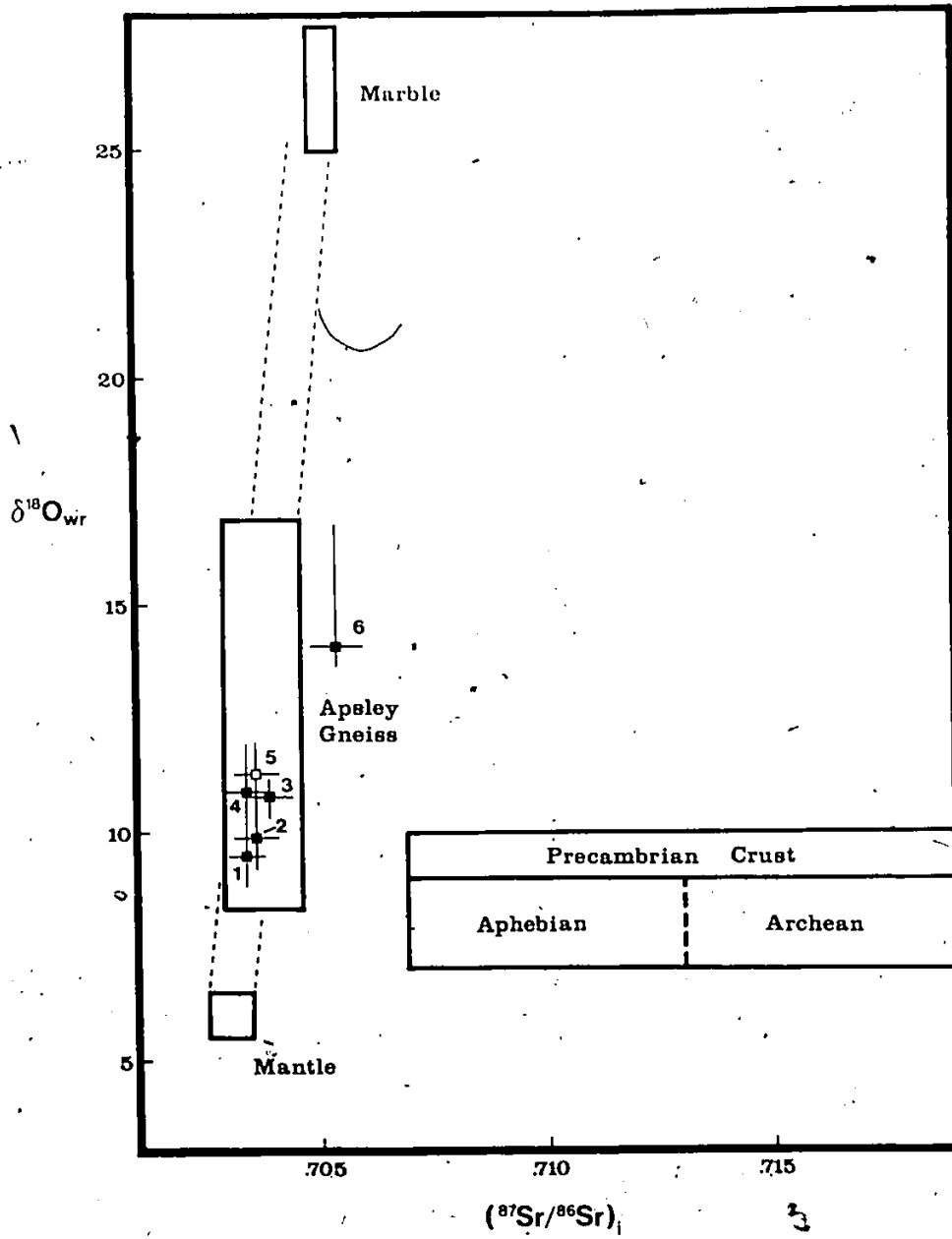
There are several high initial strontium ratios (ie. > 0.708) in Figure 42a but the fact that they coincide with ages that are considered geologically "suspect" and are

removed by the filtering technique (compare Figures 42a and b) indicates that these ratios have likely been elevated by secondary disturbances that affected the Rb-Sr system. It is difficult to argue against the possibility that some of these high initial strontium ratios do reflect involvement with upper crustal material and the associated data scatter is a result of a heterogeneous initial strontium composition in the magma. In such a case, however, a Rb-Sr age determination would be geologically meaningless because a fundamental assumption in Rb-Sr dating, that all samples had identical initial strontium ratios at the time of their formation, is violated.

5.5.2 Sr-O Relationships

Recent attempts have been made to use combined stable and radiogenic isotopic studies to obtain information regarding the source material from which granitic magma has been derived and the processes that have affected this magma during its emplacement (Taylor, 1980; Harmon and Halliday, 1980). The strontium and oxygen isotopic composition for six granitoid bodies from the CMB are plotted on a Sr-O diagram in Figure 43 along with various crustal and mantle isotopic reservoirs. The initial strontium ratios are those determined from Rb-Sr whole rock studies (this study and Krogh and Hurley, 1968) and the oxygen isotopic compositions represent an average whole rock value (this study; Shieh, 1985; Heaman,

Figure 43 Sr-O correlation diagram for granitoid rocks from the CMB. Solid squares - post-1100 Ma plutons, open square - 1250 Ma granitoid. 1 - Loon Lake monzonite, 2 - Westport pluton, 3 - Coe Hill pluton, 4 - Loon Lake quartz monzonite, 5 - Tallan Lake granodiorite, 6 - Lyndehurst pluton. The various isotopic reservoirs are discussed in the text.



et al. 1982a). The various reservoirs shown in Figure 43 were constructed using the following information. The oxygen isotope composition of the mantle (5.5 to 6.5%) is taken from Taylor (1978) and the initial strontium ratio is calculated for a 1100 Ma mantle ($R_i=0.69899$) assuming a range in $^{87}\text{Rb}/^{86}\text{Sr}$ between 0.07 and 0.09. The isotopic composition for a Precambrian crustal reservoir was calculated using Rb-Sr data for an Archean tonalite ($t=2800$ Ma; $R_i=0.701$; $^{87}\text{Rb}/^{86}\text{Sr}=0.5$) reported by Beakhouse (1983) and the oxygen isotopic composition for normal granitoid rocks (Taylor, 1978). The reservoirs for marble and quartzo-feldspathic gneiss (Apsley gneiss) from the Grenville Supergroup have been constructed using data from Heaman (unpublished data), Shieh et al. (1976), and Krogh and Hurley (1968).

The majority of granitoids plotted in Figure 43 are post-tectonic (solid squares) with radiometric ages younger than 1100 Ma, with the exception of the Tallan Lake granodiorite (open square, #5). The majority of these granitoids plot within the field for Grenville Supergroup quartzo-feldspathic gneisses and are enriched in ^{18}O compared to normal granitic rocks (Taylor, 1978). These data can be interpreted to indicate that these plutons:

- a) were derived from quartzo-feldspathic rock, similar in age and composition to the Apsley gneiss
- b) were derived in the mantle and/or lower crust and involved some contamination with rocks like the Apsley

gneiss

- c) were derived in the mantle or, more likely, lower crust and have subsequently interacted at depth with carbonate metasediments

The first two interpretations are less probable because the Apsley gneiss reservoir shown in Figure 43 was calculated for the sodic Apsley gneiss only ($^{87}\text{Rb}/^{86}\text{Sr}$ varies from 0.1 to 1.0) but doesn't include the potassic members. If an average for the Apsley Formation is used, then the anticipated initial strontium ratio obtained during partial melting of the entire Apsley Formation would result in granitoid rocks with more radiogenic initial strontium ratios. Although the latter interpretation (c) is preferred here, there is clearly no indication that these plutons have interacted with early Precambrian crust of the composition shown in Figure 43.

TABLE 5.2 - Age Compilation For CMB Granitoid Rocks

ONTARIO

UNIT ^a	n ^b	MSWD ^c	Ri	Rb-Sr ^c	U-Pb ^d	Ref ^e
1 Tallan Lake	12	25.7 (M2)	.7051±8	1089±83		1
2 Tallan Lake	6	0.92(M1)	.7037±4	1244±32	1254	1
3 Tallan Lake	6	0.38(M1)	.7059±4	1023±17		1
4 Tallan Lake	2		.7075	1100		1
5 Methuen	21	25.6 (M2)	.7027±20	1234±56		1
6 Methuen	8	3.98(M2)	.7080±53	1129±109	1242	1
7 Methuen	7	4.67(M2)	.7222±94	1053±107		1
8 Silent Lake*	5	20.5 (M2)	.7110±72	990±181		1
9 Silent Lake*	7	49.6 (M2)	.7204±103	862±137		1
10 Silent Lake*	7	25.6 (M2)	.7096±12	988±53		1
11 Silent Lake* 18/19		27.5 (M2)	.7097±12	1005±39		1
12 Loon Lake*	6	2.86(M1)	.7034±4	1055±22	1090	3(1,2)
13 Loon Lake*	8	2.99(M1)	.7034±4	1071±18		3
14 Loon Lake*	14	2.83(M1)	.7034±2	1066±14		3
15 Loon Lake*	4	17.4 (M2)	.7037±14	1254±170		4
16 Coe Hill*	9	2.69(M1)	.7039±5	1038±20		5
17 Blue Mountain* 6/8		0.32(M1)	.7043±8	1253±34		6
18 Ridge*	2		.7005	1119		6
19 Westport*	6	1.37(M1)	.7036±5	1019±27		6
20 Gananoque*	5	0.28(M1)	.7054±6	1085±44		6
21 Kaladar*	6	19.4 (M2)	.7127±126	1027±142		6
22 Cheddar	6	(Y1)	.6909±158	1207±92		7
23 CD-G-B	8	(Y1)	.7054±40	959±30		7
24 Deloro*	6	2.14(M1)	.7048±24	1087±37		8
25 Addington	3/6	0.3	.7068±14	1060±30		9
26 Northbrook	4/5	0.5	.7032±8	1030±120		9
27 Mellon Lake	5/7	2.0	.7019±6	1120±90		9
28 Elzevir	4/5	0.7	.7020±5	1240±50		9
29 Mazinaw Lake	4/5	0.4	.6990±2	1185±25		9
30 Skootamatta	4/5	2.4	.7032±3	1020±50		9
31 Trooper Lake 8/17		2.07(Y2)	.7038±2	1165±17		10
32 Nogies Lake					1219	(10)
33 Hinchinbrooke					1254	(11)
34 Bishop Corners					(1118)	(12)
35 Madawaska					1020	(13)
36 Tory Hill					(1064)	(14)
37 Tory Hill					(983)	(14)
38 Cardiff					(976)	(14)

TABLE 5.2 - CON'D

QUEBEC						
UNIT ^a	n ^b	MSWD ^c	Ri	Rb-Sr ^c	U-Pb ^d	Ref ^e
39 Mont Laurier	5	(YI)	.7028±16	948±64		7
40 Mont Laurier	6	(YI)	.7044±16	959±64		7
41 Mont Laurier	6	(YI)	.7048±10	937±60		7
42 Mont Laurier	6	(YI)	.7050±38	1009±48		7
43 Mont Laurier	7	(YI)	.7039±8	1107±74		7
44 Guenette	8	(YI)	.7043±46	999±100		7
45 Loranger	5	1.9	.7030±5	1120±60		9
46 St-Diadicet*	8	1.86(M1)	.7028±6	1126±51		15
47 Grand Meret*	6	8.38(M2)	.7034±26	1227±44		15
48 Lac Crochet*	7	3.64(M2)	.7083±6	953±52		16
49 Lac Crochet*	6	0.29(M1)	.7044±12	1071±210		16
50 Lac Crochet*	4	0.16(M1)	.7040±18	1172±671		16
51 Lac Crochet*	13	0.17(M1)	.7042±6	1097±126		16
52 Lac Crochet*	6	0.85(M1)	.7027±12	1113±31		16

Notes:

- a - For a description of the units presented in this compilation consult the appropriate references. Unit 35 (CD-B-B) represents a composite age determined for samples from three widely spaced pegmatite dikes near Bancroft. The published data for units indicated with an asterisk were re-calculated using the two-error regression program REBROSS (Brooks et al., 1972) with the 1.42×10^{-11} ^{87}Rb decay constant recommended by Steiger and Jager (1977).
- b - Indicates the number of samples used in the age calculation. For example, 6/8 means that 6 out of a total of 8 analyses were used in the age calculation.
- c - For published data that have been re-calculated using REBROSS, results from the McIntyre 1 model are quoted if the MSWD value is less than 3 and results from the McIntyre 2 model are quoted if this parameter is greater than 3. Where possible, errors are quoted at the 95% confidence level and all ages, if necessary, are re-calculated using the 1.42×10^{-11} yr^{-1} decay constant. All other results are presented as they occur in the literature. In the cases where the $^{87}\text{Rb}/^{86}\text{Sr}$ and $^{87}\text{Sr}/^{86}\text{Sr}$ ratios are not published a MSWD value could not be calculated. YI and YII refer to the York regression treatments (York, 1967; 1969).
- d - The zircon ages in parentheses represent $^{207}\text{Pb}/^{206}\text{Pb}$ ages.
- e - The number in parentheses corresponds to the appropriate reference for the U-Pb zircon data.

TABLE 5.2 - CON'D


References

- | | |
|------------------------------|--------------------------------|
| 1 Heaman (this study) | 2 Heaman and Krogh (1985) |
| 3 Heaman et al. (1982) | 4 Heaman (1980) |
| 5 Atkins (1983) | 6 Krogh and Hurley (1968) |
| 7 Fowler and Doig (1983) | 8 Wanless and Loveridge (1972) |
| 9 Bell and Blenkinsop (1980) | 10 Miller (1984) |
| 11 Wallach (1974) | 12 Boutcher et al. (1965) |
| 13 Rimsaite (1981) | 14 Tilton et al. (1957) |
| 15 Barton and Doig (1974) | 16 Barton and Doig (1972) |

REFERENCES

- ABBEY, S. (1977). Studies in "Standard Rock Samples" for use in the general analysis of silicate rocks and minerals. Part 5: 1977 edition of "Usable Values". Geol. Surv. Can. Paper 77-34, 31p.
- ADAMS, F.D. and BARLOW, A.E. (1910). Geology of the Haliburton and Bancroft areas, Province of Ontario. Geol. Surv. Can., Memoir 6, 419p.
- ALDRICH, L.T., WETHERILL, G.W., DAVIS, G.L., and TILTON, G.R. (1958). Radioactive ages of micas from granitic rocks by Rb-Sr and K-Ar methods. Trans. Am. Geophys. Union, 39, 1124-1134.
- ALLSOPP, H.L. (1961). Rb-Sr age measurements on total rock and separated mineral fractions from the Old Granite of the Central Transvaal. J. Geophys. Res., 66, 1499-1508.
- ANDERSON, A.T. and GREENLAND, L.P. (1969) Phosphorus fractionation diagram as a quantitative indicator of crystallization differentiation of basaltic liquids. Geochim. Cosmochim. Acta, 33, 493-505.
- ATKINS, T.R. (1983). Petrography, geochemistry, and geochronology of the Coe Hill granite, Hastings County, Ontario. Unpubl. B.Sc. thesis, McMaster Univ., Hamilton, Ontario, 74p.
- BAER, A.J. (1981). Two orogenies in the Grenville Belt. Nature, 290, 129-131.
- BAKSI, A.K. (1982). $^{40}\text{Ar}/^{39}\text{Ar}$ incremental heating studies on the Tudor gabbro, Grenville Province, Ontario: Its bearing on the North American apparent polar wander path in late Proterozoic times. Geophys. J. Roy. Astr. Soc., 70, 545-562.
- BARKER, F., ARTH, J.G., PETERMAN, Z.E., and FRIEDMAN, I. (1976). The 1.7 to 1.8 G.Y. old trondhjemites of southeastern Colorado and northern New Mexico: Geochemistry and depths of genesis. Geol. Soc. Am. Bull., 87, 189-198.
- BARTON, J.M. and DOIG, R. (1972). Rb-Sr isotopic studies of the Lac Croche Complex, Grenville Province, Quebec. Can. J. Earth Sci., 9, 1180-1186.

- BARTON, J.M. and DOIG, R. (1974). Temporal relationships of rock units in the Shawinigan area, Grenville Province, Quebec. *Can. J. Earth Sci.*, 11, 686-690.
- BEAKHOUSE, G.P. and HEAMAN, L.M. (1980). The chemical separation of Rb and Sr for mass spectrometric analysis. McMaster University Technical Memoir 80-7, 21p.
- BEAKHOUSE, G.P. (1983). Geological, geochemical and Rb-Sr and U-Pb zircon geochronological investigations of granitoid rocks from the Winnipeg River Belt, northwestern Ontario and southeastern Manitoba. Unpubl. Ph.D. thesis, McMaster Univ., Hamilton, Ontario, 376p.
- BELL, K. and BLENKINSOP, J. (1980). Whole rock Rb-Sr studies in the Grenville Province of southwestern Ontario and western Quebec - A summary report. *Geol. Surv. Can. Paper* 80-1C, 152-154.
- BENDER, J.F., HANSON, G.N., and BENICE, A.E. (1982). The Cortlandt Complex: Evidence for large-scale liquid immiscibility involving granodiorite and diorite magmas. *Earth Plan. Sci. Lett.*, 58, 330-344.
- BERGER, G.W., YORK, D., and DUNLOP, D.J. (1979). Calibration of Grenvillian palaeopoles by $^{40}\text{Ar}/^{39}\text{Ar}$ dating. *Nature*, 277, 46-47.
- BERGER, G.W. and YORK, D. (1981). Geothermometry from $^{40}\text{Ar}/^{39}\text{Ar}$ dating. *Geochim. Cosmochim. Acta*, 45, 795-811.
- BERGER, G.W. and YORK, D. (1981). $^{40}\text{Ar}/^{39}\text{Ar}$ dating of the Thanet gabbro, Ontario: Looking through the Grenville metamorphic veil and implications for paleomagnetism. *Can. J. Earth Sci.*, 18, 266-273.
- BERGERON, M., BUFFET, G., HIGGINS, M.D., and SHAW, D.M. (1983). Variations in boron distribution in altered basalts. *Geol. Assoc. Can.*, 8, A6.
- BERGERON, M. and HEAMAN, L.M. (1985). Determining the abundance of gadolinium in geological samples by prompt-gamma neutron activation analysis. *Chem. Geol.* (in press).
- BEST, M.G. (1966). Structural geology of the Precambrian rocks south of Bancroft. *Can. J. Earth Sci.*, 3, 441-455.

- BIRK, W.D. (1978). The nature and timing of granitoid plutonism in the Wabigoon volcanic-plutonic belt, NW Ontario. Geochemistry, Rb/Sr geochronology, petrology and field investigations. Unpubl. Ph.D. thesis, McMaster Univ., Hamilton, Ontario, 496p.
- BOUTCHER, S.M.A., DAVIS, G.L., and MOORHOUSE, W.W. (1965). Potassium-argon and uranium-lead ages from two localities. Can. Mineral., 8, 198-203.
- BREAKS, F.W. (1971). Origin of the Silent Lake pluton and its quartz-sillimanite nodules, near Bancroft, Ontario. Unpubl. M.Sc. thesis, McMaster Univ., Hamilton, Ontario, 119p.
- BREAKS, F.W. and SHAW, D.M. (1973). The Silent Lake pluton, Ontario: A nodular, sedimentary, intrusive complex. Lithos, 6, 103-122.
- BRIGHT, E.G. (1977). Regional structure and stratigraphy of the Eels Lake area, Haliburton and Peterborough Counties. In: Summary of field work. Ont. Geol. Surv. Miscellaneous Paper 75, 110-117.
- BROCK, B.S. (1982). Basement and Grenville Supergroup, Madawaska Highlands, Renfrew County, Ontario. (Abstr) 1982 Workshop on the Grenville Province, Rideau Ferry, 3.
- BROOKS, C., HART, S.R., and WENDT, I. (1972). Realistic use of two-error regression treatments as applied to rubidium-strontium data. Rev. Geophy. Space Phys., 17, 526-531.
- BURRHUS, K.D. and HART, S.R. (1972). Constant-level liquid feed control for high purity distillation apparatus. Anal. Chem., 44.
- BUTLER, J.C. (1982). Artificial isochrons. Lithos, 15, 207-214.
- CATANZARO, E.J. and HANSON, G.N. (1971). U-Pb ages of sphene from Early Precambrian igneous rocks in northeastern Minnesota-northwestern Ontario, Can. J. Earth Sci., 8, 1319-1324.
- CHESWORTH, W. (1971). Metamorphic conditions in a part of the Haliburton Highlands of Ontario. Lithos, 4, 219-229.
- 

- CHIANG, M.C. (1965). Element partition between hornblende and biotite in rocks from the Loon Lake aureole, Chandos twp., Ontario. Unpubl. M.Sc. thesis, McMaster Univ., Hamilton, Ontario, 328p.
- CLOOS, E. (1934). The Loon Lake pluton, Bancroft area, Ontario, Canada. *J. Geol.*, 42, 393-399.
- COMPSTON, W. and JEFFERY, P.M. (1959). Anomalous "common strontium" in granite. *Nature*, 184, 1792-1793.
- COMPSTON, W. and JEFFERY, P.M. (1961). Metamorphic chronology by the rubidium-strontium method. *Annals of the New York Academy of Science*, 91, 185-191.
- COMPSTON, W., JEFFERY, P.M., and RILEY, G.H. (1960). Age of emplacement of granites. *Nature*, 186, 702-703.
- CONDIE, K.C. and MOORE, J.M. Jr. (1977). Geochemistry of volcanic rocks from the Grenville Province, eastern Ontario. In: *Volcanic regimes in Canada*. Ed. W.R.A. Baragar, L.C. Coleman, and J.M. Hall. *Geol. Ass. Can. Spec. Paper 16*, 149-168.
- CORFU, F. and AYRES, L.D. (1983). U-Pb age and genetic significance of the heterogeneous zircon populations in rocks from the Favourable Lake area, northwestern Ontario. *Contrib. Mineral. Petrol.*, 88, 86-101.
- DALLMEYER, R.D. and RIVERS, T. (1983). Recognition of extraneous argon components through incremental-release $^{40}\text{Ar}/^{39}\text{Ar}$ analysis of biotite and hornblende across the Grenville metamorphic gradient in southwestern Labrador. *Geochim. Cosmochim. Acta*, 47, 413-428.
- DALY, J.S., PARK, R.G., and CLIFF, R.A. (1983). Rb-Sr isotopic equilibrium during Sveconorwegian (=Grenville) deformation and metamorphism of the Orust dykes, southwestern Sweden. *Lithos*, 16, 307-318.
- DAVIDSON, A., BRITTON, J.M., BELL, K., and BLENKINSOP, J. (1979). Regional Synthesis of the Grenville Province of Ontario and western Quebec. In: *Current Research, Part B*, *Geol. Surv. Can. Paper 79-1B*, 153-172.
- DAVIDSON, A. (1982). Tectonite zones in the southwestern Grenville Province. (Abstr.) Workshop on the Grenville Province, Rideau Ferry, 3. ✓

- DAVIS, D.W. (1982). Optimum linear regression and error estimation applied to U-Pb data. *Can. J. Earth Sci.*, 19, 2141-2149.
- DODSON, M.H. (1973). Closure temperatures in cooling geochronological and petrological systems. *Contrib. Mineral. Petrol.*, 40, 259-274.
- DOERING, W.P. (1968). A rapid method for measuring the Rb-Sr ratio in silicate rocks. *U.S. Geol. Surv. Prof. Paper* 600-C, 164-168.
- DOIG, R. and BARTON, J.M. (1968). Ages of carbonatites and other alkaline rocks in Quebec. *Can. J. Earth Sci.*, 16, 1401-1407.
- DOIG, R. (1977). Rb-Sr geochronology and evolution of the Grenville Province in northwestern Quebec, Canada. *Geol. Soc. Am. Bull.*, 88, 1843-1856.
- DOSTAL, J. (1973). Geochemistry and petrology of the Loon Lake pluton, Ontario. Unpubl. Ph.D. thesis, McMaster Univ., Hamilton, Ontario, 328p.
- DOSTAL, J. (1975). Geochemistry and petrology of the Loon Lake pluton, Ontario. *Can. J. Earth Sci.*, 12, 1331-1345.
- DOSTAL, J., DUPLUY, C., CARRON, J.P., LE GUEN DE KERNEIZON, M.L., and MAURY, R.C. (1983). Partition coefficients of trace elements: Application to volcanic rocks from St. Vincent, West Indies. *Geochim. Cosmochim. Acta*, 47, 525-534.
- DRURY, S.A. (1973). The geochemistry of Precambrian granulite facies rocks from the Lewisian Complex of Tiree, Inner Hebrides, Scotland. *Chem. Geol.*, 11, 167-188.
- EASTON, R.M. (1983). Howland area: Haliburton, Peterborough and Victoria Counties. In: Summary of field work. *Ont. Geol. Surv. Miscellaneous Paper* 116, 74-79.
- ENGEL, A. and ENGEL, C. (1958). Progressive metamorphism and granitization of the major paragneiss, northwest Adirondack mountains, New York. Part 1: Total rock. *Bull. Geol. Soc. Am.*, 69, 1369-1414.
- FAILEY, M.P., ANDERSON, D.L., ZOLLER, W.H., and GORDON, G.E. (1979). Neutron-capture prompt gamma-ray activation

analysis for multi-element determination in complex samples. *Anal. Chem.*, 51, 2209-2221.

- FAIRBAIRN, H.W., HURLEY, P.M., and PINSON, W.H. (1961). The relation of discordant Rb-Sr mineral and whole rock ages in an igneous rock to its time of crystallization and to the time of subsequent $^{87}\text{Sr}/^{86}\text{Sr}$ metamorphism. *Geochim. Cosmochim. Acta*, 23, 135-144.
- FARHAT, J.S. and WETHERILL, G.W. (1975). Interpretation of apparent ages in Minnesota. *Nature*, 257, 721-722.
- FAURE, G. (1977). Principles of Isotope Geology. John Wiley and Sons, New York, 464p.
- FIELD, D. and RAHEIM, A. (1979). Rb-Sr total rock isotope studies on Precambrian charnockitic gneisses from south Norway: Evidence for isochron resetting during a low-grade metamorphic-deformational event. *Earth Plan. Sci. Lett.*, 45, 32-44.
- FIELD, D. and RAHEIM, A. (1980). Secondary geologically meaningless Rb-Sr isochrons, low $^{87}\text{Sr}/^{86}\text{Sr}$ initial ratios and crustal residence times of high-grade gneisses. *Lithos*, 13, 295-304.
- FLETCHER, I.R. and FARQUHAR, R.M. (1982). The proto-continental nature and regional variability of the Central Metasedimentary Belt of the Grenville Province: Lead isotope evidence. *Can. J. Earth Sci.*, 19, 239-253.
- FOWLER, A.D. and DOIG, R. (1983). The age and origin of Grenville Province uraniferous granites and pegmatites. *Can. J. Earth Sci.*, 20, 92-104.
- FRANKE, W. and GHOBARKAR, H. (1980). The morphology of titanite grown from aqueous supercritical solutions. *N. Jb. Miner. Mh.*, 12, 564-568.
- GAST, P.W. (1980). Limitations on the composition of the upper mantle. *J. Geophys. Res.*, 65, 1287-1297.
- GITTINS, J., HAYATSU, A., and YORK, D. (1969). A strontium isotope study of metamorphosed limestones. *Lithos*, 3, 51-58.
- GRIEP, J.L. (1975). Petrochemistry and metamorphism of the Tallan Lake sill, Bancroft area, Ontario. Unpubl. M.Sc. thesis, McMaster Univ., Hamilton, Ontario, 166p.

- HANSON, G.N., CATANZARO, E.J., and ANDERSON, D.H. (1971). U-Pb ages for sphene in a contact metamorphic zone. *Earth Plan. Sci. Lett.*, 12, 231-237.
- HARMON, R.S. and HALLIDAY, A.N. (1980). Oxygen and strontium isotope relationships in the British late Caledonian granites. *Nature*, 283, 21-25.
- HART, S.R. (1961). Mineral ages and metamorphism. *Annals of the New York Academy of Sciences*, 91, 192-197.
- HAWTHORNE, F.C., GRIEP, J.L., and CURTIS, L. (1980). A three-amphibole assemblage from the Tallan Lake sill, Peterborough County, Ontario. *Can. Mineral.*, 18, 275-284.
- HAYATSU, A. and PALMER, H.C. (1975). K-Ar isochron study of the Tudor gabbro, Grenville Province, Ontario. *Earth Plan. Sci. Lett.*, 25, 208-212.
- HEAMAN, L.M. (1980). Rb-Sr geochronology and Sr isotope systematics of some major lithologies in Chandos township, Ontario. Unpubl. M.Sc. thesis, McMaster Univ., Hamilton, Ontario, 140p.
- HEAMAN, L.M., McNUTT, R.H., and SHAW, D.M. (1980a). Rb-Sr whole rock ages from the Hastings Basin, Grenville Province, Ontario. *Geol. Assoc. Can.*, 5, 59.
- HEAMAN, L.M., SHIEH, Y.N., McNUTT, R.H., and SHAW, D.M. (1980b). Interpretation of strontium and oxygen isotope data from the Loon Lake pluton and Apsley gneiss, Grenville Province, Ontario. *Trans. Am. Geophys. Union (EOS)*, 61, 387.
- HEAMAN, L.M., SHIEH, Y.N., McNUTT, R.H., and SHAW, D.M. (1982a). Isotopic and trace element study of the Loon Lake pluton, Grenville Province, Ontario. *Can. J. Earth Sci.*, 19, 1045-1054.
- HEAMAN, L.M., McNUTT, R.H., and SHAW, D.M. (1982b). Rb-Sr data for high grade metamorphic rocks from Chandos township, Grenville Province, Ontario. *Geol. Assoc. Can.*, 7, 55.
- HEAMAN, L.M., SHAW, D.M., and McNUTT, R.H. (1982c). The Tallan Lake sill: Geochemical evidence for a large scale nappe structure in the NW portion of the Grenville Province. *Geol. Soc. Am.*, 14, 512.

- HEAMAN, L.M. (1983). Constant-level feed device for continuous acid distillation. McMaster University Technical Memoir 83-1, 6p.
- HEAMAN, L.M., SHAW, D.M., McNUTT, R.H., CROCKET, J.H., and SHIEH, Y.N. (1983). The effect of fluid interaction on the geochemistry and isotopic composition of the Tallan Lake sill, Grenville Province, Ontario. Geol. Assoc. Can., 9, A31.
- HEAMAN, L.M., McNUTT, R.H., and SHAW, D.M. (1984). Rb-Sr systematics of the 1100 Ma Grenville granitoids; Metamorphic resetting or crustal contamination? Geol. Assoc. Can., 9, 72.
- HEAMAN, L.M. and KROGH, T.E. (1985). The Loon Lake pluton revisited: A U-Pb zircon study. Geol. Assoc. Can., 10, 26.
- HEWITT, D.F. (1956). The Grenville region of Ontario. In: The Grenville Problem. Ed. J.E. Thomson. Roy. Soc. Can. Spec. Publ. 1, 22-41.
- HEWITT, D.F. and JAMES, W. (1956). Geology of Dungannon and Mayo townships, County of Hastings. Ont. Dept. Mines, 64, Part B, 1-61.
- HEWITT, D.F. (1959). Geology of Cardiff and Faraday townships. Ont. Dept. Mines, 66, Part 3, 82p.
- HEWITT, D.F. (1961). Geology of Methuen township. In: Nepheline syenite deposits of southern Ontario. Ont. Dept. Mines, 69, Part B, 194p.
- HEWITT, D.F. (1962a). Geology of Wollaston township. Ont. Dept. Mines Geol. Report #11, 29-55.
- HEWITT, D.F. (1962b). Some tectonic features of the Grenville Province of Ontario. Roy. Soc. Can. Spec. Publ. 4, 102-117.
- HIGGINS, M.D. (1984). Abundance of boron in international geochemical standards by prompt-gamma neutron activation analysis. Geostandards Newsletter, 8, 31-34.
- HIGGINS, M.D., TRUSCOTT, M.G., SHAW, D.M., BERGERON, M., and BUFFET, H.G. (1984). Prompt-gamma neutron activation analysis at the McMaster nuclear reactor. Atomkern-energie Kertechnik, supplement to v.44, 690-697.

- HILDRETH, W.E. (1979). The Bishop tuff: Evidence for the origin of compositional zonation in silicic magma chambers. *Geol. Soc. Am., Special Paper 180*, 43-76.
- HOERNES, S. and HOFFER, E. (1979). Equilibrium relations in prograde metamorphic mineral assemblages. A stable isotope study of rocks of the Damara orogen, from Namibia. *Contrib. Mineral. Petrol.*, 68, 377-389.
- HOFMANN, A.W. (1979). Rb-Sr dating of thin slabs: An imperfect method to determine the age of metamorphism. In: Lectures in Isotope Geology, Ed. E. Jager and J.C. Hunziker. Springer-Verlag, N.Y., 329p.
- HOLM, P., SMITH, T., HUANG, C., GERASIMOFF, M., GRANT, B., FILBEY, B., and McLAUGHLIN, K. (1984). Geochemistry of Grenville meta-igneous rocks from a portion of the Hastings Lowlands. *Geol. Assoc. Can.*, 9, 74.
- IRVINE, T.N. and BARAGAR, W.R.A. (1972). A guide to the classification of the common volcanic rocks. *Can. J. Earth Sci.*, 8, 523-548.
- JAKLEVIC, J.M. and WALTER, R.L. (1977). Chapter 5 in X-ray Fluorescence Analysis of Environmental Samples. Ed. T.G. Dzubey, Ann Arbor Sciences, Ann Arbor, Michigan.
- JENNINGS, D.S. (1969). Origin and metamorphism of a part of the Hermon Group near Bancroft, Ontario. Unpubl. Ph.D. thesis, McMaster Univ., Hamilton, Ontario, 225p.
- KROGH, T.E. and HURLEY, P.M. (1968). Strontium isotope variation and whole-rock isochron studies, Grenville Province of Ontario. *J. Geophys. Res.*, 73, 7107-7125.
- KROGH, T.E. (1973). A low-contamination method for hydrothermal decomposition of zircon and extraction of U and Pb for isotopic age determinations. *Geochim. Cosmochim. Acta*, 37, 485-494.
- KROGH, T.E. and DAVIS, G.L. (1973). The effect of regional metamorphism on U-Pb systems in zircons and a comparison with Rb-Sr systems in the same whole rock and its constituent minerals. *Carn. Inst. Wash. Yearbook*, 72, 601-610.
- *KROGH, T.E. (1982a). Improved accuracy of U-Pb zircon ages by the creation of more concordant systems using an air abrasion technique. *Geochim. Cosmochim. Acta*, 46, 637-649.

- KROGH, T.E. (1982b). Improved accuracy of U-Pb zircon dating by selection of more concordant fractions using a high gradient magnetic separation technique. *Geochim. Cosmochim. Acta*, 46, 631-636.
- KROGH, T.E. and WARDLE, R. (1984). U-Pb ages along the Grenville Front. *Geol. Assoc. Can.*, 9, 80.
- LAASKO, R.K. (1968). Geology of Lake township, Hastings County, Ontario. *Ont. Dept. Mines Geol. Report* 54, 36p.
- LOGAN, W.E. (1846). Report of progress, 1845-1846. *Geol. Surv. Can.*, 40-51.
- LOPEZ-MARTINEZ, M. and YORK, D. (1983). Further thermochronometric unravelling of the age and palaeomagnetic record of the southwest Grenville Province. *Can. J. Earth Sci.*, 20, 953-960.
- LOWDON, J.A. (1960). Age determination by the Geological Survey of Canada. *Geol. Surv. Can. Paper* 61-17.
- LUMBERS, S.B. (1964). Preliminary report on the relationship of mineral deposits to intrusive rocks and metamorphism in part of the Grenville Province of southeastern Ontario. *Ont. Dept. Mines, Preliminary Report*, 1964-4, 37p.
- LUMBERS, S.B. (1967). Stratigraphy, plutonism, and metamorphism in the Ottawa River remnant in the Bancroft-Madoc area of the Grenville Province of SE Ontario. Unpubl. Ph.D. thesis, Princeton Univ., Princeton, New Jersey.
- LUMBERS, S.B. (1969). Geology of Limerick and Tudor townships. *Ont. Dept. Mines Geol. Report* #67, 110p.
- LUMBERS, S.B. (1982). Summary of metallogeny, Renfrew County area. *Ont. Geol. Surv. Report* #212, 58p.
- MacINTYRE, R.M., YORK, D., and MOORHOUSE, W.W. (1967). Potassium-argon age determination in the Madoc-Bancroft area in the Grenville Province of the Canadian Shield. *Can. J. Earth Sci.*, 4, 815-828.
- MacLEAN, W.H., SEYMOUR, K.St., and PRABHU, K.M. (1982). Sr, Y, Zr, Nb, Ti, and REE in Grenville amphibolites at Montauban-les-Mines, Quebec. *Can. J. Earth Sci.*, 19, 633-644.

- MARCHAND, M. (1973). Determination of Rb, Sr and Rb/Sr by XRF. McMaster University Technical Memoir 73-2, 16p.
- MARTIGNOLE, J. and SCHRIJVER, K. (1970). Tectonic setting and evolution of the Morin anorthosite, Grenville Province, Quebec. Geol. Soc. Finlande Bull., 42, 165-209.
- MATTINSON, J.M. (1972). Preparation of HF, HCl, and HNO₃ at ultralow lead levels. Anal. Chem., 44, 1715-1716.
- MCCAMMON, B.W. (1968). A geochemical study of some igneous rocks from the Loon Lake complex using spectrographic methods. Unpubl. B.Sc. thesis, McMaster Univ., Hamilton, Ontario, 34p.
- McINTYRE, G.A., BROOKS, C., COMPSTON, W., and TUREK, A. (1966). The statistical assessment of Rb-Sr isochrons. J. Geophys. Res., 71, 5456-5469.
- McLELLAND, J. (1984). Structural geology of the Adirondacks. Geol. Assoc. Can., 9, 87.
- MENZIES, M. and MURTHY, V.R. (1980). Enriched mantle: Nd and Sr isotopes in diopsides from kimberlite nodules. Nature, 283, 634-636.
- MILLER, R.R. (1984). Tectonic significance of nepheline-bearing rocks in the Haliburton-Bancroft area of the Grenville Province. Geol. Assoc. Can., 9, 89.
- MOORE, J.M.Jr. (1982). Stratigraphy and tectonics of the Grenvillian orogen in eastern Ontario. Workshop on the Grenville Province, Rideau Ferry, 7.
- MOORE, J.M.Jr. and THOMPSON, P.H. (1980). The Flinton Group: A late Precambrian metasedimentary succession in the Grenville Province of eastern Ontario. Can. J. Earth Sci., 17, 1685-1707.
- MORRISON, M.A. (1978). The use of "immobile" trace elements to distinguish the palaeotectonic affinities of metabasalts: Applications to the Paleocene basalts of Mull and Skye, northwest Scotland. Earth Plan. Sci. Lett., 39, 407-416.
- MORTON, R.L. (1978). Harvey township, Peterborough County. In: Summary of field work. Ont. Geol. Surv., Miscellaneous Paper 82, 128-130.

- NICOLAYSEN, L.O. (1961). Graphic interpretation of discordant age measurements on metamorphic rocks. *Annals of the New York Academy of Sciences*, 91, 198-206.
- NIER, A.O. (1939). The isotopic composition of radiogenic leads and the measurement of geological time. *Phys. Rev.*, 55, 153-163.
- NOCKOLDS, S.R. (1954). Average chemical compositions of some igneous rocks. *Bull. Geol. Soc. Am.*, 65, 1007-1032.
- PAGE, R.W. (1978). Response of U-Pb zircon and Rb-Sr total rock and mineral systems to low-grade regional metamorphism in Proterozoic igneous rocks, Mount Isa, Australia. *J. Geol. Soc. Australia*, 25, 141-164.
- PALMER, H.C., HAYATSU, A., WABOSO, C.E., and PULLAN, S. (1979). A paleomagnetic and K-Ar study of the Umfraville gabbro, Ontario. *Can. J. Earth Sci.*, 16, 459-471.
- PATCHETT, P.J. (1980). Thermal effects of basalt on continental crust and crustal contamination of magmas. *Nature*, 283, 559-561.
- PEARCE, J.A. and CANN, J.R. (1973). Tectonic setting of basic volcanic rocks determined using trace element analyses. *Earth Plan. Sci. Lett.*, 19, 290-300.
- PEARCE, J.A. and NORRY, M.J. (1979). Petrogenetic implications of Ti, Zr, Y, and Nb variations in volcanic rocks. *Contrib. Mineral. Petrol.*, 69, 33-47.
- PETTIJOHN, F.J. (1963). Chemical composition of sandstones - excluding carbonate and volcanic sands. In: *Data of Geochemistry* (6th ed.). Ed. M. Fleischer. U.S. Geol. Surv. Prof. Paper 440-S, S1-S21.
- PRABHU, M.K. and WEBBER, G.R. (1984). Origin of quartzofeldspathic gneisses at Montauban-les-Mines, Quebec. *Can. J. Earth Sci.*, 21, 336-345.
- PRIDE, C. and MOORE, J.M.Jr. (1983). Petrogenesis of the Elzevir batholith and related trondhjemitic intrusions in the Grenville Province of eastern Ontario, Canada. *Contrib. Mineral. Petrol.*, 82, 187-194.
- RAPELA, C.W., HEAMAN, L.M., McNUTT, R.H. (1982). Rb-Sr geochronology of granitoid rocks from the Pampean Ranges, Argentina. *J. Geol.*, 90, 574-582.

- RAYLEIGH, J.W.S. (1896). Theoretical considerations respecting the separation of gases by diffusion and similar processes. *Phil. Mag.*, 42, 493-498.
- REYNOLDS, R.C. (1963). Matrix corrections in trace element analysis by X-ray fluorescence. Estimation of the mass absorption coefficient by Compton scattering. *Am. Mineral.*, 48, 1133-1143.
- REYNOLDS, R.C. (1967). Estimation of mass absorption coefficients by Compton scattering. Improvements and extensions of the method. *Am. Mineral.*, 52, 1493-1502.
- RIMSAITE, J. (1981). Isotope, scanning electron microscope, and energy dispersive spectrometer studies of heterogeneous zircons from radioactive granites in the Grenville Structural Province, Quebec and Ontario. *Geol. Surv. Can. Paper* 81-1B, 25-35.
- RODDICK, J.C. and COMPSTON, W. (1977). Strontium isotopic equilibration: A solution to a paradox. *Earth Plan. Sci. Lett.*, 34, 238-246.
- ROEDDER, E. (1979). Silicate liquid immiscibility in magmas. In: *The Evolution of Igneous Rocks (50th anniversary perspectives)*. Ed. H.S. Yoder. Princeton Univ. Press, Princeton, N.J., 588p.
- ROMEY, W., ELBERTY, W.T., JACOBY, R.S., CHRISTOFFERSEN, R., SHRIER, T., and TIETBOHL, D. (1980). A structural model for the northwestern Adirondacks based on leucogranitic gneisses near Canton and Pyrites, New York: Summary. *Geol. Soc. Am. Bull.*, 91, 97-100.
- SAHA, A.K. (1957). Mode of emplacement of some granitic plutons in SE Ontario. Unpubl. Ph.D. thesis, Univ. of Toronto, Toronto.
- SAHA, A.K. (1959). Emplacement of three granitic plutons in SE Ontario, Canada. *Geol. Soc. Am. Bull.*, 70, 1293-1326.
- SCHREINER, G.D.L. (1958). Comparison of the ^{87}Rb - ^{87}Sr ages of the red granite of the Bushveld Complex from measurements on the total rock and separated mineral fractions. *Proc. Roy. Soc. London, Series A*, 245, 1499-1508.
- SEYFRIED, W.E. Jr., JANECKY, D.R., and MOTT, M.J. (1984). Alteration of oceanic crust: Implications for geochemical cycles of lithium and boron. *Geochim. Cosmochim. Acta*, 48, 557-570.

- SHAW, D.M. (1962). Geology of Chandos township, Peterborough County, Ontario. Ont. Dept. Mines Geol. Report#11, 1-28.
- SHAW, D.M. (1972). The origin of the Apsley gneiss, Ontario. *Can. J. Earth Sci.*, 5, 561-583.
- SHAW, D.M. and KUDO, A.M. (1965). A test of the discriminant function in the amphibolite problem. *Mineral. Mag.*, 34, 423-435.
- SHIEH, Y.N. and SCHWARCZ, H.P. (1974). Oxygen isotope studies of granite and migmatite, Grenville Province of Ontario, Canada. *Geochim. Cosmochim. Acta*, 38, 21-45.
- SHIEH, Y.N., SCHWARCZ, H.P., and SHAW, D.M. (1976). An oxygen isotope study of the Loon Lake pluton and the Apsley gneiss, Ontario. *Contrib. Mineral. Petrol.*, 54, 1-16.
- SHIEH, Y.N. (1980). Oxygen isotopic compositions of granitic and syenitic plutons in the Central Metasedimentary Belt, Grenville Province of Ontario. *Trans. Am. Geophys. Union (EOS)*, 61, 410.
- SHIEH, Y.N. (1985). High- 100 granitic plutons from the Frontenac Axis, Grenville Province, Ontario, Canada. *Geochim. Cosmochim. Acta*, 49, 117-123.
- SILVER, L.T. and LUMBERS, S.B. (1966). Geochronological studies in the Bancroft-Madoc area of the Grenville Province, Ontario, Canada. *Geol. Soc. Am. Spec. Publ.*, 87, 156.
- SIMONY, P.S. (1960). Origin of the Apsley paragneiss. Unpubl. M.Sc. thesis, McMaster Univ., Hamilton, Ontario, 79p.
- SMITH, R.E. and SMITH, S.E. (1976). Comments on the use of Ti, Zr, Y, Sr, K, P, and Nb in classification of basaltic magmas. *Earth Plan. Sci. Lett.*, 32, 114-120.
- STEIGER, R.H. and JAGER, E. (1977). Subcommittee on geochronology: Convention on the use of decay constants in geology and cosmochronology. *Earth Plan. Sci. Lett.*, 36, 359-362.
- TAYLOR, H.P.Jr. (1968). The oxygen isotope geochemistry of igneous rocks. *Contrib. Mineral. Petrol.*, 19, 1-71.
- TAYLOR, H.P.Jr. (1974). The application of oxygen and hydrogen isotope studies to problems of hydrothermal

alteration and ore deposition. *Econ. Geol.*, 69, 843-883.

- TAYLOR, H.P.Jr. (1978). Oxygen and hydrogen isotope studies of plutonic granitic rocks. *Earth Plan. Sci. Lett.*, 38, 177-210.
- TAYLOR, H.P.Jr. (1980). The effects of assimilation of country rocks by magmas on $^{18}O/^{16}O$ and $^{87}Sr/^{86}Sr$ systematics in igneous rocks. *Earth Plan. Sci. Lett.*, 47, 243-254.
- THIVIERGE, R.H. (1977). The geology of the Mount Moriah syenite, Grenville Province, southeast Ontario. Unpubl. B.Sc. thesis, Carleton Univ., Ottawa, 64p.
- THIVIERGE, R.H. (1982). Structural relationships of Grenville gneisses in Bangor township, southeastern Ontario: A preliminary evaluation. Workshop on the Grenville Province, Rideau Ferry, 9.
- TILTON, G.R., PATTERSON, C., BROWN, H., INGRAM, M., HAYDEN, R., HESS, D., and LARSON, E.Jr. (1955). Isotopic composition and distribution of lead, uranium and thorium in a Precambrian granite. *Bull. Geol. Soc. Am.*, 66, 1131-1148.
- TILTON, G.R., DAVIS, G.L., WETHERILL, G.W., and ALDRICH, L.T. (1957). Isotopic ages of zircon from granites and pegmatites. *Trans. Am. Geophys. Union*, 38, 360-371.
- TILTON, G.R., DAVIS, G.L., WETHERILL, G.W., ALDRICH, L.T., and JAGER, E. (1959). The ages of rocks and minerals. *Carn. Inst. Wash. Yearbook*, 58, 171-178.
- TILTON, G.R. and GRUNENFELDER, M.H. (1968). Spinel: Uranium-lead ages. *Science*, 159, 1458-1461.
- TINDLE, A.G. and PEARCE, J.A. (1981). Petrogenetic modelling of in situ fractional crystallization in the zoned Loch Doon pluton, Scotland. *Contrib. Mineral. Petrol.*, 78, 196-207.
- TUREK, A., RIDDLE, C., and SMITH, T.E. (1977). Determination of Rb and Sr by X-ray fluorescence in the measurement of radiometric ages. *Can. J. Spectroscopy*, 22, 20-24.
- VAN DE KAMP, P.C. (1968). Geochemistry and origin of metasediments in the Haliburton-Madoc area, southeastern Ontario. *Can. J. Earth Sci.*, 5, 1337-1372.

- VAN DE KAMP, P.C., LEAKE, B.E., and SENIOR, A. (1976). The petrography and geochemistry of some Californian arkoses with application to identifying gneisses of metasedimentary origin. *J. Geol.*, 84, 195-212.
- WAGER, L.R. and BROWN, G.M. (1969). Layered igneous rocks. Freeman, San Francisco.
- WALKER, K.R. (1969). A mineralogical, petrological, and geochemical investigation of the Palisades sill, New Jersey. *Geol. Soc. Am. Memoir*, 115, 175-187.
- WALLACH, J.L. (1974). Origin and age of the Hinchinbrooke gneiss and its relationship to the Grenville Group rocks of southeastern, Ontario. *Geol. Assoc. Can., meeting in St. John's, NFLD.*, 96.
- WANLESS, R.K. and LOVERIDGE, W.D. (1972). Rb-Sr isochron age studies, Report 1. *Geol. Surv. Can. Paper* 72-23, 77p.
- WASSERBURG, G.J., ALBEE, A.L. and LANPHERE, M.A. (1964). Migration of radiogenic strontium during metamorphism. *J. Geophys. Res.*, 69, 4395-4401.
- WATSON, E.B. (1982). Basalt contamination by continental crust: Some experiments and models. *Contrib. Mineral. Petrol.*, 80, 73-87.
- WENDT, I. (1969). Derivation of the formula for a regression line based on a least squares analysis. Internal Report, Bundesanstalt für Bodenforschung, Hanover, W. Germany.
- WYLLIE, P.J. (1961). Fusion of Torridonian sandstone by a picritic sill in Soay (Hebrides). *J. Petrol.*, 2, 1-37.
- WYNNE-EDWARDS, H.R. (1972). The Grenville Province. In: Variations in Tectonic Styles in Canada. Ed. R.A. Price and R. Douglas. *Geol. Assoc. Can. Special Paper* 11.
- YODER, H.S.Jr. (1973). Contemporaneous basaltic and rhyolitic magmas. *Am. Mineral.*, 58, 153-171.
- YORK, D. (1967). The best isochron. *Earth Plan. Sci. Lett.*, 2, 479-482.
- YORK, D. (1969). Least squares fitting of a straight line with correlated errors. *Earth Plan. Sci. Lett.*, 5, 320-324.

- YORK, D. (1978). A formula describing both magnetic and isotopic blocking temperatures. *Earth Plan. Sci. Lett.*, 39, 89-93.
- ZARTMAN, R.E. (1969). Lead isotopes in igneous rocks of the Grenville Province as a possible clue to the presence of older crust. *Geol. Assoc. Can., Special Paper 5*, 193-205.

APPENDIX A

ANALYTICAL PROCEDURES

A1 SAMPLE PREPARATION

Rock samples weighing approximately 5 kilograms were collected from relatively homogeneous portions (ie. areas that are visibly devoid of alteration, weathering, inclusions, veins or fractures) of a sampling site. These samples were often broken into smaller chips in the field so that they could be introduced directly into the jaw crusher. To reduce these samples to a fine powder, each sample collected in the field was passed through the following three pulverizing apparatus; jaw crusher, Bico ceramic disk mill and Spex tungsten-carbide shatterbox. Before crushing a sample, each apparatus was thoroughly cleaned with compressed air, acetone and a wire brush (jaw crusher only). At the start of a crushing session and when samples of vastly different composition (ie. basalt and granite) were comminuted in succession, the first aliquot of sample at each step in the crushing procedure was discarded (pre-

contamination).

The samples collected for the U-Pb study were crushed at the Jack Satterly geochronology laboratory, Royal Ontario Museum, Toronto. Each sample, weighing between 15 and 60 kilograms, was processed through a jaw crusher and a Bico steel disk mill. The jaw crusher and disk mill are designed to be disassembled so that all steel parts that come into contact with the sample can be thoroughly cleaned with a wire brush (attached to an electric drill), compressed air and alcohol.

A2 X-RAY FLUORESCENCE SPECTROSCOPY (XRF)

The major element and some of the trace element abundances listed in Appendix B2 were determined using a Phillips PW 1450 automated X-ray fluorescence spectrometer. Details of the procedure for preparing fused disks (major element analyses) and pressed pellets (trace element analyses) are outlined by Beakhouse (1983) and Heaman (1980). The XRF operating conditions for determining the abundance of the major elements (Beakhouse, 1983; Table A1.1) and trace elements (Heaman, 1980; Table 2.1) are presented elsewhere. Rb and Sr abundances were determined following the Mo-Compton peak method described by Reynolds (1963, 1967) and Turek et al. (1977) and Rb/Sr ratios were determined as ratios of the total corrected peak counts (Doering, 1968; Marchand, 1973).

A2.1 Precision and Accuracy

The precision and accuracy of the major element analyses were evaluated by repeatedly analysing the international rock standard JG-1 (granodiorite) as an unknown. This standard was chosen because it is one of the few well studied international standards that is not used to establish calibration curves in the various XRF programs and, therefore, can be analysed as an "unknown" and because the abundance of major and trace elements in this standard are comparable to the values measured for many granitoid rocks. The individual analyses are presented in Table A1, along with average values, standard deviations (SD) and a normalized set of "usable" values reported by Abbey (1977). The precision of the major element analyses is quite good (often better than $\pm 2\%$) except for MgO, Na₂O and P₂O₅. The precision of the Na₂O data is much better if analysis #4 is omitted from the calculation (mean = 3.36; SD = 0.11). There is generally good agreement between the average major element compositions for JG-1 determined in this study (Table A1) and the "usable" values reported by Abbey (1977).

The results for replicate analyses of the standard JG-1 analysed for Y, Zr and Nb using the Rb-Sr-Y-Zr-Nb program are presented in Table A2. The precision of these determinations is approximately $\pm 10\%$. There is good agreement between the average Y value determined in this study (30 ppm) and the recommended value of 31 ppm reported by Abbey (1977).

The average Zr abundance determined in this study (126 ppm) is noticeably higher but within error (2 sigma) of the recommended value of 110 ppm for JG-1.

As a measure of the reproducibility of the Rb and Sr analyses, a single powder pellet of JG-1 was analysed routinely throughout this study. A summary of the results for 31 analyses of this standard are presented in Table A3 including the average Rb, Sr and Rb/Sr values and the corresponding "usable values" reported by Abbey (1977). The estimated uncertainty (one standard deviation) in the abundance of Rb and Sr based on these 31 determinations is 1.6%. The uncertainty is less than 1% if the three anomalous determinations (#15, 16, 17) are omitted. The uncertainty in the Rb/Sr ratio for JG-1 is 0.6% so the blanket error of 1% for the Rb/Sr ratios used to calculate the error associated with the Rb-Sr age determinations reported in this study is considered a generous estimate of this error. The absolute abundances of Rb and Sr in JG-1 measured in this study are slightly lower than the recommended values reported by Abbey (1977).

TABLE A1 - Precision and accuracy of major elements based on replicate analyses of the international rock standard JG-1 (run as an unknown)

	<u>JG-1</u>						Ave	SD	*
	1	2	3	4	5	6			
SiO ₂	72.58	72.50	72.93	71.42	73.43	73.43	72.70	0.75	72.78
Al ₂ O ₃	14.39	14.41	14.25	14.24	13.88	14.09	14.21	0.20	14.28
Fe ₂ O ₃	2.24	2.20	2.18	2.14	2.27	2.27	2.22	0.05	2.18
HgO	0.82	0.74	1.09	0.79	0.22	0.26	0.65	0.34	0.76
CaO	2.23	2.14	1.93	2.11	2.19	2.16	2.13	0.11	2.18
Na ₂ O	3.40	3.45	3.24	4.84	3.46	3.26	3.61	0.61	3.41
K ₂ O	3.96	4.04	3.93	3.98	4.09	4.10	4.02	0.07	3.98
TiO ₂	0.27	0.25	0.24	0.25	0.28	0.26	0.26	0.02	0.27
MnO	0.05	0.08	0.08	0.09	0.09	0.08	0.08	0.02	0.06
P ₂ O ₅	0.04	0.17	0.12	0.16	0.11	0.11	0.12	0.05	0.09
TOTAL	100	100	100	100	100	100	100		100

TABLE A2 - Precision and accuracy of selected trace elements based on replicate analyses of the international rock standard JG-1

	<u>JG-1</u>							Ave	SD	*
	1	2	3	4	5	6	7			
Y	36	28	29	35	26	26	29	30	4	31
Zr	157	127	124	112	120	122	121	126	14	110
Nb	15	20	17	14	14	15	15	16	2	?

* - "Usable Values" reported by Abbey (1977)

TABLE A3 - Precision and accuracy of Rb, Sr and Rb/Sr determinations based on replicate analyses of the international rock standard JG-1 run as an unknown during the period 1979 to 1984

	Date	Rb (ppm)	Sr (ppm)	Rb/Sr
1	15/09/79	174	181	0.9621
2	15/09/79	176	180	0.9779
3	13/12/79	175	181	0.9662
4	13/01/80	174	179	0.9728
5	13/01/80	178	181	0.9794
6	15/06/81	179	185	0.9653
7	31/08/81	177	182	0.9714
8	31/08/81	176	178	0.9851
9	31/08/81	174	179	0.9717
10	31/08/81	179	184	0.9666
11	08/09/81	178	182	0.9787
12	08/09/81	178	183	0.9746
13	08/09/81	176	181	0.9714
14	24/06/82	178	182	0.9777
15	24/06/82	184	190	0.9689
16	24/06/82	185	190	0.9714
17	24/06/82	184	190	0.9686
18	24/06/82	178	182	0.9751
19	24/06/82	177	180	0.9842
20	25/03/83	174	180	0.9631
21	25/03/83	175	181	0.9636
22	14/04/83	175	181	0.9659
23	14/04/83	174	180	0.9643
24	14/04/83	176	182	0.9686
25	14/04/83	176	183	0.9641
26	14/04/83	176	183	0.9640
27	07/08/84	178	183	0.9725
28	07/08/84	176	182	0.9676
29	07/08/84	178	183	0.9707
30	07/08/84	178	183	0.9722
31	07/08/84	178	182	0.9780
		-----	-----	-----
	Average (1 σ)	177 \pm 3	182 \pm 3	0.9711 \pm 62
	Abbey (1977)	185	185	1.0000

A3 INSTRUMENTAL NEUTRON ACTIVATION ANALYSES (INAA)

A total of 20 samples were analysed by INAA to determine the abundances of the REE, Th, Ta, and Hf. These samples were irradiated in two batches. For the first batch, two aliquots of each sample plus two standards (AGV-1 and ACOURS) were weighed into silica ampules and polypropylene vials, respectively. The 0.5 to 1.2 gram samples in the polypropylene vials were irradiated for 1 hour with epithermal neutrons then allowed to cool for 6 days before counting for La and Sm while the silica ampules, containing between 200 and 400 mg of sample powder, were irradiated for 6 hours in a total neutron flux of approximately 1×10^{13} $\text{ncm}^{-2}\text{sec}^{-1}$ at the McMaster University Nuclear Reactor. The irradiation procedure for the second batch of samples was modified slightly such that the sample aliquots in the polypropylene vials used for the epithermal irradiation were re-irradiated after 23 days for 3 hours. During irradiation the samples (plus standards) were surrounded with 5 cm of Pb shielding and rotated (1 revolution/minute) using a Lasy Susie rotating table. After the second irradiation the samples were allowed to cool for 8 to 12 days, counted for Eu, Lu and Tb, then allowed to cool for an additional 2 to 5 weeks before counting for Ce, Hf, Nd, Ta, Th, Tm and Yb.

The samples and standards were counted for 3600 seconds using a coaxial intrinsic germanium detector (12% efficiency; 1.8 keV resolution at 1332 keV; peak:compton

ratio = 35:1) that is coupled to a Canberra Industries Series 80 Multichannel Analyser and a B604 Processor (8192 channels). The accuracy of the REE analyses determined by INAA was evaluated by analysing the international standard AGV-1 as an "unknown" with each batch. These results are presented in Table A4 along with the "usable" values for this standard reported by Abbey (1977) and the average of numerous analyses determined in the McMaster lab (A. Kabir, personal communication). The results reported in Table A4 for batches 1 and 2 are generally in good agreement, except for Ce and Nd, and generally agree with the values reported by Abbey (1977). This disparity in the Ce and Nd data from batch 1 to batch 2 is also reflected in the data obtained for two samples that were analysed in both batches (Table A5). Considering that the Ce and Nd data obtained for AGV-1 in batch 1 are in good agreement with the results routinely obtained in the McMaster lab (compare the results in Table A4), the Ce and Nd abundances determined for batch 2 are considered anomalously low.

TABLE A4 - Accuracy of the REE analyses determined by INAA

AGV-1

	Batch 1	Batch 2	Abbey	Kabir
La	39	38	36	40
Ce	77	69	71	76
Nd	36	32	37	36
Sm	6.3	6.3	5.9	6.1
Eu	1.7	1.6	1.6	1.7
Tb	0.8	0.8	0.7	0.8
Yb	1.9	1.8	1.9	2.0
Lu	0.3	0.3	0.3	0.3

TABLE A5 - Comparison of REE data determined for samples irradiated in both batches

	<u>TL1</u>		<u>TL16</u>	
	#1	#2	#1	#2
La	7.7	6.1	64	64
Ce	20	17	185	172
Nd	15	11	145	134
Sm	5.9	5.7	40	40
Eu	1.8	1.9	7.7	8.9
Tb	1.0	1.0	5.8	6.8
Yb	3.2	3.0	26	26
Lu	0.7	0.5	3.8	4.0

A4 PROMPT-GAMMA NEUTRON ACTIVATION ANALYSES (PGNAA)

A number of samples were analysed for boron and gadolinium by prompt-gamma neutron activation. This technique is based on the measurement of gamma-rays emitted from excited nuclei that are produced by irradiating a sample with thermal neutrons. The principal advantage of the method is that the gamma-ray spectrum for certain elements are free from any interference and the samples generally have a low activity after irradiation. Both B and Gd are ideal elements for PGNAA because they have high thermal neutron capture cross-sections (Failey et al., 1979) and a gamma-ray peak that is free from interference. A summary of the PGNAA method is presented by Failey et al. (1979).

The prompt-gamma system used at McMaster University is described in detail by Higgins et al. (1984) and the procedure for measuring the abundance of B and Gd is outlined by Higgins (1985) and Bergeron and Heaman (1985), respectively. For Gd, samples of powdered rock weighing between 1 and 3 grams are sealed in teflon tubing and introduced into a thermal neutron flux of $6 \times 10^7 \text{ n cm}^{-2} \text{ sec}^{-1}$ for 500 to 5000 seconds, depending on the quantity of Gd present. The minimum detection limit for Gd, calculated using the equation reported by Jaklevic and Walter (1977) and Failey et al. (1979), is 0.05 ug for a 1000 second counting period. The Gd blank, determined by irradiating an empty sample holder for 30,000 seconds, is negligible. The

reproducibility of the Gd analyses is estimated to be $\pm 5\%$ (1 sigma) for samples containing between 5 and 15 ug of Gd. Additional information concerning the procedure used for calibration and the results from experiments to test for matrix effects and gamma-ray attenuation are presented by Bergeron and Heaman (1985).

A5 ISOTOPIC ANALYSES

A5.1 Strontium Isotopes

The procedures for dissolving a rock powder and isolating strontium for isotopic analysis have been outlined in previous reports (Heaman, 1980; Beakhouse and Heaman, 1980, Beakhouse, 1983) so only a general description of these procedures, with an emphasis on the changes made during this study, will be presented here.

A5.1.1 Chemistry

The reagents used for dissolving the sample and for isolating strontium were distilled once. The HF and HNO₃ were distilled by sub-boiling distillation following the two-bottle still method of Mattinson (1972) while the distilled water supply, already available in the chemistry lab, was further distilled in a Corning "Mega Pure" Vycor still then subsequently passed through a Barnstead ultrapure deionizer. The procedure for distilling HCl was modified

slightly to incorporate a constant-level feed device (Heaman, 1983), similar to the apparatus described by Burrhus and Hart (1972), that is capable of supplying acid to a quartz still continuously for 3 to 4 weeks. When re-filling the 5 liter feed reservoir, equal volumes of reagent grade HCl (12N) and double distilled water are added so that the normality of the HCl in the collector reservoir remains approximately 6.2N, the composition of the HCl-H₂O azeotropic mixture.

For sample dissolution, a 250 mg aliquot of sample powder was dissolved by adding an HF-HNO₃ mixture (5 ml HF + 0.5 ml HNO₃) to Parr Teflon bombs (model #4745). The teflon bomb and encapsulating steel jacket assembly is placed in a furnace for four days at a temperature of 135 °C. After four days, the sample solution is evaporated to dryness then 1 ml of 8N HNO₃ is added and immediately evaporated so that any remaining sulphides are dissolved. The sample is then converted to chloride by first adding 5 ml of 6.2N HCl to the bomb and returning the bomb assembly to the furnace for 12 hours (again at 135 °C). Finally, the sample solution is evaporated to an incipient mush then re-dissolved in 2 ml of 2.5N HCl and is now ready to be loaded onto a cation exchange column. The cation exchange columns are filled with 15 ml of Dowex Bio-Rad AG50W-X8 (200-400 mesh) resin (hydrogen form). The procedure for elution and the separation of strontium from other cations using the exchange columns is described in detail by Beakhouse and Heaman (1980).

The total strontium blank for the entire chemical procedure, determined by processing a measured quantity of spike (enriched ^{87}Sr solution), is between 5 and 30 ng. Individual reagent blanks collectively account for most of the total strontium blank (Heaman, 1980).

A5.1.2 Mass Spectrometry

The majority of samples analysed for strontium isotopes were measured in the McMaster Geochronology Lab, however, a few samples were also analysed in the Jack Satterly Geochronology Lab, Royal Ontario Museum, Toronto (these analyses are indicated with an asterisk in Tables B3.1 to B3.4). At McMaster, the strontium isotopic ratios were determined using a single filament, 10 inch, 90° sector, Nier-type mass spectrometer interfaced with a TRS-80 microcomputer to facilitate automated peak switching and on-line data acquisition and calculations. The procedure for loading strontium onto a wide (0.03 mm) tantalum filament and the method of data collection are described in detail by Heaman (1980).

The samples analysed at the Jack Satterly Geochronology Lab were also loaded onto beads with wide tantalum filaments but the procedure differs slightly from the method described by Heaman (1980). The bases that hold the beads and the cover slips are cleaned prior to sample loading in an HCl-HNO_3 ultrasonic bath then rinsed with

double-distilled H_2O before allowing to dry. Previously outgassed beads and corresponding inserts are assembled and mounted onto a 16-sample turret. To load a sample, a small drop of 0.5N H_3PO_4 is first evaporated (at 0.5 Amps) onto the center of the filament followed by a drop of sample solution mixed with a Ta_2O_5 activator. This sample load is then slowly heated (0.2 Amp increments) until the filament shows a dull red glow. After each sample is evaporated onto the filament, a clean cover slip is installed and covered with parafilm while loading the remaining samples to prevent cross-contamination. The strontium isotopic measurements were determined using a VG354 mass spectrometer equipped with five Faraday cup collectors and a Daly photomultiplier detector. The strontium isotopic measurements were determined in dynamic mode (triple collection) using VG software with a typical analysis taking approximately 4.5 hours (this is equivalent to 140 data cycles). The sample warmup time is approximately 20 minutes with an initial aiming current of 1×10^{-12} Amps. During data acquisition the aiming current is 1×10^{-11} Amps (10^{11} ohm resistor).

The strontium isotopic results for five samples measured in both labs as an interlaboratory comparison are presented in Table A6. All measurements have been normalized to an $^{87}Sr/^{86}Sr$ ratio of 0.1194 and corrected for the deviation of the Eimer and Amend standard (E+A), measured in each lab, from 0.70800 (see section A5.1.3). The results for

TABLE A6 - Interlaboratory comparison of samples analysed for strontium isotopes in two laboratories.

Sample	McMaster	RDM
TL14	0.71181 \pm 24	0.71160 \pm 3
TL23	0.72855 \pm 28	0.72875 \pm 1
M17	0.75090 \pm 26	0.75119 \pm 10
M18	0.76440 \pm 22	0.76486 \pm 1
M19	0.74153 \pm 22	0.74101 \pm 2

* - precision of individual analyses is quoted at the 2 sigma level

three samples (TL14, TL23 and M17) agree within the estimated precision of each analysis, however, there is some discrepancy between the results for the remaining two samples. Since all the analyses are free from Rb interference, this discrepancy cannot be the result of an inaccurate correction for Rb at mass 87. An alternative explanation is the incorrect adjustment of the measured strontium isotopic composition when correcting the value of E+A to 0.70800. At McMaster, this standard was analysed once every 2 to 3 weeks of operation so there could be periods of time where a slight change in machine performance and hence the measured value of E+A might go undetected. This problem is less likely to occur with the VG354 machine because this standard was analysed with every barrel of seven samples (see section A5.1.3).

A5.1.3 Reproducibility and Accuracy

As a measure of the reproducibility of the strontium isotope measurements, seven samples were analysed in duplicate during this study (Table A7). For each duplicate,

250 mg aliquots of homogeneous sample powder were processed through the entire chemical and mass spectrometric procedure. The average error for these duplicate analyses is 0.008% so the blanket error of 0.02%, used to calculate all isochron errors (see section A5.1.4), is considered a generous estimate of the error in the strontium isotopic measurements. The results for all duplicates analysed in the McMaster geochronology lab during the period 1978 to 1985 are also listed in Table A7. The average error for all 21 duplicates is 0.014%.

To estimate the accuracy of the strontium isotopic analyses, eighteen analyses of the Eimer and Amend (E+A) SrCO_3 chemical standard were determined in the McMaster geochronology lab during this study (Table A8). The average value for all the analyses is 0.70816 ± 3 and agrees to within $\pm 0.02\%$ of the value generally accepted for this standard (0.70800). The strontium isotopic composition of all samples analysed at McMaster have been adjusted, using the average value quoted above, to correct for the discrepancy between the measured and accepted value for the E+A standard.

For the strontium isotopic analyses determined at the Royal Ontario Museum (ROM), at least one chemical standard (E+A or NBS987) was analysed with every new barrel of seven samples. A total of three analyses were determined for both E+A (0.70806 ± 4) and NBS987 (0.71028 ± 2) and these results are presented in Table A8. The isotopic composition of each

sample was adjusted according to the value obtained for the standard analysed on the same barrel. The E+A standard analysed at both McMaster and the ROM was prepared from the same stock solution so the results obtained in both labs provide a good interlaboratory comparison. The average value for 18 analyses of E+A determined at McMaster (0.70816 ± 3) is noticeably higher than the average value for 3 analyses determined at the ROM (0.70806 ± 4). A similar check can be made by comparing the results obtained for NBS987 at McMaster (0.71036 ± 13 ; Heaman, 1980) and ROM (0.71028 ± 2).

A5.1.4 Age Calculation and Isochron Errors

A number of two-error regression treatments are available for estimating the error associated with a Rb-Sr age determination (for a review see Brooks et al., 1972) and it is the responsibility of the geochronologist to decide which treatment is best suited for each age determination. For studies where the data scatter is not in excess of experimental error (ie. the data define an isochron in the terminology of Brooks et al., 1972) there is generally very little difference between the results from the McIntyre 1 (McIntyre et al., 1966), York 2 (York, 1969) and Wendt 2 (Wendt, 1969) two-error treatments so, in these cases, the selected model is often arbitrary. For consistency, the regression results reported in this study, where all data scatter is within analytical error (ie. Mean Square Weighted

Deviates < 2.5), are those from the McIntyre 1 (M1) model. In cases where geological error is detected (ie. MSWD > 2.5), the results from the McIntyre 2 (M2) model, which assumes the excess error is distributed proportional to the $^{87}\text{Rb}/^{86}\text{Sr}$ ratio, are reported. The M2 model was selected because many of the errorchrons reported in this study were determined using samples collected from relatively homogeneous portions of a single sampling site so variation in the initial strontium isotopic composition is unlikely. As discussed above (sections A2.1 and A5.1.3), a blanket error of 1.0% and 0.02%, based on replicate analyses, has been assigned to the $^{87}\text{Rb}/^{86}\text{Sr}$ and $^{87}\text{Sr}/^{86}\text{Sr}$ ratios, respectively.

All the Rb-Sr whole rock ages reported in this study were calculated using the $1.42 \times 10^{-11} \text{ yr}^{-1}$ ^{87}Rb decay constant recommended by the International Subcommission on Geochronology and Cosmochronology (Steiger and Jager, 1977).

TABLE A7 - Precision of strontium isotope measurements based on duplicate analyses of the same rock powder. The data presented in this table is a summary of all duplicates analysed at McMaster during the period 1978-1985.

Analyst*	Sample	$^{87}\text{Sr}/^{86}\text{Sr}$	$^{87}\text{Sr}/^{86}\text{Sr}^{**}$	% Error
1	AG19E1 (a) (b)	0.71978 \pm 14 0.71944 \pm 34	0.71961	0.024
1	AG19E2 (a) (b)	0.73382 \pm 20 0.73384 \pm 52	0.73383	0.001
1	HG7 (a) (b)	0.74445 \pm 186 0.74453 \pm 30	0.74449	0.005
1	HGB (a) (b)	0.75962 \pm 12 0.75969 \pm 16	0.75966	0.005
1	HG12 (a) (b)	0.76437 \pm 18 0.76440 \pm 16	0.76439	0.002
1	SL3 (a) (b)	0.90636 \pm 30 0.90621 \pm 16	0.90629	0.008
1	M10 (a) (b)	0.75111 \pm 10 0.75131 \pm 20	0.75121	0.013
2	LL8 (a) (b)	0.73474 \pm 26 0.73434 \pm 15	0.73454	0.027
2	LL27 (a) (b)	0.72029 \pm 22 0.72075 \pm 13	0.72052	0.032
2	TL12 (a) (b)	0.74639 \pm 7 0.74668 \pm 9	0.74654	0.019
2	D1 (a) (b)	0.76161 \pm 19 0.76115 \pm 20	0.76138	0.030
3	R-242 (a) (b)	0.70855 \pm 7 0.70870 \pm 9	0.70863	0.011
4	TACH30 (a) (b)	0.74649 0.74665	0.74657	0.011
5	R-5 (a) (b)	0.71411 \pm 8 0.71364 \pm 15	0.71387	0.032

TABLE A7 - Con'd

Analyst*	Sample	$^{87}\text{Sr}/^{86}\text{Sr}$	$^{87}\text{Sr}/^{86}\text{Sr}$	% Error
5	R-52 (a)	0.72733 \pm 16	0.72736	0.004
		(b) 0.72739 \pm 13		
5	R-70 (a)	0.72327 \pm 11	0.72316	0.015
		(b) 0.72305 \pm 8		
5	796006 (a)	0.72810 \pm 9	0.72816	0.008
		(b) 0.72822 \pm 13		
5	79-1 (a)	0.72189 \pm 10	0.72184	0.007
		(b) 0.72179 \pm 9		
5	79-2 (a)	0.73251 \pm 12	0.73260	0.012
		(b) 0.73239 \pm 7		
5	79-3BC (a)	0.79678 \pm 9	0.79687	0.014
		(b) 0.79698 \pm 8		
5	79-3DC (a)	0.86105 \pm 12	0.86109	0.005
		(b) 0.86113 \pm 14		

* 1 - Heaman (this study) 2 - Heaman (1980)
 3 - Rapela et al. (1982) 4 - Atkins (1983)
 5 - Beakhouse (1983)

** Average strontium isotopic composition for duplicate.
 % Error calculated from equation quoted in Heaman (1980).

TABLE AB - Accuracy of the strontium isotope measurements based on replicate analyses of the Eimer and Amend standard. This table summarizes the results obtained at McMaster and the ROM during the period 1982 to 1985.

#	**	Date	$^{87}\text{Sr}/^{86}\text{Sr}$	
			<u>McMaster</u>	E+A
1	1	3/06/82		0.70822±7
2	1	15/06/82		0.70814±7
3	1	1/07/82		0.70818±6
4	1	13/07/82		0.70803±16
5	2	6/10/82		0.70816±8
6	1	9/12/82		0.70821±4
7	2	5/01/83		0.70805±15
8	3	11/01/83		0.70815±12
9	1	2/02/83		0.70834±6
10	1	4/02/83		0.70825±5
11	1	24/02/83		0.70818±6
12	2	13/04/83		0.70899±5
13	2	26/04/83		0.70817±8
14	1	31/05/83		0.70816±3
15	1	24/11/83		0.70828±6
16	1	25/11/83		0.70833±7
17	2	13/01/84		0.70794±9
18	1	6/02/84		0.70806±7

				0.70816±3

#	**	Date	$^{87}\text{Sr}/^{86}\text{Sr}$	
			<u>ROM</u>	E+A
1	1	26/01/84		0.708045±2
2	1	26/01/84		0.708038±2
3	1	17/04/85		0.708101±4

Mean				0.70806±4

#	**	Date	$^{87}\text{Sr}/^{86}\text{Sr}$	
				NBS987
1	1	9/02/84		0.710288±2
2	1	29/03/84		0.710283±2
3	1	7/04/84		0.710262±2

Mean				0.71028±2

** 1 - L. Heaman 2 - K. Connare 3 - R. McNutt

A5.2 Uranium and Lead Isotopes

This section outlines the procedure for separating zircon and sphene from a rock powder and the isolation of U and Pb for isotopic measurements. The samples collected for U-Pb geochronology were crushed and processed at the Jack Satterly Geochronology Laboratory, Royal Ontario Museum, Toronto.

A5.2.1 Mineral Separation

The rock sample is pulverized to a fine powder (the majority of the powder is between -70 and +325 mesh) according to the procedure outlined in section A1 then passed over a Wilfley Table to obtain a heavy mineral concentrate. Only the heaviest mineral streak on the table is collected so that at this stage of the separation procedure the sample size is often reduced to less than a kilogram. The action of the Wilfley Table also performs another important function. All the very fine powder (ie. < 400 mesh) is removed so that during other stages of separation grains do not stick together. This heavy mineral concentrate is immediately washed in alcohol and allowed to dry to prevent oxidation. The minerals of interest such as zircon and sphene are concentrated using standard heavy liquid and magnetic techniques. An outline of the mineral separation procedure used at the ROM is presented in the form of a flow chart in Table A9. In the case of mafic samples, such as a gabbro, the

bromoform step is omitted. By the time the sample reaches the final Frantz stage (Frantz refers to a Frantz isodynamic separator), only minerals that have a density greater than 3.3 (the density of methylene iodide) and are weakly paramagnetic, such as anatase, graphite, rutile, pyrite and zircon, remain. Occasionally, some apatite and/or fluorite can be found at this stage. The majority of zircon fractions analysed in this study were hand picked, using a binocular microscope, from the final frantz fractions. Sphene is concentrated in the 1.0 or 1.8A initial frantz fraction.

A5.2.2 Zircon, Sphene Selection

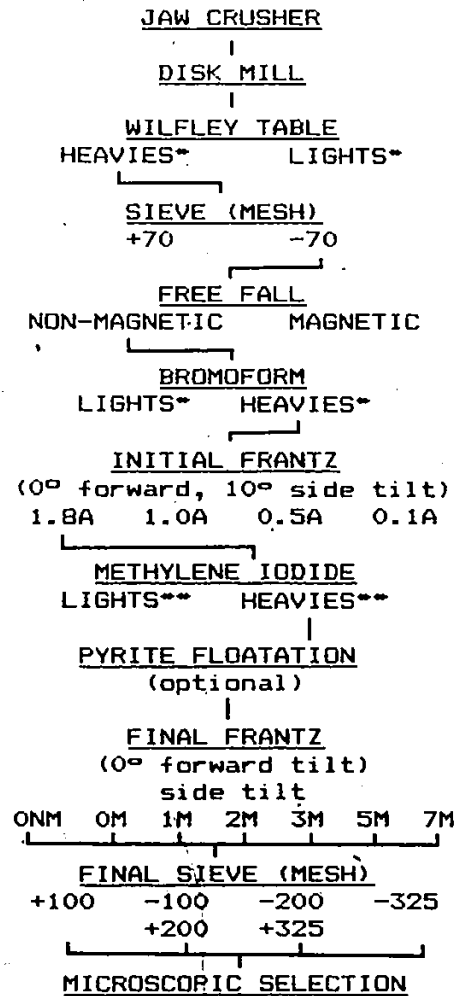
In recent years there have been significant advances in U-Pb geochronology that have been instrumental in reducing the quantity of a mineral, and also the amount of U and Pb, necessary to make a precise isotopic measurement. Most notable among these advances are the profound reduction in the Pb blank achieved by the hydrothermal decomposition of zircons (Krogh, 1973) and the improved ion transmission obtained by modern mass spectrometers. Although the nature of Pb-loss and discordance in the U-Pb system are not well understood, the ability to analyse small quantities of sample revealed that zircon grains with cracks, inclusions, or alteration contain more common Pb and also are more discordant than gem quality grains (eg. Krogh, 1982a). With this in mind, zircon and sphene fractions weighing between

0.040 and 0.652 mg were hand picked so that individual grains that contain any imperfections, such as those listed above, could be removed. As a guide to the quantity of sample analysed, the four, +100 mesh, sphene fractions analysed (Table B4) consisted of between 60 and 100 grains and weighed between 0.290 and 0.507 mg, respectively.

A5.2.3 Abrasion

To further reduce discordance caused by surface related Pb-loss, many of the selected fractions were abraded according to the method described by Krogh (1982b). The air abrasion technique was employed in two different operating modes. In the first, and most commonly used mode, selected zircon and sphene fractions were loaded into an air abrasion device with between 5 and 25 mg of pyrite. The pyrite acts to enhance polishing and prevents grains from breaking. Most zircon fractions were abraded for 6 to 10 hours at 3 to 4 psi followed by a period of abrasion at a lower pressure (2 hours at 2 psi) to produce a smooth, polished surface. For certain fractions, abrasion revealed additional grains with cracks and other imperfections so often the abraded fractions were further subdivided by hand picking into abraded best and abraded second best fractions. By comparing the isotopic composition of abraded versus non-abraded grains in Table B4, it is apparent, as suggested by Krogh (1982b), that the abraded grains are lower in U and total common Pb. The only

TABLE A9 - Flow chart illustrating the procedure for separating zircon from a rock sample.



* - washed in alcohol

** - washed in acetone

exception is the abraded zircon fraction from the Loon Lake monzonite which has a higher total common Pb content. The sphene fractions were abraded for 2 hours at 1 to 2 psi but, since the hardness of sphene is close to the hardness of pyrite, abrasion of sphene tends to result in the formation of slightly frosted spheres.

The second mode of operation is to abrade a large quantity of bulk sample (ie. 10 to 20 mg) in order to concentrate the good quality zircon grains. This approach is particularly useful when dealing with tiny grains (ie < 325 mesh) where hand picking is especially tedious.

In order to remove the pyrite remaining in an abraded fraction, the sample is transferred to a Pyrex Petri dish then washed in warm 4N HNO₃ until the majority of pyrite is dissolved or forms large particle aggregates.

A5.2.4 Sample Cleaning

Before weighing the samples, they are cleaned in the following manner. The samples, submerged in alcohol, are transferred to clean, 10 ml pyrex beakers using a disposable pipette. To ensure that all the grains are concentrated in one spot on the bottom of the beaker, the walls and bottom of the beaker are rinsed with acetone and, holding the beaker on a 45° angle, tapped repeatedly with a metal object then the acetone is decanted such that the zircon grains are never

exposed to air. The samples are then washed in warm 4N HNO₃ for one hour, covered with parafilm, and placed in an ultrasonic cleaner for thirty to sixty seconds. After rinsing with double-distilled (2X) H₂O twice, the samples are washed in warm 2X H₂O for 30 minutes, again rinsed twice with 2X H₂O, then rinsed twice with acetone before allowing to dry.

A5.2.5 Sample and Spike Weighing

The samples are transferred from the pyrex beakers to weighing boats, made from clean aluminium foil, and weighed on a Cahn (model 4700) microbalance. Before transferring the samples to clean teflon bombs, the bombs are treated with an anti-static gun so that grains do not adhere to the walls of the bomb. After the samples are weighed, an estimate of the amount of ²⁰⁷Pb in each sample is made and an appropriate amount of mixed ²⁰⁸Pb-²³⁵U enriched spike solution (Krogh, 1975) is added. In all cases, an attempt is made to slightly underspike each sample such that the ²⁰⁷Pb/²⁰⁸Pb ratio is greater than 1. The concentration of Pb and U in the spike solution is such that 0.2 mg of Grenville zircon containing 100 ppm Pb requires one big drop from the dispensing bottle. For samples that require less spike, the spike solution is added using a clean, calibrated pipette. The weight of spike solution added is calculated by subtracting the weight of the bomb plus sample from the weight of the bomb plus sample plus spike solution.

A5.2.6 U and Pb Chemistry

The procedure for dissolving zircon and isolating U and Pb for isotopic measurements follows closely the low-contamination method described by Krogh (1973). All reagents used during the extraction of U and Pb are purified following the two-bottle, sub-boiling distillation method of Mattinson (1972). Prior to loading samples into the bombs, the bombs are cleaned by first rinsing with 2X H₂O then are passed through three cleaning cycles where approximately 0.2 ml of 48% HF and 0.02 ml of HNO₃ are added and the bomb assembly is placed in the furnace at 220°C for 3 to 4 days.

After weighing the samples, 0.2 ml (20 drops) of 48% HF and 0.02 ml (2 drops) of 7N HNO₃ are added to the sample-spike mixture already loaded into the teflon bombs. The bomb assembly is placed in a furnace at 220°C for five days at which time the bombs are removed from the furnace, allowed to cool and the sample solutions are evaporated to dryness. The samples are then converted to chloride by adding approximately 0.15 ml (15 drops) of 3.1N HCl and the bombs are returned to the furnace for 12 to 24 hours. Prior to loading the samples onto the columns, an additional 15 drops of 3.1N HCl are added to the bombs to ensure that the sample solution is 3.1N. The sample solution is transferred to a corresponding clean PMP beaker prepared for collecting Pb then loaded according to the procedure outlined by Krogh

(1973).

To prepare for the extraction of U and Pb, thirteen, 30 ml PMP beakers are rinsed with 1X H₂O and cleaned for 1 hour in 6.2N HCl (reagent grade). If the beakers are cleaned for periods longer than 1 hour then significant wetting can occur. The beakers are then rinsed with 1X H₂O (twice) followed by 2X H₂O (twice). Approximately 5 ml of 6.2N HCl is added to the six best beakers (ie. beakers that show no signs of wetting); to be used to collect the Pb effluent, and placed on the hotplate for 1 hour just prior to column chemistry. The previously used resin is discarded and the columns are cleaned in an inverted position by sequentially washing the polyethylene frit with 20 drops (0.2 ml) of acetone, 7N HNO₃, 6.2N HCl and 2X H₂O. This washing procedure is repeated twice. The columns are then placed in an upright position and washed with 2 ml of 7N HNO₃ and acetone, respectively. Approximately 0.5 ml of new anion exchange resin (Dowex 1 x 8, 200 to 400 mesh, chloride form) is added as a slurry then cleaned by repeatedly filling the column (2 ml) with 2X H₂O followed by 6.2N HCl for a total of 3 passes each. Just prior to loading the sample the resin is equilibrated with 1 ml of 3.1N HCl. The sample is loaded and U and Pb are isolated according to the method described by Krogh (1973). A small drop of 0.5N H₃PO₄ is added to each U and Pb aliquot with a clean pipette so that the sample evaporates to a tiny orange-brown spot that is easily found

during bead loading.

The sphene dissolution and column chemistry deviates from the method described above for zircon. The sphene fraction and spike aliquot are weighed into a clean Salvillex digestion bomb and then passed through the following four dissolution steps:

- a) 16 hours - 48% HF (0.10 ml) + 8N HNO₃ (0.10 ml) + 6.2N HCl (0.10 ml)
- b) 5 days - 48% HF (0.05 ml) + 8N HNO₃ (0.10 ml) + 6.2N HCl (0.15 ml)
- c) 22 hours - 6.2N HCl (0.30 ml)
- d) 24 hours - 3.1N HCl (0.30 ml)

It took a total of seven days on the hotplate (medium heat) before the sphene grains were totally dissolved. Column preparation and cleaning and the 3.1N HCl sample wash are identical to the procedure described above but U was removed first by eluting with a total of 2 ml of 1N HBr then Pb was removed with 2 ml of 6.2N HCl. The 2 ml of 1N HBr and 6.2N HCl represents the total volume of solvent added and is introduced by first adding four 0.15 ml aliquots so that the resin equilibrates with the solvent followed by the 1.4 ml wash. The advantage of this column procedure for sphene is that the Pb aliquot has fewer impurities than the conventional procedure used for zircon. The U aliquot contains some impurities and can be further cleaned by re-loading onto the column in 6.2N HCl and washing with 2 ml

of 6.2N HCl followed by 4 ml of 8N HNO₃ then removing the U with H₂O.

A5.2.7 Blanks

Bomb blanks were determined on both the regular Teflon bombs and the Salvillex containers during this study. For the regular Teflon bombs, between 1 and 3 mg of ²⁰⁸Pb-enriched tracer solution (concentration of Pb is 79.64 ppm), HF (0.3 ml) and HNO₃ (0.02 ml) were added to each bomb then the bomb assembly was placed in the furnace at 220°C for five days. The total amount of common Pb contamination measured in the bombs generally varied between 2 and 20 pg with one bomb (#9) having a 98 pg blank. The U blank is generally less than 20 pg (Krogh, personal communication). A summary of the blanks determined for the bombs most often used in this study is presented in Table A10. The Pb blanks for the Salvillex containers varied between 2 and 10 pg.

The fact that the total common Pb measured in a number of the zircon fractions (Table B4) is less than 20 pg also indicates that the common Pb contamination for the entire chemical procedure must be less than 20 pg. The isotopic data presented in Table B4 have been corrected for Pb and U blanks of 12 and 20 pg, respectively except where the total common Pb measured in a zircon sample is less than the estimated blank. In this case the total measured common Pb is considered equivalent to the blank.

TABLE A10 - Summary of bomb blanks (picograms of Pb) for the period 1984 to 1985

Bomb #	04/84	02/85	06/85
1	8	10	6
12	6	5	7
14	6	19	5
16	50	9	6
17	6	5	10
18	14	4	11

A5.2.8 Mass Spectrometry

The samples analysed for U and Pb were measured on a VG354 (micromass) mass spectrometer (see section A5.1.2). The VG354 was chosen over the VG30, also available in the lab, because the former has a factor of 10 better transmission so that even with relatively small samples (ie. less than 5 ng of Pb) precise measurements can be made using the Faraday cup collectors. The Pb samples were loaded onto previously outgassed Re filaments as a sample - silica gel - phosphoric acid (0.5N) mixture. The proportion of silica gel to phosphoric acid was 2:1 with approximately 1 cm of gel used (measured in a 0.5 mm inner diameter disposable, loading pipette). This mixture was evaporated at 0.8 Amp until the mixture passed through a lumpy resinous looking stage and formed a thin, honey-coloured film on the filament. The filament was then slowly heated (0.2 Amp increments) to 1.6 to 1.7 Amps (or to a current just below where the filament shows a dull red glow). At 1.0 Amp the load turns black and with increasing temperature it starts to bubble. At 1.7 Amps

the load will eventually turn white and at this point the loading is complete. For Pb samples that contain some impurities, the load at 1.7 Amps will remain a grey colour.

To measure the isotopic composition of Pb on the mass spectrometer, the filament was slowly heated to 1350°C where blocks of data (4 runs of 8 cycles) were collected for $^{207}\text{Pb}/^{204}\text{Pb}$, $^{207}\text{Pb}/^{208}\text{Pb}$, $^{208}\text{Pb}/^{204}\text{Pb}$ (Daly detector) and $^{207}\text{Pb}/^{208}\text{Pb}$ respectively. This sequence of data collection was repeated at 50°C increments until all the Pb was burned off. For samples with less than 5 ng of ^{204}Pb , all the isotopic ratios were measured initially using the Daly photomultiplier detector until the signal at mass 206 reached 0.8×10^{-13} A (10^{11} ohm resistor). The intensity at this mass for samples with more than 5 ng of ^{204}Pb was usually greater than 0.8×10^{-13} A at 1350 °C so the isotopic ratios (except $^{208}\text{Pb}/^{204}\text{Pb}$) could be measured directly on the Faraday collector. The Daly:Faraday conversion factor used is 0.3%/amu and all Pb isotopic ratios are corrected for mass fractionation of 0.13%/amu. After all the Pb samples have been analysed, the beads are then heated to 3 Amps for three minutes so that they could be re-used for the corresponding U analyses.

Uranium extracted from zircons is loaded in a similar way as Pb, however, the U extracted from sphenes using HBr chemistry is more impure and was loaded with a Ta_2O_5 - TaPO_4 activator for a smoother run. To measure the isotopic

composition of U loaded with silica gel, the filament was heated slowly to 1450°C where blocks of data as above were collected for $^{235}\text{U}/^{238}\text{U}$. The average fractionation during an U analysis using silica gel is 0.1%/amu whereas fractionation using Ta-gel is -0.1%/amu.

The errors associated with the Pb/U and $^{207}\text{Pb}/^{206}\text{Pb}$ ratios, based on the reproducibility of standards (Krogh, personal communication), are estimated to be 0.5 and 0.1% (2 sigma), respectively. The method for estimating errors for the U-Pb ages is similar to the approach discussed by Davis (1982) and also quoted at the 2 sigma level. The decay constants for ^{238}U (9.8485×10^{-10}) and ^{235}U (1.55125×10^{-10}) used in this study are those recommended by the Subcommittee on Geochronology (Steiger and Jager, 1977).

A5.3 Oxygen Isotopes

The oxygen isotopic data presented in this dissertation were performed by Yuch Ning Shieh at Purdue University, West Lafayette, Indiana. Oxygen was extracted from the rock powders using the BrF_5 technique and isotopic ratios were measured with a Nuclide 3-60-RMS mass spectrometer. The results are reported in the conventional δ notation as per mil relative to SMOW (standard mean ocean water). The precision of the oxygen isotopic analyses is generally better than 0.2 per mil. The average value obtained for the reference sample NBS-28 is 9.6 per mil.

APPENDIX B

TABLE B1 - MODAL ANALYSES

The following modes were determined by point counting thin sections prepared by Len Zwickler. Each mode is based on a minimum of 1000 counts obtained along traverses approximately perpendicular to any foliation, if present. Only the abundance of the major and minor rock forming minerals present in any sample is presented in this table. Accessory minerals are listed in the text.

TABLE B1.1 - APSLEY GNEISS

	QUARTZ	PLAG.	K-FELD.	BIOTITE	MUSC.	GARNET	AMPH.	OPAQUES	CARB.	CHLORITE
AG2A	17.0	61.6		18.4	0.8	1.6	0.6			
AG2B	20.0	66.2		9.8	1.8	0.8		0.8	0.4	0.2
AG3	25.9	49.3	9.6	14.9				0.3	tr	
AG5	43.7	32.5	15.0	8.3				0.5		
AG7	33.6	44.7	9.6	11.3		0.2		0.6		
AG11	24.1	37.5		36.1		1.6		0.7		
AG19E3	42.7	43.1		13.1		0.1		0.1	0.9	
AG32	14.7	44.9	14.8	24.4		0.3		0.7	0.3	
AG50	27.1	52.4	2.8	15.3	0.7	0.5		0.4	0.8	tr

TABLE B1.2 - SILENT LAKE COMPLEX

	QUARTZ	PLAG.	K-FELD.	BIOTITE	MUSC.	GARNET	AMPH.	OPAQUES	CARB.	CHLORITE
HG5	40.8	15.6	34.9		5.8			1.9		
HG6	36.2	32.3	20.5	0.3	6.9			3.1	0.8	
HG8	31.7	45.5	5.2		12.8			1.3	3.5	
HG9	40.7	25.2	6.5	0.8	22.2	0.2		2.2	2.3	
HG10	32.9	31.2	17.5		15.0	0.3		1.8	1.5	
HG11	34.4	25.8	17.1	12.4	5.9	0.3	tr	1.5	2.6	
HG13	39.3	22.1	28.1		7.1			3.4		
HG15	37.2	28.4	30.2		1.6			2.6		
HG16	37.5	42.6		14.3	4.7			1.3	0.7	
HG18	29.3	33.4		30.2	3.3			3.8		
HG19	9.5	49.8		31.4	0.3			7.0	tr	
HG21	0.4	31.3			0.1		62.9	2.2	3.2	
HG22	28.8	22.1		35.4	8.8			3.7	0.5	
HG23	29.8	14.8		23.7	26.8			4.4		
Sw1	32.6	37.0	23.1	3.0	4.0			0.4		

TABLE B1.3 - TALLAN LAKE SILL

	QUARTZ	PLAG.	K-FELD.	BIOTITE	MUSC.	GARNET	AMPH.	OPAQUES	CARB.	CHLORITE
TL1		34.2					60.8	5.0		
TL2	19.5	46.0	15.1	9.9			7.3	0.2	2.0	
TL5	39.0	47.6	4.9	5.4	3.2			tr	tr	
TL11	20.4	50.8	7.8	16.6			2.8		1.0	
TL12	16.7	45.1	21.7	13.5	0.1		1.7			
TL14	21.5	48.4	10.0	9.3			9.6	tr	1.2	
TL15	31.1	41.2	2.8	23.5	0.6			tr	0.8	
TL16	15.7	53.4	5.0	25.8	0.3					
TL22	20.1	50.2	5.3	8.9			13.7	0.1	1.7	
TL23	26.7	42.8	13.7	4.5			11.1		0.7	
TL40	18.3	48.5	11.3	6.1			14.3	0.4	1.1	
TL41		54.0				1.0	44.0	1.0		
TL615S		31.0				7.6	58.9	2.2		
TL617S		30.1					64.8	5.0		

TABLE B1.4 - METHUEN COMPLEX

	QUARTZ	PLAG.	K-FELD.	BIOTITE	MUSC.	GARNET	AMPH.	OPAQUES	CARB.	CHLORITE
Site - A										
M3	15.6	42.5	32.8	6.0			2.8		0.1	0.2
M10	15.3	46.2	29.1	5.9			3.0			0.2
M12	28.0	38.8	22.6	7.7			2.3			0.1
M15	20.9	39.9	28.2	6.7			3.4			0.1
M17	19.5	45.3	23.9	6.9			3.5			0.2
Site - B										
M22	28.7	36.0	29.1	5.9					0.5	
M23	27.8	31.4	36.8	3.6			0.1		0.1	
M24	25.6	32.6	36.0	5.2					0.6	
M27	31.6	34.6	28.6	5.0					0.2	
M28	20.8	35.2	39.0	4.4					0.6	
Others										
M6	27.2	52.0	9.2	1.4			9.6			
M7	24.4	45.8	18.4	5.6					0.8	5.0
M19	21.2	49.6	10.6	13.7			1.1		3.3	
M20	33.2	27.7	26.6	9.1			8.0		2.0	

PLAG = Plagioclase K-FELD = K-feldspar MUSC = Muscovite
 AMPH = Amphibole CARB = Carbonate

TABLE B2

MAJOR AND TRACE ELEMENTS

The following tables of data contain the major and trace element compositions determined for samples collected from the Apsley Gneiss, Silent Lake Complex, Tallan Lake Sill, Methuen Complex and Coe Hill pluton. The majority of major and trace element data presented in these tables has been determined by XRF following the procedure outlined in Appendix A and Heaman (1980). In addition, many of the samples listed in Table B2.3 were also analysed for the same elements by AA (Shaw, unpublished data; Griep, 1975) and for certain elements (eg. Na_2O and MgO) the AA results are more accurate. The elements determined by AA and listed in Table B2.3 are marked with an asterisk. All the major element data are normalized to 100%, excluding loss on ignition (LOI), to facilitate comparison. For samples where only XRF major element data is available, total iron is expressed as Fe_2O_3 . Some other features of these data are:

- 1) the REE, Hf, Ta and Th abundances were determined by INAA (Appendix A) and B plus Gd by PGNAA (Higgins, 1984; Bergeron and Heaman, 1985).

- 2) the scandium data reported in Table B2.3 were determined by emission spectroscopy (Shaw and Kudo, 1965).
- 3) the abundance of thallium is reported as ppb.
- 4) "DF" in Tables B2.1 and B2.2 refers to discriminant function values determined using the equation listed in Chapter 3 (after Shaw, 1972). "K/K+N" refers to K_2O/K_2O+Na_2O .
- 5) tr = trace.

TABLE B2.1 - APSLEY GNEISS

	AG21	AG22	AG25	AG26	AG27	AG28	AG29	AG30	AG31	AG32	AG33	AG35
SiO2	71.24	68.14	53.20	57.33	59.34	61.96	58.37	64.25	75.56	75.56	73.44	72.06
Al2O3	13.61	13.80	16.30	15.66	15.64	15.09	15.89	14.65	12.02	11.87	12.83	13.26
Fe2O3	5.13	5.81	7.81	8.04	7.59	7.97	8.83	5.35	4.45	4.15	5.16	5.15
MgO	1.26	1.43	2.79	6.09	3.06	3.12	3.00	2.38	1.51	1.76	1.32	1.46
CaO	1.30	1.54	10.97	4.72	5.86	3.96	4.44	5.18	0.70	1.19	0.70	1.82
Na2O	3.46	4.83	4.71	4.00	4.15	3.74	4.57	2.65	4.35	3.92	4.59	3.74
K2O	3.26	3.66	1.94	2.59	2.80	2.61	3.22	4.10	0.93	1.00	1.33	1.74
TiO2	0.52	0.57	0.95	0.89	0.88	0.96	0.99	0.83	0.30	0.34	0.38	0.51
MnO	0.13	0.13	0.17	0.17	0.10	0.19	0.28	0.12	0.11	0.12	0.17	0.15
P2O5	0.09	0.09	1.16	0.51	0.58	0.40	0.41	0.49	0.07	0.09	0.08	0.11
TOTAL	100.00	100.00	100.00	100.00	100.00	100.00	100.00	100.00	100.00	100.00	100.00	100.00
DF	0.13	2.75	7.99	-0.31	3.35	0.87	3.27	1.84	-1.09	-1.56	-0.12	-0.37
K/K+N	0.49	0.43	0.29	0.39	0.40	0.41	0.41	0.61	0.18	0.20	0.22	0.32
Rb	50	61	47	60	58	55	95	103	15	15	21	24
Sr	81	97	732	553	542	423	567	448	67	88	72	123
Y	39	38	43	42	33	36	37	45				58
Zr	139	151	130	155	137	131	131	242				202
Nb	10	10	8	10	10	10	10	10				10

	AG36	AG37	AG38	AG39	AG40	AG41	AG42	AG43	AG44	AG50A	AG50B
SiO2	65.73	66.88	72.09	73.35	72.84	70.45	71.20	60.21	68.62	73.11	70.11
Al2O3	13.51	13.88	13.80	12.69	13.90	15.33	13.58	16.08	13.85	13.54	14.66
Fe2O3	5.56	4.87	5.28	4.73	4.77	4.74	5.17	9.13	5.24	4.93	5.96
MgO	4.50	3.94	0.91	2.00	0.96	1.02	1.38	3.12	1.96	1.21	1.14
CaO	0.76	0.35	1.10	0.92	0.55	0.97	1.31	1.81	1.90	0.57	0.48
Na2O	5.62	6.72	3.10	3.35	4.70	5.03	3.87	4.98	5.52	4.31	4.86
K2O	3.49	2.69	2.89	2.25	1.70	1.83	2.72	3.49	2.07	1.75	2.08
TiO2	0.57	0.40	0.52	0.43	0.36	0.41	0.50	0.81	0.56	0.37	0.43
MnO	0.13	0.16	0.16	0.16	0.14	0.11	0.14	0.19	0.14	0.12	0.17
P2O5	0.13	0.11	0.15	0.12	0.08	0.11	0.13	0.18	0.14	0.09	0.11
TOTAL	100.00	100.00	100.00	100.00	100.00	100.00	100.00	100.00	100.00	100.00	100.00
DF	0.96	2.43	-0.59	-1.83	0.76	1.99	0.32	1.97	2.65	-0.13	1.18
K/K+N	0.38	0.29	0.48	0.40	0.27	0.27	0.41	0.41	0.27	0.29	0.30
Rb	52	36	37	32	34	37	46	70	34	34	40
Sr	95	70	104	97	97	116	82	129	140	91	95
Y	41	65	44	42	50	46	27	22	29	51	58
Zr	227	254	205	186	219	206	150	108	155	224	236
Nb	10	8	10	8	10	8	7	8	11	8	9

TABLE B2.2 - SILENT LAKE COMPLEX

	H68	H69	H610	H613	H615	H616	H621	H622	H623	SL2	SL5	SL7
SiO2	77.22	77.31	77.29	78.97	78.35	78.85	48.56	62.11	62.25	78.01	78.35	81.74
Al2O3	11.81	11.69	11.38	11.48	11.27	10.85	16.10	15.85	16.81	12.45	12.39	11.48
Fe2O3	2.95	3.41	4.03	3.38	3.25	3.89	13.78	9.32	9.62	1.94	1.78	0.95
MgO	0.60	0.04	0.77	0.05	0.04	0.93	6.96	3.81	3.49	0.65	0.41	0.63
CaO	1.00	0.96	0.39	0.41	0.08	0.09	10.86	3.40	0.49	0.08	0.08	0.08
Na2O	3.50	3.22	2.86	2.03	2.82	3.60	1.00	0.17	0.20	3.63	2.92	4.78
K2O	2.61	3.03	2.94	3.42	3.96	1.31	0.45	4.00	5.79	3.11	3.96	0.21
TiO2	0.23	0.21	0.21	0.19	0.18	0.22	1.68	0.90	1.01	0.08	0.08	0.08
MnO	0.05	0.09	0.10	0.05	0.04	0.24	0.29	0.23	0.14	0.03	0.02	0.02
P2O5	0.03	0.03	0.02	0.02	0.02	0.02	0.31	0.20	0.20	0.02	0.02	0.02
TOTAL	100.00	100.00	100.00	100.00	100.00	100.00	100.00	100.00	100.00	100.00	100.00	100.00
LOI	0.31	0.36	0.36	0.85	0.54	0.52	1.20	1.80	1.57	0.30	0.30	0.38
DF	-0.24	-0.05	-1.86	-2.24	-0.80	-2.27	-3.31	-5.03	-5.44	-0.18	-0.54	-0.52
K/K+N	0.43	0.48	0.51	0.63	0.58	0.27	0.31	0.96	0.97	0.46	0.58	0.04
B										6.59		
Rb	66	66	57	67	68	38	12	143	153	72	110	3.7
Sr	53	87	340	28	15	33	323	195	64	17	17	17
Y	175	187	187	171	175	158	41	42	40	52	40	48
Zr	807	712	697	679	641	623	112	210	201	131	135	133
Nb	43	40	37	40	40	39	7	15	15	2	15	11
La										30.3		
Ce										63.8		
Nd										25.0		
Sm										5.13		
Eu										0.43		
Gd										4.02		
Tb										1.12		
Yb										5.12		
Lu										0.86		
Th										11		

TABLE B2.2 - SILENT LAKE COMPLEX

	HG1	HG2	HG3	HG4	HG5	HG6	HG7	HG11	HG12	HG14	HG17	HG18
B					9.00							
Rb	117	143	112	108	63	49	79	78	41	96	89	127
Sr	12	31	25	22	19	51	101	48	31	31	32	132
Y	177	137	155	149	142	191	177	165	185	182	216	43
Zr	1040	1054	1075	1022	1015	726	812	666	710	615	697	218
Nb	38	42	40	39	39	38	36	37	42	34	40	15
La					107							
Ce					224							
Nd					110							
Sm					26.2							
Eu					1.85							
Gd					21.6							
Tb					3.98							
Yb					16.8							
Lu					2.71							
Th					18							
	HG19	HG20	SL1	SL2	SL4	SL6	JN24M	JN24M	JN43N	JN43M	JM62N	JM62M
B							43.8	3.39				
Rb	96	61	84	93	79	66	40	195	24	108	35	154
Sr	148	95	20	19	45	20	23	18	1.7	16	3.4	18
Y	39	43	40	50	66	40	76	27	54	38	73	36
Zr	211	222	136	130	148	135	113	143	160	177	130	163
Nb	14	15	16	12	13	15	10	13	11	13	10	13
La							13.8	36.8				
Ce							34.8	70.6				
Nd							17.1	29.3				
Sm							5.32	6.40				
Eu							0.09	0.68				
Gd							6.30	4.04				
Tb							1.79	1.08				
Yb							10.3	3.3				
Lu							1.69	0.55				
Th							14	9				

TABLE B2.3 - TALLAM LAKE SILL
AMPHIBOLITE

	729-4X	729-5X	729-6X	729-7X	802-2X	612SX	613SX	614SX	615SX	616SA	617SX	68763X	69295X	69298X
SiO ₂	45.49	47.49	49.48	46.04	37.59	53.24	48.17	45.95	51.91	47.18	46.55	57.94	43.24	42.44
Al ₂ O ₃	13.05	15.12	14.86	12.14	15.21	12.05	11.76	11.00	13.12	13.51	12.20	13.58	11.06	10.15
Fe ₂ O ₃ *	3.55	3.23	2.47	3.50	3.75	3.55	3.91	4.01	2.89	3.48	3.90	4.41	3.62	3.80
FeO*	14.75	10.28	9.12	14.81	17.35	15.85	16.65	14.54	14.64	13.59	14.24	10.13	17.09	17.35
MgO*	4.79	8.14	7.86	5.04	8.60	1.86	3.40	4.42	2.09	5.16	4.92	0.89	4.96	4.65
CaO	8.80	9.28	11.21	8.37	6.30	5.20	6.55	9.16	6.23	7.75	8.44	4.88	8.75	10.82
Na ₂ O*	3.57	4.19	2.90	3.21	2.27	3.80	3.00	3.18	4.71	2.80	3.04	5.12	2.80	2.37
K ₂ O	0.67	0.09	0.45	0.98	0.90	1.48	1.51	0.52	0.88	0.71	0.52	1.03	0.58	0.39
TiO ₂	4.47	1.81	1.33	5.09	6.64	1.91	3.03	4.50	2.18	5.01	5.45	1.35	5.32	4.02
MnO	0.27	0.19	0.19	0.35	0.26	0.40	0.45	0.33	0.42	0.29	0.34	0.38	0.39	0.44
P ₂ O ₅	0.58	0.18	0.15	0.48	1.13	0.65	1.56	2.39	0.92	0.54	0.40	0.30	2.19	3.55
TOTAL	100.00	100.00	100.00	100.00	100.00	100.00	100.00	100.00	100.00	100.00	100.00	100.00	100.00	100.00
LOI	0.99	1.27	1.25	1.69	1.95	1.27	1.36	1.24	1.00	1.94	0.70	0.64	2.64	1.48
Li*	16	23	21	24	45	11	21	7	18	15	14	15	20	12
B						16.1	18.6	11.8	14.2		10.3			
Sc						25	26	43	44	43	42		66	
V*	590	350	310	530	520	tr	160	320	30	490	520	tr	310	300
Cr*	16	150	230	15	41	10	30	30	20	30	20	10	10	13
Co*	57	62	60	55	60	16	57	61	43	66	64	9	64	46
Ni*	42	65	52	23	42	10	20	30	30	20	30	12	10	14
Cu	52	53	55	18	15	tr	2	5	tr		tr	6	tr	3
Zn	163	148	135	131	206	212	264	196	244		147	218	225	247
As	tr	tr	tr	tr	tr	tr	tr	tr	tr		tr	tr	tr	tr
Rb	8	5	5	22	49	25	42	12	15	37	5	18	17	3
Sr	244	180	219	299	75	174	153	233	305	250	254	329	294	298
Y	63	40	35	63	60	124	111	101	116		59	124	100	120
Zr	159	86	64	199	178	631	288	215	377		177	353	146	163
Nb	tr	2		3	1						10			
Ba*	130	90	160	360	220	400	280	180	300	400	210	350	210	90
La						22.2	22.8	21.6	22.6		8.17			
Ce						65.2	64.5	61.1	61.5		23.9			
Nd						51.4	56.8	58.1	50.0		20.3			
Sm						18.3	17.1	17.3	17.6		7.51			
Eu						5.93	5.81	5.34	5.93		2.75			
Gd						19.6	18.2	17.1	18.1		7.81			
Tb						2.57	2.63	2.70	2.25		1.44			
Yb						10.8	8.77	7.57	8.82		4.49			
Lu						2.03	1.56	1.34	1.52		0.83			
Hf														
Ta														
Tl*	120	110	110	380	1370	280			240			200		95
Pb	9	13	10	13	11	11	12	8	13		11	18	9	7
Th						2.82	1.72	1.80	2.27		0.93			

TABLE B2.3 - TALLAM LAKE SILL

	AMPHIBOLITE						TRANSITION				GRANODIORITE	
	TL4X	TL6X	TL10X	TL20X	TL21X	TL41X	105A	606A	69305X	TL22X	TL2X	TL8X
SiO ₂	58.14	50.53	53.93	48.98	54.21	55.42	63.99	57.54	64.88	66.39	68.96	68.78
Al ₂ O ₃	13.47	12.39	14.00	13.18	13.52	14.01	13.49	16.78	13.86	13.63	14.18	14.06
Fe ₂ O ₃ *	15.82	18.17	17.15	19.86	17.07	16.36	2.45	3.02	3.12	8.62	6.16	5.29
FeO*							7.82	8.30	7.02			
MgO*	0.45	2.56	0.09	1.44	0.64	1.51	0.58	0.98	0.13	0.44	0.01	1.82
CaO	5.28	7.18	6.02	6.74	6.08	6.02	3.14	3.99	3.02	3.15	2.50	0.97
Na ₂ O*	4.29	3.62	5.30	5.04	5.02	3.90	5.16	6.50	6.25	4.92	5.16	6.16
K ₂ O	0.50	0.99	1.18	1.67	1.06	1.00	2.13	1.11	0.61	1.79	2.25	2.42
TiO ₂	1.03	3.33	1.27	1.96	1.35	1.17	0.88	1.22	0.73	0.56	0.40	0.40
MnO	0.47	0.36	0.44	0.41	0.43	0.40	0.18	0.27	0.28	0.22	0.18	0.06
P ₂ O ₅	0.54	0.86	0.61	0.73	0.61	0.22	0.20	0.29	0.09	0.26	0.20	0.04
TOTAL	100.00	100.00	100.00	100.00	100.00	100.00	100.00	100.00	100.00	100.00	100.00	100.00
LOI							2.79	2.40	0.77			
Li*										13		
B						9.30				7.83		5.48
Sc												
V*	38	211	52	92	54				tr	23		
Cr*	tr	21	53	33	54				8	58		
Co*	39	52	45	48	39				34	19		
Ni*	38	31	35	33	38				9	9		
Cu	5	6	8	3	6				tr	tr		
Zn	185	295	243	267	296				159	227		
As	tr	tr	tr	tr	tr				tr	tr		
Rb	7	18	15	47	8		54	30	7	24	16	44
Sr	286	244	333	341	324	334			171	192	143	80
Y	156	126	129	108	121	88			182	224	296	298
Zr	1529	323	1193	400	763	981			1210	1392	1083	1149
Nb						19						
Ba*									300			
La						17.6				44.0		71.6
Ce						53.2				122		201
Nd						35.5				87.4		151
Sm						16.1				26.8		46.6
Eu						6.67				9.86		10.4
Gd						16.7				28.7		43.7
Tb						2.30				4.15		7.02
Yb						9.62				23.3		26.8
Lu						2.01				3.96		4.17
Hf						23.7				40.3		
Ta						1.01				1.90		
Tl*									150			
Pb	11	11	8	12	11				12	17		
Th						2.00				5.80		9.80

TABLE B3

Rb-Sr WHOLE ROCK DATA

The Rb-Sr data for the Apsley Gneiss (Table B3.1), Silent Lake Complex (Table B3.2), Tallan Lake Sill (Table B3.3) and the Methuen Complex (Table B3.4) are presented in this section. The Rb and Sr concentrations for all samples have been determined by XRF using the procedure outlined in Appendix A and Heaman (1980). The Rb/Sr ratios were determined as ratios of the total corrected peak counts. The majority of strontium isotopic data were determined using a single sample, 10 inch, 90° sector, Nier-type mass spectrometer (Heaman, 1980). The following comments explain the codes used with this data:

- 1) the samples marked with a single asterisk were analysed previously (Heaman, 1980) but these data have been revised to include additional Rb/Sr data determined in this study.
- 2) the number in parentheses beside the Rb/Sr ratio refers to the total number of analyses used to calculate the average Rb and Sr concentrations and the Rb/Sr ratio. Using AG11, and an example, the total of nine analyses refers to the results for three pellets analysed on three different occasions.

- 3) the strontium isotope data for the samples marked with a double asterisk were obtained at the Royal Ontario Museum (ROM) using a VG354 multi-collector mass spectrometer. The lower two sigma errors reported for these analyses reflect the precision that can be obtained using triple collectors in dynamic mode.
- 4) the oxygen isotope data reported in Table B3.3 were determined by Y.N. Shieh (Purdue University) and are reported in the conventional per mil notation relative to SMOW (Standard Mean Ocean Water).

TABLE B3.1 - Rb-Sr data for samples from
the Apsley Gneiss

SAMPLE	Rb (ppm)	Sr (ppm)	$^{87}\text{Rb}/^{86}\text{Sr}$	$^{87}\text{Sr}/^{86}\text{Sr}$
<u>Regional</u>				
AG1*	52	79	1.902 (10)	0.73935 \pm 18
AG2*	13	37	0.9928(16)	0.72091 \pm 26
AG3*	41	69	1.730 (10)	0.73636 \pm 26
AG5*	33	48	2.001 (9)	0.74299 \pm 26
AG7*	31	47	1.884 (8)	0.74261 \pm 12
AG11*	47	94	1.470 (9)	0.73036 \pm 32
<u>Site-#1</u>				
AG20A	39	101	1.110 (10)	0.72502 \pm 10
AG20B	25	88	0.8196(12)	0.71923 \pm 19
AG22	61	97	1.814 (9)	0.73700 \pm 6
AG50A	34	91	1.092 (9)	0.72424 \pm 12
AG50B	40	95	1.227 (9)	0.72702
<u>Site-#2</u>				
AG25	47	732	0.1867(10)	0.70720 \pm 10
AG26	60	553	0.3121 (9)	0.70928 \pm 18
AG28	55	423	0.3730(10)	0.71025 \pm 26
AG29	95	567	0.4863(10)	0.71266 \pm 26
AG30	103	648	0.4596(10)	0.71125 \pm 18
<u>Site-#3</u>				
AG31**	15	67	0.6226 (6)	0.71460 \pm 2
AG32**	15	88	0.4924 (6)	0.71270 \pm 2
AG33**	21	72	0.8054 (3)	0.71857 \pm 2
AG36**	52	95	1.592 (7)	0.72828 \pm 2
AG37**	36	70	1.471 (7)	0.72851 \pm 2
AG38**	37	104	1.029 (7)	0.72219 \pm 2
<u>Slabs</u>				
AG19D1	62	145	1.250 (10)	0.72591 \pm 16
AG19D2	48	143	0.9703(10)	0.72218 \pm 14
AG19D3	56	148	1.088 (10)	0.72382 \pm 30
AG19D4	66	157	1.229 (10)	0.72575 \pm 22
AG19E1A	32	111	0.8356(10)	0.71978 \pm 14
AG19E1B				0.71944 \pm 34

TABLE B3.1 - CON'D

SAMPLE	Rb (ppm)	Sr (ppm)	$^{87}\text{Rb}/^{86}\text{Sr}$	$^{87}\text{Sr}/^{86}\text{Sr}$
<u>Slabs</u>				
AG19E2A	26	104	0.7218(10)	0.73382 \pm 20
AG19E2B				0.73384 \pm 52
AG19E3	7.6	82	0.2667(10)	0.71005 \pm 34
AG19E4	21	84	0.7160(10)	0.71661 \pm 24
AG19E5	28	111	0.7326(10)	0.71777 \pm 20
AG50S2**	25	80	0.9165 (1)	0.72088 \pm 1
AG50S3**	25	80	0.9069 (2)	0.72021 \pm 2
AG50S4**	26	74	1.024 (1)	0.72202 \pm 2
AG50S5**	24	84	0.8174 (1)	0.71923 \pm 1
AG50S6**	22	96	0.6504 (1)	0.71691 \pm 2
AG50S7**	25	77	0.9317 (1)	0.72079 \pm 2
AG50S8**	26	79	0.9478 (1)	0.72160 \pm 1
AG50S9**	30	85	1.010 (1)	0.72223 \pm 2
AG50S10**	28	84	0.9580 (1)	0.72177 \pm 1
AG50S11**	28	88	0.9305 (1)	0.72156 \pm 1

TABLE B3.2 - Rb-Sr data for samples from the Silent Lake Complex

SAMPLE	Rb (ppm)	Sr (ppm)	$^{87}\text{Rb}/^{86}\text{Sr}$	$^{87}\text{Sr}/^{86}\text{Sr}$
<u>Site-#1</u>				
HG5	63	19	9.455 (3)	0.83365
<u>Site-#2</u>				
HG6	49	51	2.816 (3)	0.75164 \pm 10
HG7A	79	101	2.274 (3)	0.74445 \pm 186
HG7B				0.74453 \pm 30
HG8A	66	53	3.623 (3)	0.75962 \pm 12
HG8B				0.75969 \pm 16
HG9	66	87	2.183 (3)	0.74107 \pm 16
HG10	57	34	4.942 (3)	0.78306 \pm 16
<u>Site-#3</u>				
HG11	78	48	4.764 (3)	0.78135 \pm 24
HG12A	41	31	3.910 (3)	0.76437 \pm 18
HG12B				0.76440 \pm 16
HG13	67	28	7.016 (3)	0.80732 \pm 8
HG14	96	31	9.143 (3)	0.83100 \pm 16
HG15	68	15	13.58 (3)	0.87609 \pm 20
HG16	38	33	3.347 (3)	0.76261 \pm 14
HG17	89	32	8.080 (3)	0.83006 \pm 8
<u>Site-#4</u>				
HG18	127	132	2.793 (3)	0.75516 \pm 16
HG19	96	148	1.878 (3)	0.74017 \pm 132
HG20	61	95	1.848 (3)	0.73561 \pm 10
HG21	12	323	0.1056 (3)	0.70583
HG22	143	195	2.123 (3)	0.74184 \pm 12
HG23	153	64	7.038 (3)	0.81012 \pm 16
<u>Site-#5</u>				
SL1	84	20	12.74 (8)	0.88796 \pm 34
SL2	71	17	12.28 (10)	0.88284 \pm 18
SL3A	93	19	14.81 (8)	0.90636 \pm 30
SL3B				0.90621 \pm 16

TABLE 3.2 - CDN'D

SAMPLE	Rb (ppm)	Sr (ppm)	$^{87}\text{Rb}/^{86}\text{Sr}$	$^{87}\text{Sr}/^{86}\text{Sr}$
<u>Site-#5</u>				
SL4	79	44	5.182 (10)	0.78967 \pm 24
SL5	110	17	19.20 (10)	0.97582 \pm 20
SL6	65	19	9.727 (9)	0.84762 \pm 18
SL7	3.4	17	0.6178(10)	0.71828 \pm 26
<u>Nodules-Matrix</u>				
JN24N	38	2.3	53.56 (6)	1.21093 \pm 16
JN24M	200	14	33.90 (6)	1.22652 \pm 31
JN43N	20	1.7	41.23 (6)	1.09624 \pm 48
JN43M	109	12	20.14 (6)	1.02332 \pm 30
JN62N	33	3.4	31.51 (6)	1.07643 \pm 76
JN62M	157	14	25.85 (6)	1.09580 \pm 110

TABLE B3.3 - Rb-Sr data for samples from
the Tallian Lake Sill

SAMPLE	Rb (ppm)	Sr (ppm)	$^{87}\text{Rb}/^{86}\text{Sr}$	$^{87}\text{Sr}/^{86}\text{Sr}$	age
<u>Amphibolite</u>					
TL1*	11	276	0.1123 (14)	0.70552 \pm 30	9.0
TL6*	19	243	0.2255 (11)	0.70707 \pm 30	-
TL10	15	330	0.1355 (6)	0.70572 \pm 12	-
TL20	47	339	0.4037 (6)	0.71021 \pm 24	-
TL41	7.8	334	0.0680 (3)	0.70455 \pm 28	-
TL61-2S	24	174	0.4100 (3)	0.71044 \pm 22	9.5
TL61-3S	42	153	0.7883 (3)	0.71489 \pm 16	10.5
TL61-4S	12	233	0.1438 (3)	0.70523 \pm 16	10.1
TL61-5S	16	305	0.1447 (3)	0.70635 \pm 14	10.7
TL61-7S	5.3	254	0.0605 (3)	0.70440 \pm 14	8.1
69311	135	262	1.487 (7)	0.72541 \pm 32	-
<u>Transition</u>					
TL22	25	191	0.3675 (7)	0.71007 \pm 30	10.4
<u>Granodiorite - North Limb</u>					
TL5	23	60	1.113 (6)	0.72437 \pm 32	-
68764	28	40	2.067 (3)	0.74007 \pm 28	-
<u>Granodiorite - South Limb</u>					
TL2*	17	143	0.3129 (14)	0.71036 \pm 28	10.8
TL8*	44	79	1.575 (12)	0.73176 \pm 48	11.5
TL11*	29	129	0.6513 (6)	0.71542 \pm 26	10.7
TL12*	140	147	2.780 (9)	0.74662 \pm 18	10.8
TL12F	121	151	2.325 (3)	0.73990 \pm 58	10.8
TL12FR	149	155	2.981 (6)	0.74938 \pm 16	-
TL14**	21	140	0.4310 (6)	0.71162 \pm 3	11.1
TL15*	35	84	1.185 (9)	0.72486 \pm 28	12.0
TL16*	45	75	1.691 (8)	0.73389 \pm 16	11.4
TL23A**	76	141	1.546 (7)	0.72875 \pm 1	10.9
TL23B				0.72865 \pm 28	*
69303	319	143	6.553 (7)	0.80105 \pm 52	-

TABLE B3.4 - Rb-Sr data for samples from
the Methuen Complex

SAMPLE	Rb (ppm)	Sr (ppm)	$^{87}\text{Rb}/^{86}\text{Sr}$	$^{87}\text{Sr}/^{86}\text{Sr}$
<u>Site-A</u>				
M3**	125	95	3.843 (3)	0.76822 \pm 3
M10A	102	114	2.617 (3)	0.75111 \pm 10
M10B				0.75131 \pm 20
M11	114	97	3.422 (3)	0.76310 \pm 10
M12**	120	89	3.922 (3)	0.77298 \pm 5
M13	117	94	3.631 (3)	0.76701 \pm 16
M14	130	84	4.512 (3)	0.78094 \pm 22
M15	122	88	4.013 (3)	0.77286 \pm 14
M17A	107	114	2.727 (3)	0.75090 \pm 26
M17B**				0.75119 \pm 10
<u>Site-B</u>				
M4**	137	78	5.114 (3)	0.79957 \pm 3
M22**	124	57	6.368 (3)	0.82106 \pm 1
M23**	126	64	5.755 (3)	0.80726 \pm 1
M24**	134	53	7.411 (3)	0.83533 \pm 6
M27	139	40	10.22 (3)	0.87368 \pm 22
M28**	112	63	5.193 (3)	0.79939 \pm 2
<u>Regional</u>				
M2**	130	39	9.813 (3)	0.85708 \pm 1
M5**	119	40	8.694 (3)	0.84388 \pm 1
M6**	43	147	0.8406 (3)	0.71727 \pm 2
M7**	97	142	1.984 (3)	0.73491 \pm 1
M18A	112	99	3.293 (3)	0.76440 \pm 22
M18B**				0.76486 \pm 1
M19A	91	124	2.132 (3)	0.74153 \pm 22
M19B**				0.74101 \pm 2
M20	124	134	2.691 (3)	0.75272 \pm 16

TABLE B4

U-Pb ZIRCON AND SPHENE DATA

The U-Pb zircon and sphene data obtained for the Apsley Gneiss, Tallan Lake Sill, Methuen Complex and Loon Lake Pluton are presented in this table. These analyses were performed at the Royal Ontario Museum following the procedures outlined in Appendix A.

* - the following codes have been used to describe the mineral fractions analysed:

Mineral analysed: Z = zircon S = sphene
Grain Size (Mesh): a) +100 b) -100+200 c) -200+325 d) -325
Magnetic Susceptibility: N,M = non-magnetic and magnetic at the indicated angle of tilt of a Frantz isodynamic separator
Colour: cl = colourless o = orange
A = abraded

** - Atomic ratios corrected for blank and common Pb. The Pb and U blanks are estimated to be 12 and 20 pg., respectively. For samples where the common Pb is less than the estimated blank, the total common Pb is considered equivalent to the blank.

TABLE B4. U-Pb results for zircon and sphene fractions from units in the Chandos Township area, Ontario

Sample Number	Description	Sample Weight (mg)	Concentration			Atomic Ratios**					Apparent Age (Ma)		
			U (ppm)	Pb (ppm)	Common Pb (pg)	²⁰⁶ Pb/ ²⁰⁴ Pb	²⁰⁸ Pb/ ²⁰⁶ Pb	²⁰⁶ Pb/ ²³⁸ U	²⁰⁷ Pb/ ²³⁵ U	²⁰⁷ Pb/ ²⁰⁶ Pb	²⁰⁶ Pb/ ²³⁸ U	²⁰⁷ Pb/ ²³⁵ U	²⁰⁷ Pb/ ²⁰⁶ Pb
Apsley Gneiss (AG50; LH84-1)													
1	Z, d, 2N, cl, A	0.40	-	46	47	3,355	0.0616	-	-	0.08131	-	-	1229
2	Z, d, 2N, cl	0.176	-	57	49	16,994	0.0699	-	-	0.07947	-	-	1184
3	S, a, 10N, o, A	0.290	130	23	717	598	0.0859	0.1806	1.877	0.07535	1070	1073	1078
Tallan Lake Granodiorite (TL40)													
4	Z, a, ON, cl, A	0.053	355	80	13	671,314	0.1411	0.2137	2.425	0.08225	1249	1250	1251
5	Z, a, ON, cl, A	0.166	329	72	28	44,553	0.1279	0.2110	2.384	0.08196	1234	1238	1244
6	Z, a, ON, cl, A	0.258	341	74	91	14,230	0.1282	0.2095	2.363	0.08181	1226	1231	1241
7	Z, b, 1N, cl, A	0.046	396	89	10	5.023E7	0.1445	0.2131	2.414	0.08216	1245	1247	1249
Tallan Lake Sill - Amphibolite (TL41)													
8	Z, a, ON, cl, A	0.236	65	14	30	10,997	0.0897	0.2090	2.353	0.08164	1223	1228	1237
9	Z, a, ON, cl	0.329	78	16	59	6,996	0.0759	0.2080	2.340	0.08161	1218	1225	1236
Methuen Complex (LH84-3)													
10	Z, b, ON, cl, A	0.204	326	69	82	12,182	0.0962	0.2091	2.348	0.08146	1224	1227	1232
11	Z, b, ON, cl, A	0.154	205	49	8	2.998E6	0.1275	0.2276	2.686	0.08559	1332	1325	1329
Methuen Complex (LH84-4)													
12	Z, b, ON, cl, A	0.207	263	55	19	110,603	0.0878	0.2097	2.359	0.08157	1227	1230	1235
13	Z, b, ON, cl, A	0.132	262	55	22	47,110	0.0888	0.2097	2.356	0.08151	1227	1229	1234
14	Z, c, 3N, cl, A	0.223	311	64	39	32,317	0.0819	0.2049	2.288	0.08098	1202	1209	1221
15	S, a, 10N, o, A	0.368	136	25	934	615	0.0692	0.1829	1.906	0.07560	1083	1083	1085
Loon Lake Pluton - Monzonite (LLZ1)													
16	Z, b, ON, cl, A	0.134	99	21	122	1,363	0.2659	0.1836	1.919	0.07580	1087	1088	1090
17	Z, b, ON, cl	0.652	107	22	116	7,266	0.2564	0.1796	1.874	0.07568	1065	1072	1087
18	Z, d, 3N, cl	0.250	151	31	19	62,083	0.2432	0.1782	1.858	0.07562	1057	1066	1085
19	S, a, 10N, o, A	0.507	27	13	984	172	1.9286	0.1836	1.916	0.07568	1087	1087	1086
Loon Lake Pluton - Quartz Monzonite (LLZ2)													
20	Z, c, ON, cl, A	0.190	311	64	14	620,955	0.0808	0.2067	2.304	0.08083	1211	1214	1217
21	Z, b, ON, cl, A	0.147	376	76	17	147,285	0.0748	0.2028	2.243	0.08022	1190	1195	1202
22	Z, b, ON, cl	0.471	409	81	60	48,362	0.0710	0.1977	2.174	0.07974	1163	1173	1190
23	Z, d, 3N, cl	0.146	552	100	74	14,483	0.0763	0.1831	1.990	0.07883	1084	1112	1168
24	S, a, 10N, o, A	0.383	73	20	867	399	0.5411	0.1938	2.019	0.07555	1142	1122	1083